Adsorption of Freshwater Dissolved Organic Matter to Clay and Polyethylene Particles

A Thesis submitted to the Faculty of the University of Minnesota by

Alvin Cameron Burrows

In partial fulfillment of the requirements for the degree of Master of Science in Chemistry

Dr. Elizabeth Austin-Minor

August 2019

Acknowledgements

After working on this thesis for the past two years there's a long list of people that contributed to its completion. I would first like to thank my advisor, Dr. Elizabeth C. Austin-Minor for providing guidance and support throughout my time in her group. Special thanks to my committee members, Dr. Kathryn Schreiner and Dr. John Evans for their assistance and advice while undergoing research. I would also like to thank Sarah Grosshuesch and Julia Halbur for their assistance with instrumentation as well as numerous other lab tasks. Thank you to the captain and crew of the R/V Blue Heron. To the office workers at both the LLO and UMD's Chemistry and Biochemistry department, Yvonne, Paige, Dawna, Jen and Carrie: I appreciate your help with every work-related issue and how pleasant you all always were with every request. Thank you to my roommates Maeve, Daniel and Alex for making our house truly feel like a home. Thank you to my friends and fellow graduate students for their support and the great memories: Daniel, Maeve, Alex, Anh, Michael, Faith, Ben, Cody and Robby.

Abstract

Organic matter (OM), especially dissolved organic matter (DOM), plays several integral roles in aquatic systems. OM acts as a short-term sink of carbon and a food source for heterotrophs and shields biota from harmful UV radiation. It also facilitates the transport of nutrients, trace metals and pollutants in the environment. The uptake and transport of these compounds are related to the fate of the DOM to which they are bound. Suspended solids such as clays or microplastics can adsorb DOM into their interlayer spaces or onto their surfaces leading to: 1. Possible physical protection of OM that would have been mineralized or degraded by biota; 2. Increased transport of OM through the water column to the sediments (for sinking particles) or increased time for OM in the surface water (for less-dense microplastic particles); 3. Increased uptake by larger aquatic organisms. Increased particle-associated mobility (either by sinking through the water column or being transported at the surface via wind-driven processes) also increases associated nutrient, trace metal and pollutant transport, which in sufficient quantities, may perturb the aquatic system's equilibrium and affect its chemistry. Microplastics, a new particle-type in aquatic systems, have been observed and documented in the world's oceans since the 1970s, but their presence in the Laurentian Great Lakes was first recorded in 2013. The roles that microplastics and other particulates (both naturally occurring and anthropogenically impacted) play in aquatic environments need to be thoroughly studied so that a better understanding of their fate and environmental impact can be gained. The goal of this study was to qualitatively examine and compare the adsorption of open water Lake Superior DOM and DOM from a tributary stream to polyethylene microplastic spheres and to clays (kaolinite and montmorillonite). UV-VIS optical proxies were used to

monitor changes in aromaticity (A_{254}, SUVA) and molecular weight (E_2:E_3, $S_{250\text{-}400}$, S_R) within the remaining dissolved phase. Aromaticity proxies suggest that clays preferentially adsorbed aromatic species, while polyethylene had no significant effect on DOM composition. Changes in the amount of carbon remaining in the dissolved phase were measured using dissolved organic carbon (DOC) analysis while the amount adsorbed to the surface of the particulates was measured using elemental analysis (EA). DOC analysis did not show significant changes in the amount of dissolved organic carbon after sorption testing. EA was unable to provide a definitive answer for carbon adsorbed by polyethylene but suggests that kaolinite and montmorillonite adsorb similar amounts of carbon in both environments.

Table of Contents

List of Tables

List of Figures

List of Acronyms

CEC – Cation Exchange Capacity
DOM - Dissolved Organic Matter
EA – Elemental Analyser
FA – Fulvic Acid
FTIR – Fourier transform infrared spectroscopy
HA – Humic Acid
HDPE – High-Density Polyethylene
HOC – Hydrophobic Organic Contaminants
HPB – Hydrophobic
HPL – Hydrophilic
HTCO – High temperature catalytic oxidation
Kaol – Kaolinite
KHP – Potassium hydrogen phthalate
LOI – Loss on ignition
MMT – Montmorillonite
NOM – Natural Organic Matter
NPOC – Non-purgeable organic carbon
OM - Organic Matter
PA - Polyamide
PAH – Polyaromatic Hydrocarbons
PAHA – Purified Aldrich humic acid
PAR – Photosynthetically Active Radiation
PCBs – Polychlorinated Biphenyls
PE – Polyethylene
PET – polyethylene terephthalate
POM – Particulate Organic Matter
POP – Persistent Organic Pollutants
PP – Polypropylene
PS – Polystyrene
PVC – Polyvinvyl Chloride
SEM/EDS – Scanning Electron Microscopy/ Energy Dispersive X-Ray Spectroscopy
SPE – Solid Phase Extraction
S_R – Slope Ratio
SRFA – Suwannee River fulvic acid
SUVA – Specific UV absorbance
TSS – Total Suspended Solids
UV – Ultraviolet
UV-Vis – Ultraviolet-visible spectroscopy
WEOC – Water Extractable Organic Carbon

Chapter 1. Introduction

1.1 Freshwater Lakes

About 87% of the earth's surface liquid freshwater is found in lakes (USGS, 2019). This means that lakes play a key role in providing much needed resources, such as drinking water, water for irrigation, hydro-electric power generation and food. There are aesthetic benefits associated with lakes as well, such as the natural beauty of the area and the tranquility it may provide for homeowners (Al-Khudhairy et al., 2001). Lakes, and large water bodies in general, also provide economic opportunities. Entire industries may be built around fishing for large scale consumption, shipping services to import and export goods, and tourism due to aesthetic appeal or recreational activity lakes provide (Al-Khudhairy et al., 2001; Austin et al., 2007). Lakes also serve as home to a plethora of biodiverse organisms, providing protection and nutrients to sustain their growth (Garn et al., 2003; O'Beirne et al., 2017).

The Laurentian Great Lakes, bordering southern Canada and the northern United States, contain about 84% of the surface fresh water in North America and about 21% of the world's surface fresh water (EPA, 2018). These lakes also sustain the 30 million people that live in the surrounding areas (Austin et al., 2007). Lake Superior, the location for this study, is the most upstream, deepest, and most pristine of the Laurentian Great Lakes.

Climate change has led to increased intensity and frequency of major storm events around the world (Villarini et al., 2011; Ban et al., 2015; Fischer and Knutti, 2016). In the United States midwestern states have experienced some of the greatest increases in precipitation with this trend predicted to continue well into the rest of this century (Hayhoe et al., 2018). The Minnesota Department of Natural Resources has predicted that

Minnesota's climate will continuously get wetter and warmer with increased frequency of larger storm events (Minnesota DNR, 2019). These events can drastically increase nutrient loadings as well as induce the mobilization of biogenic and anthropogenic material into local waterways. Notably, in 2012 a "mega-rain event" in Minnesota and Wisconsin led to a plume of mud, clay and other debris inundating western Lake Superior's waters. This drastically increased the average total suspended solid (TSS) concentration (1.1mg/L to 83mg/L (Minor et al., 2014a)) and tinted waters light brown. TSS concentrations are dependent upon factors such as soil erosion, sediment resuspension and run-off.

1.2 Clays

Clays constitute a major portion of TSS in natural water and are responsible for organic matter (OM) and inorganic matter transport in these systems (Sondi and Pravdic, 1998). The southwestern shore of Lake Superior sits on an abundance of red clay which is constantly eroded and dispersed throughout the lake. Clays, also referred to as phyllosilicates, are hydrated silicates of aluminum, iron and magnesium arranged in various combination of layers (Birkeland, 1984). These natural particles have high mobility, high surface areas due to their small size as well as variable surface charge depending on the pH of the system and mineral type. Another characteristic of clays is their ability to exchange interlayer cations with those present in their surroundings, also known as cation exchange capacity (CEC). These characteristics affect element cycling, pollutant transport and interactions with microbial communities (Day et al., 1994).

In the Lake Superior region, more densely populated areas such as Thunder Bay (121,621 according to the 2016 census (Statistics Canada)), Duluth (85,884 estimate in 2018 (U.S. Census Bureau)), and Superior (26,101 estimate in 2018 (U.S. Census Bureau))

are likely sources of anthropogenic pollutants, such as microplastics. The extent to which these pollutants are mobilized will vary depending on the magnitude of the storm event (Guan et al., 2016). In general, sediment loads to aquatic bodies are sensitive to numerous factors such as reservoir construction, land clearance and land use change, as well as other forms of land disturbance (Walling and Fang, 2003). Clearing land for cultivation or urbanization commonly increases soil erosion and loads to rivers by up to several orders of magnitude (Walling and Fang, 2003). Land disturbances such as construction and mining have variable results on sediment loads (Wood and Armitage, 1997), in some instances these disturbances may only affect a smaller area and be short-lived (Walling and Fang, 2003).

1.3 Microplastics

In recent years microplastics have gained attention due to increased identification in the environment and not fully understood environmental effects. Microplastics are plastic particles <5mm whose robust properties make them an ever-growing contaminant throughout the world. Due to their relative chemical inertness, microplastics can travel far from their source and collect in even the most remote aquatic environments. In 1971 Edward Carpenter and his colleagues were the first to report the presence of plastic particles on the ocean's surface in the Atlantic (Carpenter and Smith, 1972). Since then, more researchers have taken notice of these particles in the environment prompting plastic assessments and identification in marine and freshwater systems throughout the world (Eriksen et al., 2013, 2014; Anderson et al., 2017; Sruthy and Ramasamy, 2017; Hendrickson et al., 2018). With increased yearly production of plastics (1.5 million tonnes in 1950 to 335 million tonnes in 2016 (Plastics Europe Market Research Group (PEMRG)

/ Consultic Marketing & Industrieberatung GmbH, 2015; PlasticsEurope, 2017)) accumulation in aquatic systems has the potential to escalate. There are a plethora of polymers that make up microplastics in the environment, but those used in packaging material and personal care products are more likely to end up as contaminants (Andrady, 2011). Examples of common microplastic polymers are polyethylene terephthalate (PET), polyvinylchloride (PVC), polystyrene (PS), polyethylene (PE), and polypropylene (PP) (Andrady, 2011; Gewert et al., 2015). Possible sources of microplastic pollutants to aquatic environments include wastewater treatment plants, high precipitation events leading to sewage overflow and storm water/snow melt run off, atmospheric deposition, the fishing industry, and beach debris (Eriksen et al., 2013; Sruthy and Ramasamy, 2017; Hendrickson et al., 2018).

Because microplastics are now ubiquitous in water bodies, aquatic life has been burdened by their presence. Microplastics may damage organisms upon ingestion by blocking digestive tracts, inducing false satiation, impairing reproductive capabilities, leaching toxins to body tissue and causing death (Eerkes-Medrano et al., 2015; Baldwin et al., 2016). Humans that feed on these organisms may then indirectly ingest these plastics leading to potential health risks, but the effects that ingested microplastics have on humans still need to be studied in greater detail. Furthermore, due to their large surface area and varying chemical composition, microplastics tend to sorb potentially harmful compounds such as heavy metals, polyaromatic hydrocarbons (PAHs) and polychlorinated biphenyls (PCBs) (Fries and Zarfl, 2012; Van et al., 2012; Driedger et al., 2015; Eriksen et al., 2017). Dissolved organic matter (DOM) may also be adsorbed to the surface of microplastics. The

significance of DOM here is that it can affect the edibility or "taste" of particles, as well as affect the transport of pollutants in aquatic environments.

Because clays and microplastics can sorb OM to their external surfaces or to portions of their interior, and because they have different surface properties in an aqueous environment, the role that these particulates play in the presence of DOM should be carefully assessed. The retention of DOM in soils has been attributed to its clay content (Kaiser and Zech, 2000). Plastics have the potential to sorb and concentrate hydrophobic organic contaminants (HOC) in aquatic environments (Hong et al., 2018). HOC association with plastic in the presence of DOM has been studied with varied results as discussed later in this section, however vigorous study of DOM-microplastic interactions is lacking.

1.4 Dissolved Organic Matter

DOM is defined as the dissolved organic constituents of water that pass through a filter whose pore size may range from 0.7μm-0.1μm. Any organic compounds retained on the filter are defined as particulate organic matter (POM). The characteristics of DOM, such as concentration, composition and chemistry, vary considerably between locations. The primary sources of DOM are often described as being autochthonous, native to the system, or allochthonous, coming from outside the system. Autochthonous DOM comes from the primary production of macrophytes, algae, and bacteria that take in simple inorganic species and convert them to complex organic matter, autolysis of dead organisms and excretions from aquatic species (Leenheer and Croué, 2003; Lin, 2015). Allochthonous material is usually soil run off and vegetation from the surrounding landscape that gets leached or broken down to dissolved or smaller particulate organic material and transported to an aquatic system (Amy, 2008). Thus, terrestrial DOM is often dominant in areas with

an abundance of vegetation in the watershed relative to water area, such as rivers, streams, creeks, and swamps. Conversely, autochthonous DOM is abundant in locations with low terrestrial inputs such as the marine environment and open water locations in large lakes. DOM consists primarily of carbon, so it is often characterized by its carbon content and referred to as dissolved organic carbon (DOC). There is an estimated 55 Pmol of DOC that has accumulated over thousands of years and is being stored in the oceans (Holland and Turekian, 2014) making this pool of carbon comparable in terms of size to that of carbon in the atmosphere, so small changes in marine DOC respiration or formation can directly influence atmospheric CO_2 budgets and the earth's radiative balance making it an important constituent in the carbon cycle. Aside from being an important source and sink of carbon in exchange with the atmosphere, DOM also plays several other crucial environmental roles. Many essential trace metals in aquatic systems are soluble due to organic ligand complexes formed with DOM (Holland and Turekian, 2014). Autotroph-produced DOM is also a major source of energy for bacterial heterotrophs in aquatic environments (Carlson et al., 2007). As previously mentioned, DOM can increase the transport of contaminants and nutrients within a system. If nutrient transport increases the limiting reagent in an aquatic ecosystem, there will be growth in phytoplankton and algal species in the environments leading to a reduction in water clarity, changes in primary production, and increases in anoxic water volumes (Carpenter et al., 1998). As for pollutant transport, DOM has been shown to increase the transport of persistent organic pollutants (POPs) such as PAHs, phenols, pesticides, and pharmaceuticals (Magee et al., 1991; Ohlenbusch et al., 2000; Chabauty et al., 2016). DOM also has the ability to attenuate ultraviolet (UV) radiation as well as photosynthetically active radiation (PAR) allowing it

to act as sunscreen in surface water (Minor et al., 2014b). This protects organisms from harmful UV rays, but can also limit the amount of light available for sunlight driven processes such as photosynthesis.

1.5 Organic Matter Sorbent Interactions

The binding of DOM to mineral surfaces affects the stability and composition of DOM (Armanious et al., 2014). Binding stabilizes the bound fraction of the DOM in the environment (Hedges and Oades, 1997) leading to protection from enzymatic degradation, ultimately increasing organic carbon sequestration in sediments. Selective sorption may also fractionate DOM, changing the chemical composition of the unbound solution in the dissolved phase (Hur and Schlautman, 2004; Fleury et al., 2017). OM-coated mineral surfaces display different physicochemical properties than bare minerals which alters their reactivity and particle aggregation affecting their fate in the environment (Tombácz et al., 2004; Gao et al., 2018).

Due to the various functionalities of DOM and the various particulate characteristics of sorbents available within the aquatic environment, sorption is a complex process that is difficult to explain through a single mechanism. Six commonly used mechanisms to explain these sorption processes are hydrophobic interactions, van der Waals interactions, ligand exchange, chelation, cation bridging and H-bonding (Philippe and Schaumann, 2014). Hydrophobic interactions involve non-polar OM that interacts unfavourably with water leading to uptake onto a surface resulting in a favorable change in entropy. Van der Waals interactions are weak short-range, additive associations. Ligand exchange for DOM in natural water systems generally refers to the exchange of hydroxyl groups on adsorbent surfaces for acidic hydroxyl groups (carboxylic acids and phenols)

within organic matter. Cation bridges form when cations link negatively charged adsorbent surfaces and anionic or polar functional groups within OM. Water bridges may also form between the cation and the polar functional group through hydrogen bonds. Hydrogen bonds form through the interactions of hydrogen atoms polar covalently bound to a more electronegative atom with surrounding strongly electronegative atoms such as oxygen and nitrogen.

Evidence of OM's ability to form micelles in solution has led Kleber et al. (2007) to propose that OM sorbs to mineral surfaces in three discrete zonal sequences. The first zone is the contact zone, which favors the formation of strong organo-mineral associations made primarily of polar, possibly amphiphilic, functional groups that bind through ligand exchange or form stable inner sphere complexes. Strong bonds may also form through the unfolding of proteinaceous species adding hydrophobic interactions to electrostatic binding. This is followed by the hydrophobic zone, which comprises the hydrophobic portion of amphiphilic molecules that are favourably shielded from the polar aqueous phase through interactions with other hydrophobic moieties of other amphiphilic species. These components may exchange with species in the surrounding solution more readily than those in the contact zone but are still bound with some strength. The third and final region is referred to as the kinetic zone. This zone includes species that are bound to the exterior coating, thus they are only weakly held and readily exchanged with the surrounding mixture.

1.6 Factors that affect sorption

The extent to which OM sorbs depends on the characteristics of the particulates, properties of the DOM and environmental conditions. Some of these environmental factors

include pH, ionic strength, the ions present and the concentration of OM. Numerous authors (Day et al., 1994; Hyung and Kim, 2008; Zhang et al., 2012) observed an inversely proportional relationship between pH and OM adsorption with increased adsorption at lower pH values. Studies have also reported increased OM-particulate interactions with increasing ionic strength (Day et al., 1994; Hyung and Kim, 2008; Zhang et al., 2012). The type of ions present also plays a role in either facilitating increased uptake of DOM onto particulate surfaces or decreasing uptake by competitively binding to reactive sites. Hiemstra et al. (2010) observed variations in the amount of natural phosphate bound to top soils due to competition from natural organic matter (NOM) complexes. Weng et al. (2008) observed a similar phenomenon when studying the interactions of phosphate with goethite in the presence of fulvic acid but observed no effect when humic acid (HA), rather than fulvic acid(FA), was present. Conversely, studies have found that the presence of divalent cations, such as calcium, facilitate increased uptake of DOM onto mineral surfaces (Feng et al., 2005; Majzik and Tomba, 2007). The concentration of DOM within a system may also affect how well it is protected against chemical degradation by OM-mineral interactions. Kaiser and Guggenberger (2007) observed that at higher DOM loadings OM attached to goethite was more chemically degradable than at lower concentrations. The authors attributed this to more OM being intimately bound directly to the mineral's surface at lower OM concentrations through innersphere complexation, whereas at higher OM concentrations, bulky agglomerates form which are primarily bound through weaker outersphere complexes, decreasing their protection.

The adsorbent characteristics for mineral-surface interactions depend on size, shape, surface charge, surface topography and degree of particle aggregation (Philippe and

Schaumann, 2014; Kleber et al., 2015). Particle size affects the amount of adsorbent that may interact with the adsorbate. The number of reactive surface groups per mass in minerals is inversely related to particle size, increasing with decreasing particle size due to an increase in specific surface area. Complicating the relationship with size, pores in swelling clays such as smectites expose internal surface area allowing absorption to occur on these surfaces, if the pores are large enough, leading to increased enzymatic protection of OM. In general, OM tends to show stronger affinity for oxide and hydroxide minerals than aluminosilicates (Meier et al., 1999; Fleury et al., 2017). This has been attributed to more favourable electrostatic interactions on oxide/hydroxide surfaces relative to those of clays (Philippe and Schaumann, 2014). Fleury et al. (2017) found that in the case of alumina the main binding mechanism was through ligand exchange, while for kaolinite (Kaol) it was H-bonding leading to varied fractionation patterns.

The sorbent interactions exhibited by plastic particles depend on factors similar to those discussed above in addition to type of plastic, crystallinity and temperature. Plastic surface activity may be influenced by surface defects such as kinks and pits that change the interactions of the surface atoms and create internal surface area for absorption. Crystallinity refers to the degree of order within a structure. Polymers may be highly crystalline with molecules regularly arranged or amorphous where the structure is randomly oriented. The highly ordered crystalline region requires more energy for molecules to interrupt the regular arrangement, however in the amorphous region sorption is more favourable where the polymeric structure is less restricted (Endo and Koelmans, 2010). Semi-crystalline polymers such as PE or PP can absorb chemicals in their amorphous regions. Temperature affects the bulk properties of a polymer such as

crystallinity and glassiness (Endo and Koelmans, 2010). The glass transition temperature of a polymer is the temperature at which it changes from a rubbery state that can freely move which promotes sorption, as opposed to a glassy state that is rigid which inhibits sorption.

Non-polar plastics such as PE or PP exert only van der Waals forces, in absence of polar functional groups on their surface. Van der Waals interactions and hydrogen bonding play a major role in the sorption of neutral organic chemicals to different compounds (Endo and Koelmans, 2010). As previously mentioned, studies have shown that plastics sorb numerous HOCs and persistent organic pollutants (POPs), but the effects of these interactions in the presence of DOM along with DOM-plastic interactions themselves need further study to understand whether DOM inhibits HOC uptake (Xu et al., 2018) or increases uptake (Zhang et al., 2018). Physical properties should also be studied such as particle size which has been shown to affect OM-microplastic interactions, as was seen when smaller fragments of polystyrene (80nm) showed a greater affinity for humic acid adsorption than larger fragments (500nm) (Chen et al., 2018).

1.7 DOM Characteristics

Because DOM is a complex mixture comprised of aliphatic and aromatic moieties with various functional groups, its affinity for adsorbents differs based on the reactivity of these groups. These common functionalities include carboxylic acids as well as their derivatives, alcohols, ethers, amines, etc. Commonly discussed species include carbohydrates, amino acids, proteins, lignin, tannins, fatty acids, HA and FA. HA and FA refer to the fractions of humic substances that are soluble in water over pH 2 and those soluble over the entire pH range, respectively (Baglieri et al., 2007). DOM's composition

varies temporally and spatially making its chemical characteristics source dependent, meaning that observations made in one environment may not necessarily hold true in another.

DOM origin controls its chemical content and reactivity. Variations in its content can change its adsorptive properties, as seen in previous studies (Day et al., 1994; Kaiser and Guggenberger, 2000; Hur and Schlautman, 2003; Hyung and Kim, 2008; Kruger et al., 2011). Day et al. (1994) compared the adsorption of NOM from Redwater Creek in Australia and NOM from Suwannee River in USA, to goethite using Langmuir adsorption isotherms. The bulk Redwater Creek OM had a greater sorption density than the Suwannee River fulvic acid (SRFA). This was attributed to the larger molecular size of the creek NOM relative to the river NOM. Hur and Schlautman (2003) observed preferential adsorption of high molecular weight species for Suwanee River FA to kaolinite and hematite. In contrast, preferential adsorption for purified Aldrich Humic Acid (PAHA) was found to vary. Fractionation patterns were explained due to differing chemical content within the SRFA and PAHA samples. Kruger et al. (2011) found inconsistencies in optical properties (E2/E3 and $SUVA_{254}$) when comparing Lake Superior and tributary stream C18-extracted DOM to bulk DOM. Changes in $SUVA_{254}$ varied depending on source without a clear trend while E2/E3 ratios were consistently lower compared to bulk DOM. Hyung and Kim (2008) studied the adsorption of NOM standards (Suwannee river HA, Nordic HA, Wakish peat HA and several others) to multi-walled carbon nanotubes using adsorption isotherms and found one of the factors that affected sorption was the type of NOM used. It was generally seen that less soluble, higher molecular weight humic acids exhibited higher adsorption capacity than fulvic acids to the multiwalled carbon nanotubes used as sorbent.

Kaiser and Guggenberger (2000) stated that the sorptive preservation of OM in soil is affected by the chemical structure of the sorbing DOM and the surface properties of the mineral matrix. DOM composition affects the strength and favoured binding mechanisms of organo-clay interactions. Thus, by comparing the sorption of DOM from different sources, insight may be gained into whether sorption favours a specific source, as well as how much DOM sorption occurs in general.

Sorption studies may use DOM from a variety of sources such as leachates from soil (Kaiser and Zech, 2000; Kaiser et al., 2001; Gao et al., 2018), water extractable organic carbon (WEOC) from compost (Nguyen and Marschner, 2014) and composted biosolids (Young et al., 2018). Due to the prevalence of humic substances in the environment, HA and FA fractions from various sources are commonly used to study these interactions as well (Hur and Schlautman, 2004; Feng et al., 2005; Fleury et al., 2017). Mahamat Ahmat et al. (2016) was able to test organic matter mineral interactions in-situ along a seawater column using clay immersion traps. Scientists may further fractionate OM to elucidate binding mechanisms from subsets such as the hydrophobic (HPB) and hydrophilic (HPL) fractions (Kaiser and Zech, 2000; Hunt et al., 2007). Avneri-Katz et al. (2017) studied the adsorption of fractionated OM to Fe (III) montmorillonite and observed preferential adsorption of the hydrophobic acid fractions based on resin separation. Using FTICR-MS the authors observed preferential uptake of polyphenolic compounds, a component of the hydrophobic acid fractions.

Although DOM reactivity varies, numerous studies have reported preferential sorption of hydrophobic, higher molecular weight species (Hur and Schlautman, 2004; Hunt et al., 2007; Pitois et al., 2008; Zhang et al., 2012) and more aromatic species (Meier

et al., 1999). Despite there being an apparent trend, studies have also reported preference for lower molecular weight species and no selectivity for aromatic species (Chorover and Amistadi,2001; Kaiser, 2003) depending on adsorbent and adsorbate. Thus, there is a need to study organic matter particulate interactions within a given environment.

When studying dissolved organic matter sorbent interactions, researchers often model soil environments, which use large amounts of adsorbent relative to TSS in aquatic systems. To this author's knowledge none of these studies have used levels of TSS relevant to lakes and streams and DOM from the Laurentian Great Lakes. Very few have investigated sorption of natural dissolved organic matter on microplastic particles. Because the roles of microplastics within the environment are still relatively unknown, it is important to understand the effects microplastics may have on DOM partitioning and ultimate fate in the environment. Due to Minnesota's shift towards a wetter climate with more intense rain events, the transfer of anthropogenic, biogenic, and geogenic material into aquatic environments needs to be studied to determine effects of increased loadings. This thesis uses batch adsorption to examine DOM-clay and DOM-microplastic interactions using DOM from Lake Superior and a tributary stream, Chester Creek. The goals of this thesis are: 1. to determine the amount of C adsorbed to clays and microplastic particles; 2. to determine what bulk property changes can be seen in the dissolved phase; and 3. to characterize the initial material in hopes of elucidating what in the dissolved phase drives these changes. The sorbents were montmorillonite (MMT), kaolinite and high-density polyethylene (HDPE) microspheres. Scanning electron microscopy (SEM) was used to size adsorbents. Filtrate underwent DOC analysis while adsorbents were subjected to elemental analysis to determine loss or uptake of C. Ultraviolet-visible spectroscopy

(UV-VIS) was used to observe bulk chemical changes in filtrate. Fourier transform infrared spectroscopy (FTIR) was used to characterize OM extracts and freeze-dried material in hopes of gaining structural information.

Chapter 2. Methods

2.1 Description of Sample Sites

Figure 1. The top figure is a google maps image showing the location of the offshore (Lake Superior) and inland (Chester Creek) sampling sites. The bottom left figure is the Chester Creek at St. Scholastica site. The bottom right picture is open water Lake Superior.

Two sample sites were chosen for this study based on their contrasting characteristics. The first site is a Lake Superior tributary stream, Chester Creek in Duluth, Minnesota. The tributary's watershed has an area of 18.4 km^2. The watershed consists of 49% forests, 24% rural and urban areas and 0.3% open water. (Lakesuperiorstreams, 2009).

With the majority of its watershed consisting of forest and urbanized areas it is expected that Chester Creek will have a higher DOM concentration (8-10mg/L (Macdonald and Minor, 2013)) than open water Lake Superior and the DOM will be primarily allochthonous in origin. Due to its proximity to urban areas the stream is susceptible to anthropogenic pollutants such as microplastics and debris during runoff events.

Lake Superior holds 10% of the world's freshwater (Minnesota Sea Grant) and is the world's largest fresh water lake by surface area (82,000 km^2) and third largest by volume (12,000 km^3) (Herdendorf, 1982). Its watershed is 127,700 km^2, the smallest watershed to surface area ratio of all the Laurentian Great Lakes. Its environment is relatively well preserved compared to other Great Lakes due to a lack of industrialization and development although it borders three U.S. states and one Canadian province (Minnesota Sea Grant). Lake Superior is the least populated Laurentian Great Lake basin with a human population of approximately 600,000 (Minnesota Sea Grant) which is significantly less than the fourth most populated basin, Lake Huron, whose human population is about 3 million (US Department of Commerce). The Lake is oligotrophic with DOM concentrations ranging from 1.7-3.2 mg/L (Stephens and Minor, 2010) and has a water residence time of 191 years. Due to its large size and lack of significant allochthonous inputs Lake Superior's DOM is expected to be primarily autochthonous in origin; however, based on previous ESI-FTICR-MS and FTIR studies, its DOM appears to be a mixture of reworked terrestrial material containing large amounts of aromatics, carbohydrates and aliphatics (Minor and Stephens, 2008; Minor et al., 2012).

2.2 Sample Collection

Chester Creek (46°48'59.5"N 92°06'09.2"W; November 2018) whole water was collected in a submerged 10L carboy, previously cleaned with soap and water, rinsed with 10% HCl, and further rinsed with deionized water. The carboy was rinsed with sample three times prior to collection. Within 24 hours of collection the whole water was filtered through a previously combusted 0.7μm glass microfiber filter (Whatman 1825-047) followed by a 0.22μm PVDF membrane filter (Durapore GVWP04700) to remove POC and bacteria. Filtrate was then combined in a fresh acid clean 10L carboy and stored in the fridge at 37˚C until time for use. A subset was collected in an acid cleaned 1L Nalgene bottle, frozen overnight (-4˚C) and freeze dried for Fourier transformed infrared spectroscopy (FTIR). The surface (5m depth) open water Lake Superior (46°47.04'N, 91º49.23'W; May 2018) sample was collected on the R/V Blue Heron. This sample was collected in 5 20L carboys (cleaned similarly to the carboy) using a diaphragm pump (ARO Ingersoll Rand Model # PDO2P-APS-PTA) equipped with silicone tubing. Initially, a 0.8/0.2μm capsule filter (Whatman Polycap 150 TC), flushed with DI water for 1 hour and site water for 5 minutes, was placed on-line before the carboys to filter on site. However, after filling one of the 20L carboys, due to harsh weather conditions it was decided that filtering in lab was best. Whole water samples were filtered in lab using the previously mentioned capsule filter within 24 hours of collection and stored in a refrigerator at 37˚C. A 2L subset of this Lake Superior filtrate was then frozen and freeze dried similarly to the Chester Creek sample.

2.3 PPL Cartridge Solid Phase Extraction (SPE)

Solid phase extraction was conducted as described in Dittmar et al., (2008) using a Varian PPL cartridge (6mL, 500mg) made of a modified styrene divinyl benzene polymer. Briefly, sterile filtered water samples were acidified to pH~2 using 6N HCl, and an aliquot of this acidified sample was taken for DOC analysis. The resin was conditioned by allowing one cartridge volume of methanol to elute through the cartridge. After conditioning, sample water was passed through the cartridge with the assistance of a peristaltic pump using masterflex (PharMed NSF-51) tubing. Due to previously reported extraction efficiencies, which vary for open-water and tributary samples, Lake Superior extraction passed 4L of water through the cartridge while Chester Creek used 2L. Aliquots of filtrate were collected for DOC analysis to determine extraction efficiency. After DOM elution 12mL of 0.01M HCl was passed through the cartridge to remove any salts. The cartridge was then dried under N_2 for 10 minutes. After drying, 6mL of methanol was passed through the cartridge to elute retentate using gravity filtration. The retentate was collected in pre-weighed ashed glass vials and dried under N_2. The dried retentate was then stored in a desiccator for further analysis. Extraction efficiencies were calculated using the following formula:

$$1 - \frac{DOC_{filtrate}}{DOC_{initial}} * 100$$

Samples were stored in the dark in a refrigerator for several months before SPE extraction was done.

2.4 Loss on Ignition

Loss on ignition (LOI) was used to isolate inorganic species from freeze dried material. LOI included combusting a known amount of freeze-dried material from Chester

Creek and Lake Superior 5 hours at 450℃ in a pre-weighed glass vial until no change in mass was observed.

2.5 Sorption Substrates

The sorption substrates are bentonite/montmorillonite (MMT) (≤25μm Sigma-Aldrich), kaolinite (1-1.8μm Fisher Scientific) and high density polyethylene microspheres (HDPE) (10-45μm Cospheric). The choice in sizes of each substrate were limited by what was commercially available, but all substrates used have similar surface areas. Using particle diameter values determined by measuring SEM images of particles, the mass used in the experiment and particle geometry, the number of particles present was calculated and used to approximate external surface area available for sorption. MMT's surface area was calculated as a sphere as this was the approximate shape of what was seen using SEM. HDPE was clearly spherical and Kaol was treated as rectangular sheets with the thickness of the sheet assumed to be the minimum diameter value measured. The structure of Kaol was aggregated leading to difficulty finding individual particles. Depending on the magnification of the image, numerous Kaol particles were unmeasured due to their small size (believed to be in the manufacturer's range of <1.8μm). Due to the difficulty of easily identifying shapes in some of the images and because only a limited number of scans of each particulate were taken the size ranges must be considered approximate. Nonetheless, the average particle size of HDPE and MMT agreed with manufacturer specification while Kaol was slightly larger; results may be found in Table S-6. The external surface areas were found to be 0.26, 0.51 and 0.15 m^2/g respectively for MMT, Kaol and HDPE respectively. Unlike Kaol, MMT is a swelling clay which means it expands and has an

internal surface area potentially available for sorption of DOM. It has been shown that this internal surface area is much larger than the external surface area (Diamond, 1956; Pennell, 2016); at the current time we do not have an estimate for this internal surface area. The adsorption of organic matter to montmorillonite and kaolinite has been extensively studied making them reasonable choices for comparison to other studies. Polyethylene was chosen because it is a commonly used plastic making it a likely environmental contaminant, and because it has been identified in Lake Superior surface waters (Hendrickson et al, 2018).

2.6 Adsorption Study

Before sorption studies began, the stored water samples were re-filtered through 0.22um PVDF membrane filters (Millipore GVWP). Apart from montmorillonite, which was dried for 2 hours in a vacuum oven (>150˚C, -10in Hg) to remove preabsorbed water, substrates were used with no prior treatment. Adsorption studies were conducted by placing approximately 20mg of particulates (MMT, Kaol and HDPE) in separate combusted glass Erlenmeyer flasks followed by 250mL of sterile filtered sample water (containing DOM). The flasks were capped with previously-ashed foil and parafilm, placed in a dark enclosure and shaken for 4 days. In addition to the substrates a control for each experiment was analysed; this control, which consisted of sterile filtered sample water without particulates but otherwise treated similarly to the particulate samples. Day 0 samples were prepared simultaneously with day 4 samples using the methodologies above but were analysed immediately after being placed in their respective flasks. The experiment was conducted using 3 replicates with the results averaged to give a final value. A HOBO pendant was used to measure the temperature every hour within the enclosure for the duration of the experiment.

At the given time point the flask's contents were filtered through individual pre-weighed 0.22μm membrane filters (Durapore GVWP04700) into combusted 500mL vacuum flasks. A subset of filtrate was collected in combusted 40mL amber vials that were rinsed once with a small washing of filtrate before being filled for TOC analysis. These vials were immediately acidified with 40μL of 6N HCl (Fisher Chemical Certified ACS Plus) and stored in a refrigerator until they could be analysed. The remainder of the filtrate was placed in combusted glass kimax bottles, filled similarly to the TOC vials, for immediate UV-Vis analysis. All filters were loosely wrapped in foil and placed in a vacuum oven overnight to dry at 50˚C and -10 inHg. Dried filters were left in a desiccator to cool before being reweighed. To recover substrate from filters the particulates were resuspended in a previously-ashed glass petri dish. The filter was shaken using metal forceps and rinsed several times with Milli-Q water (18.2 Ω*cm) using an ashed glass pipette. The washings were transferred to 20mL pre-weighed glass vials and frozen overnight. The vials were then freeze-dried and reweighed.

To ensure there was no significant leaching of carbon from any sorption substrate, a blank study using the same amount of Milli-Q water (18.2 Ω*cm) and particulates as the lake and tributary experiments was conducted. TOC analysis showed that there were no significant changes in the amount of carbon present in the filtrate before and after the experiment (Supplementary information Table S-6). UV-Vis analysis showed that any contributions from the particulates to absorption spectra in the 250-400nm range used for calculations were insignificant.

Analytical Methods

2.7 UV-VIS

Spectra were taken on a Genesys 10 UV-VIS spectrophotometer. Samples were scanned from 800nm to 200nm in either a 1cm (Chester Creek site) or 5cm (Lake Superior site) pathlength quartz cuvette. A blank, consisting of MilliQ water, was taken before analyses began and after every 6 analyses thereafter. Blank correction was done by averaging the two blanks surrounding each group of sample analyses and subtracting the average blank from the samples it surrounds. To remove the effects of potential particulates in the sample, a backscatter correction was performed by subtracting the average absorbance from 700-800nm from the blank corrected absorbances for all wavelengths of that sample. The Naperian absorption coefficient was then calculated as done in Massicotte et al. (2017):

$$a(\lambda) = \frac{2.303 * A_{\lambda}}{L}$$

Where $a(\lambda)$ is the wavelength-specific absorption coefficient (m^{-1}), A_{λ} is the backscatter corrected decadal absorbance value and L is the cuvette pathlength (m).

The E_2/E_3 ratio was calculated by comparing the absorption coefficients at 250nm (E_2) and 365nm (E_3). This parameter has been used in numerous studies (Haan, 1987; Hunt et al., 2007; Helms et al., 2008) to track changes in the average molecular weight of DOM and is inversely proportional to molar mass with larger E_2/E_3 ratios being indicative of a lower average molecular weight. This is significant because an increase or decrease in this ratio indicates whether there is a preference between the average sorption of higher or lower MW DOM.

The absorption coefficient at 254nm (A_{254}) has been shown to be highly correlated to a sample's aromaticity. Specific UV absorption (SUVA) is a measure of ultraviolet absorption at a given wavelength normalised to the sample's DOC content in mg C L^{-1} (Weishaar et al., 2003; Minor et al., 2014b). SUVA may be calculated by dividing the Naperian absorption coefficient or the decadal absorbance value (normalized to pathlength) by the sample's DOC content. Both methods are used throughout literature, but in this study Naperian absorption coefficient SUVA values are reported. Weishaar et al., (2003) found that SUVA at 254nm was correlated to aromaticity based on ^{13}C NMR studies of OM isolates from numerous aquatic environments (Weishaar et al., 2003). Spectral slope (S_λ) is a robust parameter that uses wavelength intervals, as opposed to a single wavelength, to derive information such as source, degradation state, and MW ranges from chromophoric dissolved organic matter (CDOM) (Del Vecchio and Blough, 2002; Helms et al., 2008; Minor and Stephens, 2008). $S_{250\text{-}400}$ was calculated by fitting the absorption coefficients to an exponential function using the equation:

$$a(\lambda) = a(\lambda)_{ref} e^{S(\lambda - \lambda_{ref})}$$

The $S_{275\text{-}295}$ and $S_{350\text{-}400}$ were calculated using a linear regression on the natural log transformed absorption coefficients. The ratio of these slopes ($S_{275\text{-}295}$: $S_{350\text{-}400}$) was then used to calculate the spectral slope ratio (S_R) which has been used as a proxy for shifts in DOM molecular weight (Helms et al., 2008), with increases in S_R reflecting decreases in average molecular weight. The benefit of S_R is that it uses shorter wavelength intervals which show strong characteristic changes in UV-Vis spectra and that it avoids using wavelengths near a spectrophotometer's limit of detection. Optical parameters were found

for each replicate and then the replicate values were averaged (n=3). Descriptions of each parameter and their affiliated references can be found in Table S-3.

2.8 TOC/DOC

DOC analysis was performed on the filtrate following previously established methods as described in Zigah et al., (2014). The filtrate was collected in ashed 40mL vials after a single rinse of sample. This aliquot was acidified with 40µL of 6M HCl and refrigerated until analysis. DOC content was analysed using high temperature catalytic combustion (HTCO) on a Shimadzu V_{CSH} analyser calibrated with potassium hydrogen phthalate (KHP) and measuring DOC as non-purgeable organic carbon (NPOC). The DOC was also acidified by the instrument using HCl and was sparged with CO_2 free air to remove all inorganic carbon. The sample was injected 3-5 times until the standard deviation between injections was <2.5%. The 3 injections that met this criterion were averaged for sample concentration. Milli Q water (Milli Q, Millipore Corp) that had been acidified with 40µL of 6M HCl added to 40 mL of water were dispersed throughout the analytical run to be used as blanks. The average of these Milli Q blanks was then subtracted from calculated sample concentrations to give a corrected DOC concentration. A pre-acidified Deep-Sea Standard (0.50mg C/L, Batch 11 Lot #03-11) was included in the run to act as a check standard for the method. Values within ±25% of the expected value for this standard were deemed acceptable. At the end of the sample runs a secondary calibration curve of the initial standards was made to account for instrument drift. Deviation of <5% in secondary calculated standard concentrations using the first calibration curve was deemed acceptable.

2.9 Scanning Electron Microscopy (SEM)

Imaging was conducted using a Jeol JSM-6490LV scanning electron microscope equipped with an INCAx-act energy dispersive x-ray detector for elemental analysis. Sorbents were mounted to metal SEM stubs using double sided carbon tape. The electron accelerating voltage was varied between 5-15kV depending on the sample and under low vacuum to minimize charging under the electron beam. Samples were imaged at 230x – 4,000x using the SEM's backscattered electron (BSE) detector. Chester Creek and Lake Superior LOI samples underwent (EDS) analysis in addition to imaging (Figure S-13 – S-16). SEM/EDS allows for qualitative determination of elemental composition. Scandium™ software was used to size images.

2.10 FTIR Analysis

FTIR spectra were taken using a Nicolet 380 FTIR spectrophotometer equipped with a DTGS detector and KBr beam splitter using nitrogen as a purge gas. DOM stock mixtures were prepared by mixing 2mg freeze dried <0.22μm DOM with 400mg KBr (Alfa Aesar, FTIR grade) that had previously been dried in a vacuum oven for at least one hour at 110°C and -10in Hg. Montmorillonite and Kaolinite stocks were made using 1:500 clay to KBr ratio due to the strong absorbances of these clays in the IR region. High density polyethylene stock was made using a 1:500 plastic to KBr ratio for the same reason. MMT was also dried in a vacuum oven at the same conditions as the KBr due to its hydrophilic nature. Stock mixtures were then homogenised using a Wig-L-bug grinding mill. After homogenisation, pellets were made by pressing approximately 100mg of sample mixture, at no more than 10,000lbs of pressure, between two methanol cleaned pellet casings.

Spectra were collected using 200 scans, a resolution of $1cm^{-1}$, Happ-Genzel apodization, ranging from $4000cm^{-1}$ to $400cm^{-1}$. A pure KBr background was taken every 3 scans. A 4-minute lag time between closing the FTIR chamber and collecting the spectra was introduced to reduce atmospheric CO_2 and water signals. All spectra were collected in triplicate and baseline corrected using a plain KBr pellet in OMNIC software. Peak deconvolutions were done on Origin 2019 using its Peak Deconvolution application to deconvolute peaks and determine peak areas.

2.11 Elemental Analysis

Elemental analysis measurements were done following previously established methods (Zigah et al., 2014). The freeze-dried particulates from the experimental treatments were wet with several drops of Milli Q water to aid in the transfer of particulates plus associated DOM. An ashed pipette was used to transfer the particulates to tin capsules. The capsules were dried overnight at 50˚C. The capsules were closed and underwent carbon and nitrogen analysis on a Costech ECS 4010 elemental analyser (EA) calibrated with either 2,5-(Bis(5-tert-butyl-2-benzo-oxazol-2-yl)thiophene (BBOT) (Costech) for species expected to contain more carbon (freeze-dried DOM, HDPE) or B-2153 (Elemental Microanalysis, low organic content soil) for species expected to contain less carbon (MMT, Kaol). Freeze-dried DOM samples were weighed out in silver capsules, followed by the addition of 50µL of Milli Q water via pipette. The silver capsules were then acid fumigated for at least 6 hours in a dessicator with 12M HCl to remove inorganic carbon. After fumigation the capsules were loosely wrapped in foil and allowed to dry in a fume hood for 48 hours. After drying the silver capsules were placed inside tin capsules, closed and

left in a desiccator for EA analysis. Because 100% of the original particulates could not be collected for EA, the amount transferred to the tin cup was recorded and the mass of carbon and nitrogen within this fraction was measured. This amount was then scaled up to the original amount of particulate used in the study. The final amount of adsorbed carbon was corrected to account for carbon already present on the particulates. This correction was done by performing EA analysis on a known amount of raw particulates and scaling the amount of C present to the initial amount of carbon used in each adsorption study. The raw particulate carbon amount was then subtracted from the adsorbed sample. This was followed by subtracting the total amount of carbon found on the control filter from the raw particulate corrected amount of carbon adsorbed. The control filter refers to the filter from the adsorption study that did not use particulates. Replicate samples were analysed and averaged to give the reported value (n=3) with its standard deviation.

2.12 Statistical Analysis

The Microsoft Excel Data Analysis Toolpak was used to conduct T-tests which determined whether there were significant differences between Day 0 and Day 4 samples. Q-tests were used to determine whether outliers could reasonably be removed from a data set. This test was performed manually using Q criteria from Dixon's Q-test. Both tests used an alpha of 0.05 to determine significance, thus any $p<0.05$ was deemed significant.

Chapter 3. Results

3.1 FTIR Characterization of initial water samples used in the sorption studies

Although the peaks in Figure 2 have tentatively been identified there appears to be significant overlap of peaks from organics and inorganics (see Table 1 for peak assignments and references). Thus, to elucidate the bands associated with solely inorganic species, LOI was conducted on the freeze-dried material to remove the organic species.

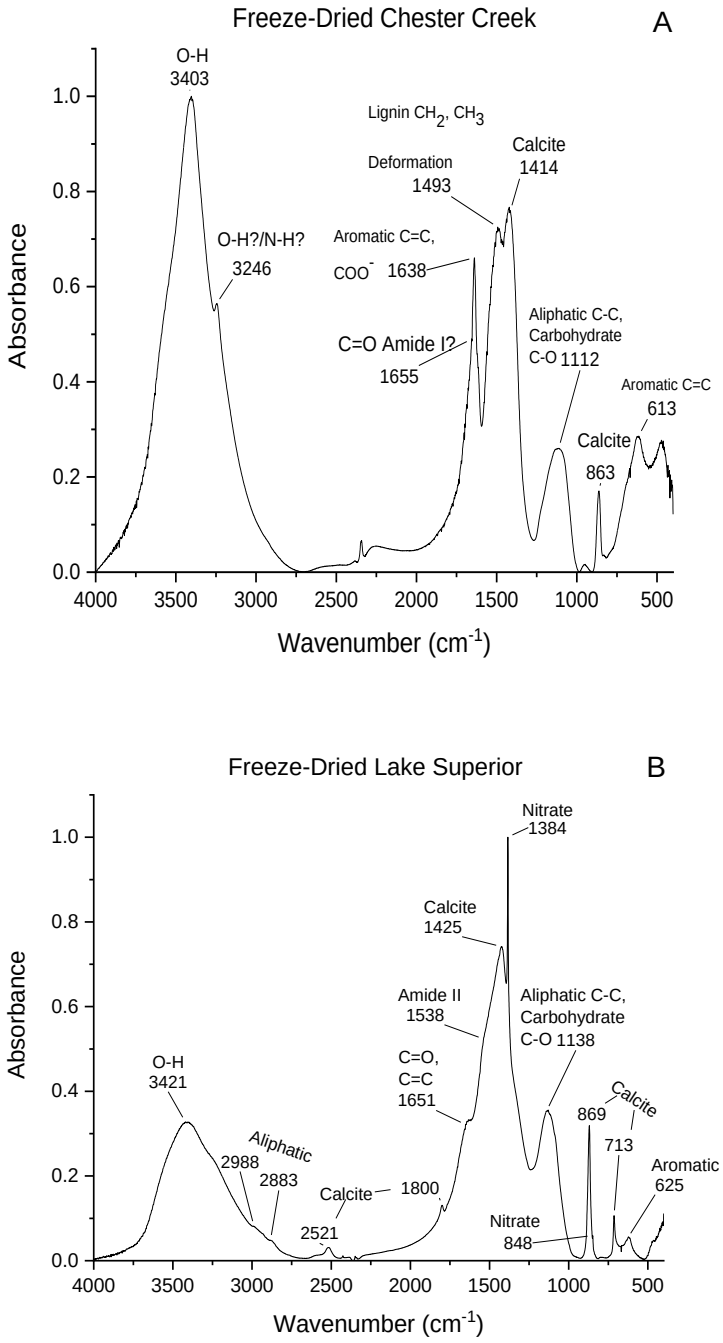

Figure 2. FTIR spectra (KBr Pellet) of freeze-dried (a) Chester Creek and (b) Lake Superior sterile filtered water

Figure 3 shows the inorganic (LOI) FTIR spectra of Chester Creek and Lake Superior (see Table 1 for peak assignments and references). Short sharp bands above 3300 cm^{-1} can be attributed to hydroxyl stretching of minerals. In Lake Superior the stretch at 3619 cm^{-1} can be attributed to inner hydroxyl groups, located between the tetrahedral and octahedral sheets, while the stretch at 3697 cm^{-1} is due to in-phase symmetric stretching of OH groups forming weak hydrogen bonds (Madejova, 2003). In Chester Creek the band at 3571 cm^{-1} could possibly be attributed to OH groups from FeOH groups in minerals (Madejova, 2003). Broadbands located at 3417 and 3425 cm^{-1} are indicative of H-O-H vibrations of water strongly bound to minerals. There also appear to be weak aliphatic stretches for Chester Creek at 2919 and 2850 cm^{-1} and Lake Superior at 2990 and 2880 cm^{-1} (Leenheer et al., 2004; Lumsdon and Fraser, 2005; Artz et al., 2008; Minor and Stephens, 2008; Abdulla et al., 2010; Parolo et al., 2017). These signals indicate that some of the organic matter remained after combustion. Silica can be attributed to sharp stretches at 1112, 1033 and 1011 cm^{-1} in Lake Superior, while in Chester Creek it is attributed to a weaker shoulder at 1120 cm^{-1} (Madejova, 2003; Diko et al., 2016). Due to the strength and number of bands relating to silica in the Lake Superior sample it appears the relative abundance of silica is greater in Lake Superior than Chester Creek. The sharp band at 913 in Lake Superior is due to Al-OH bending (Madejova, 2003). Both spectra also show that calcite has a strong presence in both waters, but more so in Lake Superior due to the identification of all its characteristic peaks. The peaks located at 1426 and 875 cm^{-1} in Chester Creek and 2524, 1802, 1421, 872 and 713 cm^{-1} in Lake Superior are attributed to calcite (Minor and Stephens, 2008; Parolo et al., 2017).

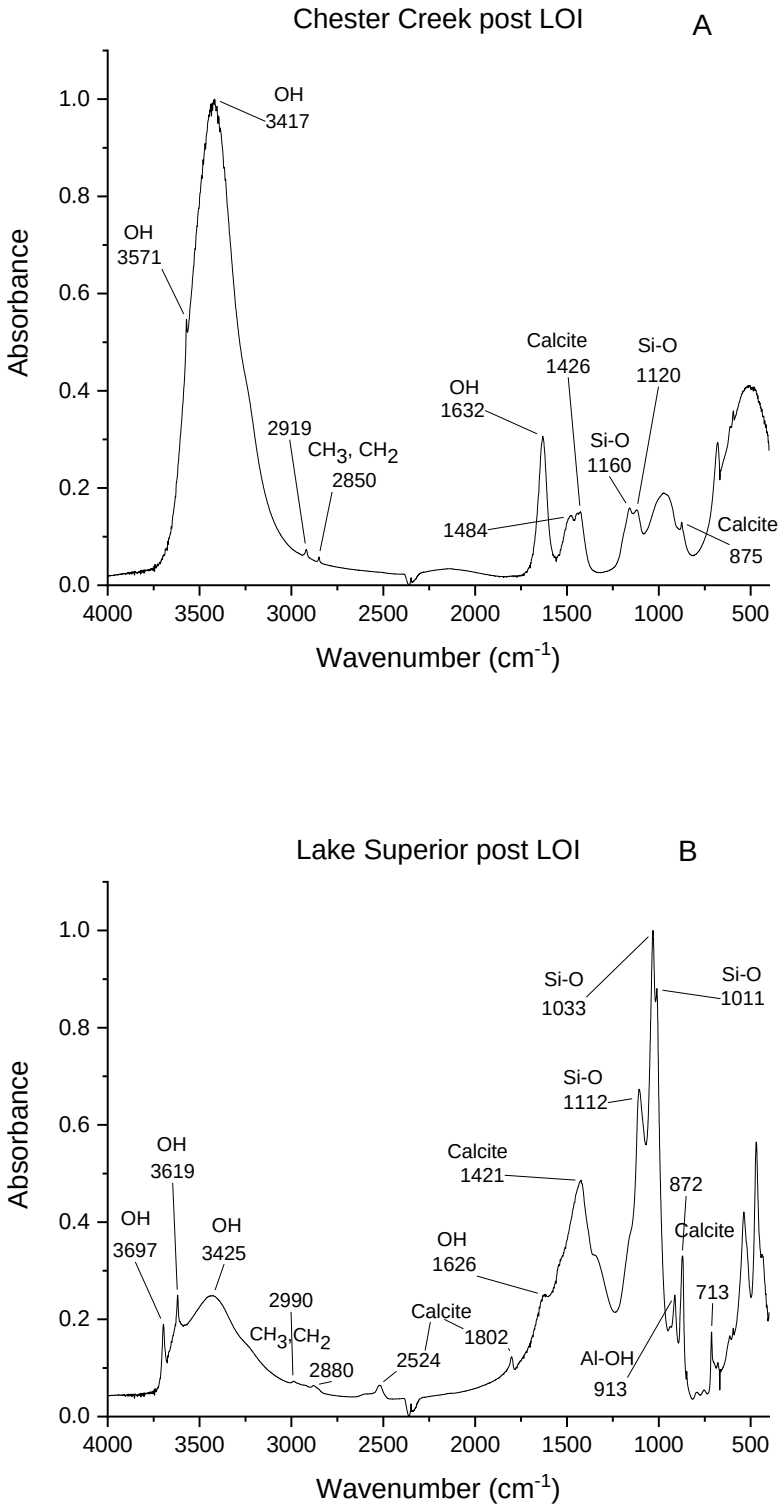

Figure 3. FTIR spectra (KBr Pellet) of material remaining after LOI removal of organic material from (a) Chester Creek and (b) Lake Superior

Figure 4 shows the FTIR spectra of the SPE organic matter from Chester Creek and Lake Superior. The broad bands at 3429 and 3417 cm^{-1} which spread to about 2500 cm^{-1} in Chester Creek and Lake Superior respectively are indicative of OH from carboxylic acids. The bands at 2981 and 2943 cm^{-1} in Chester Creek as well as 2978 and 2938 cm^{-1} in Lake Superior are attributed to CH_3/CH_2 stretching from aliphatics (Leenheer et al., 2004; Lumsdon and Fraser, 2005; Artz et al., 2008; Minor and Stephens, 2008; Abdulla et al., 2010; Parolo et al., 2017). The strong sharp peak located at 1721 and 1725 cm^{-1} in Chester Creek and Lake Superior are attributed to C=O stretching from carbonyl groups (Leenheer et al., 2004; Lumsdon and Fraser, 2005; Abdulla et al., 2010). Due to its position it is most likely from the carboxylic acid functional group. While a subtle difference, the ratio of the areas of the carboxylic and the aliphatic peaks is higher in the Chester Creek extract (1.33 ± 0.07) than in the Lake Superior sample (1.00 ± 0.02). The shoulder at 1631 and 1630 cm^{-1} in Chester Creek and Lake Superior may be attributed to C=O from amides, COO^- asymmetric stretching or C=C stretching from aromatics (Kovac et al., 2002; Artz et al., 2008; Minor and Stephens, 2008; Abdulla et al., 2010; Li et al., 2014; Parolo et al., 2017). The shoulder located at 1454 and 1457 cm^{-1} in Chester Creek and Lake Superior respectively could be due to CH_2 scissoring from aliphatics (Abdulla et al., 2010). The shoulder located near 1413 cm^{-1} is attributed to O-H bend in plane from a carboxylic acid (Abdulla et al., 2010). The weaker sharp band at 1389 cm^{-1} in both spectra is attributed to the CH_3 umbrella mode (Abdulla et al., 2010). The broad band located at 1224 and 1207 cm^{-1} in Chester Creek and Lake Superior respectively, may be due to C-O stretching from phenolic species or C-O stretching from carboxylic acids (Abdulla et al., 2010). The shoulder located at 1055 and 1057 cm^{-1} in Chester Creek and Lake Superior may be

attributed to aliphatic C-C stretching or C-O stretching from carbohydrates (Leenheer et al., 2004; Lumsdon and Fraser, 2005; Artz et al., 2008; Minor and Stephens, 2008; Abdulla et al., 2010; Li et al., 2014; Parolo et al., 2017). The shoulder at 955 cm^{-1} in Lake Superior corresponds to O-H out of-plane bending from the carboxylic acid group (Abdulla et al., 2010).

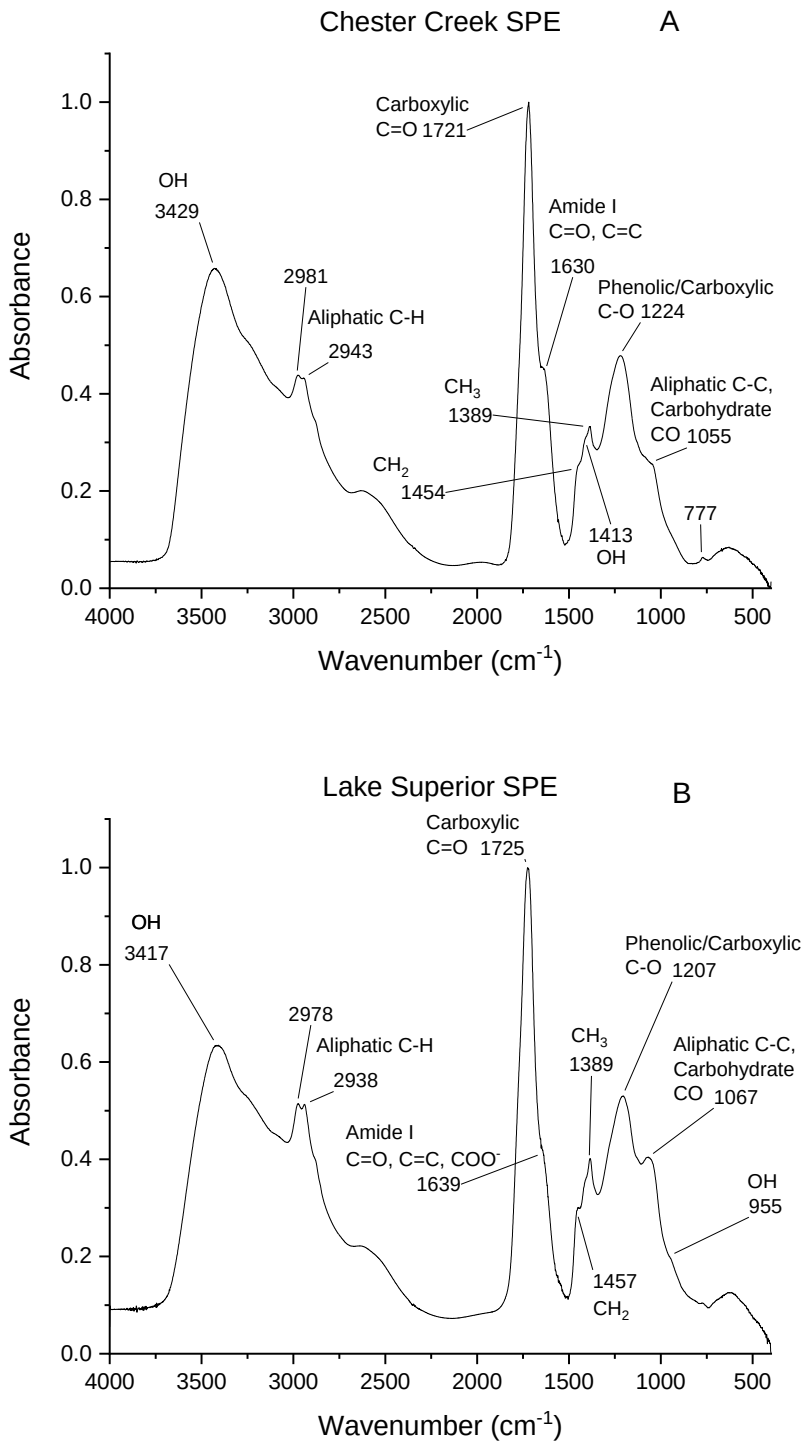

Figure 4. FTIR Spectra (KBr pellet) of SPE DOM from (a) Chester Creek and (b) Lake Superior

Table 1. IR peak assignments for Fig. 2-4. of freeze-dried (FD), LOI and SPE material for Chester Creek (CC) and Lake Superior (LS)

Assignment	*Band Position (cm^{-1})*						*Reference*
	CC FD	LS FD	CC LOI	LS LOI	CC SPE	LS SPE	
OH Crystalline hydroxyl	-	-	3571	3697, 3619	-	-	a
O-H stretching	3402	3421	3417	3425	3429	3417	a,b,c,d, e,f,g,h
OH/ NH??? Stretching	3242	-	-	-	-	-	b, e
Aliphatic C-H stretching	-	2960, 2872	2919, 2850	2990, 2880	2981, 2943	2978, 2938	b,c,e,f,h,i
C=O	-	1655	-	-	1721	1725	c,e,i
H-O-H	-	-	1632	1626	-	-	a
Amide I, aromatic C=C, COO-	1639	1642	-	-	1630	1639	b,c,d,f,g,h
Amide II	-	1538	-	-	-	-	c, e, g, i
CH2 Scissoring	-	-	-	-	1454	1457	c
OH in plane bend	-	-	-	-	1413	-	c
Nitrate	-	1385, 848	-	-	-	-	c,h
CH3 umbrella mode	-	-	-	-	1389	1389	c
Phenolic/C arboxylic C-O	-	-	-	-	1224	1207	c
Si-O	-	-	1160, 1120	1112, 1033, 1011	-	-	a,j
Aliphatic C-C, Carbohydr ate C-O	1129	1121	-	-	1055	1067	b,c,e,f,g,h, i
OH out of plane bend	-	-	-	-	-	955	c
Al-OH	-	-	-	913	-	-	a
Calcite	1420, 862	2521, 1800, 1421, 869, 713	1426, 875	2524, 1802, 1421, 872, 713	-	-	b, h

(a) (Madejova, 2003) (b) (Minor and Stephens, 2008) (c) (Abdulla et al., 2010) (d) (Kovac et al., 2002) (e) (Leenheer et al., 2004) (f) (Artz et al., 2008) (g) (Li et al., 2014) (h) (Parolo et al., 2017) (i) (Lumsdon and Fraser, 2005) (j) (Diko et al., 2016)

Sorption study results

3.2 DOC Analysis

Chester Creek and Lake Superior had average initial DOC concentrations of 7.69 mg C L^{-1} and 1.40 mg C L^{-1} respectively (Figure 5). These values fall within the range of previously reported DOC concentrations in the area (Minor and Stephens, 2008). In terms of DOC concentration neither sample showed significant changes relative to the control in the presence of any adsorbent.

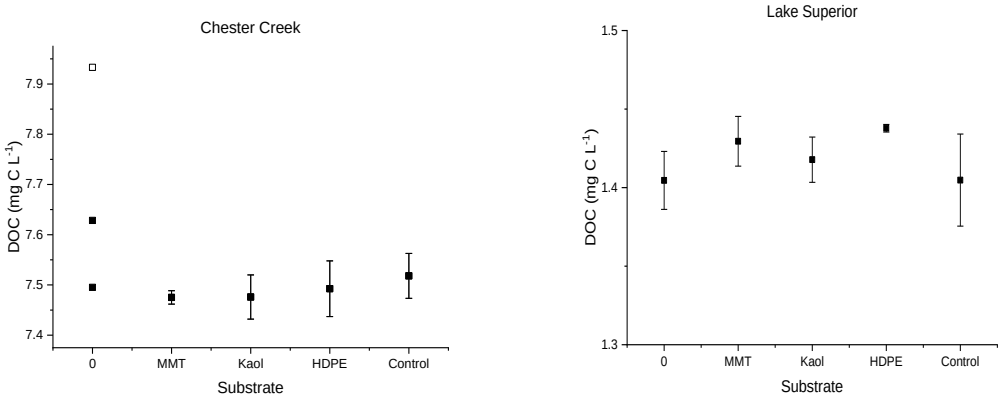

Figure 5. DOC data for Chester Creek and Lake Superior filtrate used in sorption studies. Graphs contain data for Day 0, Control (Day 4) and each adsorbent (MMT, Kaol, HDPE). □ Represents a replicate that was stored differently. While being an outlier it did not fail a Q-test, thus the 3 points were plotted instead of an average with its standard deviation. Note that the higher DOC concentration in Chester Creek compared to Lake Superior is reflected in the scaling of the y-axis.

3.3 Elemental Analysis

Table 2 shows the amount of C adsorbed to each clay. Data for HDPE is not provided as this study was not able to determine the amount of C present after adsorption due to its initial high C content. Kaol, on average, adsorbed more C in Chester Creek (n = 3, P = 0.3)

and Lake Superior (n=3, P = 0.07) than MMT, but no significant difference was observed. In general, more C was adsorbed in Lake Superior water than in the Chester Creek sample, but no significant difference was seen when comparing Kaol (n = 3, P = 0.07) and MMT (n = 3, P = 0.4) adsorption between sites.

Table 2. Particulate elemental analysis results and SSA determined via SEM particulate diameter measurement.

	Chester Creek ug C /mg substrate	**Lake Superior** ug C /mg substrate	**SSA** m^2/ g
Kaol	2.4 ± 1.0	4.4 ± 1.1	0.8 ± 0.6
MMT	1.6 ± 0.8	2.2 ± 1.1	0.3 ± 0.1
HDPE	-	-	0.15 ± 0.03

3.4 Optical Analysis

A_{254}

Based on the initial values of A_{254} it is clearly seen that Chester Creek (45.57) is more aromatic than Lake Superior (4.58) (Figure 6). In the case of Chester Creek's filtrate, HDPE did not show significant changes in A_{254} when compared to the control. On the other hand, sorption to MMT and Kaol leads to statistically significant decreases in A_{254} in the filtrates of experimental vs control samples, suggesting a decrease in aromaticity in the dissolved phase and preferential sorption of aromatic material to these clay particles. Lake Superior A_{254} also showed significant decreases in the filtrate when MMT and Kaol were present relative to control filtrate, with HDPE having little effect on the parameter.

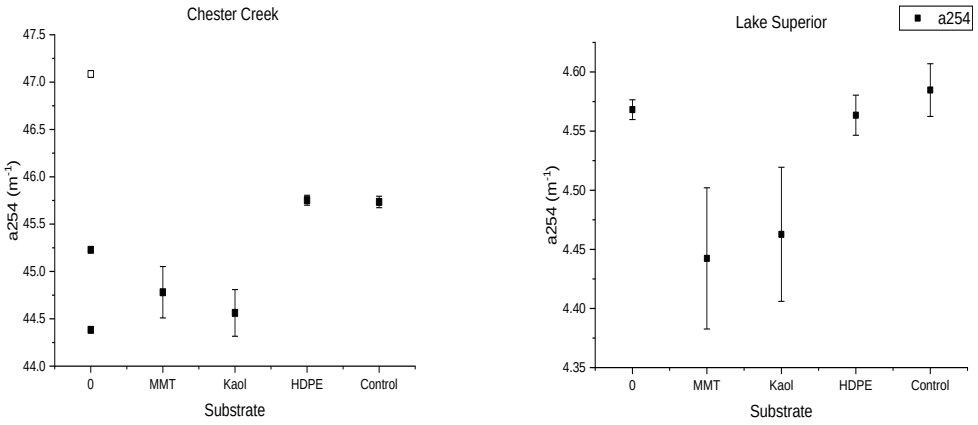

Figure 6. A_{254} data for Chester Creek and Lake Superior filtrate used in sorption studies. Graphs contain data for Day 0, Control (Day 4) and each adsorbent (MMT, Kaol, HDPE). □ Represents a replicate that was stored differently. Note the difference in y-axis scales between Chester Creek and Lake Superior.

SUVA

Chester Creek filtrate from the experimental treatments did not show significant changes in SUVA when compared to the control (Figure 7). Lake Superior experimental filtrate SUVA values follow a trend similar to its A_{254}. MMT and Kaol show significant decreases when compared to the control with MMT having the largest influence. HDPE does not show a significant difference in SUVA relative to the control. Decreases in SUVA are indicative of an increased proportion of aliphatic material in the filtrate due to the removal of aromatics (via sorption).

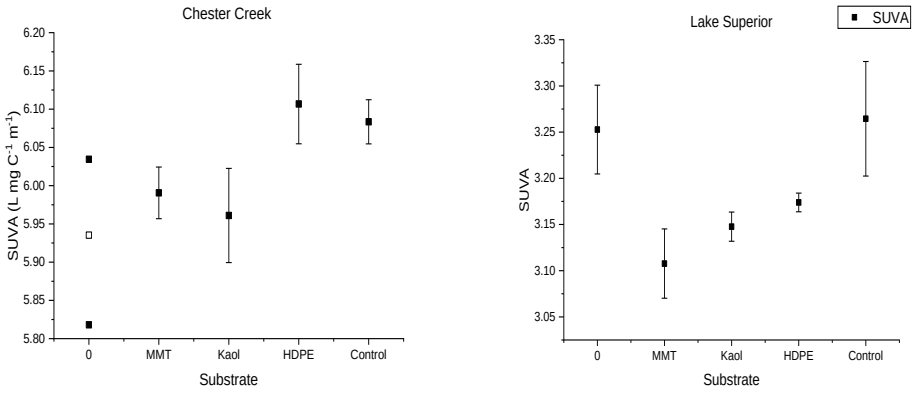

Figure 7. SUVA data for Chester Creek and Lake Superior filtrate used in sorption studies. Graphs contain data for Day 0, Control (Day 4) and each adsorbent (MMT, Kaol, HDPE). □ Represents a replicate that was stored differently. Note the difference in y-axis scales between Chester Creek and Lake Superior.

E2/E3

No significant changes in E2/E3 (Figure 8.) ratio were seen in the experimental treatments when both DOM sources were compared to their respective controls. However, there is a significant decrease in the Chester Creek control relative to day 0.

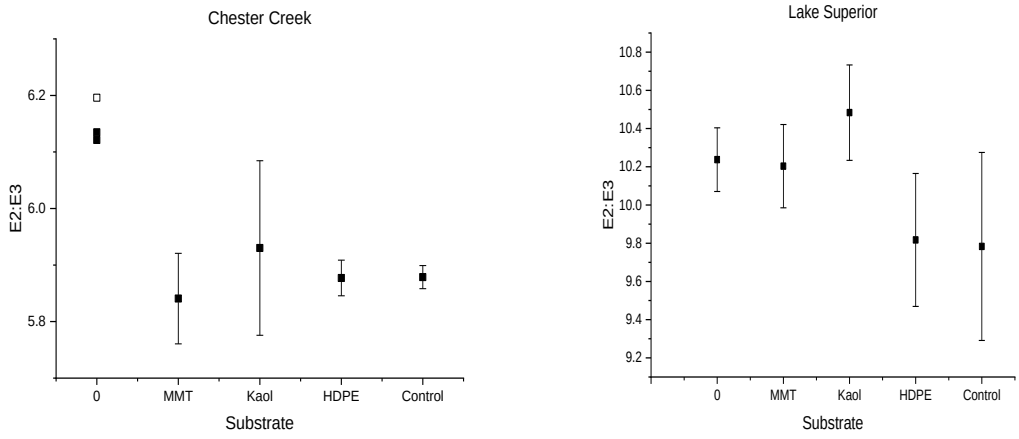

Figure 8. E2/E3 data for Chester Creek and Lake Superior filtrate used in sorption studies. Graphs contain data for Day 0, Control (Day 4) and each adsorbent (MMT, Kaol, HDPE). □ Represents a replicate that was stored differently. Note the difference in y-axis scales between Chester Creek and Lake Superior.

$S_{250\text{-}400}$

The $S_{250\text{-}400}$ is used as a proxy for the average molecular weight of DOM. Chester Creek filtrate did not show significant differences compared to the control for any adsorbent (Figure 9). In the case of Lake Superior, HDPE did not show a significant difference relative to the control. Conversely, MMT and Kaol lead to an increase in $S_{250\text{-}400}$ suggesting a decrease in the size of the DOM present in the filtrate.

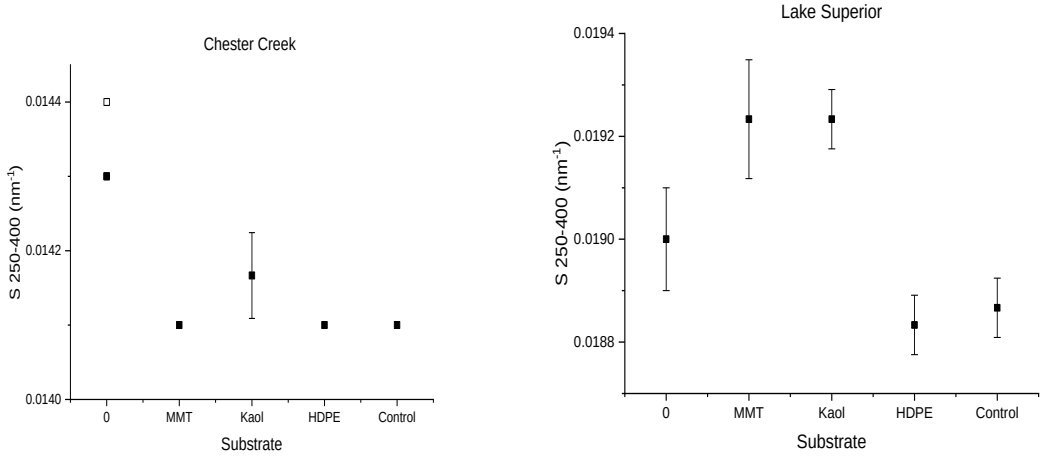

Figure 9. $S_{250\text{-}400}$ data for Chester Creek and Lake Superior filtrate used in sorption studies. Graphs contain data for Day 0, Control (Day 4) and each adsorbent (MMT, Kaol, HDPE). □ Represents a replicate that was stored differently. Note the difference in y-axis scales between Chester Creek and Lake Superior.

S_R

The S_R has been correlated to changes in molecular weight of a sample by comparing the $S_{275\text{-}295}$ to $S_{350\text{-}400}$ (Helms et al., 2008). Chester Creek filtrate did not show significant changes in the presence of particulates when compared to the control (Figure 10). Lake Superior filtrate in the presence of Kaol was the only sample to show a significant decrease compared to the control.

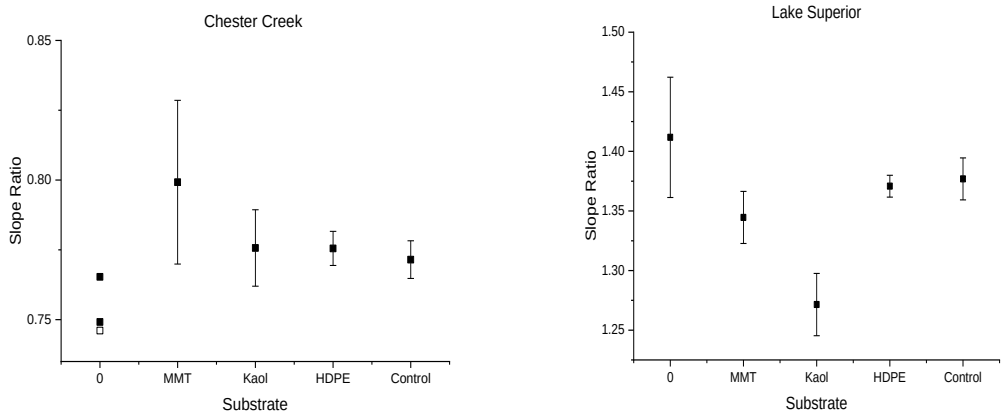

Figure 10. S_R data for Chester Creek and Lake Superior filtrate used in sorption studies. Graphs contain data for Day 0, Control (Day 4) and each adsorbent (MMT, Kaol, HDPE). □ Represents a replicate that was stored differently. Note the difference in y-axis scales between Chester Creek and Lake Superior.

Chapter 4. Discussion

4.1 FTIR

FTIR spectra of freeze dried samples from Lake Superior and Chester Creek (Figure 2) appear to mimic lake and tributary FTIR spectra from a previous study of DOM conducted on western Lake Superior (Minor and Stephens, 2008). FTIR spectra from the inorganic fractions (Figure 3) showed significant contributions from mineral phases due to the abundance of silica. Studies would need to be conducted to determine the clay composition of the soils along Chester Creek to determine which contribute to its watershed and may be chosen for further adsorption studies. Calcite was also shown to have a strong presence in both samples, with more of a contribution in Lake Superior.

The spectra from the PPL retentates gave similar absorbances for Chester Creek and Lake Superior (Figure 4). Differences in the organic fraction of the two sites could not be fully determined using this extraction technique. Dittmar et al (2008) observed that PPL is more selective (retains a smaller proportion of total DOM) when applied to marine (more autochthonous) DOM than to riverine (allochthonous) DOM, which may explain why the

Chester Creek retentate appears similar to Lake Superior's retentate. The extracts do show a strong carboxylic acid and aliphatic component of the mixture and the Lake Superior extract appears more aliphatic in nature based on its carbonyl to aliphatic ratio. Weaker phenolic and carbohydrate bands have been identified in both retentates as well (Figure 4).

The FTIR spectra of the PPL extracted OM (Figure 4b) reports similar functional groups to the FTIR spectra of C18 extracted OM from open water Lake Superior (Minor and Stephens, 2008). Both samples show strong aliphatic, carboxylic and carbohydrate components, which suggests that the even though these techniques are expected to fractionate DOM differently in Lake Superior the extractions lead to similar functional groups. Conversely, the functional groups identified in the FTIR spectrum of PPL extracted OM from Chester Creek compared to that of C18 extracted OM from another Lake Superior tributary stream, Lester River, (Minor and Stephens, 2008) are quite different. As previously mentioned, the PPL extract from the tributary stream shows similar functional groups to those found in the Lake Superior OM. The C18 extracted DOM shows strong amide and lignin signals which are absent in the PPL extract.

4.2 Sorption studies: kaolinite

Based on DOC analysis Kaol did not significantly change the DOC content of Lake Superior or Chester Creek water at the concentration used (Figure 5). EA analysis does show that adsorption occurred based on increased carbon content found on the particulates (Table 2). Based on EA analysis, Kaol adsorbed similar amounts of C in both the Chester Creek and Lake Superior sample, as a significant difference was not observed. When

compared to MMT, Kaol did not show significant differences in the amount of C adsorbed in the Chester Creek or Lake Superior sample.

It has previously been shown that the amount of OM adsorbed to mineral surfaces decreases as pH increases and increases as ionic strength increases (Feng et al., 2005; Zhang et al., 2012; Chen et al., 2017). A mineral's pH point of zero charge (pH_{PZC}) is defined as the pH at which the net particle charge becomes zero (Brezonik and Arnold, 2011). Kaol has a pH_{PZC} reported to be ~4.6 (Brezonik and Arnold, 2011) which is lower than the pH of the aquatic systems used in this study implying that the mineral has a net negative charge on its surface. It is assumed that DOM would primarily be ionic at the pHs used in this study, possibly leading to decreased electrostatic attraction and increased repulsive forces between negatively charged surface sites and DOM in solution, leading to lower values of adsorbed carbon. Due to this decrease in electrostatic attraction or increase in electrostatic repulsion, sorption at higher pHs is primarily due to hydrophobic interactions (Chen et al., 2017). Another influential mechanism may be increased H-bonding. It has been shown that fulvic acid has a greater affinity for kaolinite than polycyclic aromatic compounds due to weak H-bonding at aluminol/ silanol sites on doubly coordinated oxygens at the basal planes of the clay (Fleury et al., 2017). Thus, H-bonding and hydrophobic interactions may be the dominant forms of binding affiliated with organic matter-clay interactions in this study.

The decrease in aromaticity seen in Chester Creek and Lake Superior's filtrate based on A_{254} (Figure 6) and $SUVA_{254}$ (Figure 7) suggests that Kaol preferentially uptakes aromatic species on its surface, as seen previously (Balcke et al., 2002). On the other hand, preferential uptake of aliphatic species onto Kaol from FA and HA solutions at

concentrations <20mg C/L has also been seen (Zhang et al., 2012). It is expected that aliphatic compounds that contain carboxylic functional groups such as fatty acids would form strong chemical bonds through cation-bridging and ligand exchange reactions facilitating their uptake onto mineral surfaces (Shen, 1999; Arnason and Keil, 2000). Based on the FTIR (Figure 4b) Lake Superior's DOM contains a strong aliphatic component which agrees with previous studies (Minor and Stephens, 2008). However, as previously stated, the adsorption of OM onto mineral surfaces decreases with increasing pH due to increased electrostatic repulsion. Short and medium chain fatty acids would be deprotonated leading to a decrease in their adsorption. Phenolic species that generally have higher pKa values may still undergo ligand exchange and bind to Kaol's surface, which possibly explains the increased uptake of aromatics. It is also possible that multi substituted aromatics that contain alcohol and carboxylic acid groups may utilize both functionalities for adsorption. Thus, it is possible that the more highly oxidized species may be preferentially adsorbed through ligand exchange and H-bonding (Avneri-Katz et al., 2017).

Chester Creek and Lake Superior had initial E2/E3 ratios of 6.15 ± 0.04 and 10.24 ± 0.17 respectively (Figure 8). The initial E2/E3 values agree with the expectation that in general, tributary streams contain larger molecular weight species than in lake DOM (Minor and Stephens, 2008). In terms of size fractionation, no significant changes were observed in Chester Creek filtrate based on any of the observed parameters. However, the E_2/E_3 (Figure 8) and $S_{250\text{-}400}$ (Figure 9) for the control and filtrates from Chester Creek decreased significantly. This may be due to DOM's tendency to aggregate, which would increase the apparent MW of the DOM. DOM has been observed to assemble into microgels, with particle size dependent on the amount of available free polymers (Chin et

al., 1998). Thus, the increased concentration of DOM in Chester Creek would increase the likelihood of assembly and its size leading to possible loss. On the other hand, clays in the presence of Lake Superior DOM appear to inhibit this aggregation. This may be explained by the ratio of DOC to adsorbent in each sample. In Chester Creek and Lake Superior the ratios are 0.38 and 0.07 respectively. Thus, Chester Creek has more DOM available for aggregation than Lake Superior because more of the Lake Superior sample would be bound to the clay and less likely to aggregate.

In the Lake Superior sample there were no significant changes in E2/E3 (Figure 8), but the $S_{250\text{-}400}$ (Figure 9) increased suggesting a decrease in MW of the filtrate which means Kaol adsorbed higher MW species on its surface. This agrees with the results of Hur and Schlautman (2004) who observed a pH dependence on the size fractionation of purified aldrich humic acids onto Kaol, reporting that at pH 7-9 components with MW >3000 showed a greater adsorption affinity for Kaol than the lower molecular weight fraction suggesting increased hydrophobic interactions. With the pH for Chester Creek and Lake Superior in this study being 7.81 and 7.66 respectively, it may be expected that this pattern repeats itself in this study. However, the S_R (Figure 10) decreased suggesting that the molecular weight of the filtrate increased meaning that smaller molecular weight material was adsorbed onto Kaol's surface. Wagner et al. (2015) found that S_R was strongly correlated with microbial and protein like components. If this parameter also tracks microbial OM, primarily long chain aliphatic species, the difference displayed here may be indicative of shifts in factors other than molecular weight. The ambiguity in these results may be further elucidated in future studies through procedures such as size exclusion chromatography (SEC).

4.3 Montmorillonite

DOC analysis showed that MMT did not significantly change the amount of DOC present in the filtrate (Figure 5). Similar to Kaol, EA analysis did show that there was measurable C adsorbed to MMT at the TSS concentration used in this study (Table 2). No significant difference was observed for the adsorption of C onto MMT in Chester Creek or Lake Superior, suggesting that MMT adsorbed similar amounts of C on a per mass basis (Table 2). As stated previously, there was not a significant difference between the amount of C adsorbed on Kaol vs MMT in Chester Creek and Lake Superior. It was initially expected that MMT would adsorb more OM than Kaol as seen when comparing smectite to kaolinite in other studies (Zhang et al., 2012; Mahamat Ahmat et al., 2016; Singh et al., 2016) due to MMT's higher CEC and large surface area. The discrepancies seen in this study may be due to particle size and surface area. Kaolinite's particles are smaller than MMT (Supplementary information Fig. S-11 and S-9) and appear to aggregate as platelets as observed using SEM. Conversely, MMT particles appeared to form spherical aggregates which would decrease surface area exposed to OM (Table 2). The adsorption mechanisms for MMT are similar to those previously discussed for Kaol. Environmental factors such as pH and ions present would affect MMT similarly. MMT is negatively charged at the environmental pHs used in this study, decreasing interactions with negatively charged DOM.

Similar to Kaol, based on A_{254} (Figure 6) and $SUVA_{254}$ (Figure 7) the presence of MMT decreases the aromaticity of the Chester Creek and Lake Superior filtrates, which means that there should be increased uptake of aromatic species on MMT. This agrees with studies that have shown preferential uptake of aromatic species by MMT (Wattel-

Koekkoek et al., 2001; Young et al., 2018). Discrepancies between Kaol and MMT may be due to differences in the cation exchange capacity (CEC) of MMT and Kaol. MMT has a higher CEC than Kaol (Kleber et al., 2015) and based on the FTIR of freeze-dried aliquots of each sample (Figure 2) it appears that there is less calcite present in the Chester Creek sample relative to OM. The presence of Ca^{2+} may increase the likelihood of cation bridging (Majzik and Tomba, 2007) with reports of it accounting for as much as 41% of sorption (Feng et al., 2005). This is explained through preferential ion exchange of Ca^{2+} and complexation of HA through Ca bridges on the faces and directly on Al-OH sites. Less Ca^{2+} would decrease the contribution of cation bridging onto MMT more than it would to Kaol leading to the discrepancy observed in this study. This agrees with studies (Feng et al., 2005; Zhang et al., 2012) that have reported MMT adsorption has a greater dependence on surface exchangeable cations and ionic strength than Kaol. Determining the role that each binding mechanism plays is beyond the scope of this work and will require future studies.

This discrepancy could also be due to the OM present in each sample. Smectite in the presence of FA and HA solutions separately, lead to a decrease of $SUVA_{254}$ at lower concentration (<20mg C/L) for FA, while HA increased over the same range (Zhang et al., 2012). Similarly, C18 extracted Lake Superior DOM showed a decrease in $SUVA_{254}$ as well while the trend varied for tributary stream extracts (Kruger et al., 2011) when compared to initial sterile-filtered DOM. This was attributed to differences in source material for each stream which suggests that although tributary streams may be expected to act similarly, the source of their DOM can significantly change their reactivity in terms of sorption.

As for preference in molecular weight, the E2/E3 and spectral slope ratios do not show significant changes. The $S_{250-400}$, on average, decreased, similarly to Kaol suggesting an overall decrease in the MW of Lake Superior's filtrate, which means higher molecular weight species were adsorbed onto MMT. This result was seen in other studies (Arnason and Keil, 2000; Zhang et al., 2012). This trend is usually affiliated with increased hydrophobic interactions. The effect of pH on adsorption was previously discussed and strengthens the argument that hydrophobic interactions increased the adsorption of larger species onto MMT. It should be noted that although MMT's S_R was not significantly different than the control it appears to be decreasing similarly to Kaol, which would contradict the results of the spectral slope, but this could be due to S_R tracking changes in a specific fractions (microbial as opposed to the all OM present) of DOM (Wagner et al., 2015). In contrast to the inconsistencies seen in this study, Kruger et al (2011) observed a consistent decrease in the E2/E3 ratios in C18 extracted OM of Lake Superior open water and tributary stream samples as compared to initial sterile-filtered water samples. The study used a neutral sorbent and lower pH, which leads to more favourable interactions between the DOM and sorbent making the changes observed in the Kruger et al. (2011) study more pronounced than those seen here.

4.4 HDPE

Similarly to the clays in this study, there were no significant changes in DOC filtrate concentration in the presence of HDPE (Figure 5). There is an increase in the amount of DOC observed in the Lake Superior filtrate, which may be due to the leaching of DOC from PE into the water which has been observed for HDPE and several other plastics in artificial seawater (Romera-castillo et al., 2018). Thus, it is likely that the same phenomena

occurred with the plastic in this study. This occurrence should be further studied and quantified for natural freshwaters such as those from Lake Superior.

Elemental analysis of HDPE was inconclusive, and results are not shown. This study was unable to establish a clear baseline for C initially present in HDPE versus the amount adsorbed after the experiment due to the abundance of C originally in the plastic. HDPE had no significant effect on aromaticity or molecular weight based on the optical parameters used in this study. Because HDPE cannot undergo stronger interactions with the DOM such as ligand exchange or cation bridging it must rely on weaker sorption mechanisms, such as hydrophobic interactions. The adsorption of aromatic species onto PE has been documented and is expected to be controlled by hydrophobic interactions (Kiso et al., 1999). The lack of influence of HDPE on the parameters in this study may be due to the roles that crystallinity plays in overall sorption. Increased crystallinity hinders the diffusivity of species into the plastic when compared to more amorphous plastics, thus leading to decreased uptake of OM (Fries and Zarfl, 2012). This also suggests that the decreased uptake of OM by HDPE in this study may be fueled by the need of a longer equilibration time. Studies have reported organic species finding equilibrium in a time span ranging from 24 hours to greater than 20 days (Karapanagioti, 2007; Bakir et al., 2014; Romera-castillo et al., 2018). Thus, the results of this study may change if given a longer time frame or with varying crystallinity.

Chapter 5. Conclusions

This study has demonstrated using batch adsorption experiments that clays have the ability to affect the dissolved organic matter chemistry of aquatic bodies within the Lake

Superior watershed. The clays used in this study were able to sequester C while the polyethylene microspheres did not show measurable C adsorption in either experiment. UV-VIS analysis of optical properties (A_{254}, $SUVA_{254}$, E2/E3, $S_{250-400}$, S_R) allowed for qualitative changes in the bulk properties of DOM to be observed. The consistent decrease in A_{254} and $SUVA_{254}$ suggests that clays preferentially uptake aromatics in Lake Superior. Chester Creek showed uptake of aromatics based on A_{254}, but no significant changes were seen in $SUVA_{254}$. On the other hand, the molecular weight proxies did not provide a clear answer as to whether there was a preference for sorption of high or low molecular weight material. Polyethylene microspheres had no significant effect on any optical parameter used in this study.

PPL extracts of Chester Creek and Lake Superior water looked similar via FTIR, differing mainly in the ratio of n-alkene and n-alkane (C-H) signals relative to C=O. Because of the similarity in the extracts' FTIR spectra, which functional groups play an important role in adsorption needs to be further studied. Future studies may examine ultrafiltration retentate in conjunction with PPL extracts to obtain a more complete picture of what species are present and contribute to adsorption. These studies may also apply additional characterization techniques (such as high-resolution mass spectrometry) to further investigate dissolved organic matter composition and its effects on sorption.

Future studies could also focus on natural particles isolated from the Lake Superior watershed to gain better insight into how these particles affect the chemistry of the surrounding aquatic bodies. Likewise, more plastics should be tested as chemical reactivity in the environment will vary depending on the type of plastic used, whether the plastics have biofilms present, and whether the plastics have been oxidized.

Works Cited

Abdulla, H.A.N., Minor, E.C., Dias, R.F., Hatcher, P.G., 2010. Changes in the compound classes of dissolved organic matter along an estuarine transect: A study using FTIR and 13C NMR. Geochimica et Cosmochimica Acta 74, 3815–3838.

Al-Khudhairy, D.H.A., Bettendroffer, A., Cardoso, A.C., Pereira, A., Premazzi, G., 2001. Lakes and society: The contribution of lakes to sustainable societies. Lakes and Reservoirs: Research and Management 6, 95–101.

Amy, G., 2008. Fundamental understanding of organic matter fouling of membranes. Desalination 231, 44–51.

Anderson, P.J., Warrack, S., Langen, V., Challis, J.K., Hanson, M.L., Rennie, M.D., 2017. Microplastic contamination in Lake Winnipeg, Canada. Environmental Pollution 225, 223–231.

Andrady, A.L., 2011. Microplastics in the marine environment. Marine Pollution Bulletin 62, 1596–1605.

Armanious, A., Aeppli, M., Sander, M., 2014. Dissolved organic matter adsorption to model surfaces: Adlayer formation, properties, and dynamics at the nanoscale. Environmental Science and Technology 48, 9420–9429.

Arnason, T.S., Keil, R.G., 2000. Adsorption of marine pore water organic matter to montmorillonite. Marine Chemistry 71, 309–320.

Artz, R.R.E., Chapman, S.J., Jacqueline, M., Comont, L., Francez, A., 2008. FTIR spectroscopy can predict organic matter quality in regenerating cutover peatlands. Soil Biology and Biochemistry 40, 515–527.

Austin, J., Anderson, S., Courant, P., Litan, R., 2007. Healthy waters, strong economy: The Benefits of Restoring the Great Lakes Ecosystem. Metropolitian Policy Program, The Brooking Institute 1–16.

Avneri-Katz, S., Young, R.B., McKenna, A.M., Chen, H., Corilo, Y.E., Polubesova, T., Borch, T., Chefetz, B., 2017. Adsorptive fractionation of dissolved organic matter (DOM) by mineral soil: Macroscale approach and molecular insight. Organic Geochemistry 103, 113–124.

Baglieri, A., Ioppolo, A., Negre, M., Gennari, M., 2007. A method for isolating soil organic matter after the extraction of humic and fulvic acids. Organic Geochemistry 38, 140–150.

Bakir, A., Rowland, S.J., Thompson, R.C., Circus, D., Circus, D., 2014. Transport of persistent organic pollutants by microplastics in estuarine conditions. Estuarine, Coastal and Shelf Science 140, 1–44.

Balcke, G.U., Kulikova, N.A., Hesse, S., Kopinke, F., Perminova, I. V, 2002. Adsorption of Humic Substances onto Kaolin Clay Related to Their Structural Features. doi:10.2136/sssaj2002.1805

Baldwin, A.K., Corsi, S.R., Mason, S.A., 2016. Plastic Debris in 29 Great Lakes Tributaries: Relations to Watershed Attributes and Hydrology. Environmental Science and Technology 50, 10377–10385.

Ban, N., Schmidli, J., Schär, C., 2015. Heavy precipitation in a changing climate: Does short-term summer precipitation increase faster? Geophysical Research Letters 42, 1165–1172.

Birkeland, P.W., 1984. Soils and geomorphology. Oxford University Press.

Brezonik, P.L., Arnold, W.A., 2011. Water Chemistry: An Introduction to the Chemistry

of Natural and Engineered Aquatic Systems. Oxford University Press, New York.
Carlson, C., del Giorgio, P., Herndl, G., 2007. Microbes and the Dissipation of Energy and Respiration: From Cells to Ecosystems. Oceanography 20, 89–100.
Carpenter, E.J., Smith, K.L., 1972. Plastics on the Sargasso Sea Surface. Science 175, 1240–1241.
Carpenter, S.R., Caracao, N.F., Correll, D.L., Howarth, R.W., Sharpley, A.N., Smith, V.H., 1998. NONPOINT POLLUTION OF SURFACE WATERS WITH PHOSPHORUS AND NITROGEN. Ecological Applications 8, 559–568.
Chabauty, F., Pot, V., Bourdat-deschamps, M., Bernet, N., Labat, C., Benoit, P., 2016. Transport of organic contaminants in subsoil horizons and effects of dissolved organic matter related to organic waste recycling practices. Environmental Science and Pollution Research 23, 6907–6918.
Chen, H., Koopal, L.K., Xiong, J., Avena, M., Tan, W., 2017. Mechanisms of soil humic acid adsorption onto montmorillonite and kaolinite. Journal of Colloid and Interface Science 504, 457–467.
Chen, W., Ouyang, Z.-Y., Qian, C., Yu, H.-Q., 2018. Induced structural changes of humic acid by exposure of polystyrene microplastics: A spectroscopic insight. Environmental Pollution 233, 1–7.
Chin, W.C., Orellana, M. V., Verdugo, P., 1998. Spontaneous assembly of marine dissolved organic matter into polymer gels. Nature 391, 568–572.
Chorover, J., Amistadi, M.K., 2001. Reaction of forest floor organic matter at goethite, birnessite and smectite surfaces. Geochimica et Cosmochimica Acta 65, 95–109.
Clifford, D.J., Carson, D.M., McKinney, D.E., Bortiatynski, J.M., Hatcher, P.G., 1995. A new rapid technique for the characterization of lignin in vascular plants: thermochemolysis with tetramethylammonium hydroxide (TMAH). Organic Geochemistry 23, 169–175.
Day, G., Hart, B.T., McKelvie, I.D., Beckett, R., 1994. Adsorption of natural organic matter onto goethite. Colloids and Surfaces A: Physicochemical and Engineering Aspects 89, 1–13.
Del Vecchio, R., Blough, N. V, 2002. Photobleaching of chromophoric dissolved organic matter in natural waters: kinetics and modeling. Marine Chemistry 78, 231–253.
Diamond, S., 1956. Surface Areas of Clay Minerals as Derived from Measurements of Glycerol Retention. Clays and Clay Minerals 5, 334–347.
Diko, M., Ekosse, G., Ogola, J., 2016. Fourier transform infrared spectroscopy and thermal analyses of kaolinitic clays from South africa and Cameroon. Acta Geodynamica et Geomaterialia 13, 149–158.
Dittmar, T., Koch, B., Hertkorn, N., Kattner, G., 2008. A simple and efficient method for the solid-phase extraction of dissolved organic matter (SPE-DOM) from seawater. Limnology Oceanography Methods 230–235.
Driedger, A.G.J., Dürr, H.H., Mitchell, K., Cappellen, P. Van, 2015. Plastic debris in the Laurentian Great Lakes : A review. Journal of Great Lakes Research 41, 9–19.
Eerkes-Medrano, D., Thompson, R.C., Aldridge, D.C., 2015. Microplastics in freshwater systems: A review of the emerging threats, identification of knowledge gaps and prioritisation of research needs. Water Research 75, 63–82.
Endo, S., Koelmans, A.A., 2010. Sorption of Hydrophobic Organic Compounds to Plastics in the Marine Environment: Equilibrium, in: Hazardous Chemicals Associated with

Plastics in the Marine Environment. Springer, Cham, pp. 41–53.
EPA, n.d. Great Lakes Facts and Figures [WWW Document]. URL https://www.epa.gov/greatlakes/great-lakes-facts-and-figures (accessed 3.28.18).
Eriksen, M., Lebreton, L.C.M., Carson, H.S., Thiel, M., Moore, C.J., Borerro, J.C., Galgani, F., Ryan, P.G., Reisser, J., 2014. Plastic Pollution in the World's Oceans: More than 5 Trillion Plastic Pieces Weighing over 250,000 Tons Afloat at Sea. PLoS ONE 9, 1–15.
Eriksen, M., Mason, S., Wilson, S., Box, C., Zellers, A., Edwards, W., Farley, H., Amato, S., 2013. Microplastic pollution in the surface waters of the Laurentian Great Lakes. Marine Pollution Bulletin 77, 177–182.
Eriksen, M., Thiel, M., Prindiville, M., Kiessling, T., 2017. Microplastic : What Are the Solutions ?, in: Freshwater Microplastics. pp. 273–298.
Feng, X., Simpson, A.J., Simpson, M.J., 2005. Chemical and mineralogical controls on humic acid sorption to clay mineral surfaces. Organic Geochemistry 36, 1553–1566.
Fischer, E.M., Knutti, R., 2016. Observed heavy precipitation increase confirms theory and early models. Nature Climate Change 6, 986–991.
Fleury, G., Del Nero, M., Barillon, R., 2017. Effect of mineral surface properties (alumina, kaolinite) on the sorptive fractionation mechanisms of soil fulvic acids: Molecular-scale ESI-MS studies. Geochimica et Cosmochimica Acta 196, 1–17.
Fries, E., Zarfl, C., 2012. Sorption of polycyclic aromatic hydrocarbons (PAHs) to low and high density polyethylene (PE). Environmental Science and Pollution Research 19, 1296–1304.
Gao, J., Jansen, B., Cerli, C., Helmus, R., Mikutta, R., Dultz, S., Guggenberger, G., Vogel, C., Kalbitz, K., 2018. Organic matter coatings of soil minerals affect adsorptive interactions with phenolic and amino acids. European Journal of Soil Science 613–624.
Garn, H.S., Elder, J.F., Robertson, D.M., 2003. Why Study Lakes?: An Overview of USGS Lake Studies in Wisconsin.
Gewert, B., Plassmann, M.M., MacLeod, M., 2015. Pathways for degradation of plastic polymers floating in the marine environment. Environ. Sci.: Processes Impacts 17, 1513–1521.
Guan, M., Sillanpää, N., Koivusalo, H., 2016. Storm runoff response to rainfall pattern, magnitude and urbanization in a developing urban catchment. Hydrological Processes 30, 543–557.
Haan, D., 1987. APPLICABILITY OF LIGHT ABSORBANCE AND FLUORESCENCE AS MEASURES OF CONCENTRATION AND MOLECULAR SIZE OF DISSOLVED ORGANIC CARBON IN HUMIC LAKE TJUKEMEER. Water Research 21, 731–734.
Hayhoe, K., Wuebbles, D.J., Easterling, D.R., Fahey, D.W., Doherty, S., Kossin, J., Sweet, W., Vose, R., Wehner, M., 2018. Chapter 2: Our Changing Climate, Impacts, Risks, and Adaptation in the United States: Fourth National Climate Assessment, Volume II. Washington, DC, USA. doi:10.7930/NCA4.2018.CH2 On
Hedges, J.I., Oades, J.M., 1997. Comparative organic geochemistries of soils and marine sediments. Organic 27, 319–361.
Helms, J.R., Stubbins, A., Ritchie, J.D., Minor, E.C., Kieber, D.J., Mopper, K., 2008. Absorption Spectral Slopes and Slope Ratios As Indicators of Molecular

Weight,Source,and Photobleaching of Chromophoric Dissolved Organic Matter. Limnology And Oceanography 53, 955–969.
Hendrickson, E., Minor, E.C., Schreiner, K., 2018. Microplastic abundance and composition in western Lake Superior as determined via microscopy, Pyr-GC/MS, and FTIR. Environmental Science & Technology 52, 1787–1796.
Herdendorf, C.E., 1982. Large Lakes of the World. Journal of Great Lakes Research 8, 379–412.
Hiemstra, T., Antelo, J., Rotterdam, A.M.D.D. Van, Riemsdijk, W.H. Van, 2010. Nanoparticles in natural systems II : The natural oxide fraction at interaction with natural organic matter and phosphate. Geochimica et Cosmochimica Acta 74, 59–69.
Holland, H.D., Turekian, K.K., 2014. Treatise on geochemistry, Second. ed. Elsevier Ltd, Oxford.
Hong, S.H., Shim, W.J., Jang, M., 2018. Chemicals Associated With Marine Plastic Debris and Microplastics: Analyses and Contaminant Levels. Microplastic Contamination in Aquatic Environments 271–315.
Hunt, J.F., Ohno, T., He, Z., Honeycutt, C.W., Dail, D.B., 2007. Influence of Decomposition on Chemical Properties of Plant- and Manure-Derived Dissolved Organic Matter and Sorption to Goethite. Journal of Environment Quality 36, 135.
Hur, J., Schlautman, M.A., 2003. Molecular weight fractionation of humic substances by adsorption onto minerals. Journal of Colloid and Interface Science 264, 313–321.
Hur, J., Schlautman, M.A., 2004. Effects of pH and phosphate on the adsorptive fractionation of purified Aldrich humic acid on kaolinite and hematite. Journal of Colloid and Interface Science 277, 264–270.
Hyung, H., Kim, J.H., 2008. Natural organic matter (NOM) adsorption to multi-walled carbon nanotubes: Effect of NOM characteristics and water quality parameters. Environmental Science and Technology 42, 4416–4421.
Kaiser, K., 2003. Sorption of natural organic matter fractions to goethite (α-FeOOH): effect of chemical composition as revealed by liquid-state 13C NMR and wet-chemical analysis. Organic Geochemistry 34, 1569–1579.
Kaiser, K., Guggenberger, G., 2000. The role of DOM sorption to mineral surfaces in the preservation of organic matter in soils. Organic Geochemistry 31, 711–725.
Kaiser, K., Guggenberger, G., 2007. Sorptive stabilization of organic matter by microporous goethite : sorption into small pores vs . surface complexation. European Journal of Soil Science 58, 45–59.
Kaiser, K., Kaupenjohann, M., Zech, W., 2001. Sorption of dissolved organic carbon in soils : effects of soil sample storage , soil-to-solution ratio , and temperature. Geoderma 99, 317–328.
Kaiser, K., Zech, W., 2000. Dissolved organic matter sorption by mineral constituents of subsoil clay fractions. Journal of Plant Nutrition and Soil Science 163, 531–535.
Karapanagioti, H.K., 2007. INVESTIGATING THE PROPERTIES OF PLASTIC RESIN PELLETS FOUND IN THE COASTAL AREAS OF LESVOS ISLAND. Global Nest Journal 9, 71–76.
Kiso, Y., Kitao, T., Nishimura, K., 1999. Adsorption properties of aromatic compounds on polyethylene as a membrane material. Journal of Applied Polymer Science 74, 1037–1043.
Kleber, M., Eusterhues, K., Keiluweit, M., Mikutta, C., Mikutta, R., Nico, P.S., 2015.

Mineral-Organic Associations: Formation, Properties, and Relevance in Soil Environments, Advances in Agronomy. Elsevier Ltd. doi:10.1016/bs.agron.2014.10.005

Kleber, M., Sollins, P., Sutton, R., 2007. A conceptual model of organo-mineral interactions in soils: Self-assembly of organic molecular fragments into zonal structures on mineral surfaces. Biogeochemistry 85, 9–24.

Kovac, N., Bajt, O., Faganeli, J., Sket, B., Orel, B., 2002. Study of macroaggregate composition using FT-IR and 1H-NMR spectroscopy. Marine Chemistry 78, 205–215.

Kruger, B.R., Dalzell, B.J., Minor, E.C., 2011. Effect of organic matter source and salinity on dissolved organic matter isolation via ultrafiltration and solid phase extraction. Aquatic Sciences 73, 405–417.

Lakesuperiorstreams, 2009. Community Partnerships For Understanding Water Quality and Stormwater Impacts at the Head of the Great Lakes [WWW Document]. URL http://www.lakesuperiorstreams.org (accessed 2.18.19).

Leenheer, J.A., Croué, J.-P., 2003. Characterizing Aquatic Dissolved Organic Matter. Environmental Science & Technology 37, 18A-26A.

Leenheer, J.A., Noyes, T.I., Rostad, C.E., Davisson, M.L., 2004. Characterization and origin of polar dissolved organic matter from the Great Salt Lake. Biogeochemistry 69, 125–141.

Li, A., Zhao, X., Mao, R., Liu, H., Qu, J., 2014. Characterization of dissolved organic matter from surface waters with low to high dissolved organic carbon and the related disinfection byproduct formation potential. Journal of Hazardous Materials 271, 228–235.

Lin, V.S., 2015. Research highlights: Challenges in the characterization, storage, and isolation of natural organic matter. Environmental Sciences: Processes and Impacts 17, 2002–2005.

Lumsdon, D.G., Fraser, A.R., 2005. Infrared spectroscopic evidence supporting heterogeneous site binding models for humic substances. Environmental Science and Technology 39, 6624–6631.

Macdonald, M.J., Minor, E.C., 2013. Photochemical degradation of dissolved organic matter from streams in the western Lake Superior watershed. Aquatic Sciences 75, 509–522.

Madejova, J., 2003. FTIR techniques in clay mineral studies. Vib Spectrosc. Vibrational Spectroscopy 31, 1–10.

Magee, B.R., Lion, L.W., Lemley, A.T., 1991. Transport of Dissolved Organic Macromolecules and Their Effect on the Transport of Phenanthrene in Porous Media. Environmental Science & Technology 25, 323–331.

Mahamat Ahmat, A., Boussafir, M., Le Milbeau, C., Guegan, R., Valdès, J., Guiñez, M., Sifeddine, A., Le Forestier, L., 2016. Organic matter-clay interaction along a seawater column of the Eastern Pacific upwelling system (Antofagasta bay, Chile): Implications for source rock organic matter preservation. Marine Chemistry 179, 23–33.

Majzik, A., Tomba, E., 2007. Interaction between humic acid and montmorillonite in the presence of calcium ions I . Interfacial and aqueous phase equilibria : Adsorption and complexation. Organic Geochemistry 38, 1319–1329.

Massicotte, P., Asmala, E., Stedmon, C., Markager, S., 2017. Global distribution of dissolved organic matter along the aquatic continuum: Across rivers, lakes and oceans. Science of the Total Environment 609, 180–191.

Meier, M., Namjesnik-dejanovic, K., Maurice, P.A., Chin, Y., Aiken, G.R., 1999. Fractionation of aquatic natural organic mater upon sorption to goethite and kaolinite. Chemical Geology 275–284.

Minnesota DNR, 2019. Climate trends - Minnesota DNR [WWW Document]. URL https://www.dnr.state.mn.us/climate/climate_change_info/climate-trends.html (accessed 5.1.19).

Minnesota Sea Grant, n.d. Lake Superior | Minnesota Sea Grant [WWW Document]. URL http://www.seagrant.umn.edu/superior/ (accessed 2.17.19).

Minor, E., Stephens, B., 2008. Dissolved organic matter characteristics within the Lake Superior watershed. Organic Geochemistry 39, 1489–1501.

Minor, E.C., Forsman, B., Guildford, S.J., 2014a. The effect of a flood pulse on the water column of western Lake Superior, USA. Journal of Great Lakes Research 40, 455–462.

Minor, E.C., Steinbring, C.J., Longnecker, K., Kujawinski, E.B., 2012. Characterization of dissolved organic matter in Lake Superior and its watershed using ultrahigh resolution mass spectrometry. Organic Geochemistry 43, 1–11.

Minor, E.C., Swenson, M.M., Mattson, B.M., Oyler, A.R., 2014b. Structural characterization of dissolved organic matter: a review of current techniques for isolation and analysis. Environ. Sci.: Processes Impacts 16, 2064–2079.

Nguyen, T.T., Marschner, P., 2014. Retention and loss of water extractable carbon in soils: Effect of clay properties. Science of the Total Environment 470–471, 400–406.

O'Beirne, M.D., Werne, J.P., Hecky, R.E., Johnson, T.C., Katsev, S., Reavie, E.D., 2017. Anthropogenic climate change has altered primary productivity in Lake Superior. Nature Communications 8, 15713.

Ohlenbusch, G., Kumke, M.U., U, F.H.F., 2000. Sorption of phenols to dissolved organic matter investigated by solid phase microextraction. The Science of the Total Environment 253, 63–74.

Parolo, M.E., Savini, M.C., Loewy, R.M., 2017. Characterization of soil organic matter by FT-IR spectroscopy and its relationship with chlorpyrifos sorption. Journal of Environmental Management 196, 316–322.

Pennell, K.D., 2016. Specific Surface Area, in: Reference Module in Earth Systems and Environmental Sciences. Elsevier. doi:10.1016/B978-0-12-409548-9.09583-X

Philippe, A., Schaumann, G.E., 2014. Interactions of Dissolved Organic Matter with Natural and Engineered Inorganic Colloids: A Review. Environmental Science & Technology 48, 8946–8962.

Pitois, A., Abrahamsen, L.G., Ivanov, P.I., Bryan, N.D., 2008. Humic acid sorption onto a quartz sand surface: A kinetic study and insight into fractionation. Journal of Colloid and Interface Science 325, 93–100.

Plastics Europe Market Research Group (PEMRG) / Consultic Marketing & Industrieberatung GmbH, 2015. World Plastics Production 1950-2015.

PlasticsEurope, 2017. Plastics – the Facts. doi:10.1016/j.marpolbul.2013.01.015

Romera-castillo, C., Herndl, G.J., Pinto, M., Langer, T.M., Álvarez-salgado, X.A., 2018. Dissolved organic carbon leaching from plastics stimulates microbial activity in the

ocean. Nature Communications 1430. doi:10.1038/s41467-018-03798-5
Shen, Y.-H., 1999. Sorption of natural dissolved organic matter on soil. Chemosphere 38, 1505–1515.
Singh, M., Sarkar, B., Biswas, B., Churchman, J., Bolan, N.S., 2016. Adsorption-desorption behavior of dissolved organic carbon by soil clay fractions of varying mineralogy. Geoderma 280, 47–56.
Sondi, I., Pravdic, V., 1998. The colloid and surface chemistry of clays in natural waters. Croatica Chemica Acta 71, 1061–1074.
Sruthy, S., Ramasamy, E. V., 2017. Microplastic pollution in Vembanad Lake, Kerala, India: The first report of microplastics in lake and estuarine sediments in India. Environmental Pollution 222, 315–322.
Statistics Canada, n.d. Census Profile, 2016 Census - Thunder Bay [Census metropolitan area], Ontario and Ontario [Province] [WWW Document]. URL http://www12.statcan.gc.ca/census-recensement/2016/dp-pd/prof/details/page.cfm?Lang=E&Geo1=CMACA&Code1=595&Geo2=PR&Code2=35&Data=Count&SearchText=THUNDER bAY&SearchType=Begins&SearchPR=01&B1=All&TABID=1 (accessed 3.28.18).
Stephens, B.M., Minor, E.C., 2010. DOM characteristics along the continuum from river to receiving basin: A comparison of freshwater and saline transects. Aquatic Sciences 72, 403–417.
Tombácz, E., Libor, Z., Illés, E., Majzik, A., Klumpp, E., 2004. The role of reactive surface sites and complexation by humic acids in the interaction of clay mineral and iron oxide particles. Organic Geochemistry 35, 257–267.
U.S. Census Bureau, n.d. U.S. Census Bureau QuickFacts: Duluth city, Minnesota [WWW Document]. URL https://www.census.gov/quickfacts/fact/table/duluthcityminnesota/PST045218 (accessed 6.5.19a).
U.S. Census Bureau, n.d. U.S. Census Bureau QuickFacts: Superior city, Wisconsin [WWW Document]. URL https://www.census.gov/quickfacts/superiorcitywisconsin (accessed 6.5.19b).
US Department of Commerce, N.G.L.E.R.L.C.I. for L. and E.R., n.d. About Our Great Lakes : Lake by Lake Profiles.
USGS, n.d. Where is Earth's Water? [WWW Document]. URL https://www.usgs.gov/special-topic/water-science-school/science/where-earths-water?qt-science_center_objects=0#qt-science_center_objects (accessed 7.29.19).
Van, A., Rochman, C.M., Flores, E.M., Hill, K.L., Vargas, E., Vargas, S.A., Hoh, E., 2012. Persistent organic pollutants in plastic marine debris found on beaches in San Diego, California. Chemosphere 86, 258–263.
Villarini, G., Smith, J.A., Baeck, M.L., Vitolo, R., Stephenson, D.B., Krajewski, W.F., 2011. On the frequency of heavy rainfall for the Midwest of the United States. Journal of Hydrology 400, 103–120.
Wagner, S., Jaffé, R., Cawley, K., Dittmar, T., Stubbins, A., 2015. Associations Between the Molecular and Optical Properties of Dissolved Organic Matter in the Florida Everglades, a Model Coastal Wetland System. Frontiers in Chemistry 3, 1–14.
Walling, D.E., Fang, D., 2003. Recent trends in the suspended sediment loads of the world's rivers. Global and Planetary Change 39, 111–126.

Wattel-Koekkoek, E.J.W., Van Genuchten, P.P.L., Buurman, P., Van Lagen, B., 2001. Amount and composition of clay-associated soil organic matter in a range of kaolinitic and smectitic soils. Geoderma 99, 27–49.

Weishaar, J.L., Aiken, G.R., Bergamaschi, B.A., Fram, M.S., Fujii, R., Mopper, K., 2003. Evaluation of specific ultraviolet absorbance as an indicator of the chemical composition and reactivity of dissolved organic carbon. Environmental Science and Technology 37, 4702–4708.

Weng, L., Van, W.H., Hiemstra, T., Quality, S., 2008. Humic Nanoparticles at the Oxide - Water Interface : Interactions with Phosphate Ion Adsorption. Environmental Science & Technology 42, 8747–8752.

Wood, P.J., Armitage, P.D., 1997. Biological Effects of Fine Sediment in the Lotic Environment. Environmental Management 21, 203–217.

Xu, B., Liu, F., Brookes, P.C., Xu, J., 2018. Microplastics play a minor role in tetracycline sorption in the presence of dissolved organic matter. Environmental Pollution 240, 87–94.

Young, R., Avneri-Katz, S., McKenna, A., Chen, H., Bahureksa, W., Polubesova, T., Chefetz, B., Borch, T., 2018. Composition-Dependent Sorptive Fractionation of Anthropogenic Dissolved Organic Matter by Fe(III)-Montmorillonite. Soil Systems 2, 14.

Zhang, H., Wang, J., Zhou, B., Zhou, Y., Dai, Z., Zhou, Q., Chriestie, P., Luo, Y., 2018. Enhanced adsorption of oxytetracycline to weathered microplastic polystyrene: Kinetics, isotherms and influencing factors. Environmental Pollution 243, 1550–1557.

Zhang, L., Luo, L., Zhang, S., 2012. Integrated investigations on the adsorption mechanisms of fulvic and humic acids on three clay minerals. Colloids and Surfaces A: Physicochemical and Engineering Aspects 406, 84–90.

Zigah, P.K., Minor, E.C., Abdulla, H.A.N., Werne, J.P., Hatcher, P.G., 2014. An investigation of size-fractionated organic matter from Lake Superior and a tributary stream using radiocarbon, stable isotopes and NMR. Geochimica et Cosmochimica Acta 127, 264–284.

Supplementary Information

Table S-1. Sample site information

Sample	Date Collected	Location	Water Column Depth (m) of Sample
Chester Creek	November 26, 2018	46°48'59.5"N 92°06'09.2"W	0
Lake Superior	May 8, 2018	46°47.04'N, 91°49.23'W	5

Table S-2. Replicate blank corrected elemental analysis data of particulates from Lake Superior and Chester Creek adsorption studies. The blank values come from elemental analysis, done in triplicate, on the untreated particulates and are included as the third column here. A, B and C represent data from the replicate adsorption studies.

Kaol	Lake Superior	Chester Creek	Blank
	μg C/mg substrate		
A	3.3	3.5	0.4
B	5.4	2.0	0.4
C	4.7	1.7	0.4
MMT			
A	1.0	2.5	0.9
B	2.4	1.3	0.9
C	3.3	1.0	1.0

Table S-3. Optical Parameters

Parameter	Calculation	Proxy	Reference
A_{254} (m^{-1})	Absorption coefficient at 254nm	Correlated to aromaticity	(Weishaar et al., 2003; Minor et al., 2014b)
Specific ultraviolet absorbance [$SUVA_{254}$] (L mg C^{-1} m^{-1})	Absorption coefficient at a given wavelength in the ultraviolet region normalised by DOC concentration		
E_2:E_3	Ratio of absorption coefficients at 250nm:365nm	Inversely correlated to molecular weight (MW); Typically, higher S values indicate low molecular weight material and/or decreasing aromaticity	(Haan, 1987; Hunt et al., 2007; Helms et al., 2008)
Spectral slope [$S_{250-400}$] (nm^{-1})	Fit of absorption coefficients to a non-linear regression		(Del Vecchio and Blough, 2002; Helms et al., 2008; Minor and Stephens, 2008)
Spectral Slope Ratio [S_R]	Spectral slope $S_{275-295}$ divided by spectral slope $S_{350-400}$		(Helms et al., 2008)

Table S-4. Averaged data with standard deviations from filtrate attributes for Chester Creek adsorption study

4 Day Sorption Study Chester Creek and 20 mg MMT, Kaol and HDPE						
Sample	DOC (mg C/L)	a254 (1/m)	SUVA (L/mg C m)	E2/E3	S 250-400 (1/nm)	SR
0	7.69 ± 0.22	45.57 ± 1.38	5.94 ± 0.11	6.15 ± 0.04	0.0143 ± 0.0001	0.75 ± 0.01
MMT	7.49 ± 0.01	44.78 ± 0.27	5.99 ± 0.03	5.84 ± 0.08	0.0141 ± 0.0000	0.80 ± 0.03
Kaol	7.49 ± 0.04	44.56 ± 0.25	5.96 ± 0.06	5.93 ± 0.15	0.0142 ± 0.0001	0.78 ± 0.01
HDPE	7.51 ± 0.06	45.75 ± 0.05	6.11 ± 0.05	5.88 ± 0.03	0.0141 ± 0.0000	0.78 ± 0.01
Control	7.56 ± 0.09	45.73 ± 0.06	6.08 ± 0.03	5.88 ± 0.02	0.0141 ± 0.0000	0.77 ± 0.01

Table S-5. Averaged data values with standard deviations from filtrate from Lake Superior adsorption study

4 Day Sorption Study Lake Superior and 20 mg MMT, Kaol and HDPE						
Sample	DOC (mg C/L)	a254 (1/m)	SUVA (L/mg C m)	E2/E3	S 250-400 (1/nm)	SR
0	1.40 ± 0.02	4.57 ± 0.01	3.25 ± 0.05	10.24 ± 0.17	0.0190 ± 0.0001	1.41 ± 0.05
MMT	1.43 ± 0.02	4.44 ± 0.06	3.11 ± 0.04	10.20 ± 0.22	0.0192 ± 0.0001	1.34 ± 0.02
Kaol	1.42 ± 0.01	4.46 ± 0.06	3.15 ± 0.02	10.48 ± 0.25	0.0192 ± 0.0001	1.27 ± 0.03
HDPE	1.44 ± 0.00	4.56 ± 0.02	3.17 ± 0.01	9.82 ± 0.35	0.0188 ± 0.0001	1.37 ± 0.01
Control	1.40 ± 0.03	4.58 ± 0.02	3.26 ± 0.06	9.78 ± 0.49	0.0189 ± 0.0001	1.38 ± 0.02

Table S-6. Averaged data values with standard deviations from Milli Q water adsorption study used to determine if there was leaching of OC from adsorbates

4 Day Adsorption Study Milli Q Blank	
Sample	**Concentration (mg C/L)**
0 Milli Q	0.14 ± 0.01
MMT	0.14 ± 0.04
Kaol	0.11 ± 0.01
HDPE	0.10 ± 0.02
Control	0.18 ± 0.09

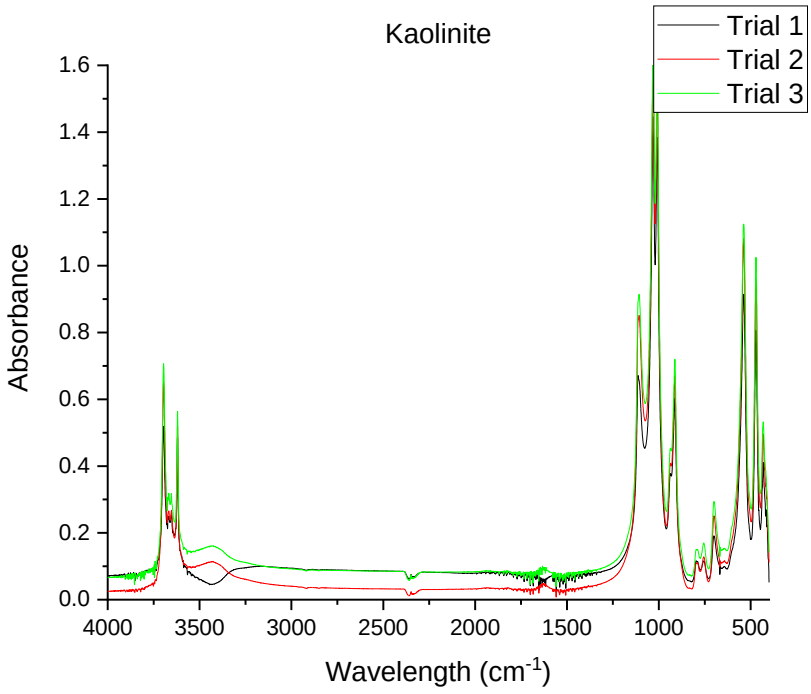

Figure S-1. FTIR (KBr pellet) of kaolinite replicates

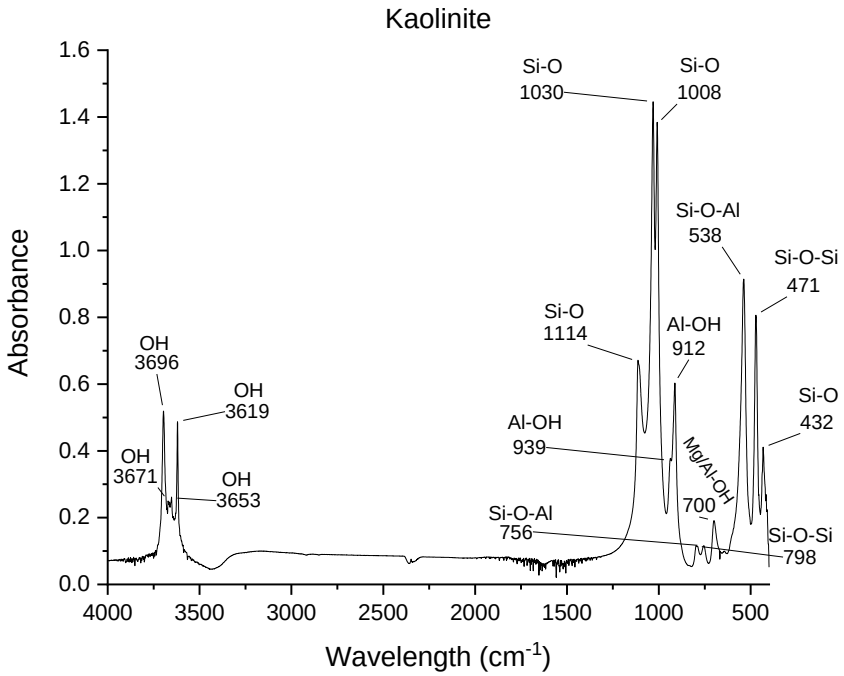

Figure S-2. FTIR (KBr pellet) of kaolinite used in this study

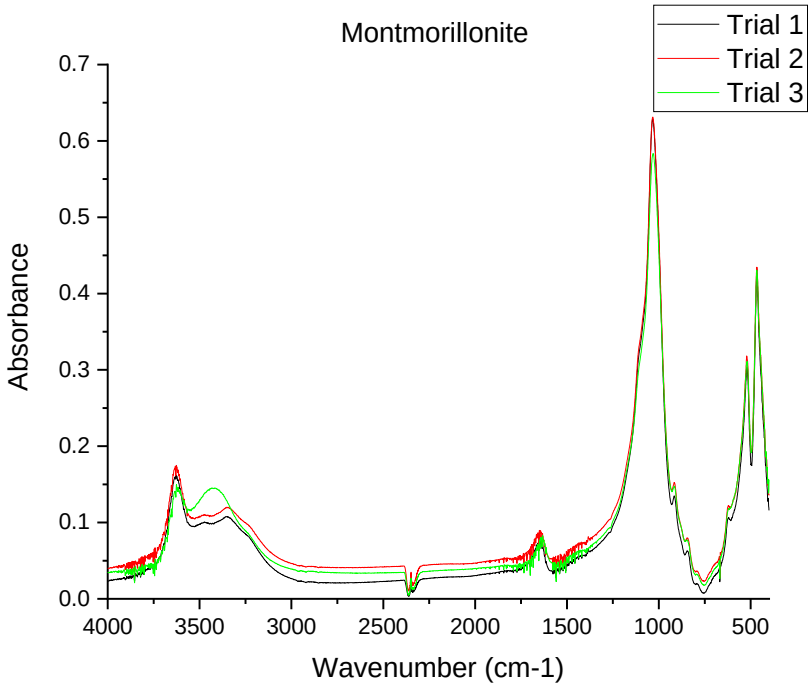

Figure S-3. FTIR (KBr pellet) of montmorillonite replicates

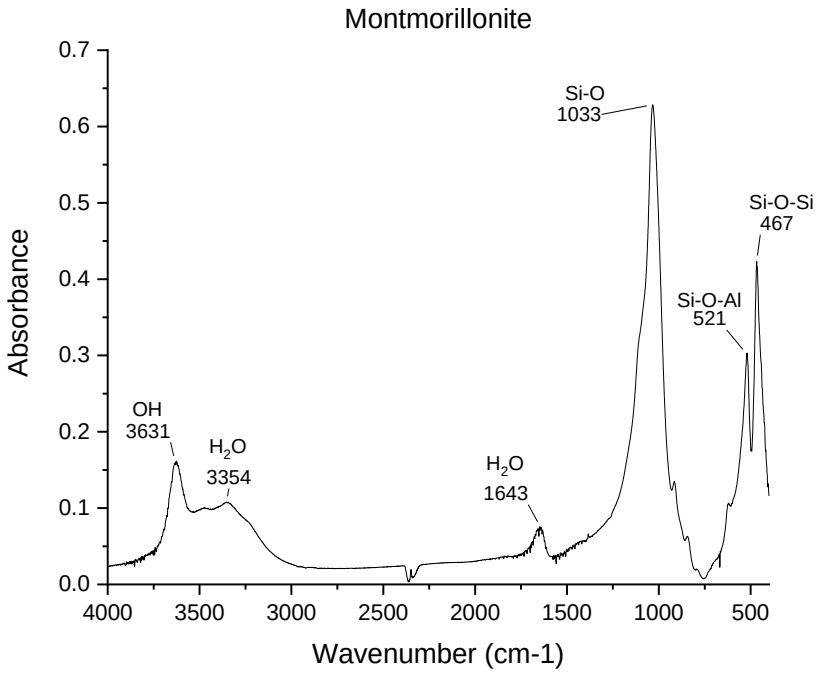

Figure S-4. FTIR (KBr Pellet) of Montmorillonite used in this study

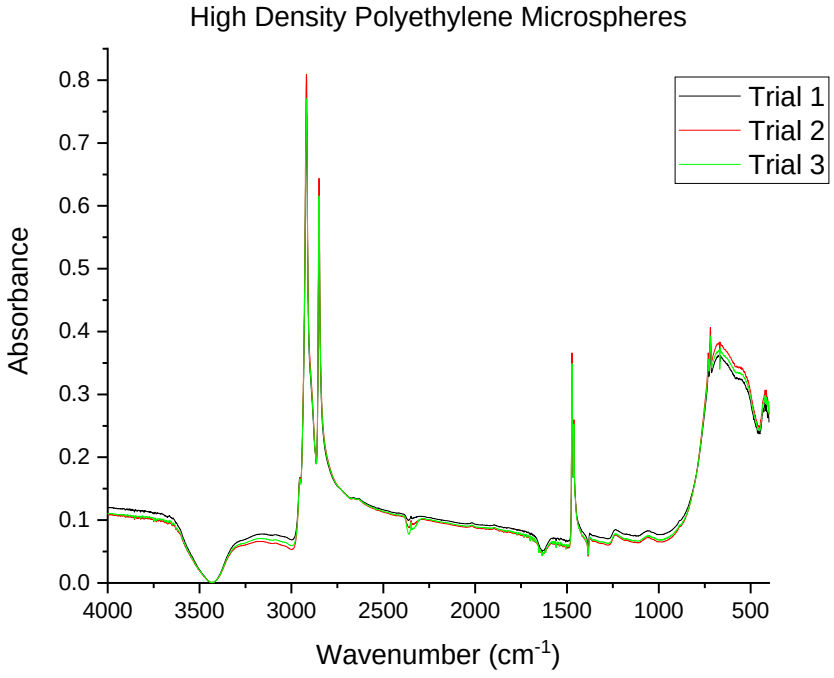

Figure S-5 FTIR (KBr pellet) of high density polyethylene microspheres replicates of this study

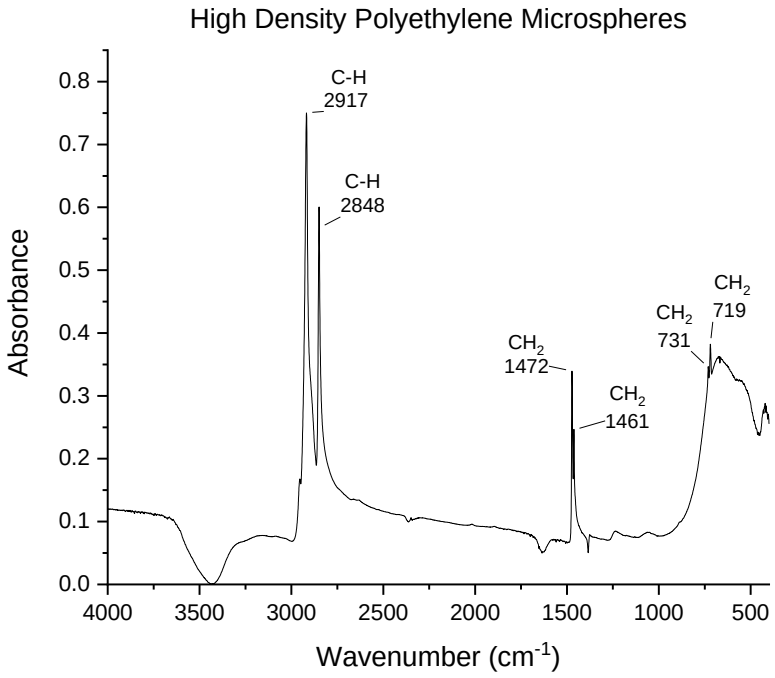

Figure S-6. FTIR (KBr Pellet) of High density polyethylene microspheres used in this study

Table S-6. Table showing diameter measurements of HDPE, MMT and Kaol from SEM imaging

	HDPE	**MMT**	**Kaol**
	Diameter (µm)		
Average	***32.18***	***9.74***	***4.65***
Std Dev	6.29	5.21	4.01
Max	56.80	44.87	33.89
Min	12.00	2.94	0.74
# of Measurements	465	336	403

Table S-7. Table of densities for MMT, Kaol and HDPE provided by the manufacturer

Particle	**Density** (g/cm^3)
MMT	2.35
Kaol	1.80
HDPE	1.25

Surface Area Calculation: $SSA = \frac{A}{\rho V}$

SSA = specific surface area (m^2/g)

A = surface area of particle (m^2)

V = volume of particle (m^3)

ρ = density of the particle (g/m^3)

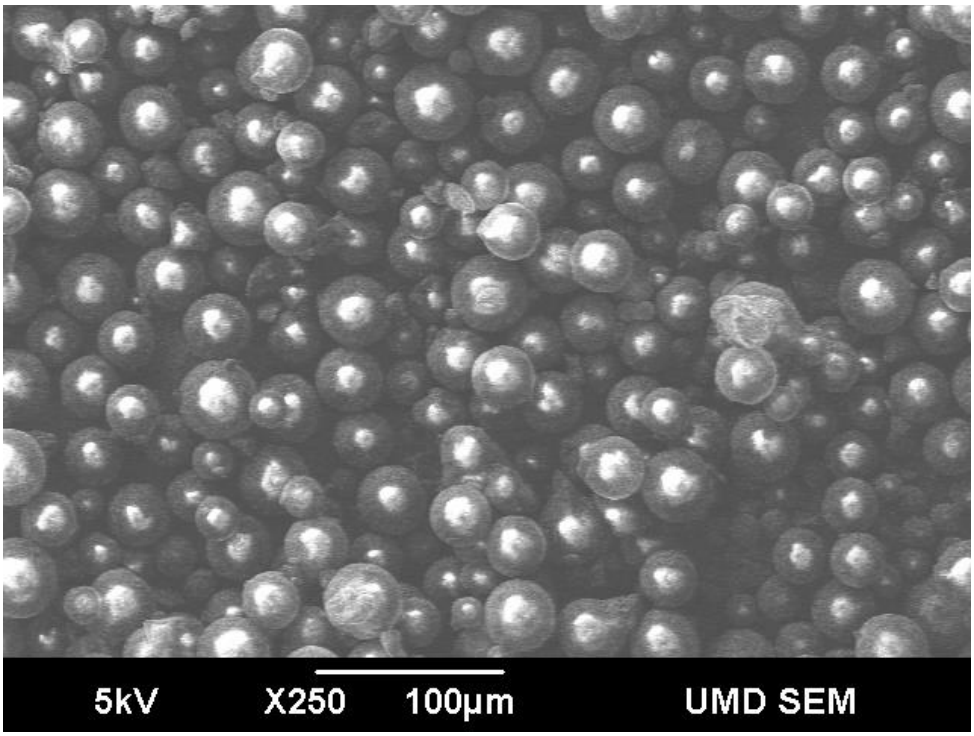

Figure S-7. SEM image of high density polyethylene microspheres

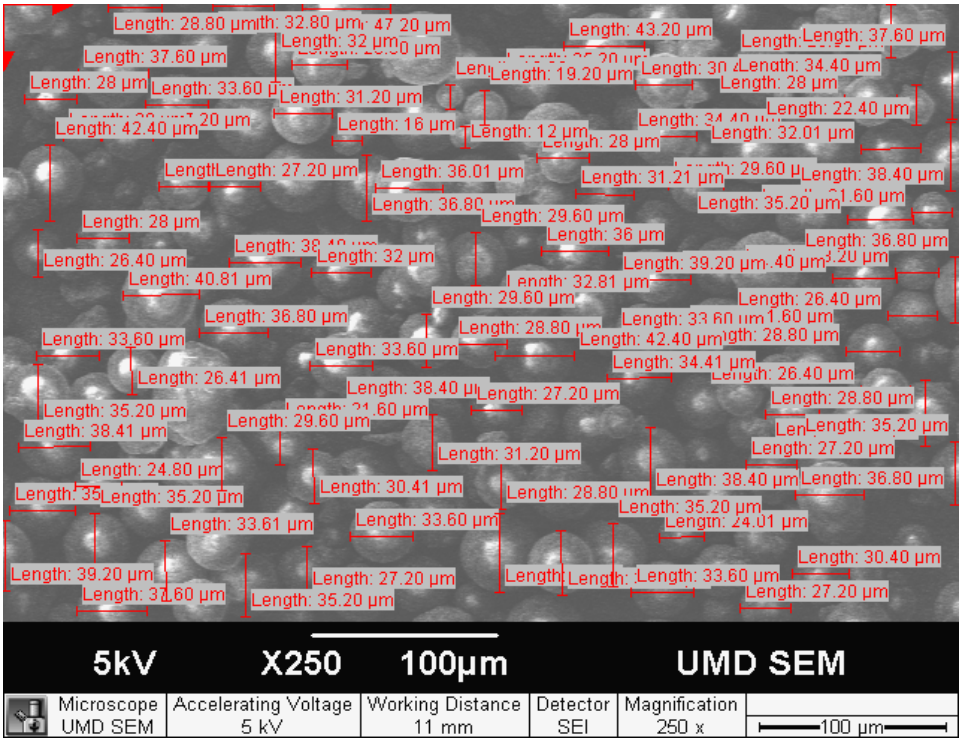

Figure S-8. SEM image of HDPE with Scandium™ measurements overlayed

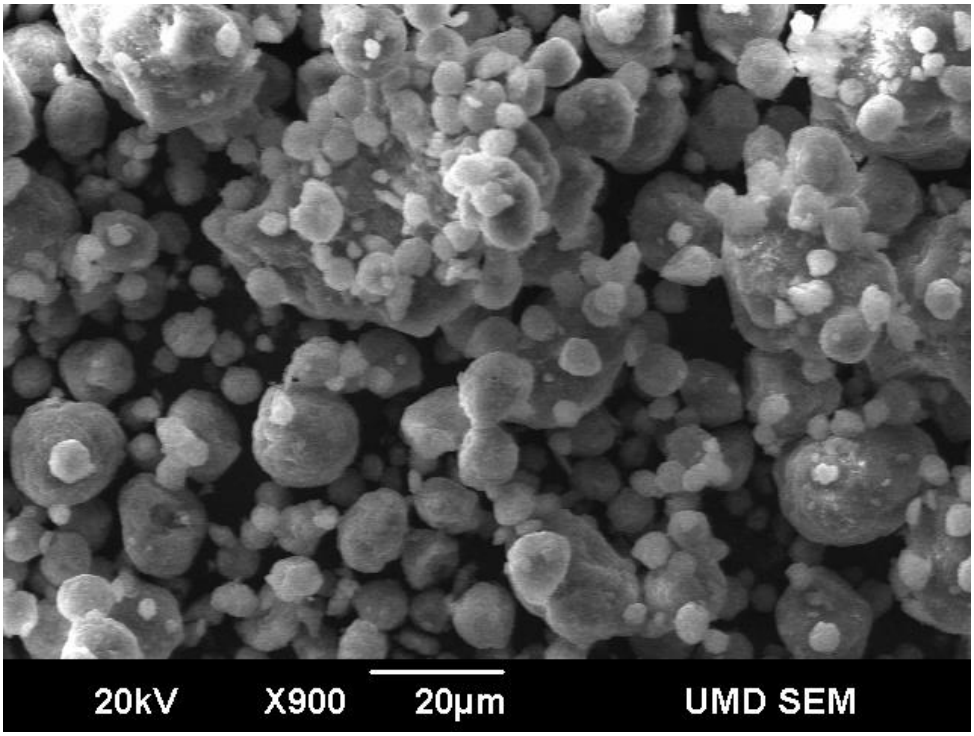

Figure S-9. SEM image of montmorillonite

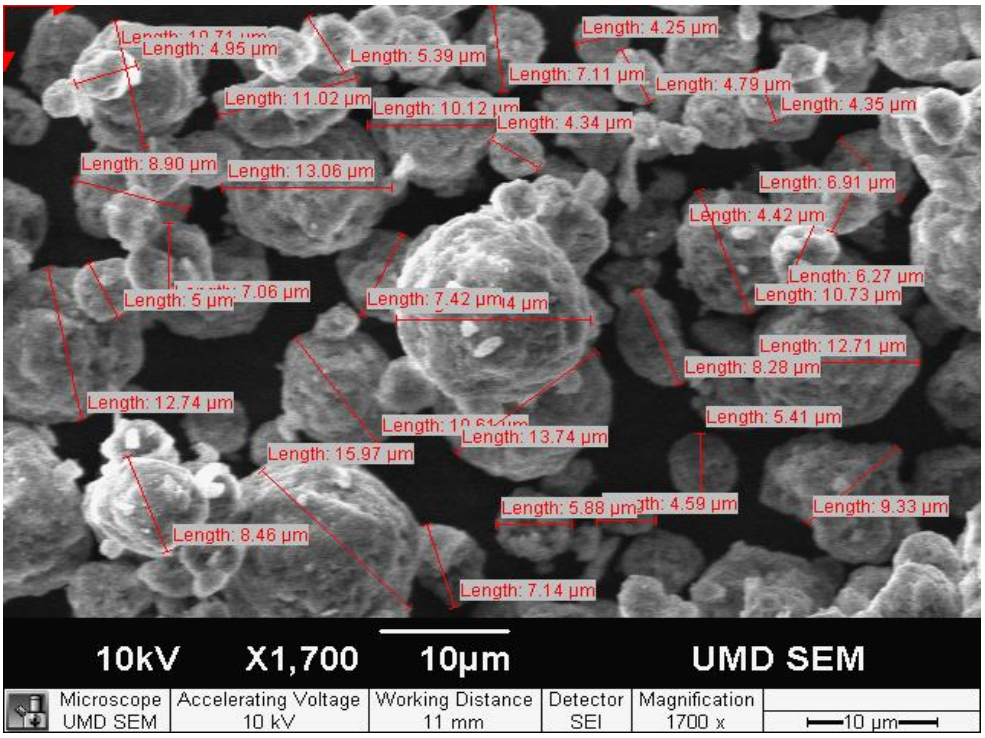

Figure S-10. SEM image of MMT with strontium measurements overlayed

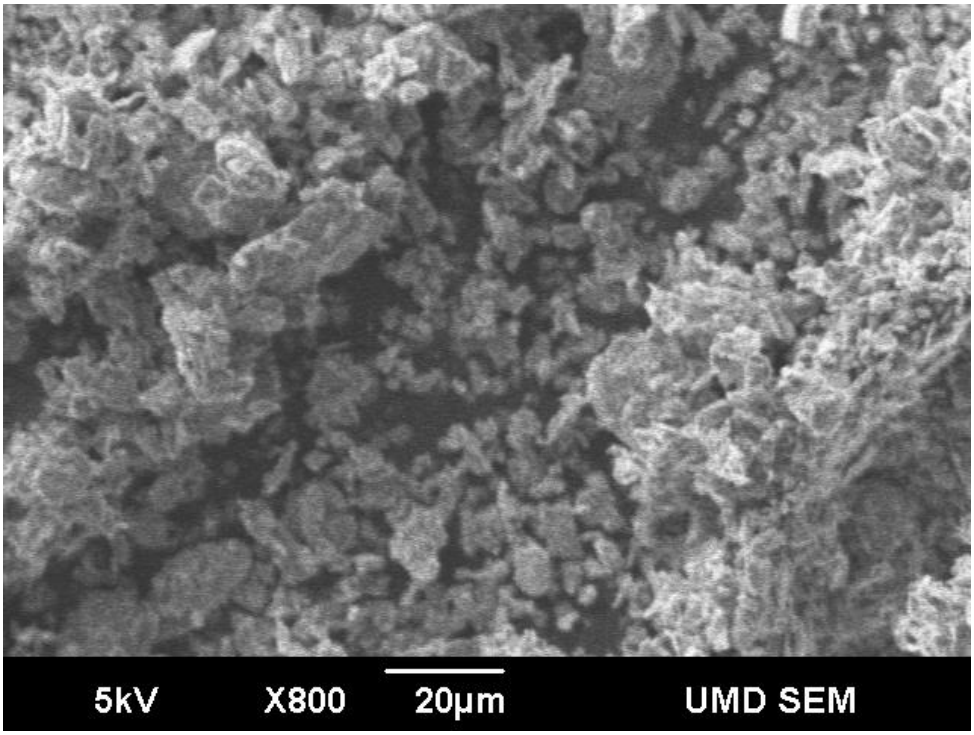

Figure S-11. Sem image of kaolinite

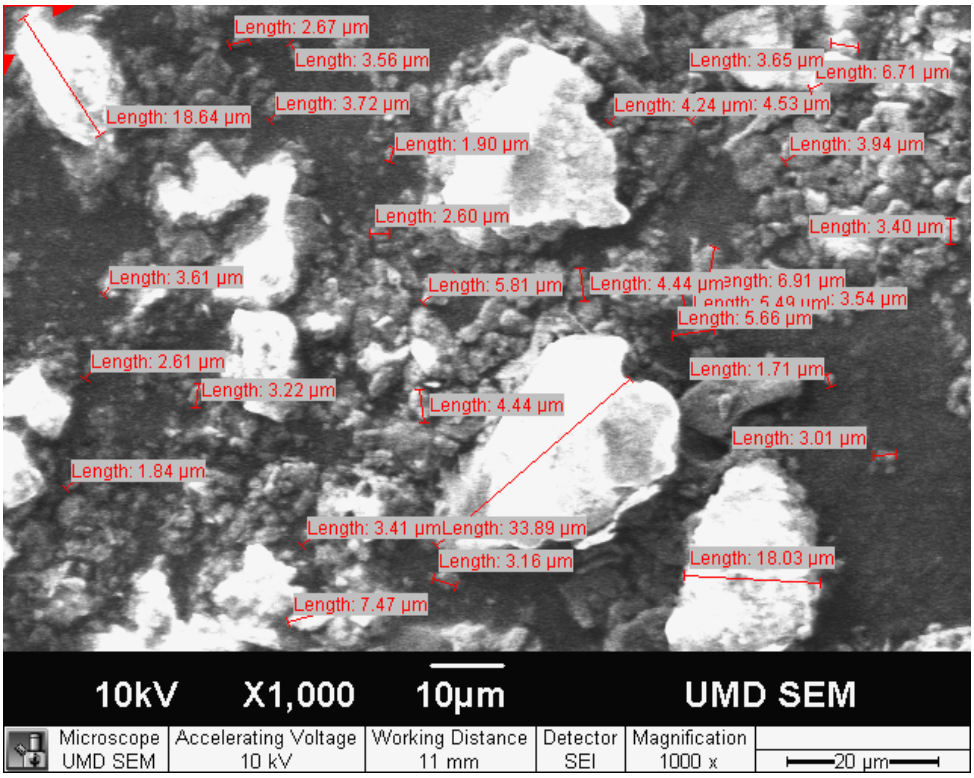

Figure S12. SEM Image of Kaol with strontium measurements overlayed

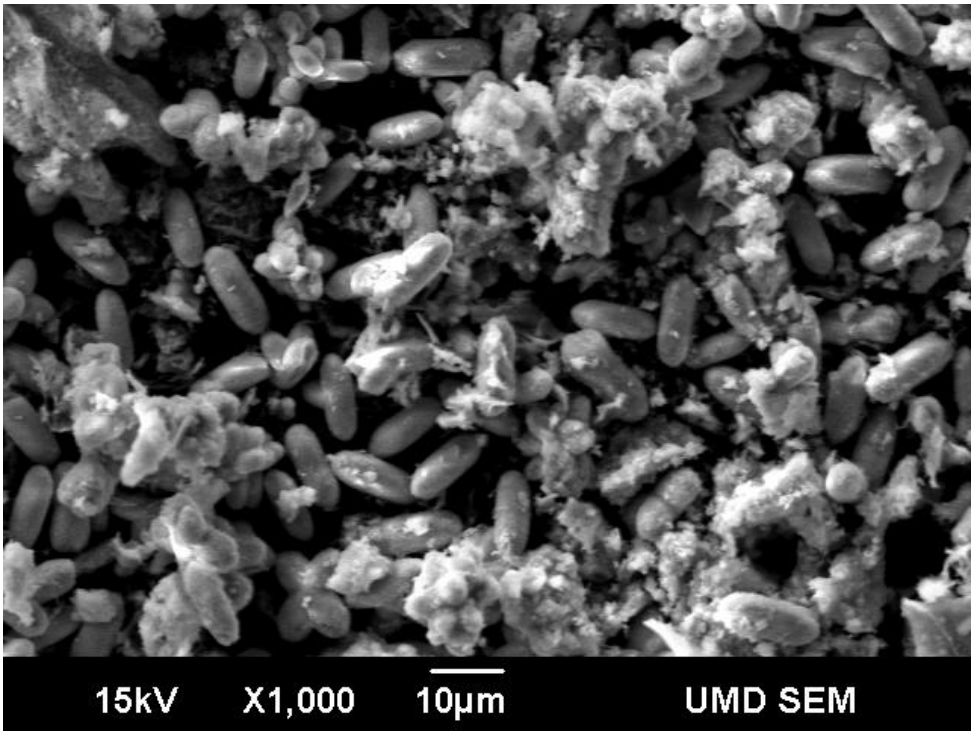

Figure S-13. SEM image of Lake Superior LOI material

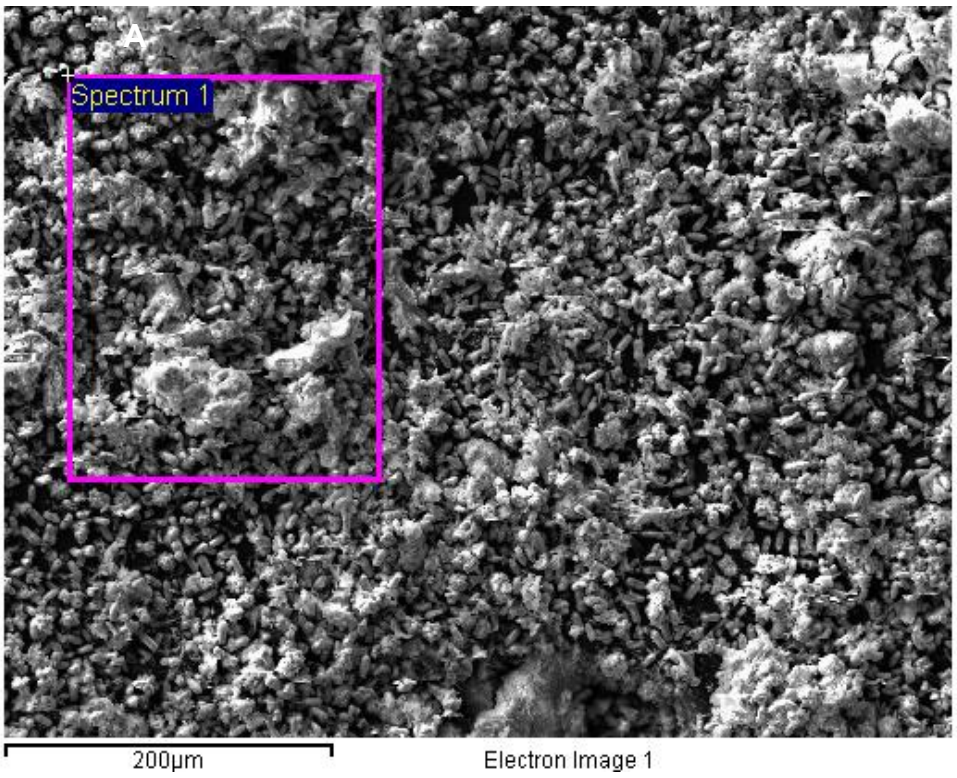

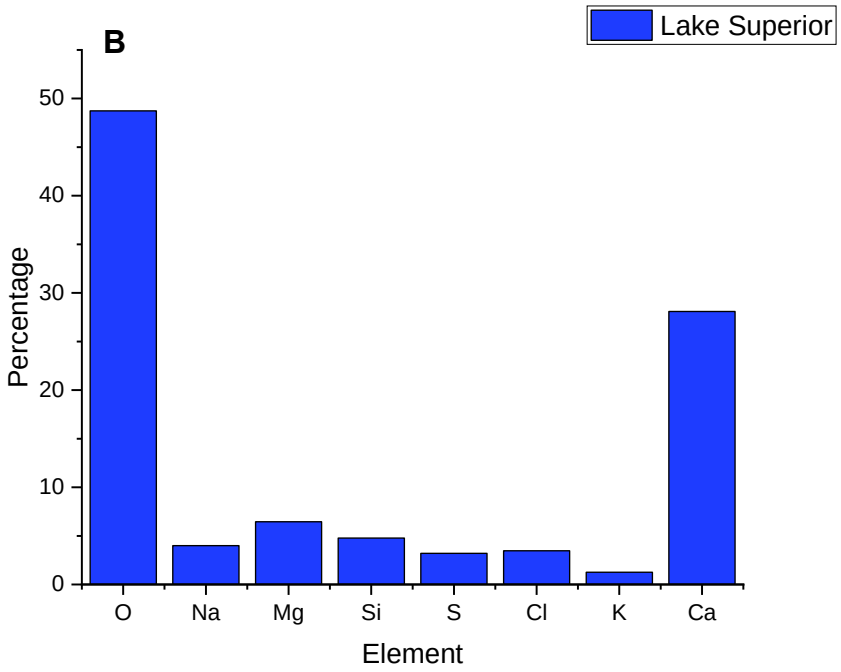

Figure S-14. A) SEM image of Lake Superior LOI sample with area used for EDS shown B) EDS analysis of A showing relative percentage of identified

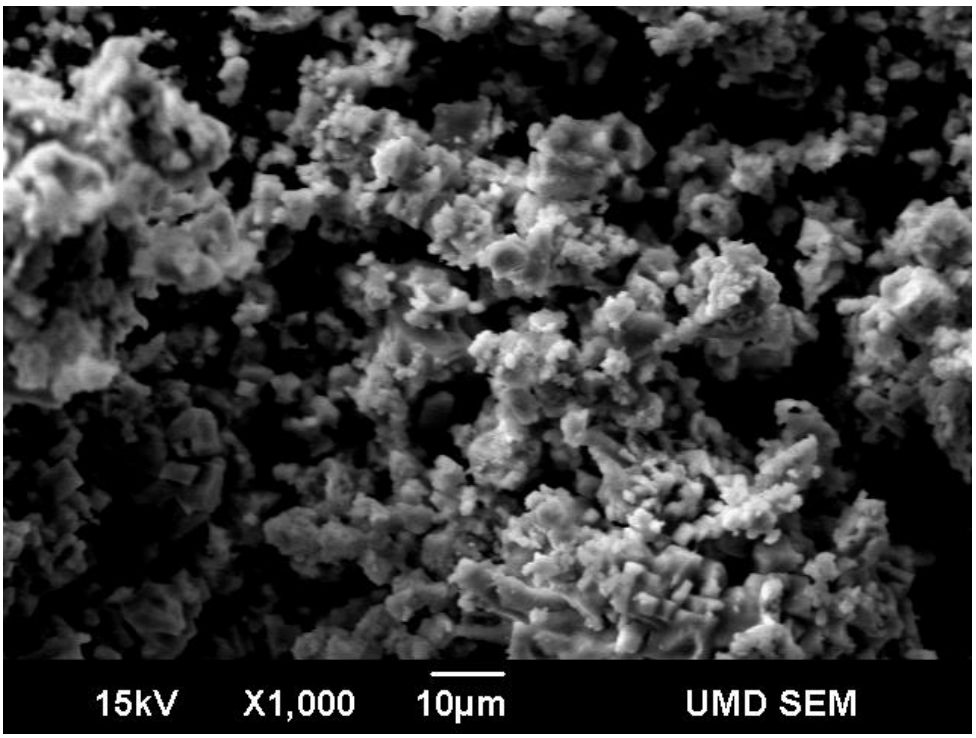

Figure S-15. A) SEM image of Chester Creek LOI material

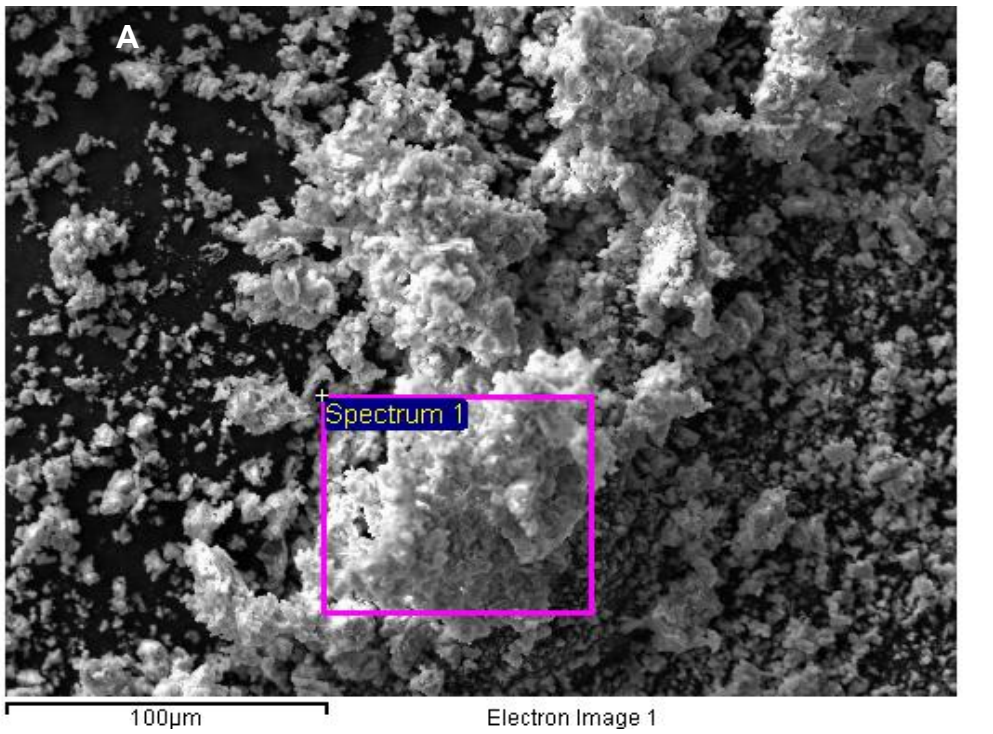

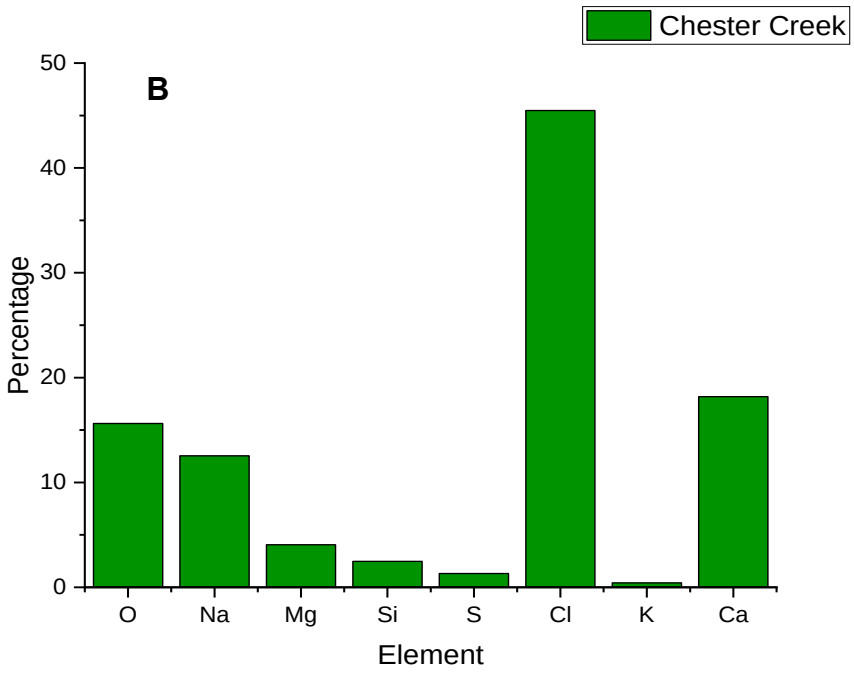

Figure S-16. A) SEM image of Chester Creek LOI sample with area used for EDS shown B) EDS analysis of A showing relative percentage of identified

Pyrolysis GC-MS

Pyrolysis was done to characterize Lake Superior and Chester Creek DOM with standards run to identify fragments. The pyrolysis procedure was based on Hendrickson et al. (2018) and modified slightly for DOM analysis. Freeze-dried DOM underwent pyrolysis in a Gerstel Thermal Desorption Unit (TDU) followed by injection into an Agilent 7890B Gas Chromatograph equipped with a 30m by 0.250mm Agilent HP-5MS and an Agilent 5977A mass-selective detector (MSD). Approximately 200mg of freeze-dried DOM was added to tared and previously ashed quartz tubes on a Mettler Toledo XP2U microbalance. This was followed by the addition of 15µL of tetramethyl ammonium hydroxide (TMAH) (Sigma Aldrich, 25 wt % in methanol) via a glass syringe. TMAH is a derivatizing agent that methylates carboxylic and hydroxyl groups leading to more GC amenable products (Clifford et al., 1995). By methylating polar functional groups the polarity of the initial group is decreased allowing for better product volatisation leading to increased detection of pyrolysis products that have to transit a GC column. The TMAH DOM mixture sat for 4 minutes before being inserted into the TDU, which was kept at an initial temperature of 50˚C. After insertion there was a 1.5-minute lag time to elute atmospheric gases from the system. The TDU then underwent a temperature ramp to 300˚C at a rate of 720˚C per minute; the final temperature was held for 1 minute. After the TDU reached its final temperature the pyrolyser began flash pyrolysis at 550˚C for 30s. The TDU transfer temperature was kept at a 320˚C. The cooled injection system (CIS) liner, which transfers sample from the pyrolyser/TDU to the GC inlet was ramped from 300˚C to 320˚C at 12˚C per minute. The GC oven held its initial temperature of 50˚C for 2 minutes. This was followed by a temperature gradient of 8˚C per minute to its final temperature 320˚C which was held for 5 minutes, giving a total run time of 42 minutes. After a run the GC equilibrated at 50˚C for 3 minutes. The transfer line between the GC and MSD was 280 ˚C. The MSD used an electron impact (EI^+, 70 eV) ionization source. The MS source and MS quadrupole had set points at 230 ˚C and 150 ˚C respectively. The MSD scanned for ions from m/z 50-550 at 2.9 scans per second. Standards were run similarly to DOM samples, but a 1:100 split ratio was introduced, and less sample was used due to purity.

Table S-7. List of standards and DOM along with source information for standards as well as corresponding page numbers of TIC and Mass Spec figures

Sample	Source	Lot #	TIC	Mass Spec
1-nonadecanol	Tokyo Chemical Industry 98%	W5MZO-MP	75-76	75
Bovine Serum Albumin	Sigma Aldrich	110M7403	77-80	76
Chitin	Sigma Aldrich	SLBN7584V	83-81	81
Coumaric Acid	MP Biomedicals, LLC	4886KA	84-85	83
Cytochrome C from equine heart	Sigma Aldrich	114K6127	86-89	85
Dextrose	Fisher Chemical	132676	90-92	90
Gallic Acid	Sigma Aldrich	111k0103	92-93	92
Lignin Alkali	Sigma Aldrich	MKCD3898	94-99	94
L-Proline	Acros Organics	A0341787	100	99
L-Serine	Acros Organics	A0333224	101-102	101
L-Tyrosine	Alfa Aesar 99%	H14Z023	103-105	103
Mannose	Acros Organics 99%	A0078007001	105-108	105
Palmitic Acid	SigmaUltra 99%	19H07011	109-110	108
Tannic Acid	Sigma Aldrich	12K0048	110-111	110
Trans-Cinnamic Acid	Acros Organics 98%	A0273868	112-113	112
Vanillin	Sigma Aldrich	101K3702	114-117	114
Freeze-Dried Lake Superior (2018) (filter <0.22 µm, depth 5m)	-	-	117-122	117
Freeze-Dried Lake Superior (2019) (filter <0.22 µm, depth 5m)	-	-	123-124	123
Freeze-Dried Chester Creek Nov 2017 (filter <0.22 µm, depth 0m)	-	-	125-127	125
Freeze-Dried Chester Creek Nov 2018 (filter <0.22 µm, depth 0m)	-	-	128-129	128

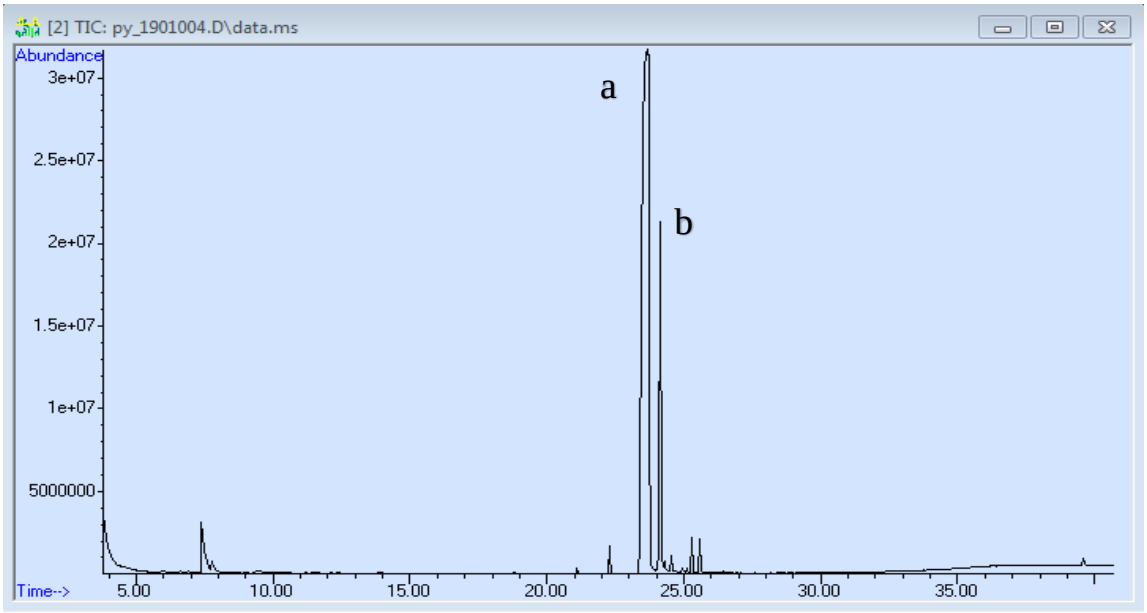

Figure S-17. TIC of 1-nonadecanol

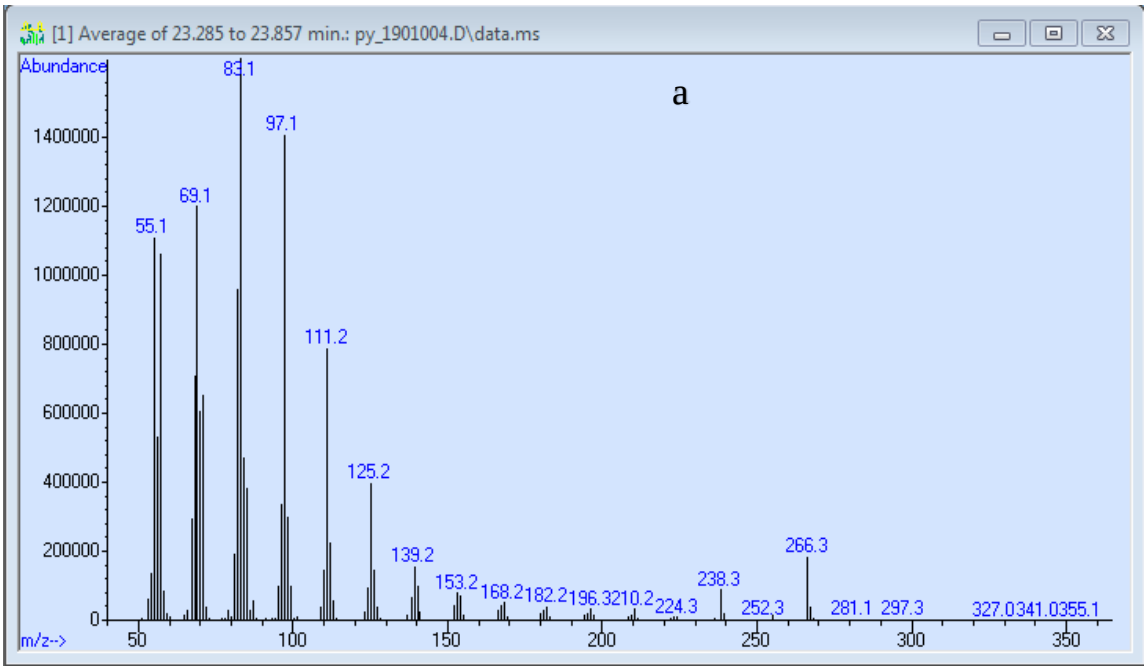

Figure S-18. MS of peak a (23.285-23.857 min) from Fig. S-17

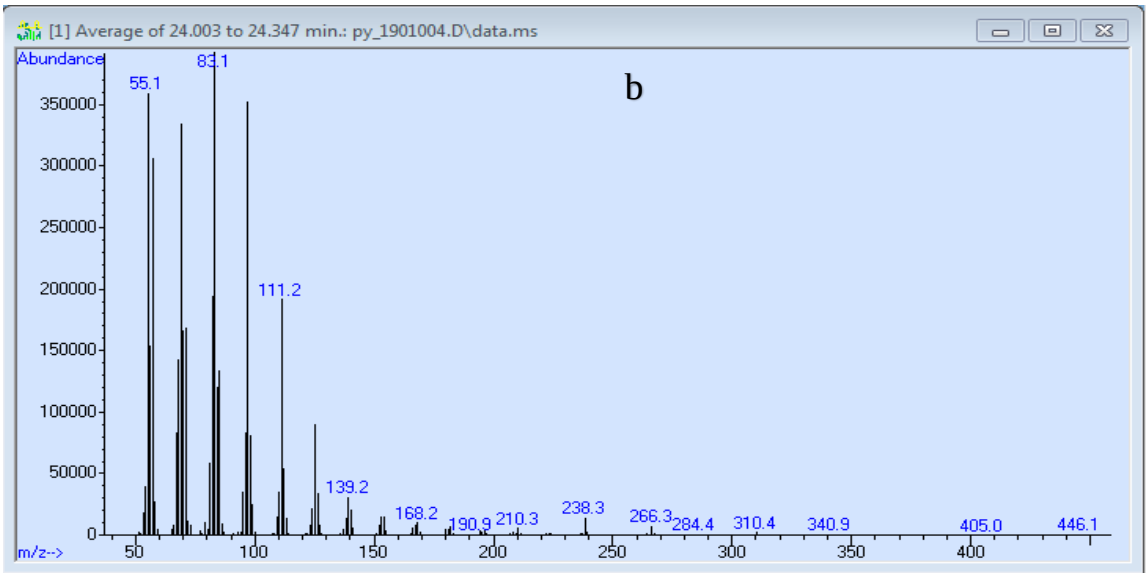

Figure S-18. MS of peak b (t=24.003 to 24.347 min) from Fig. S-17

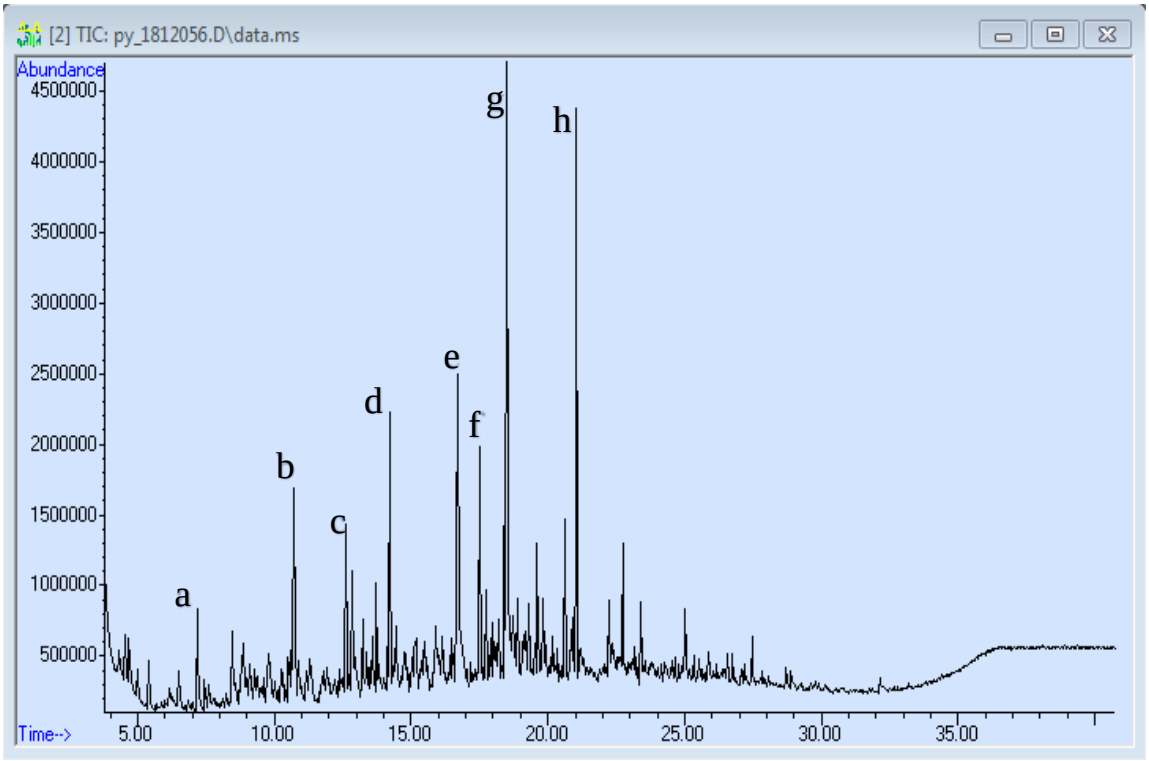

Figure S-19. TIC of Bovine Serum Albumin

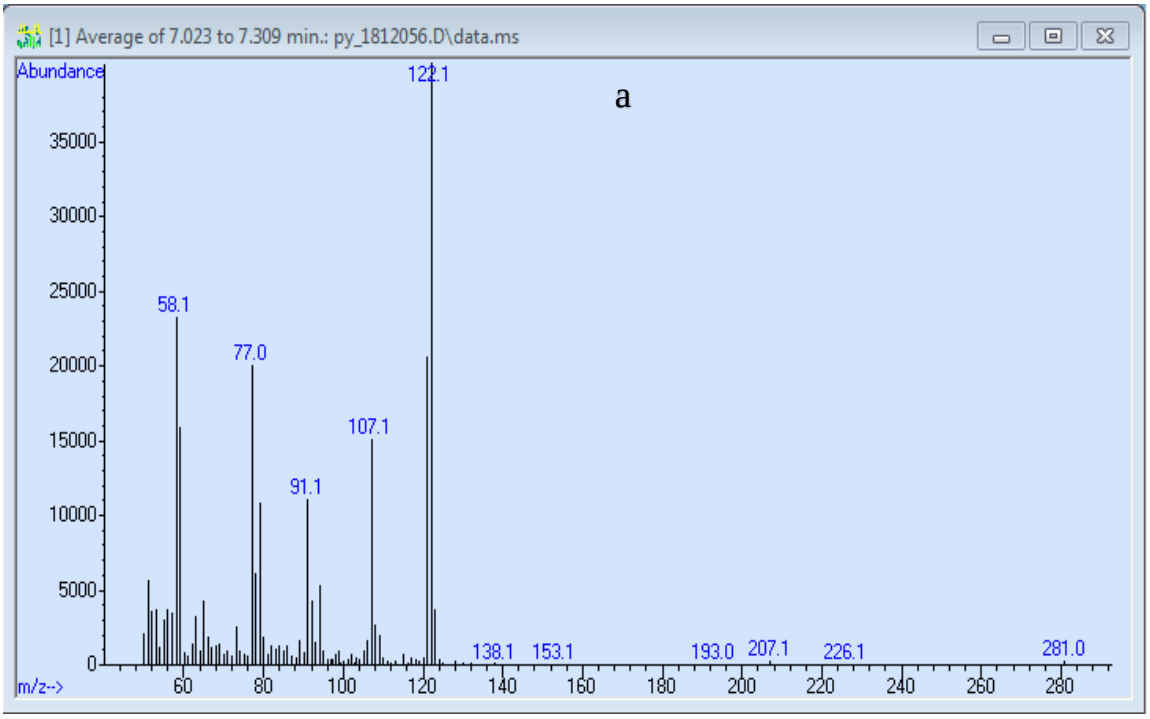

Figure S-20. MS of peak a (7.023 to 7.309 minutes) from Fig. S-19

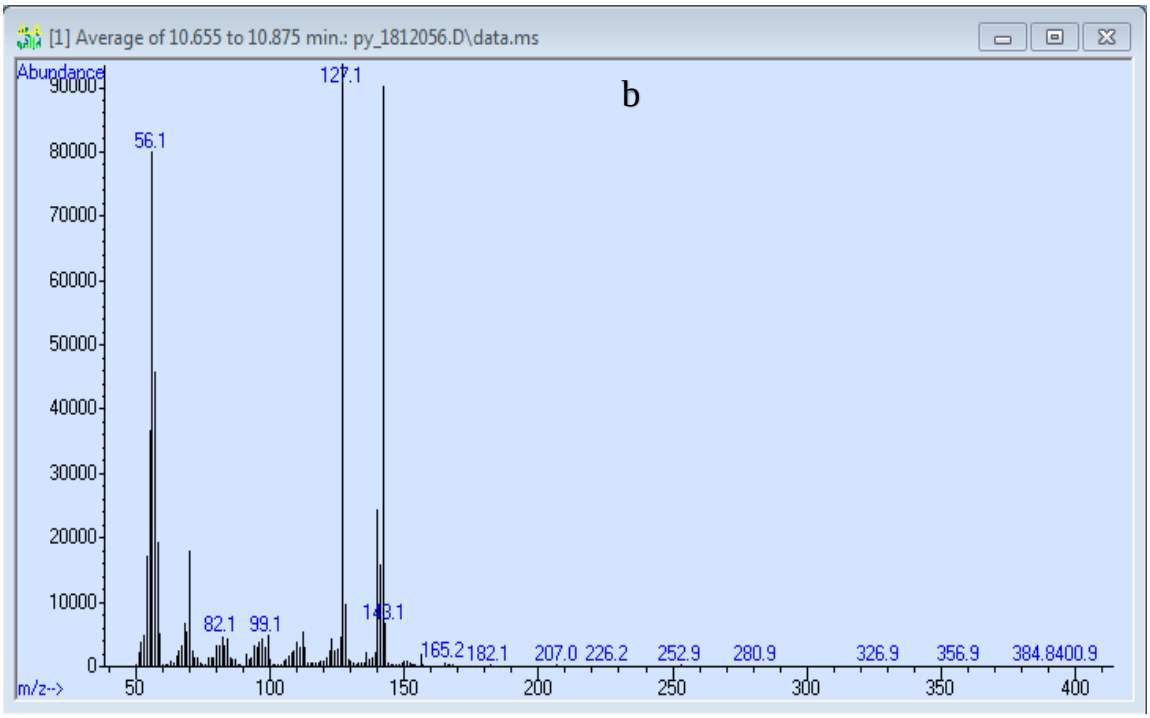

Figure S-21. MS of peak b (10.655 to 10.875 min) from Fig. S-19

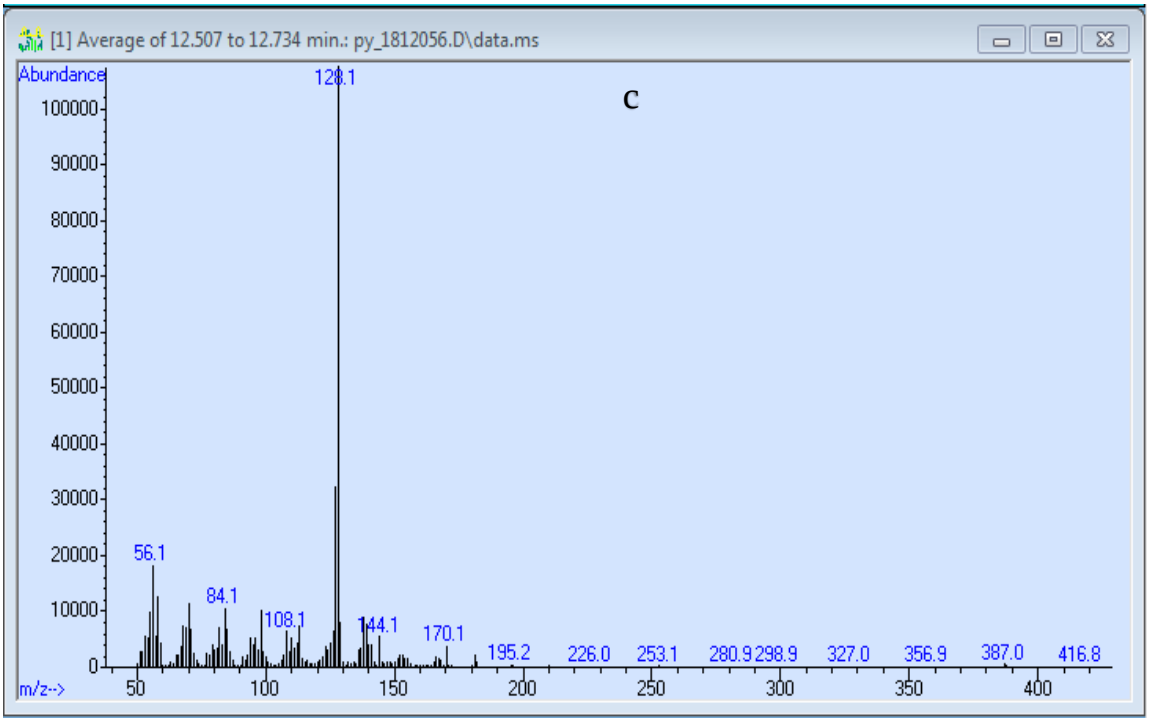

Figure S-22. MS of peak c (12.507 to 12.734 min) from Fig. S-19

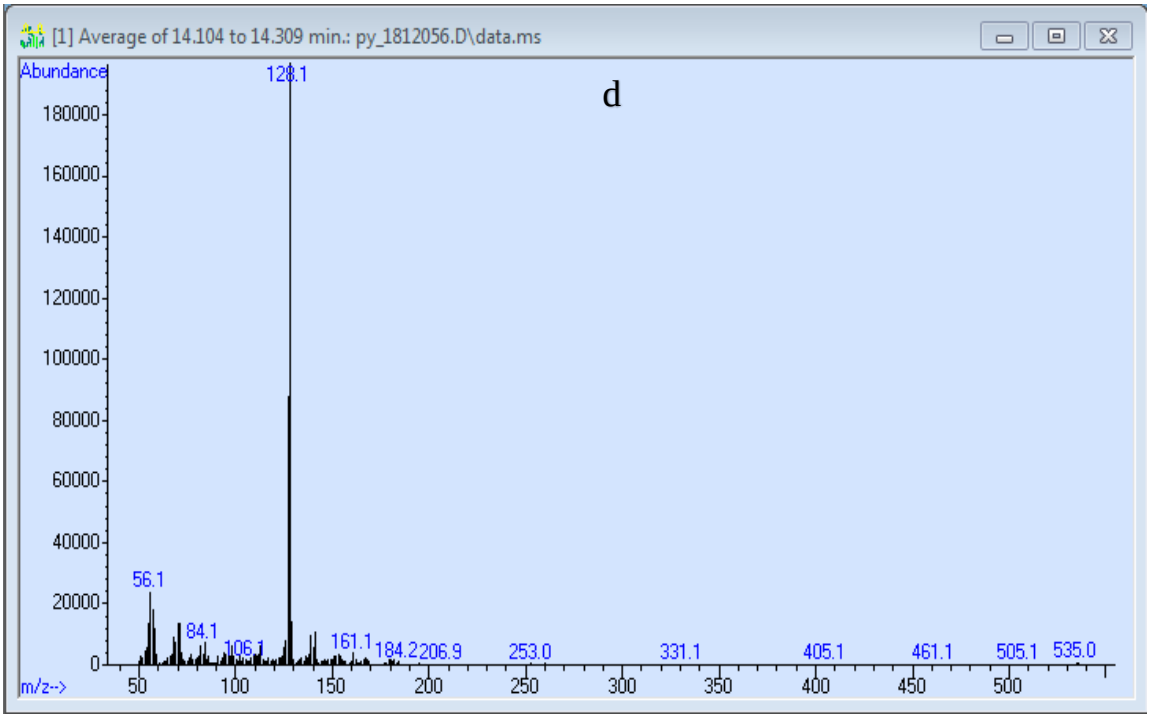

Figure S-23. MS of peak d (14.104 to 14.309 min) from Fig. S-19

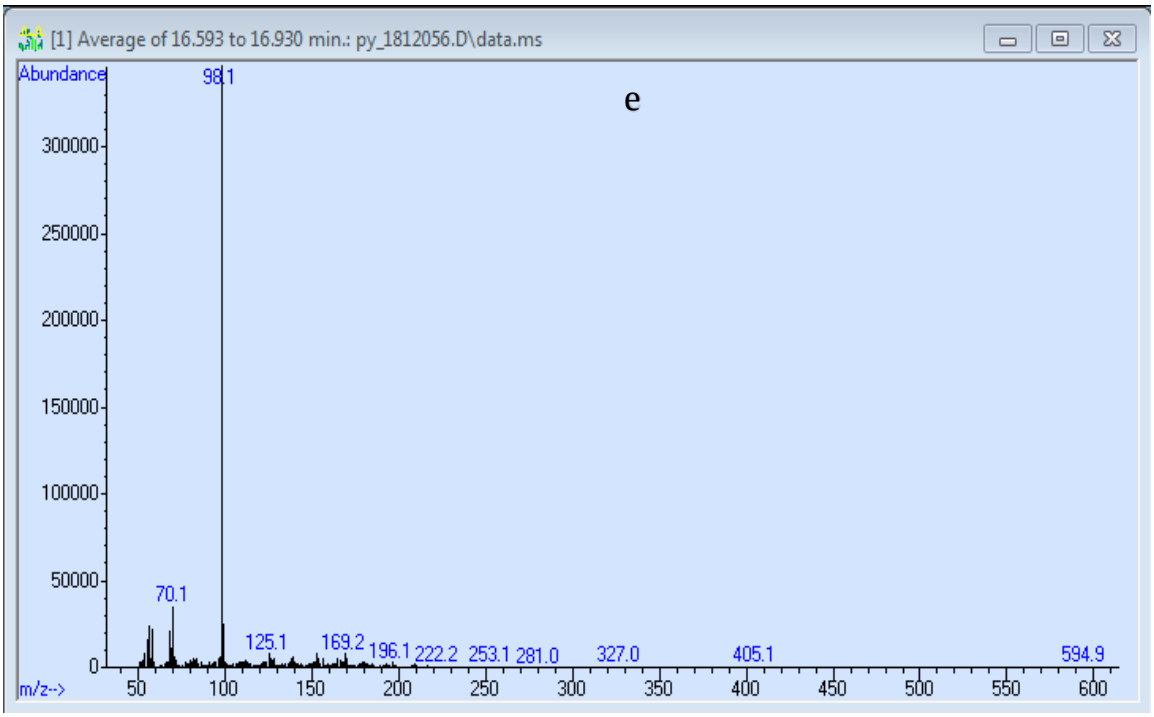

Figure S-24. MS of peak e (16.593 to 16.930 min) from Fig. S-19

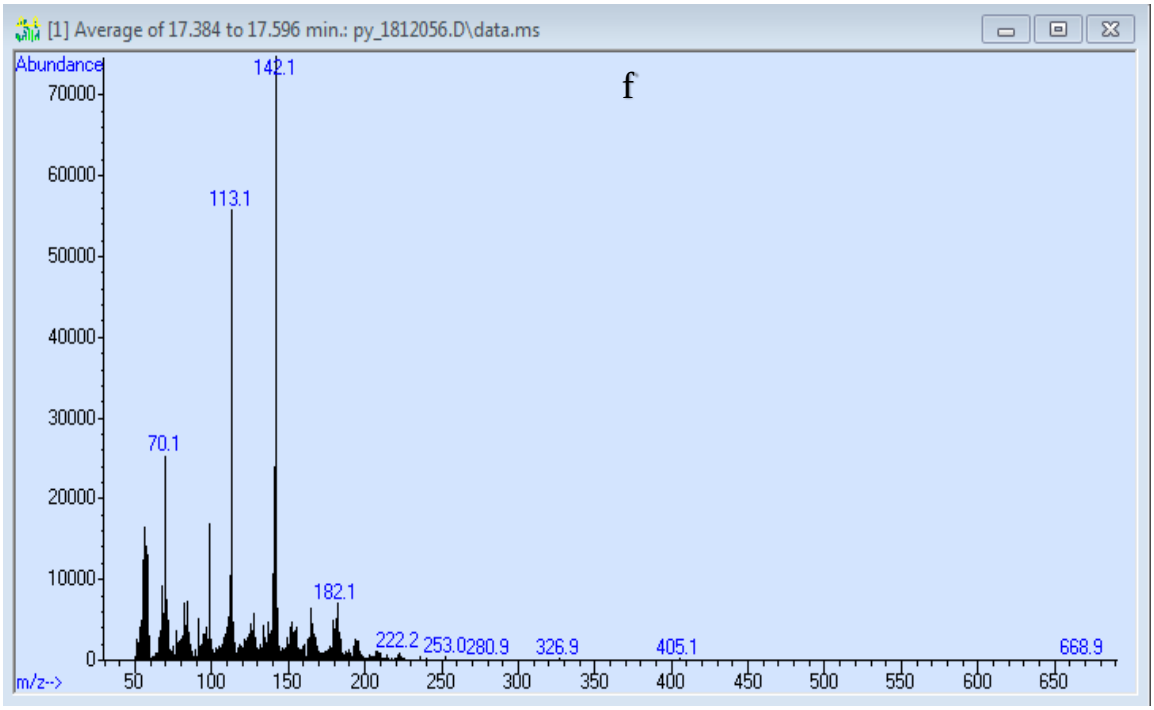

Figure S-25. MS of peak e (17.384 to 17.596 min) from Fig. S-19

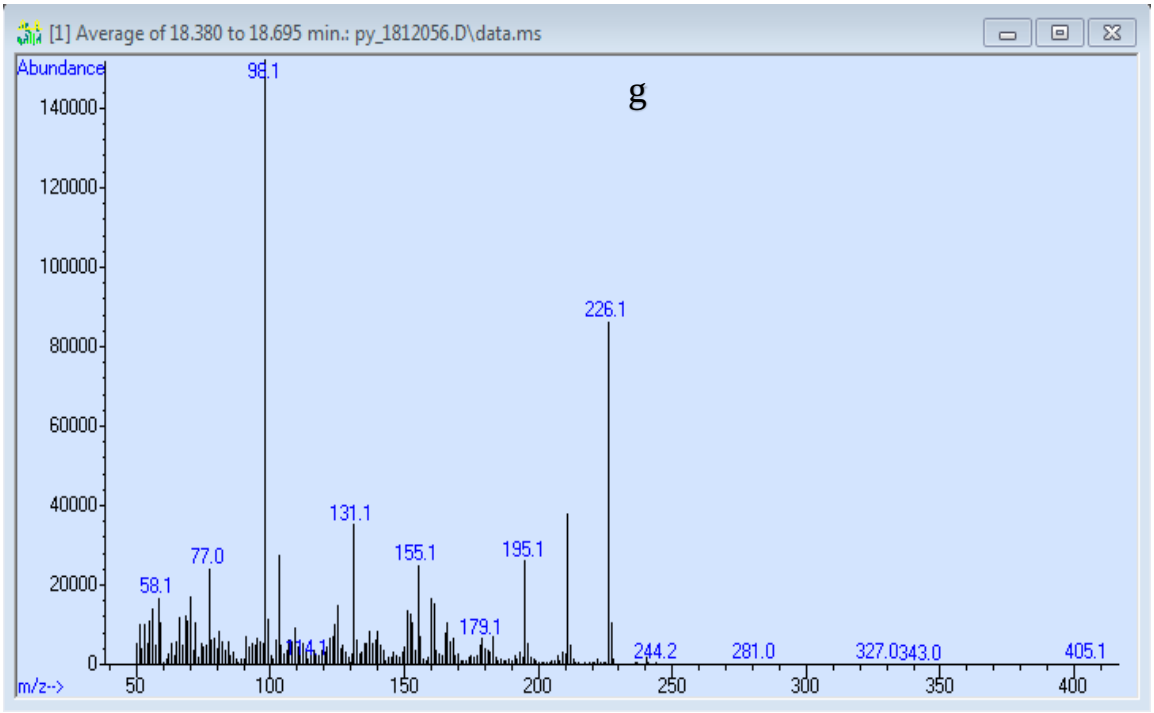

Figure S-26. MS of peak g (18.380 to 18.695 min) from Fig. S-19

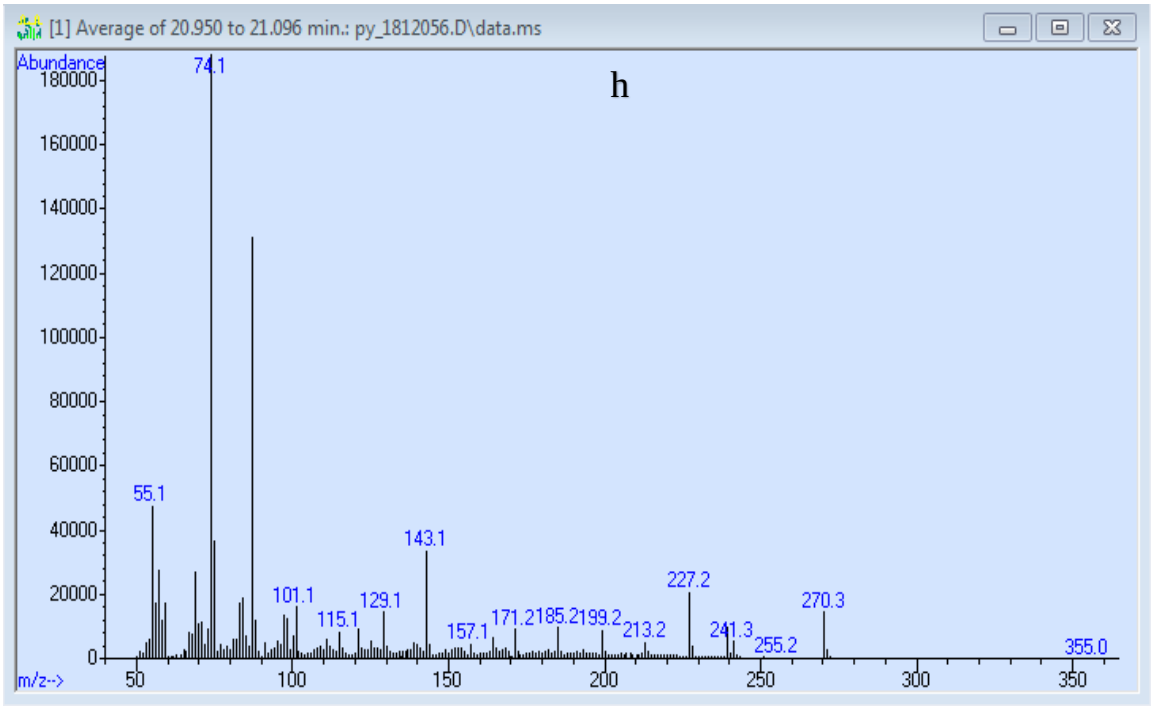

Figure S-27. MS of peak h (20.950 to 21.096 min) from Fig S-19

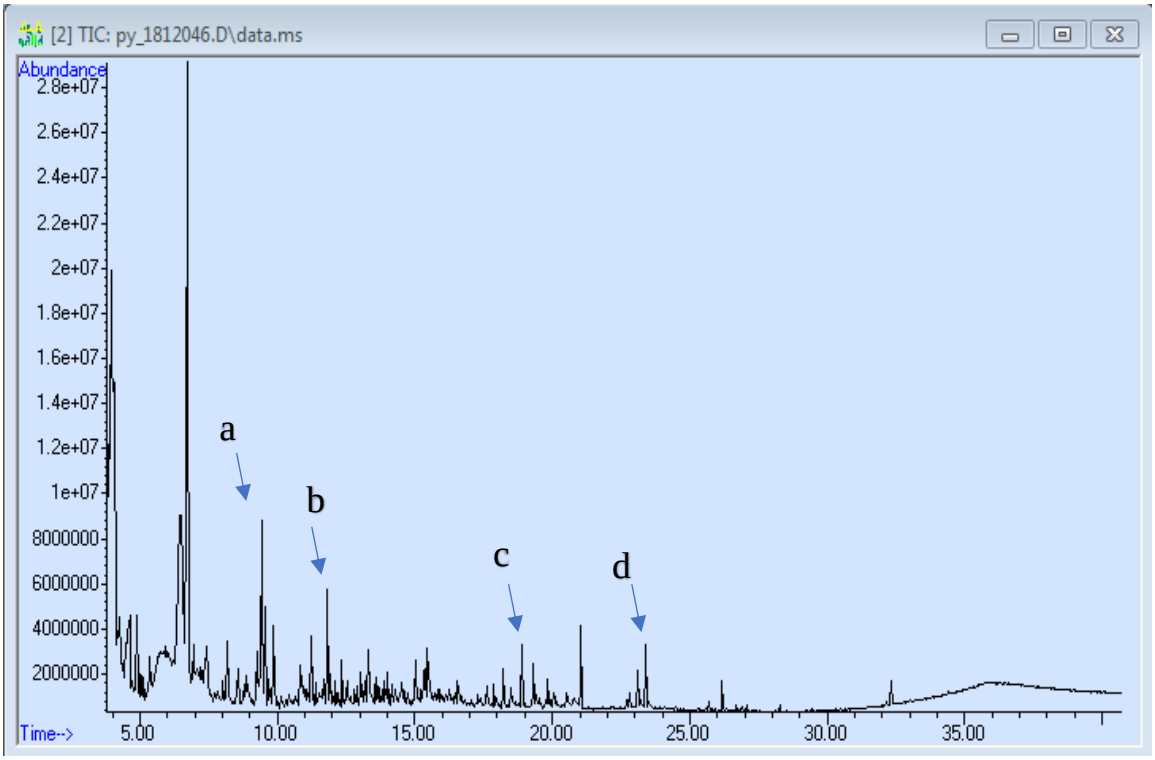

Figure S-28. TIC of Chitin

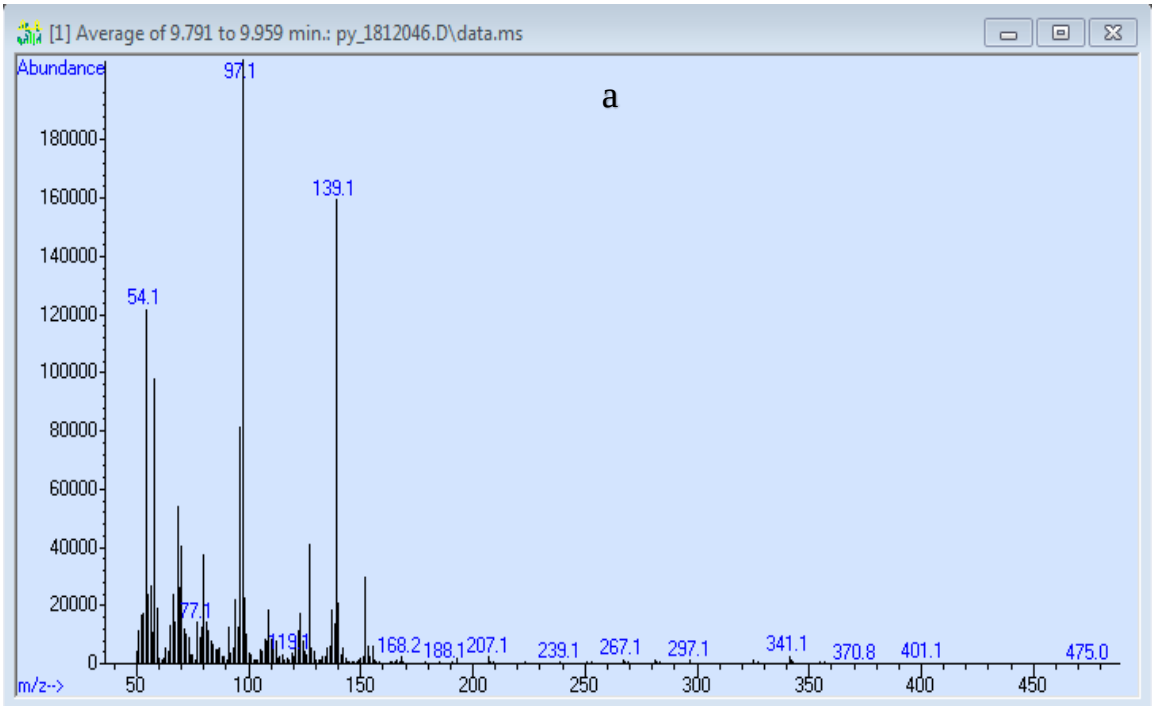

Figure S-29. MS of peak a (9.791 to 9.959 min) to Fig. S-28

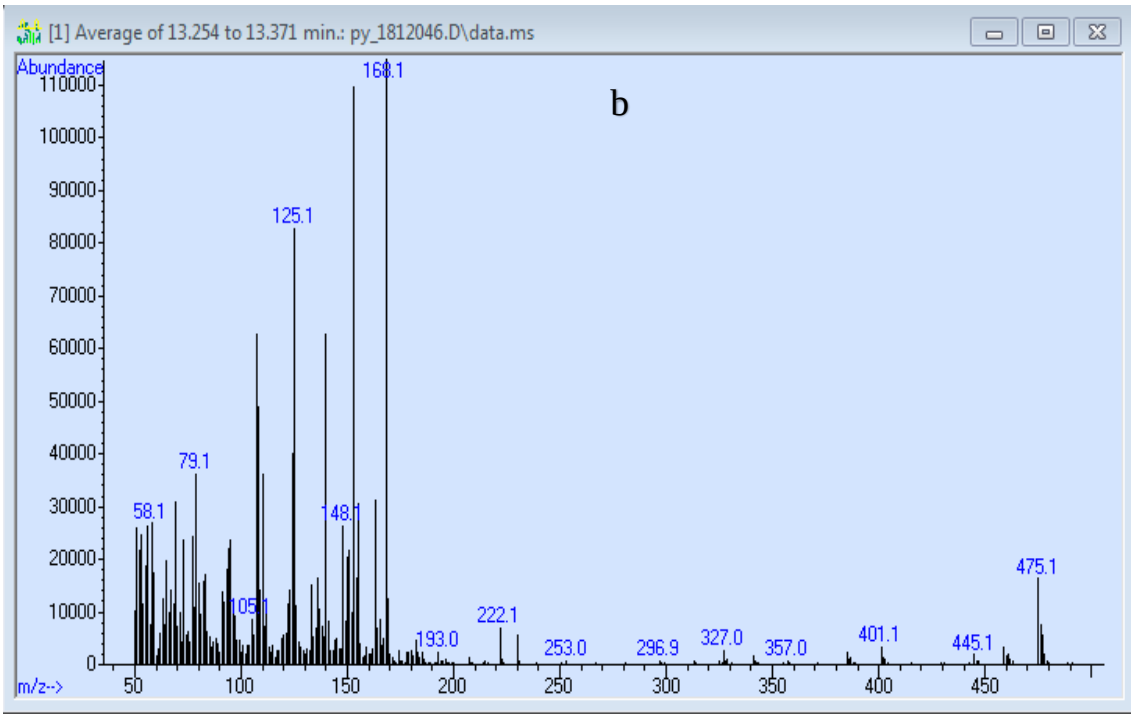

Figure S-30. MS of peak b (13.254 to 13.371 min) from Fig. S-28

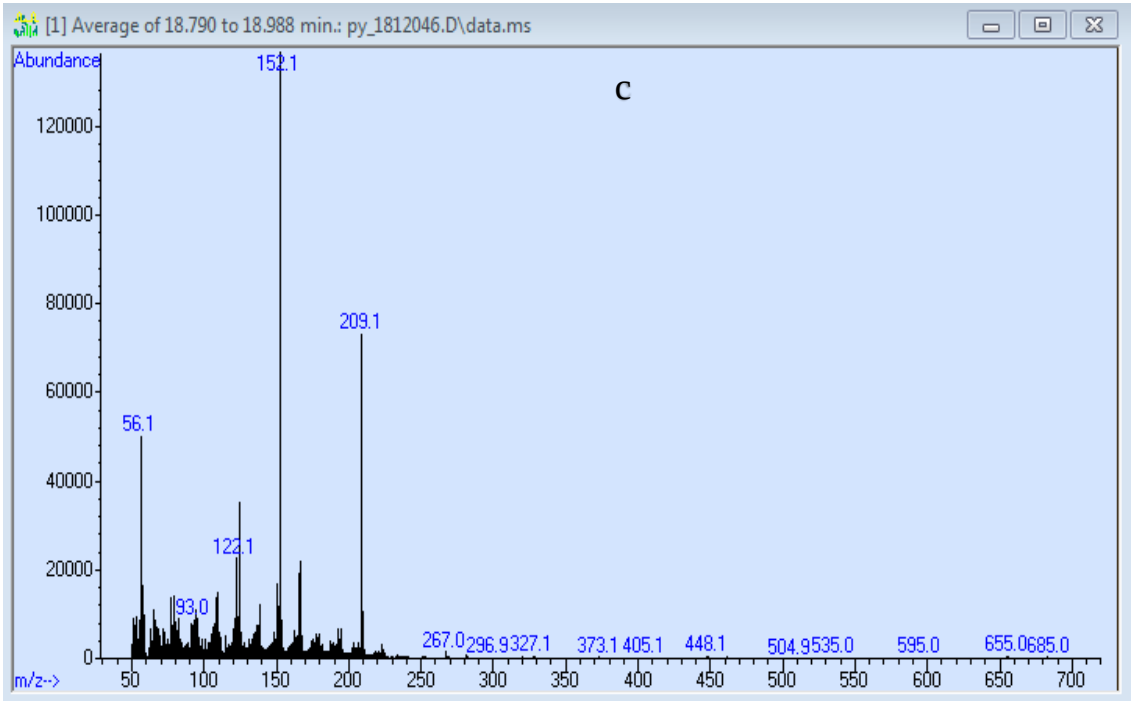

Figure S-31. MS of peak c (18.790 to 18.988 min) from Fig. S-28

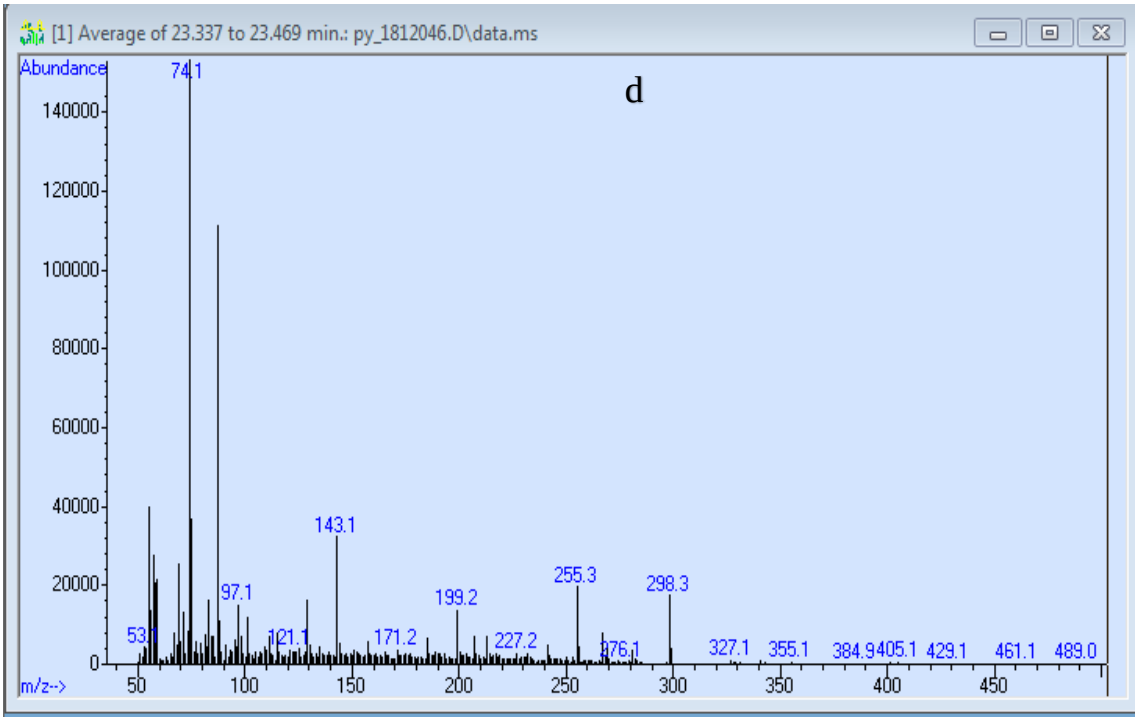

Figure S-32. MS of peak d (23.337 to 23.469 min) from Fig. S-28

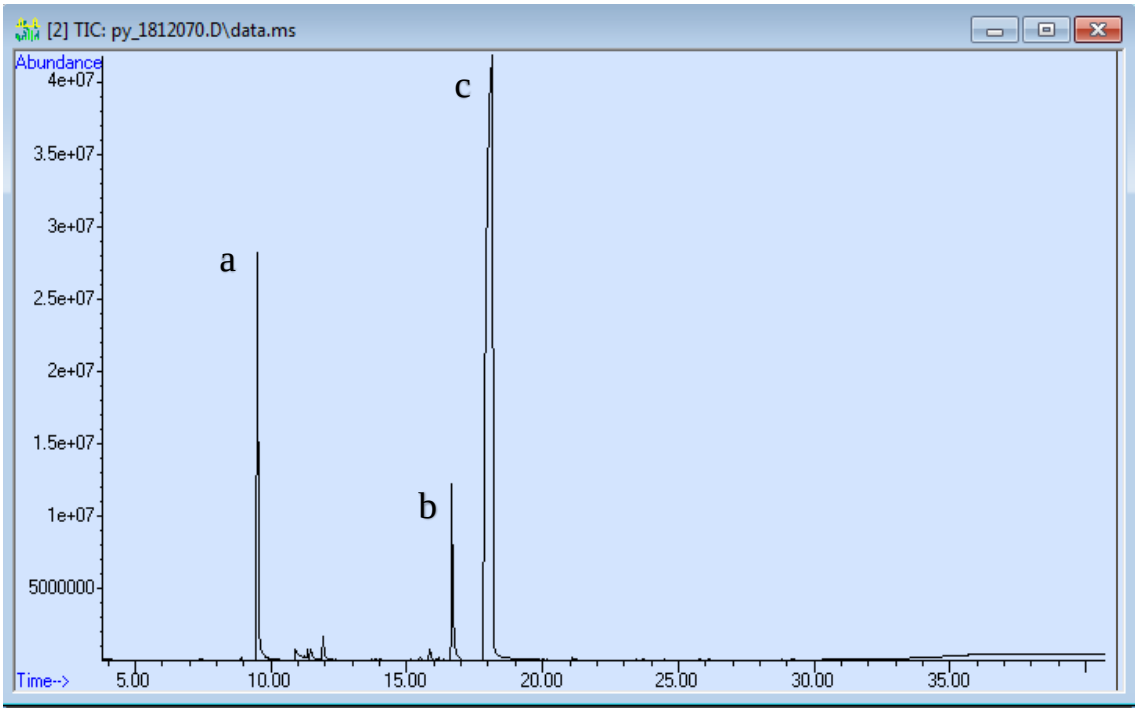

Figure S-33. TIC of p-Coumaric Acid

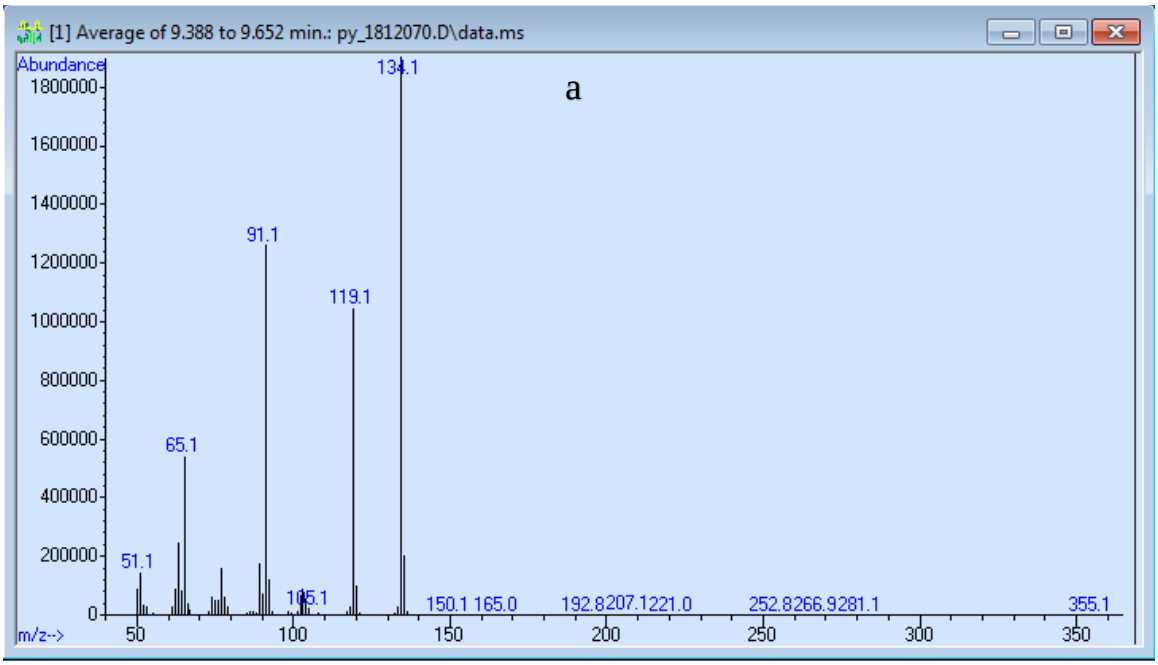

Figure S-34. MS of peak a (9.388 to 9.652 min) from Fig. S-33

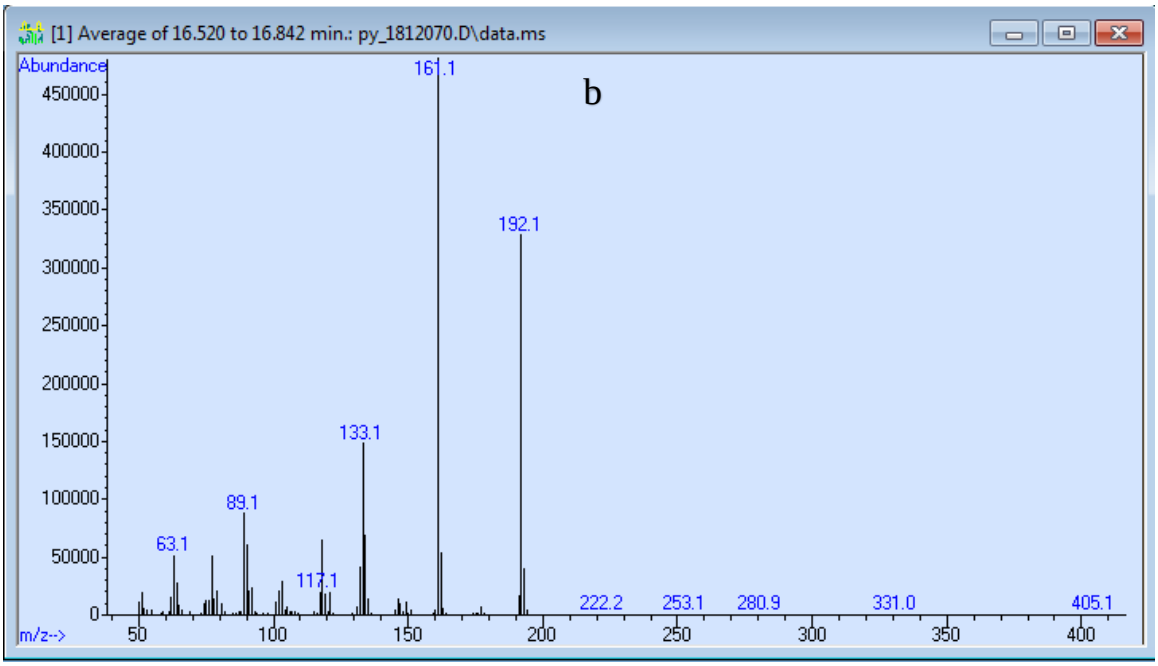

Figure S-35 of peak b (16.520 to 16.842 min) from Fig. S-33

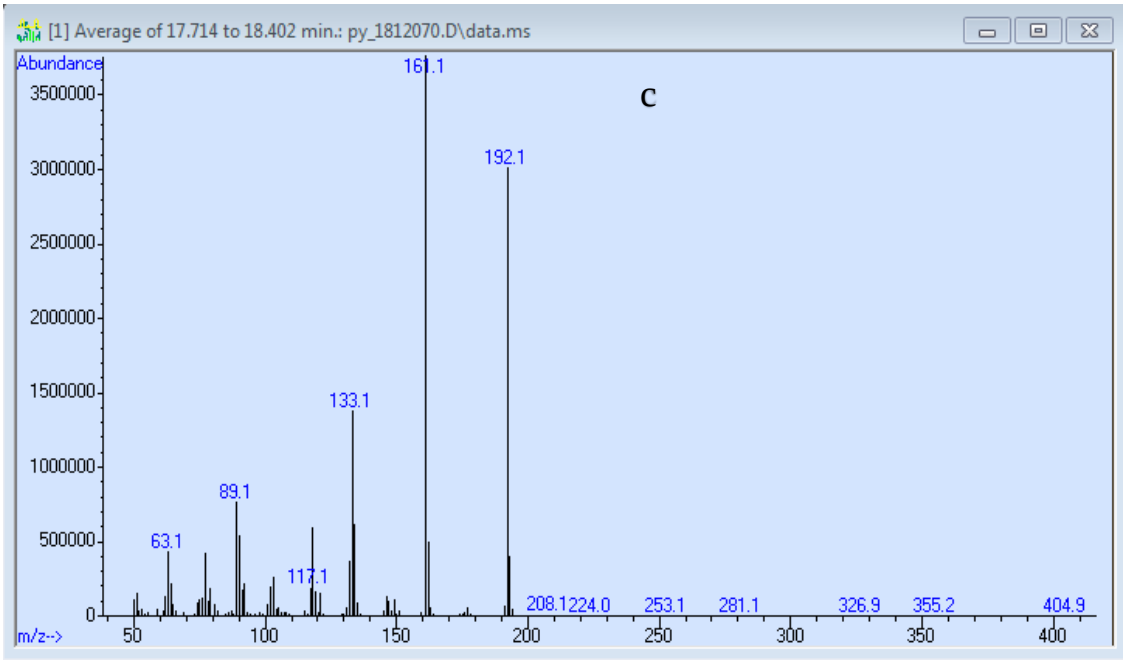

Figure S-36. MS of peak c (17.714 to 18.402 min) from Fig. S-33

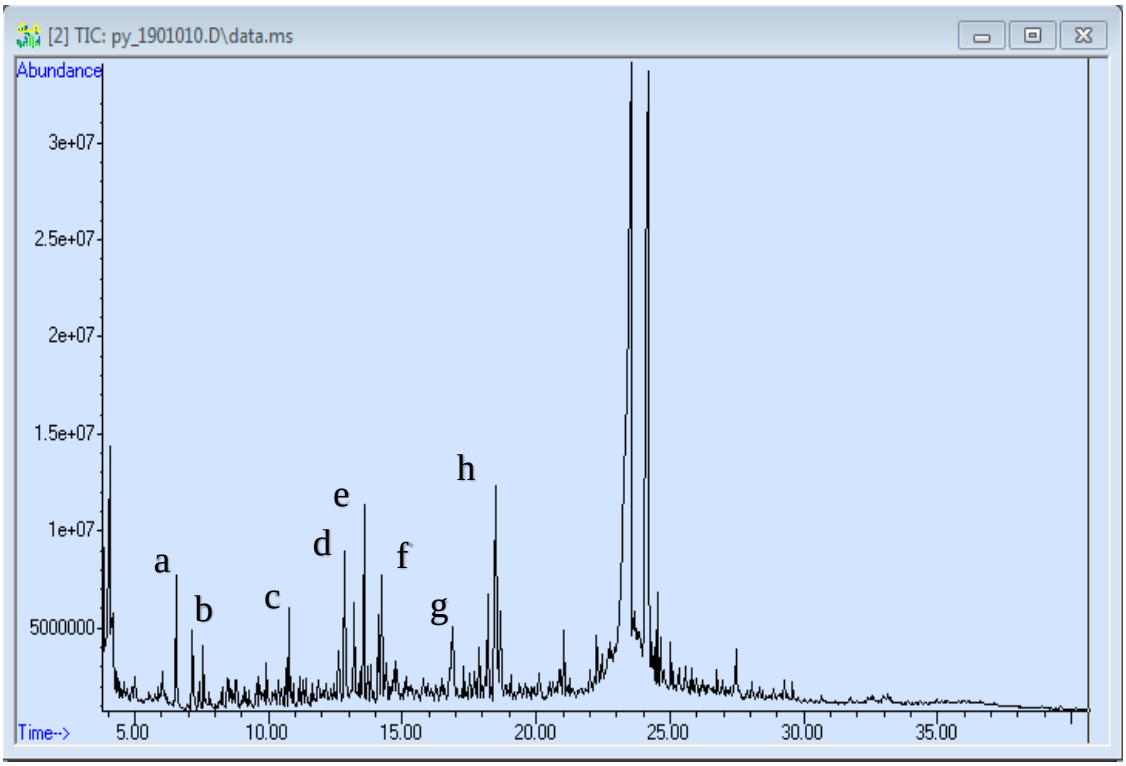

Figure S-37. TIC of Cytochrome C

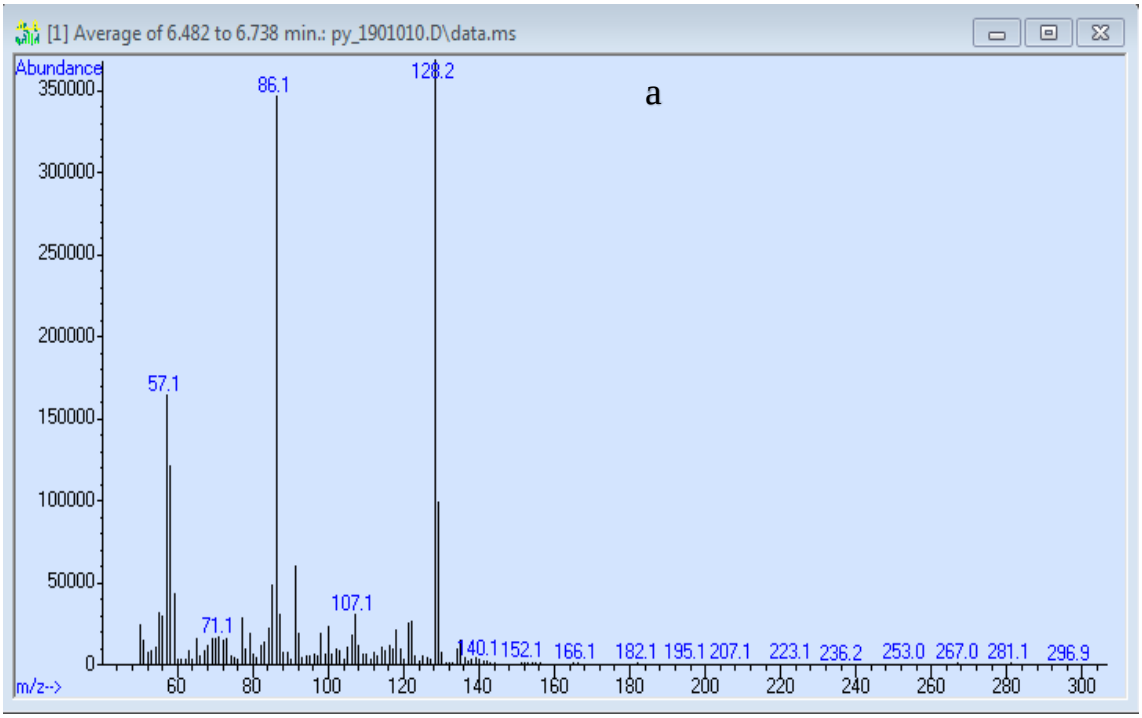

Figure S-38. MS of peak a (6.482 to 6.738 min) from Fig. S-37

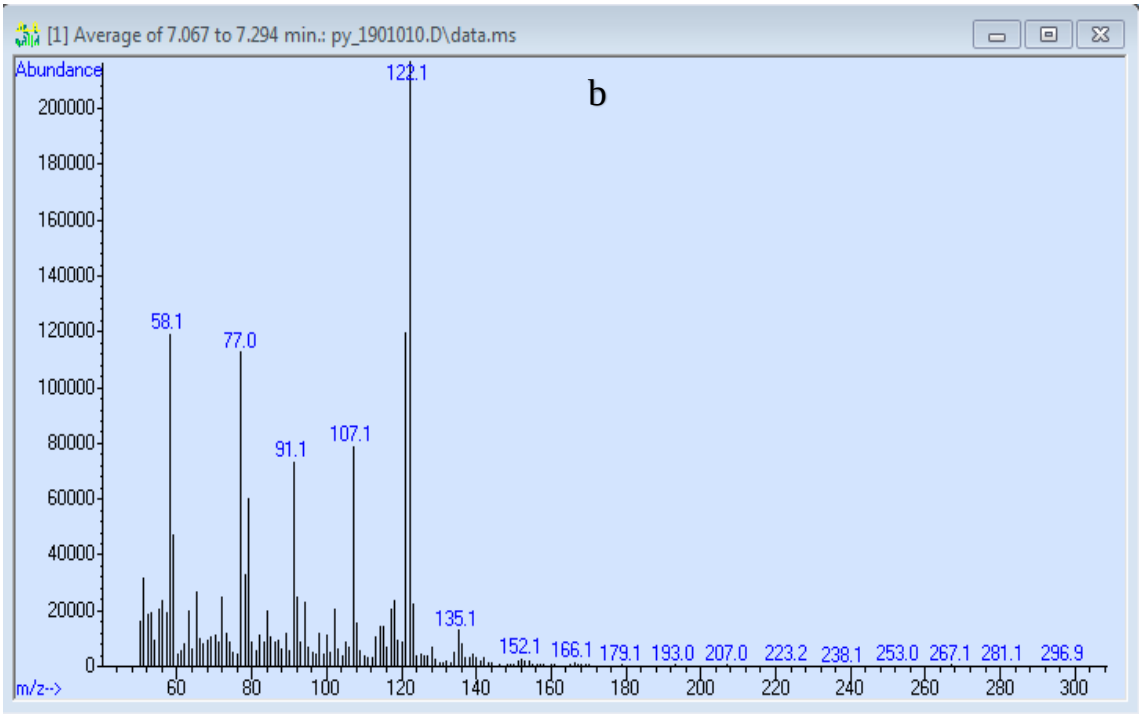

Figure S-39. MS of peak b (7.067 to 7.294 min) from Fig S-37

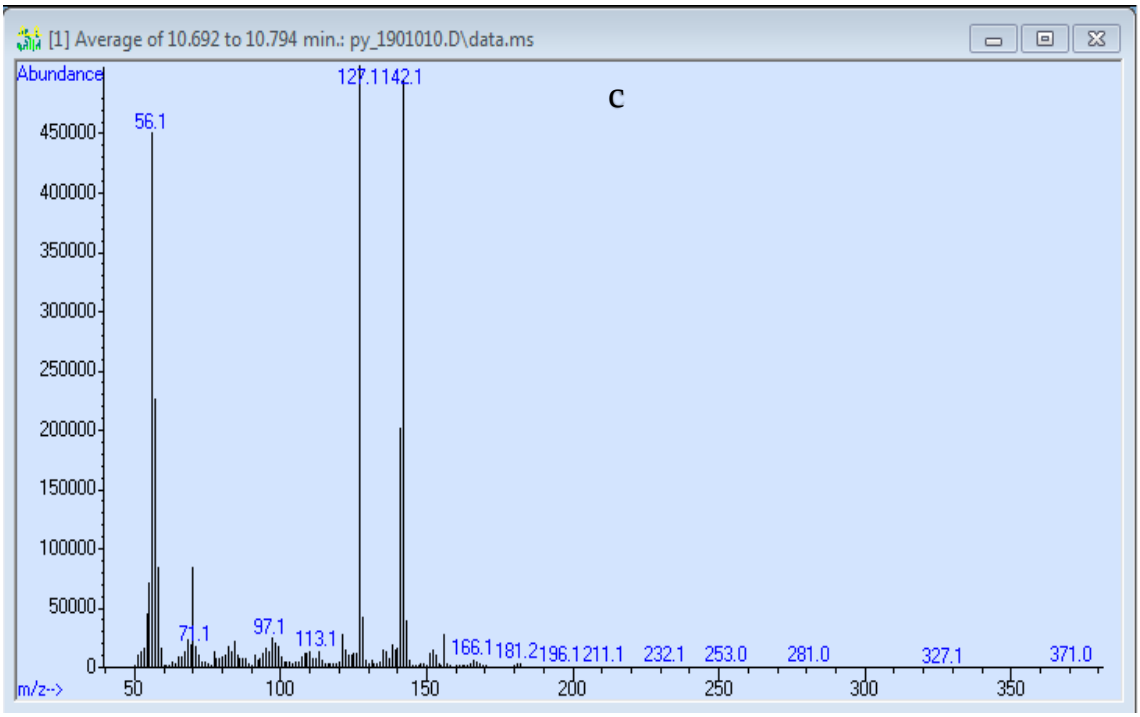

Figure S-40. MS of peak c (10.692 to 10.794 min) from Fig. S-37

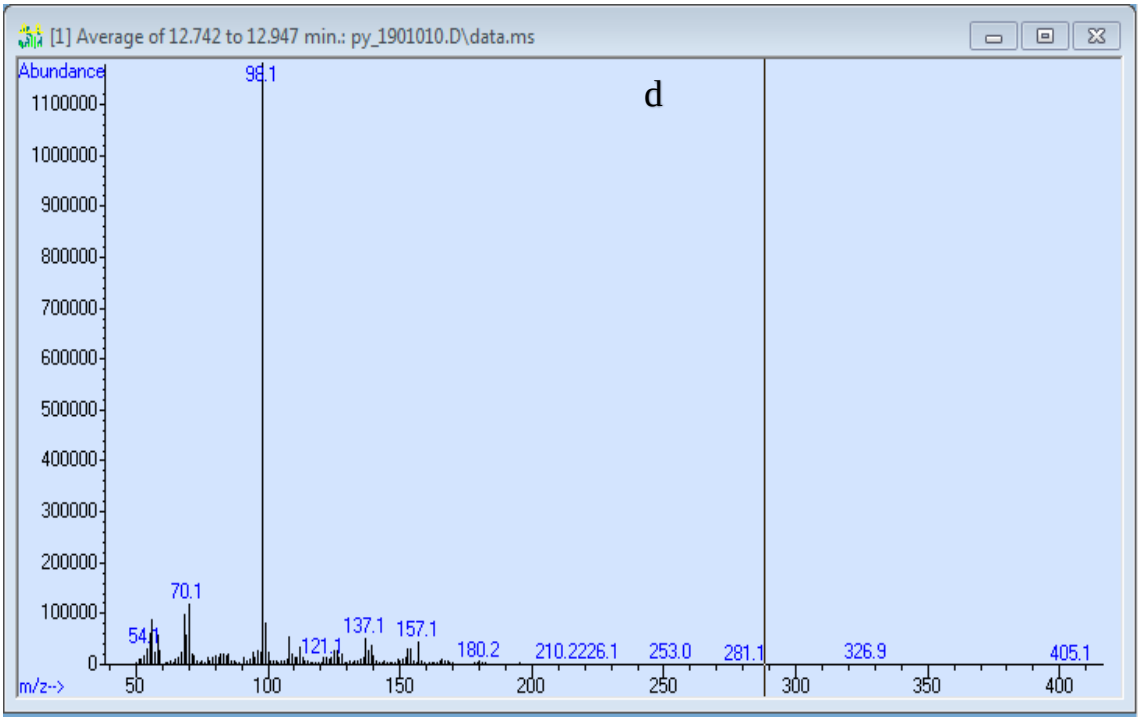

Figure S-41. MS of peak d (12.742 to 12.947 min) from Fig. S-37

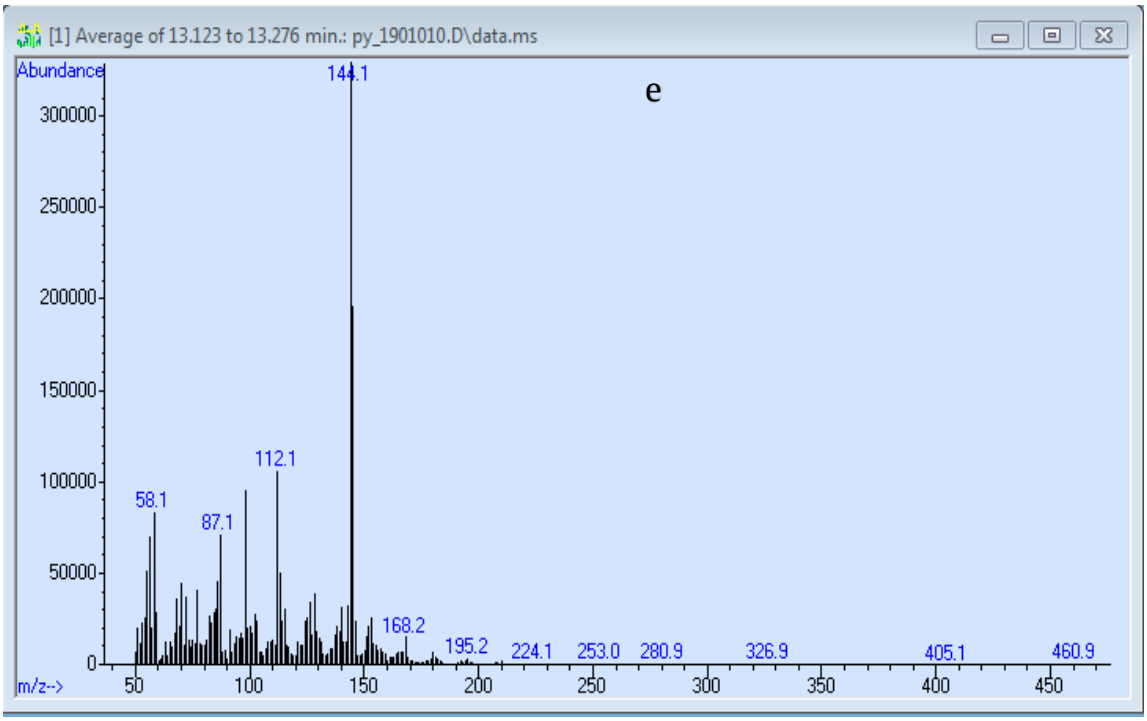

Figure S-42. MS of peak e (13.123 to 13.276 min) from Fig. S-37

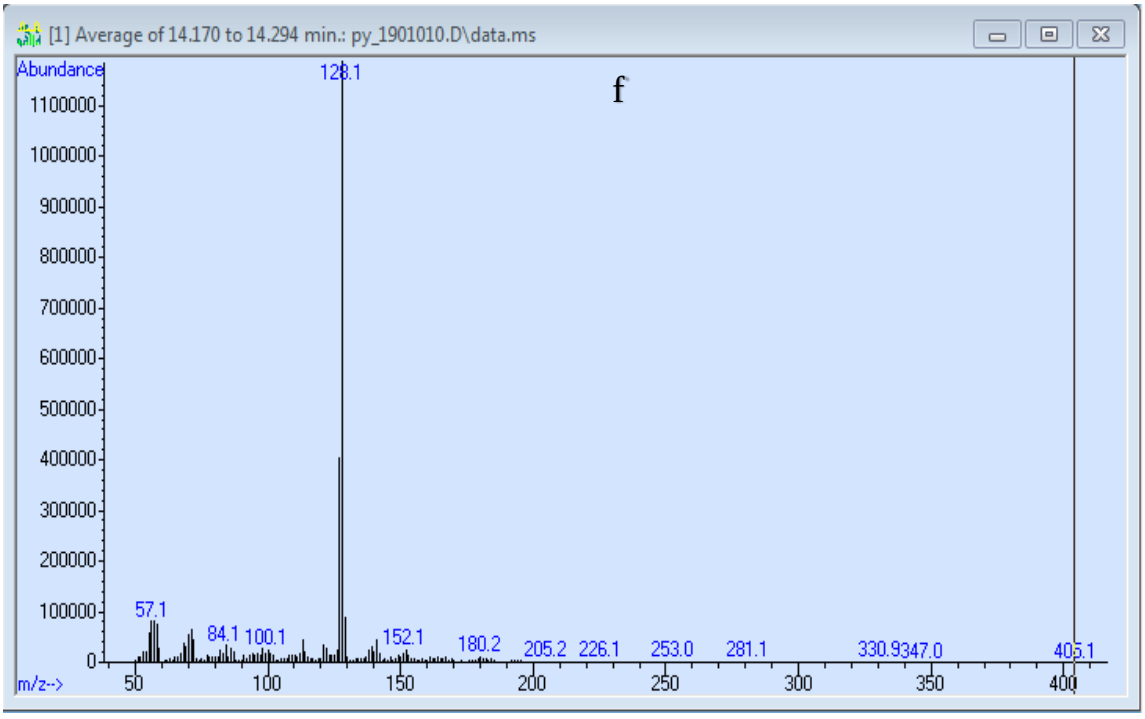

Figure S-43. MS of peak e (14.170 to 14.294 min) from Fig. S-37

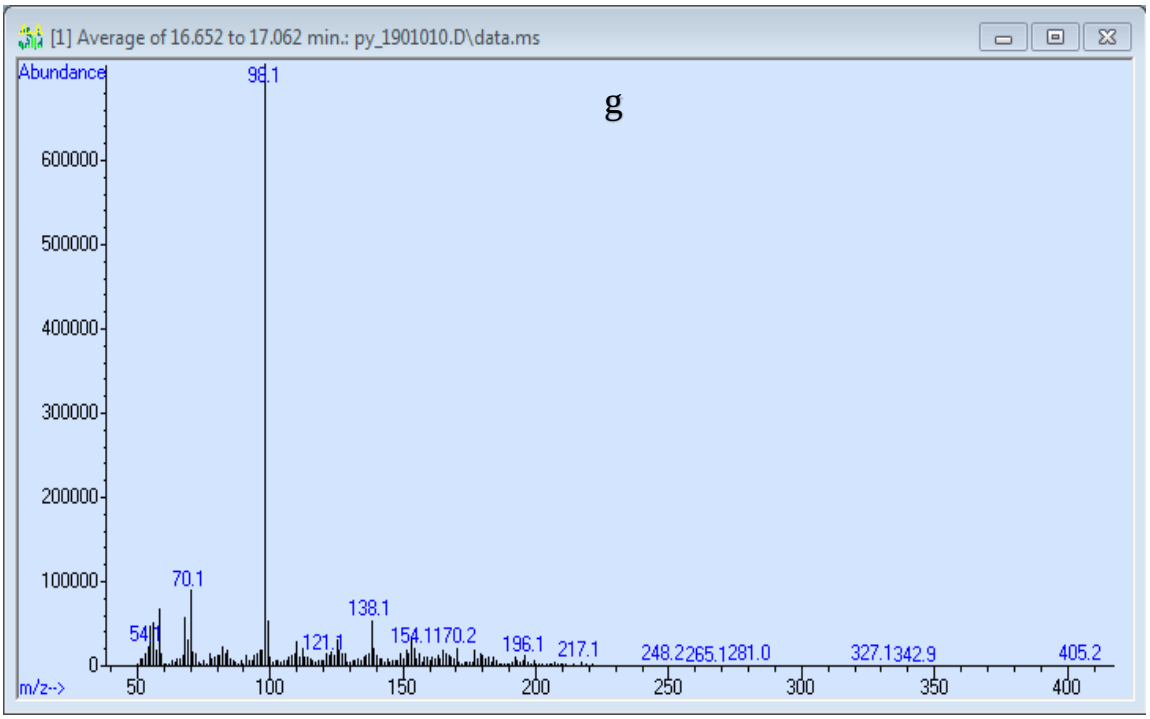

Figure S-44. MS of peak g (16.652 to 17.062 min) from Fig. S-37

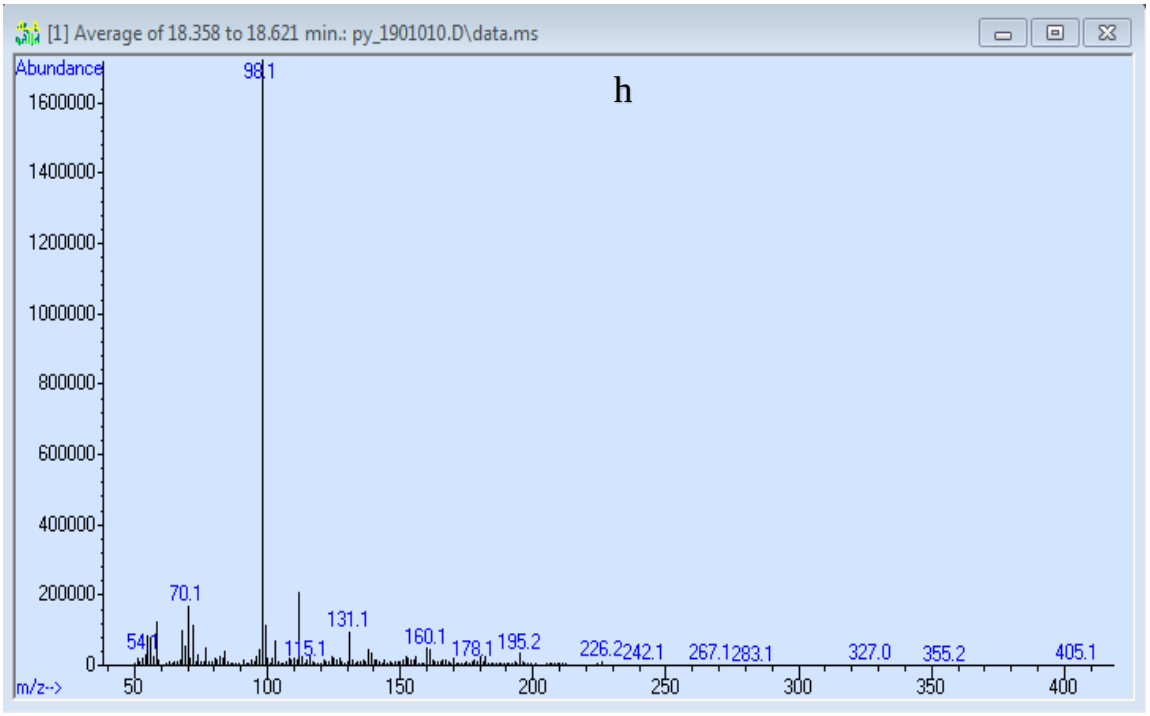

Figure S-45 of peak h (18.358 to 18.621 min) from Fig. S-37

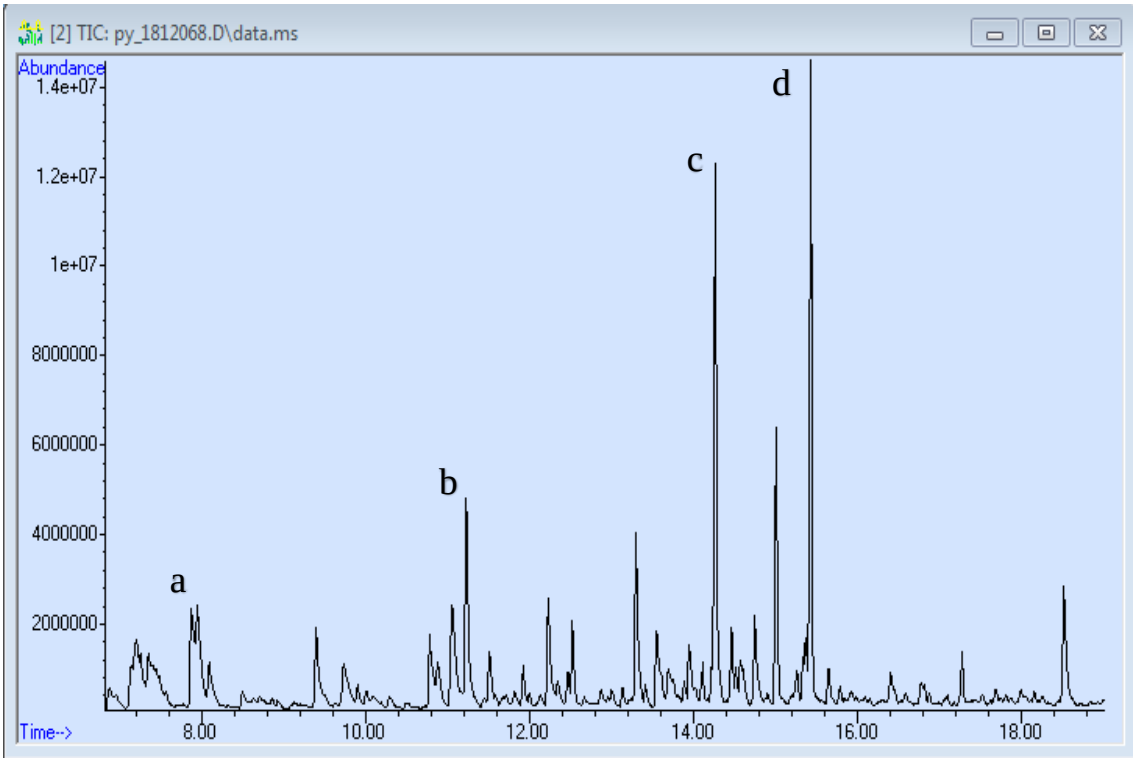

Figure S-46. TIC of Dextrose

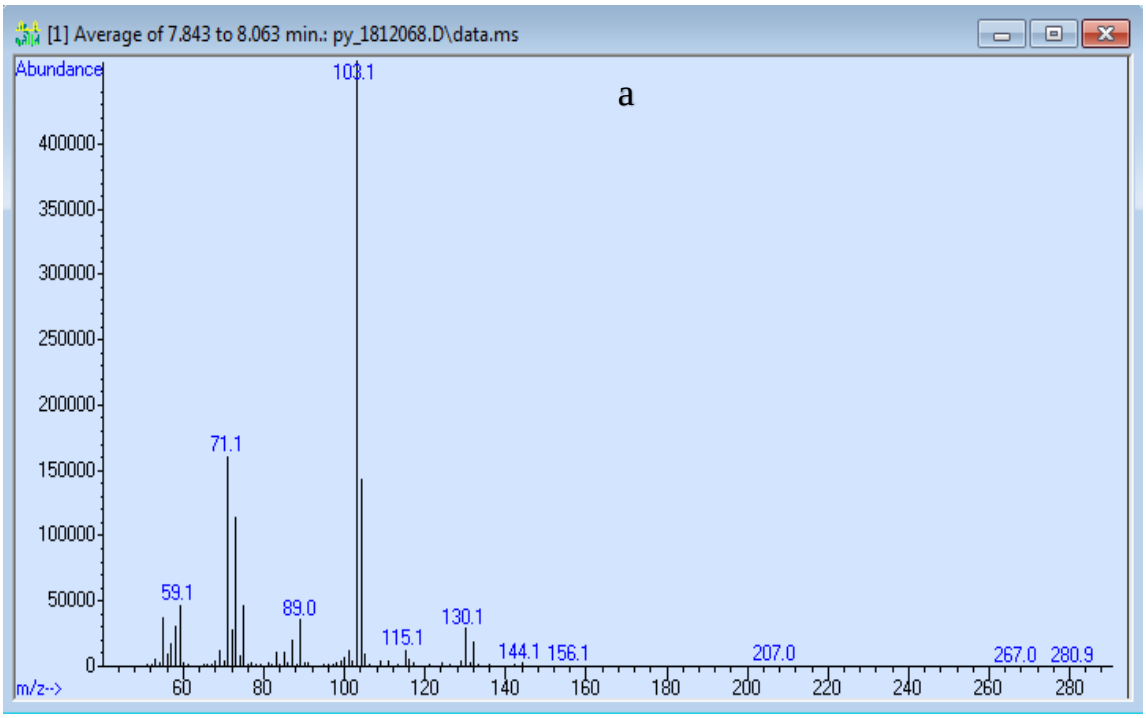

Figure S-47. MS of peak a (7.843 to 8.063 min) from Fig. S-46

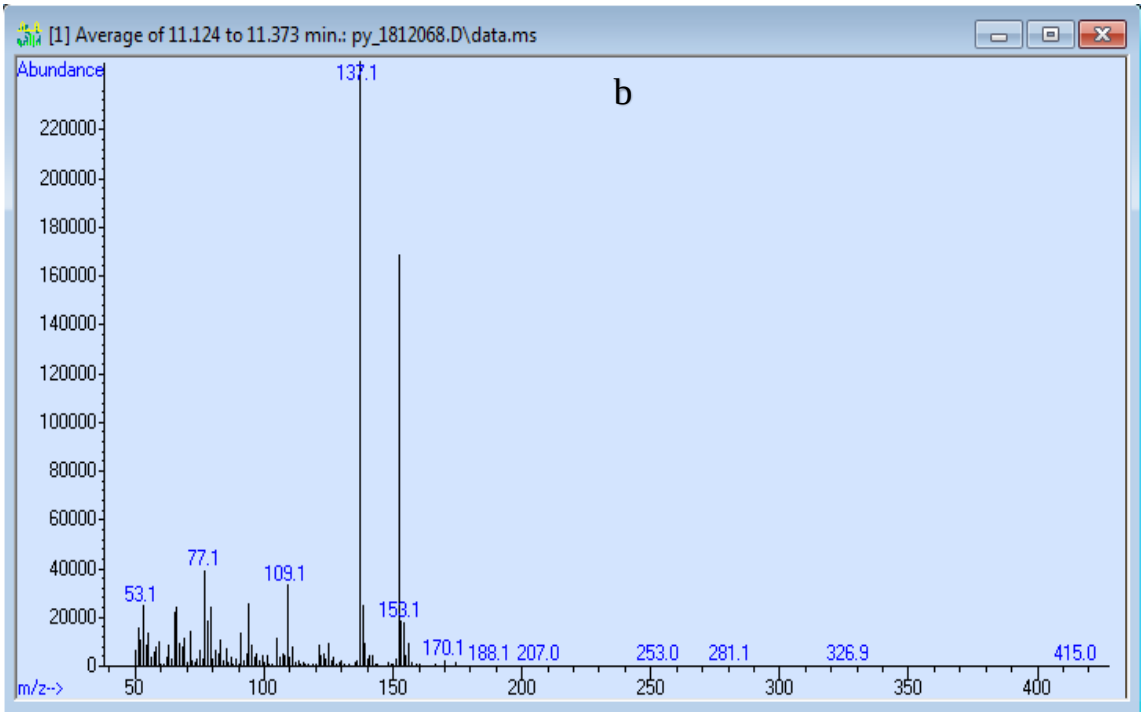

Figure S-48. MS of peak b (11.124 to 11.373 min) from Fig. S-46

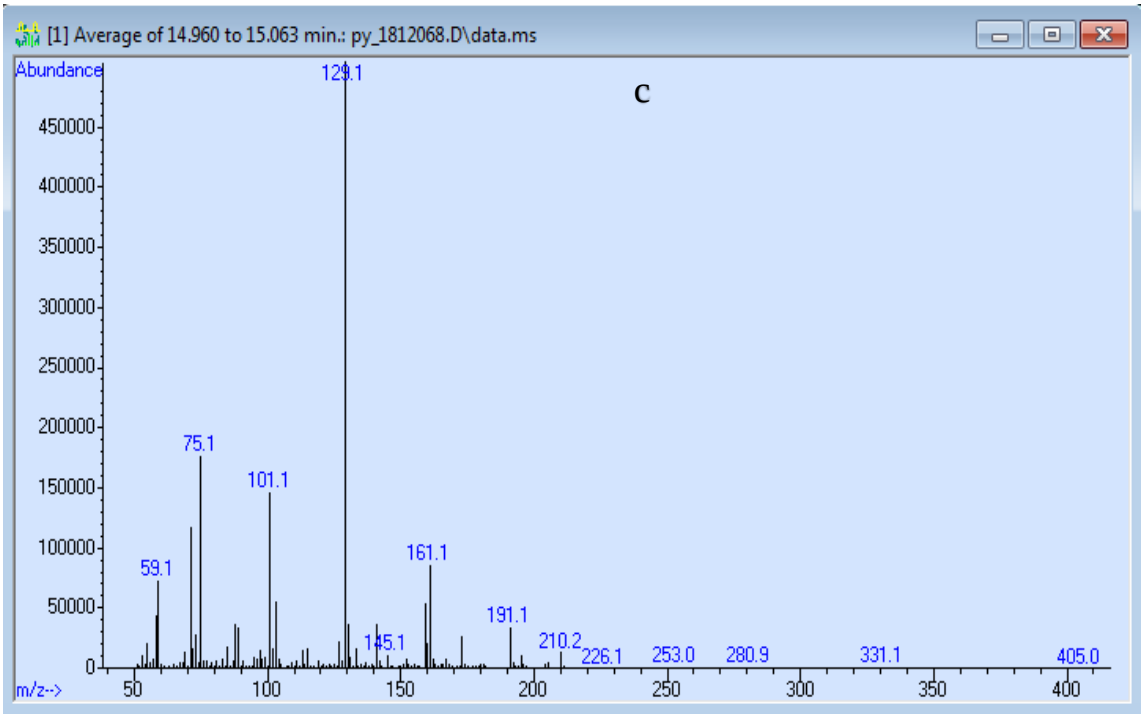

Figure S-49 of peak c (14.960 to 15.063 min) from Fig. S-46

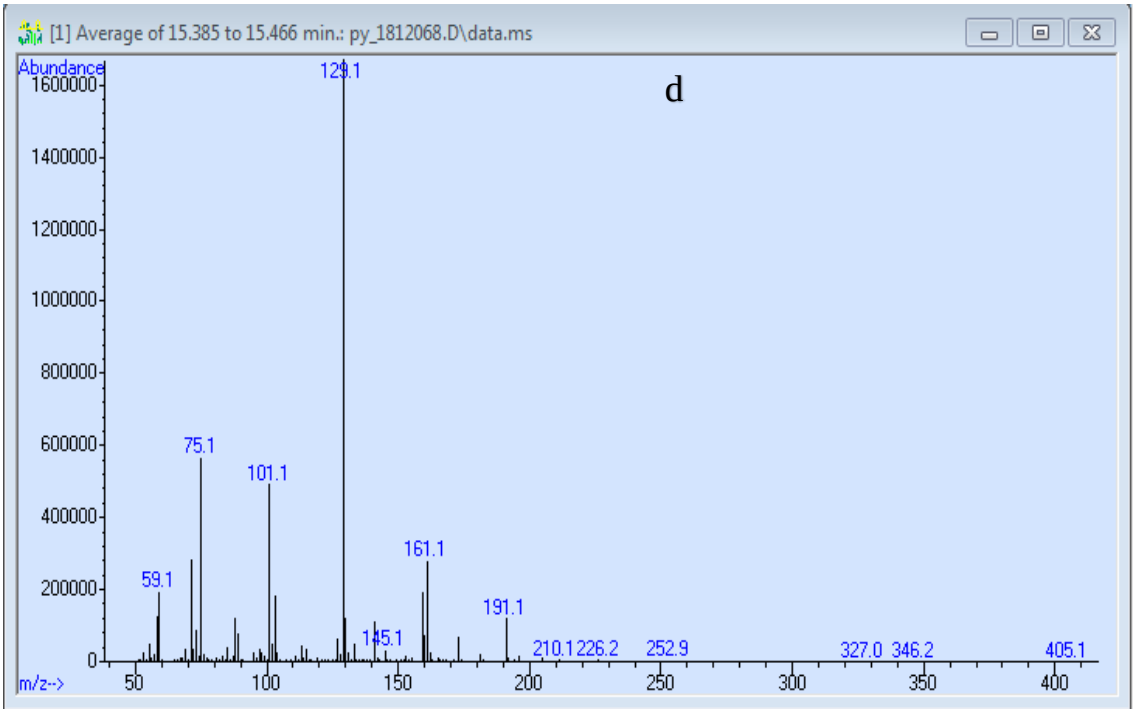

Figure S-50. MS of peak d (15.385 to 15.466 min) from Fig. S-46

Gallic Acid: TIC

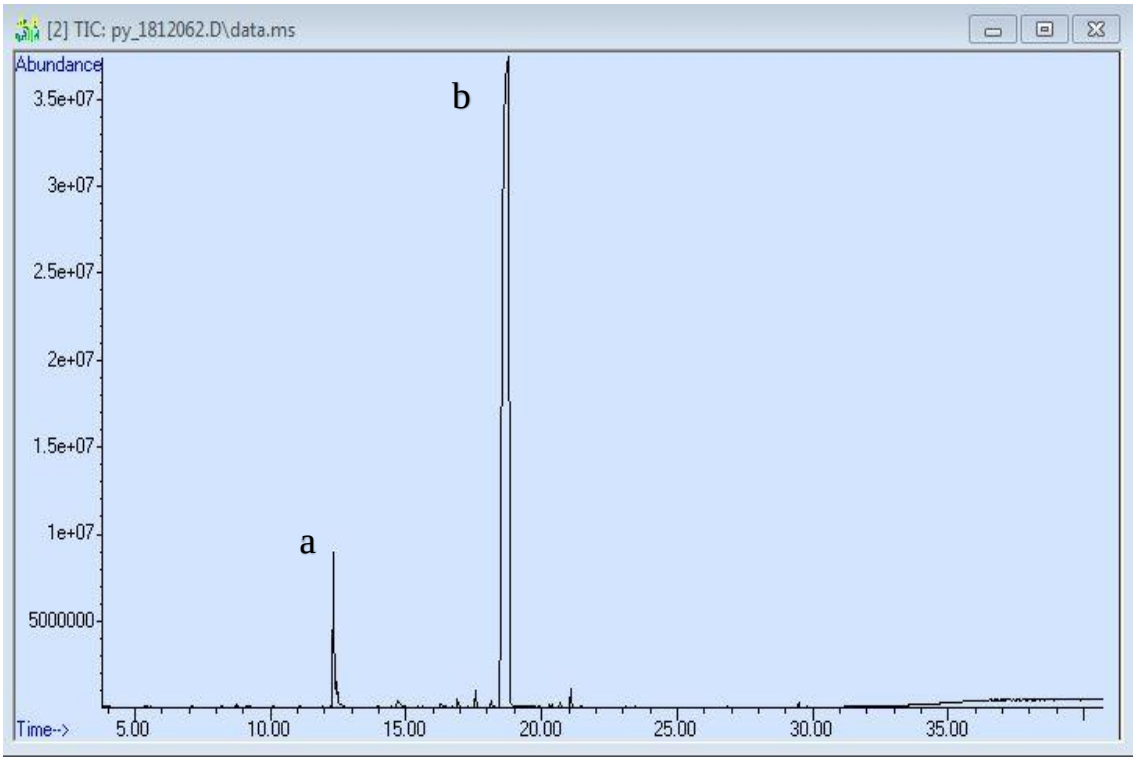

Figure S-51. TIC of Gallic Acid

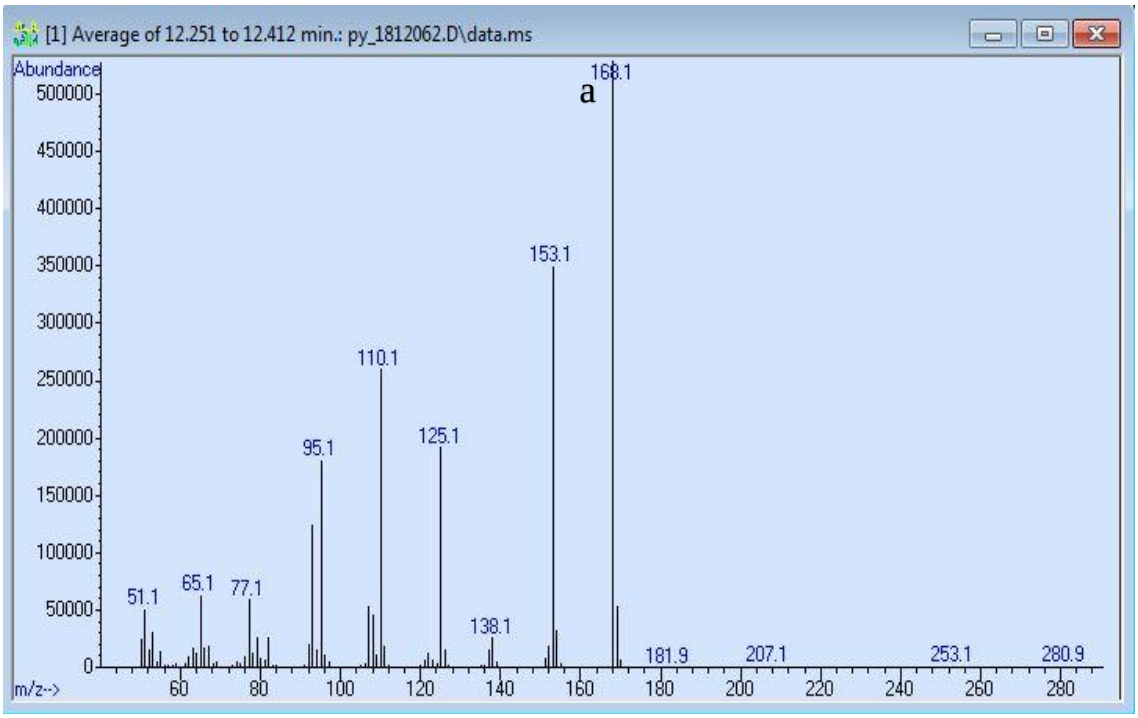

Figure S-52. MS of peak a (12.251 to 12.412 min) from Fig. S-51

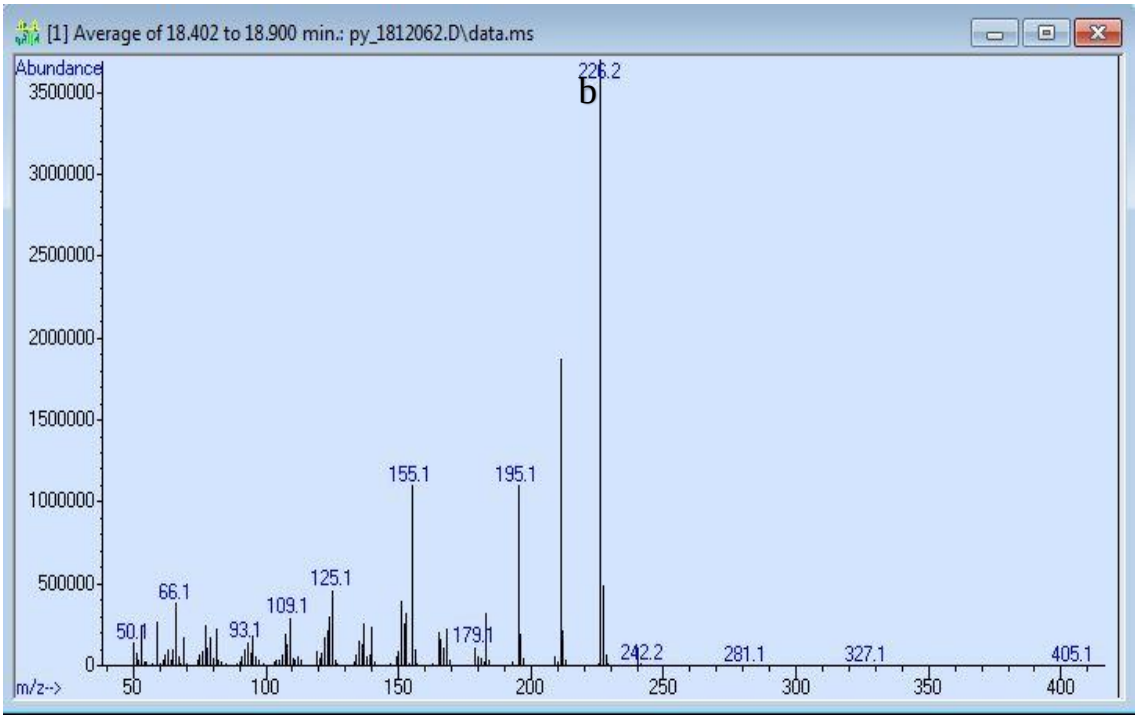

Figure S-53. MS of peak b (18.402 to 18.900 min) from Fig. S-51

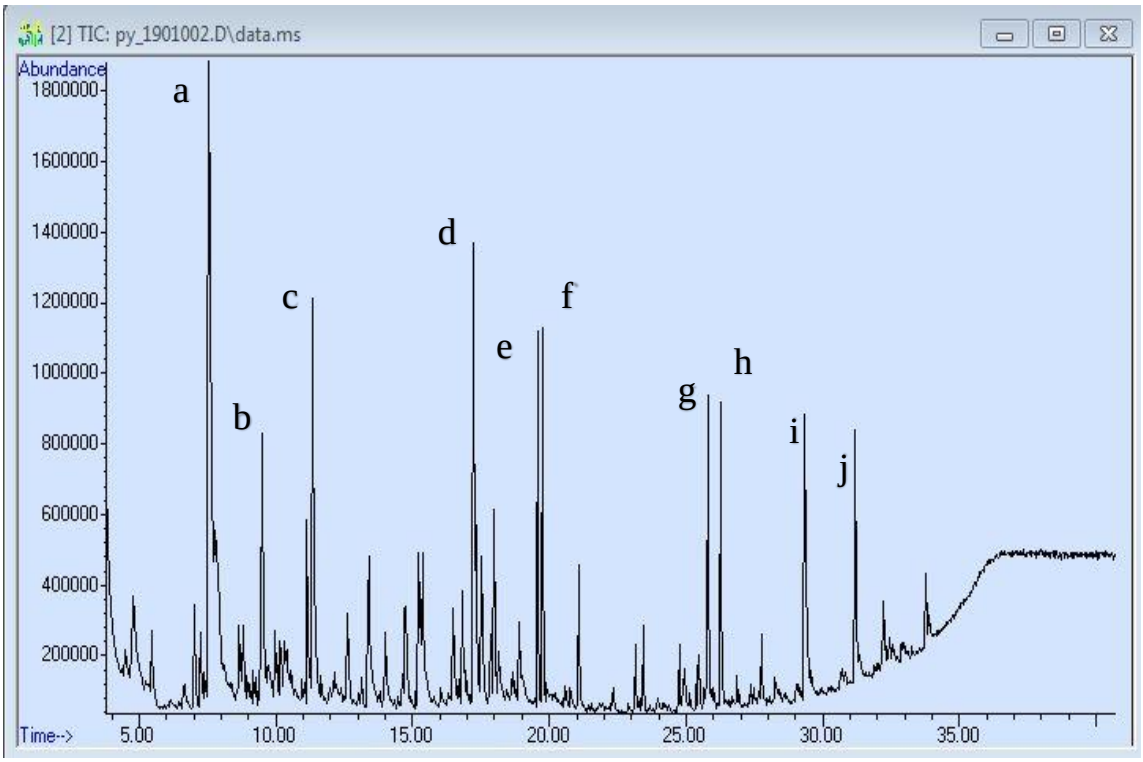

Figure S-54. TIC of Lignin Alkali

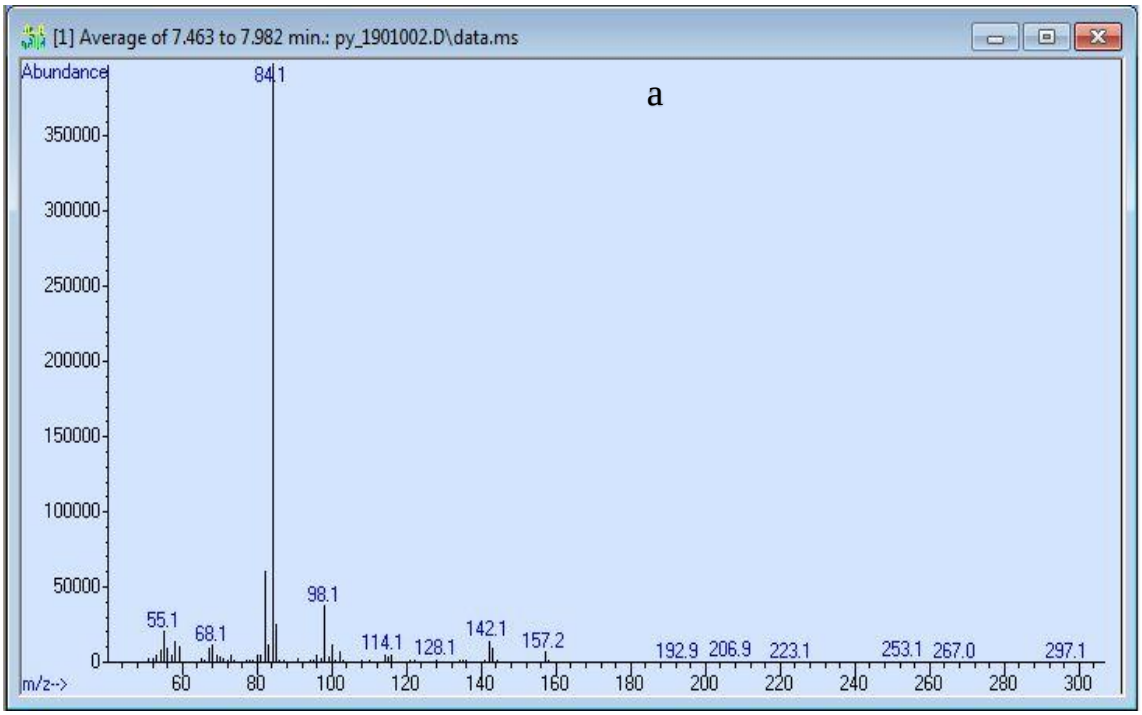

Figure S-55. MS of peak a (7.463 to 7.982 min) from Fig. S-54

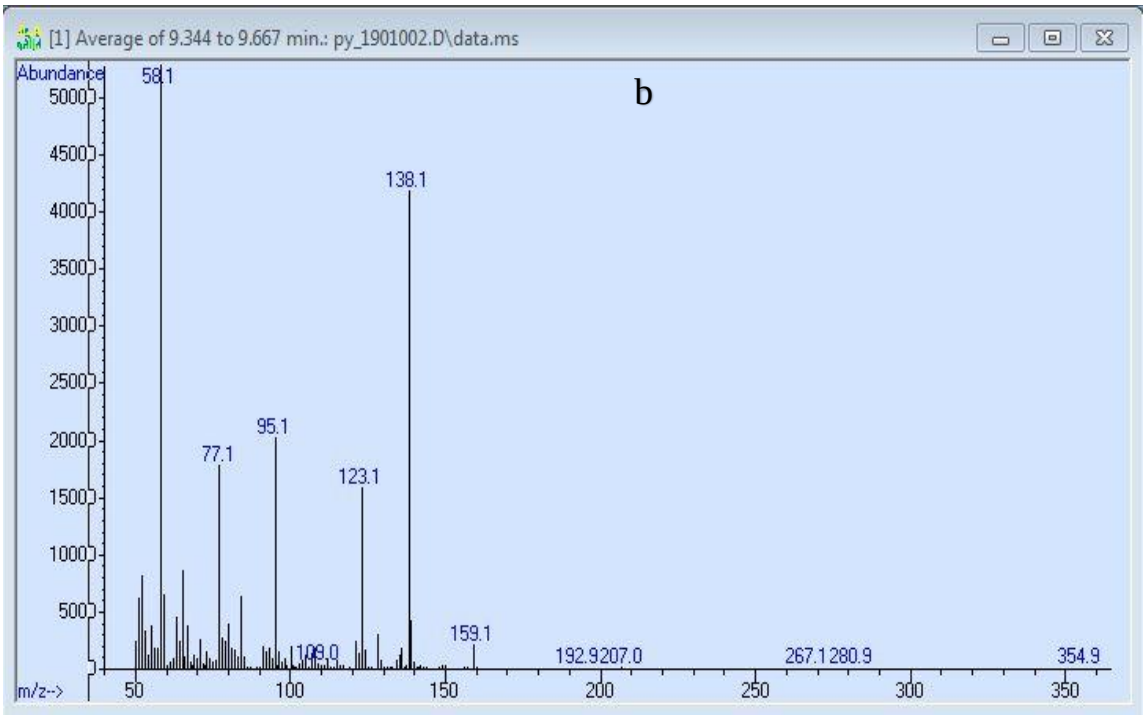

Figure S-56. MS of peak b (9.344 to 9.667 min) from Fig. S-54

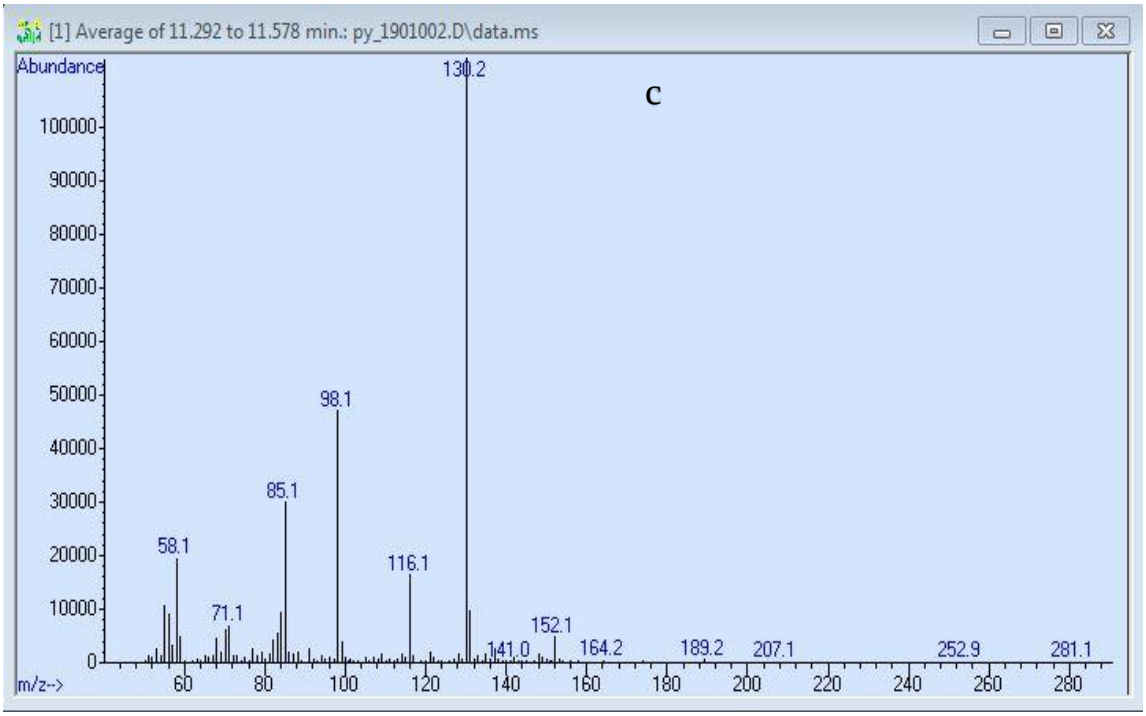

Figure S-57. MS of peak c (11.292 to 11.578 min) from Fig. S-54

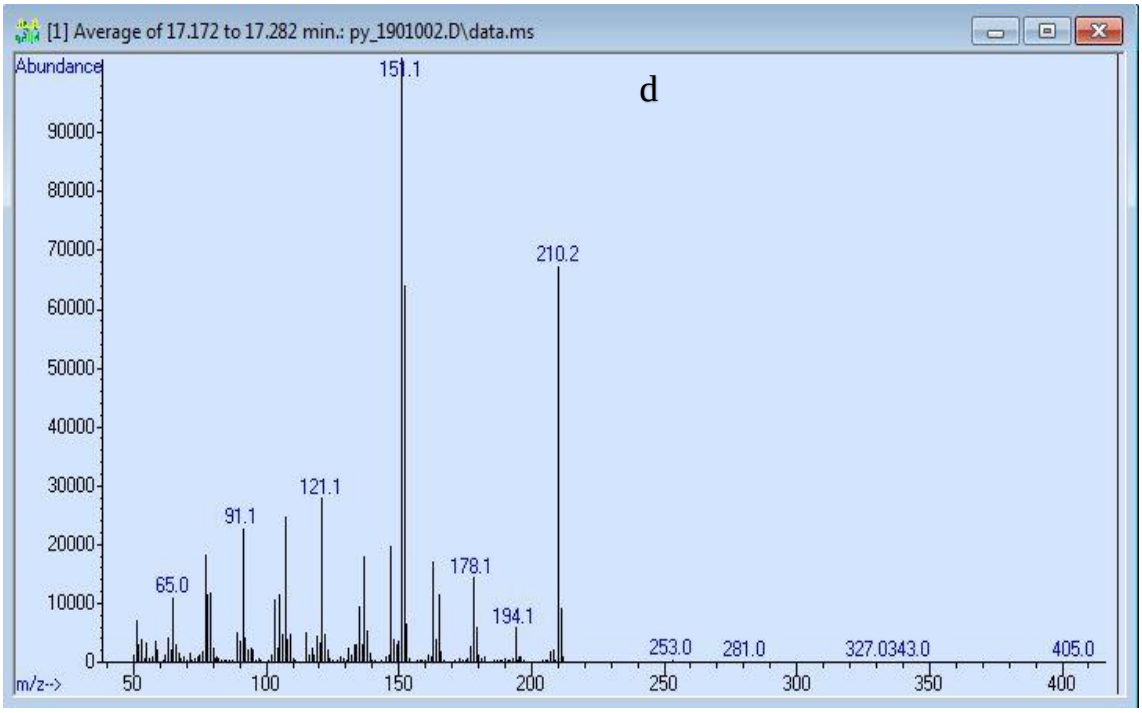

Figure S-58. MS of peak d (17.172 to 17.282 min) from Fig. S-54

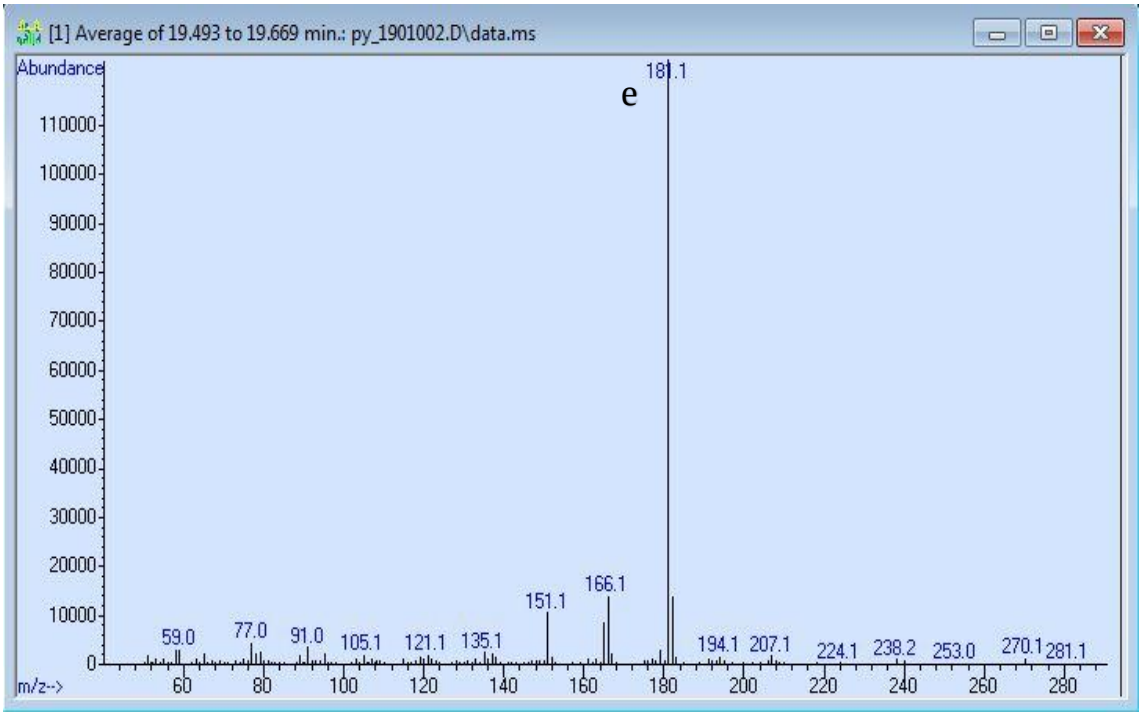

Figure S-59. MS of peak e (19.493 to 19.669 min) from Fig. S-54

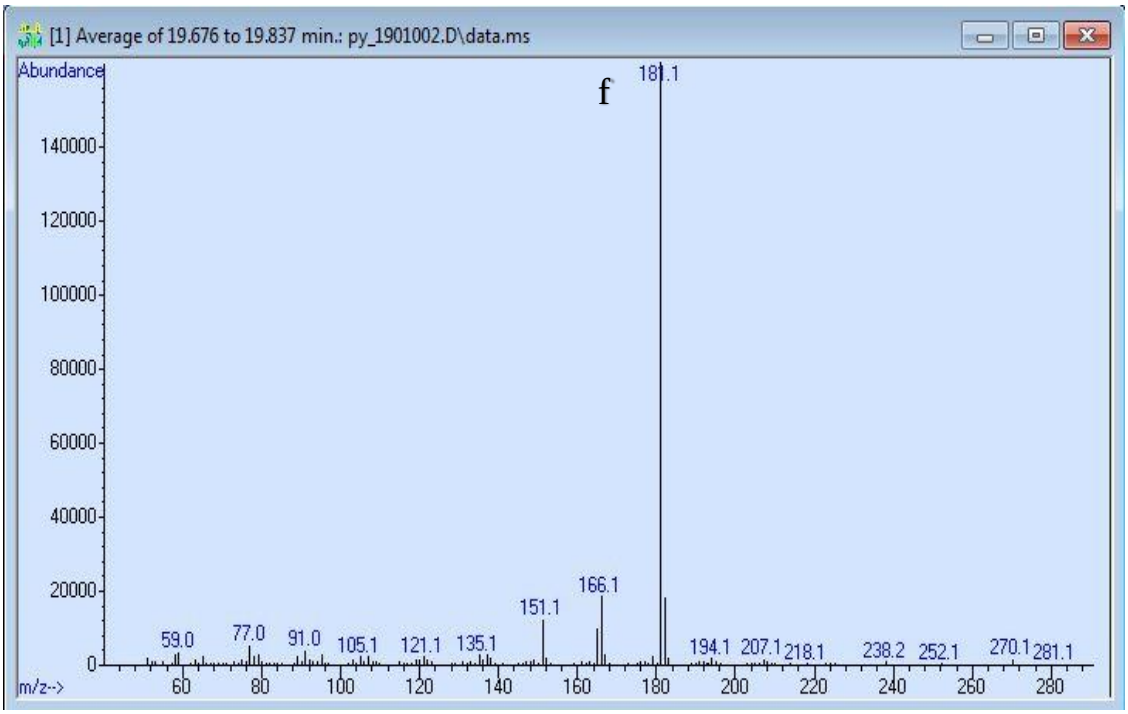

Figure S-60. MS of peak f (19.676 to 19.837 min) from Fig. S-54

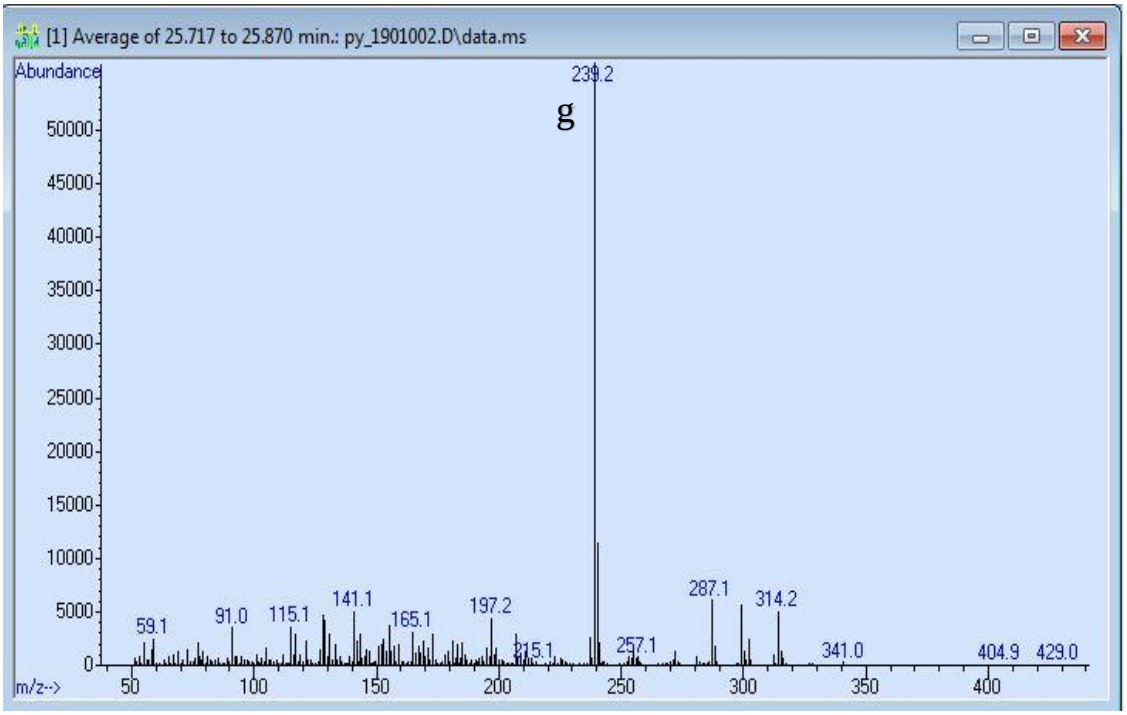

Figure S-61. MS of peak g (25.717 to 25.870 min) from Fig. S-54

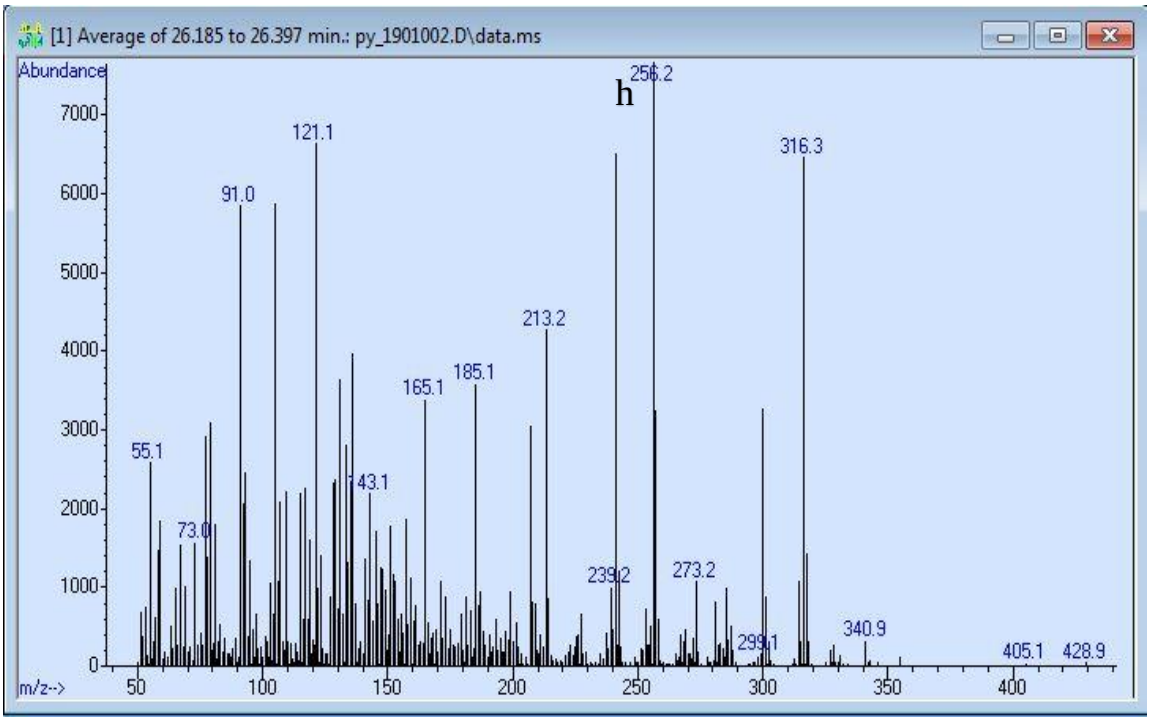

Figure S-62. MS of peak h (26.185 to 26.397 min) from Fig. S-54

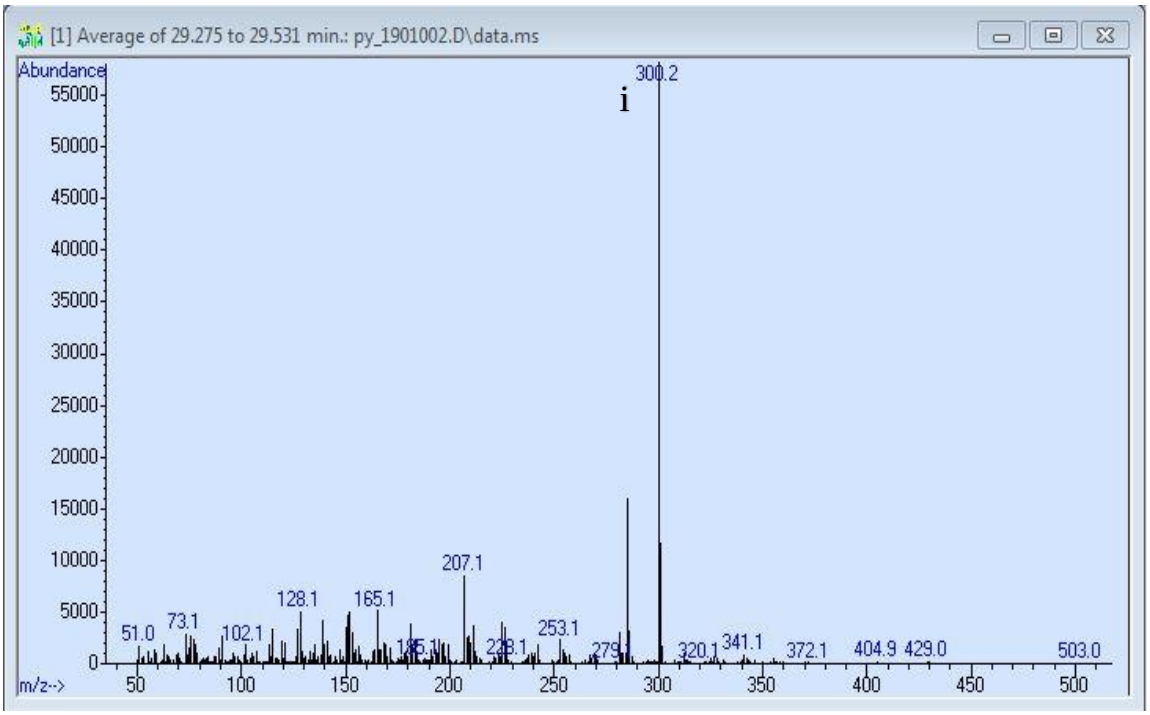

Figure S-63. MS of peak I (29.275 to 29.531 min) from Fig. S-54

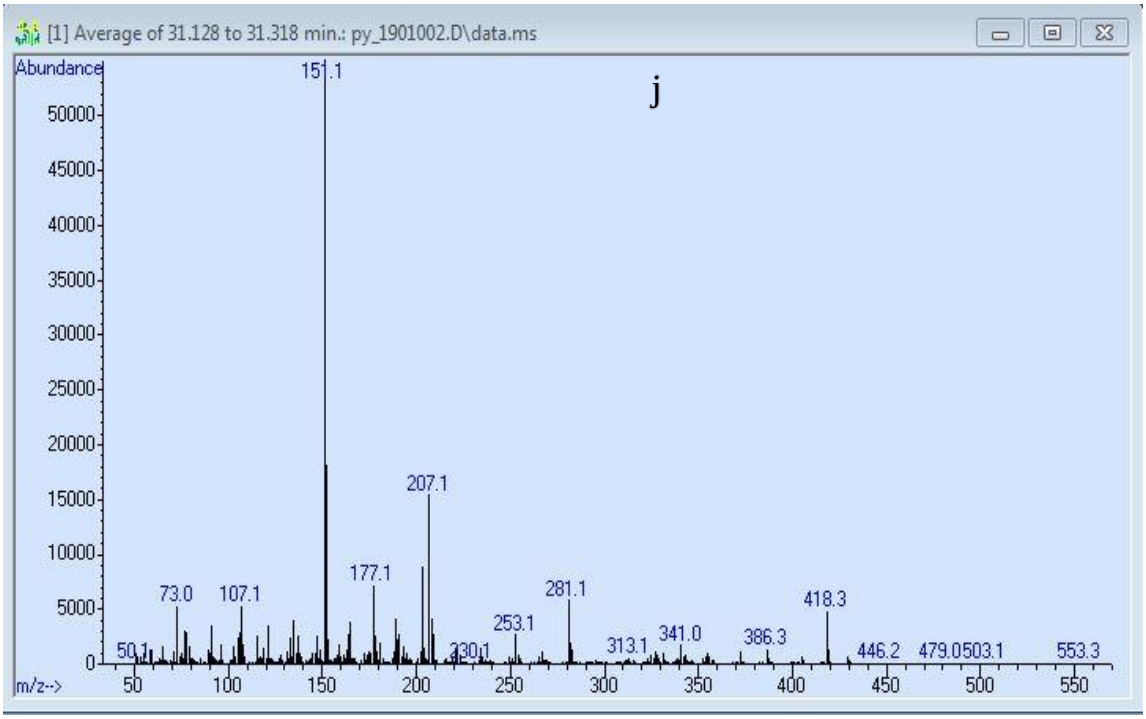

Figure S-64. MS of peak j (31.128 to 31.318 min) from Fig S-54

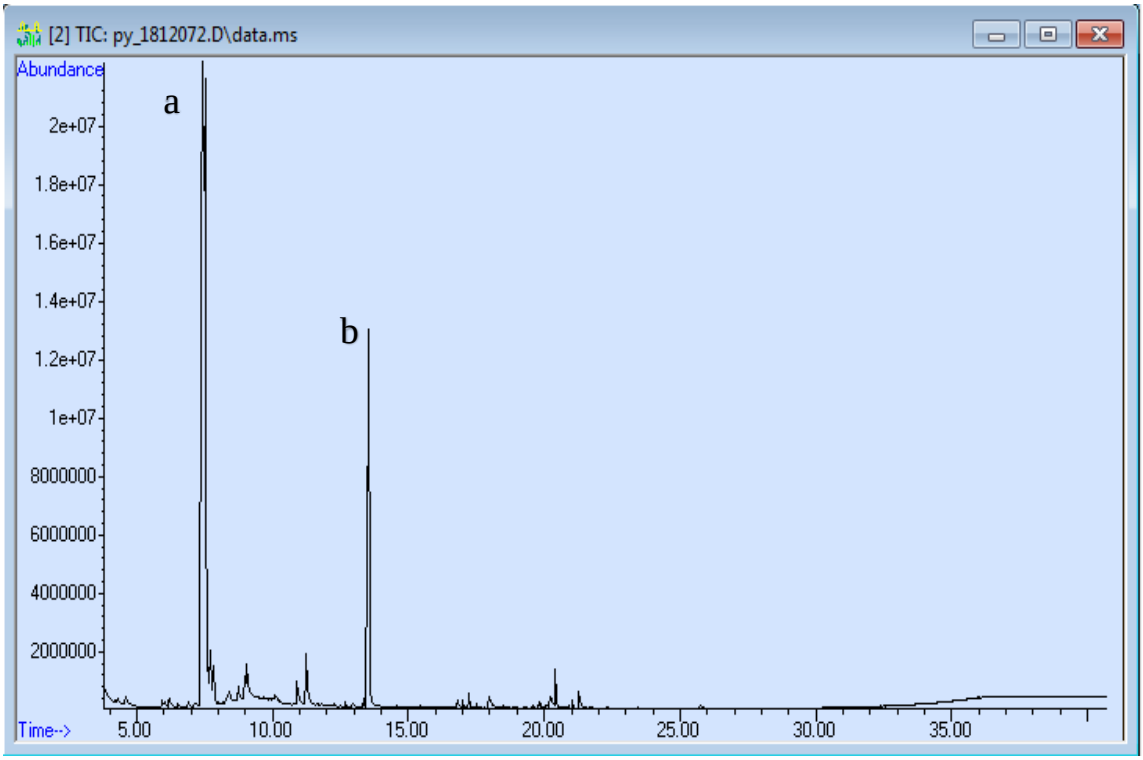

Figure S-65. TIC of L-proline

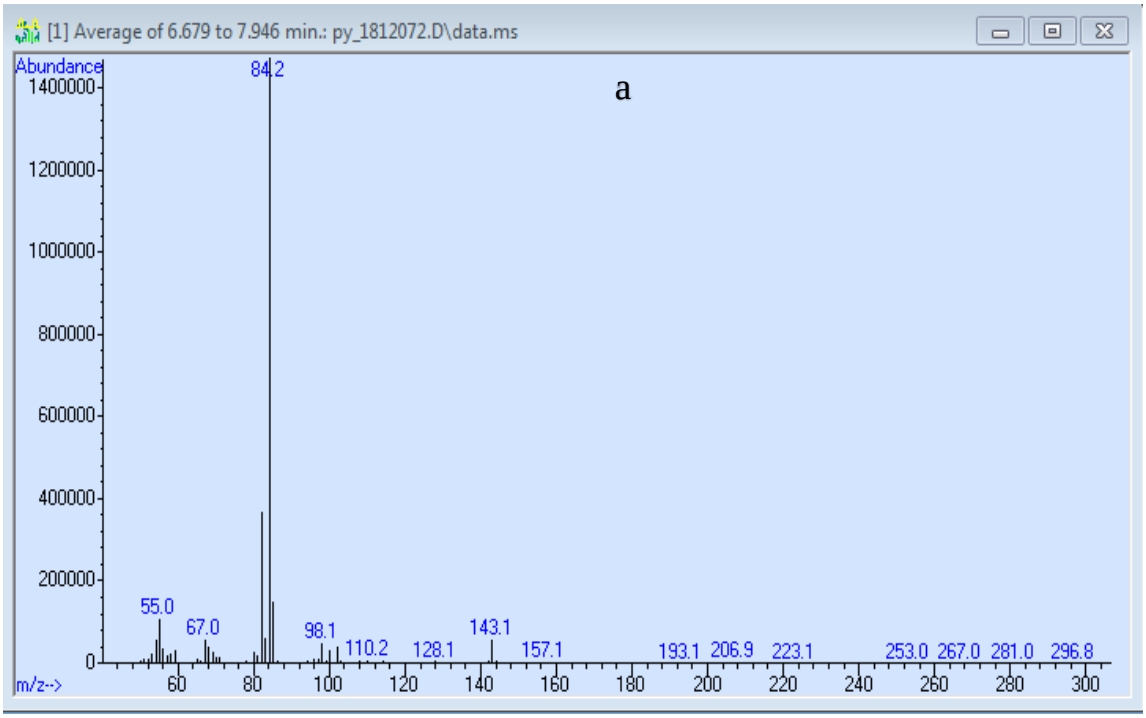

Figure S-66. MS of peak a (6.679 to 7.964 min) from Fig. S-65

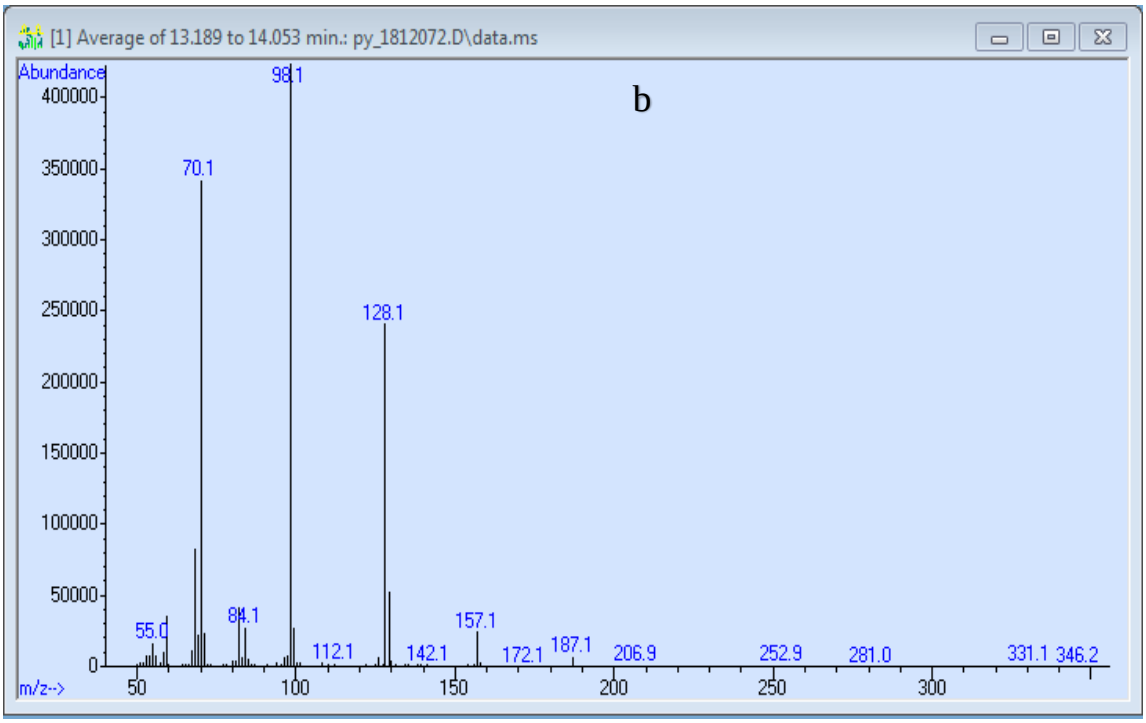

Figure S-67 peak b (13.189 to 14.053 min) from Fig. S-65

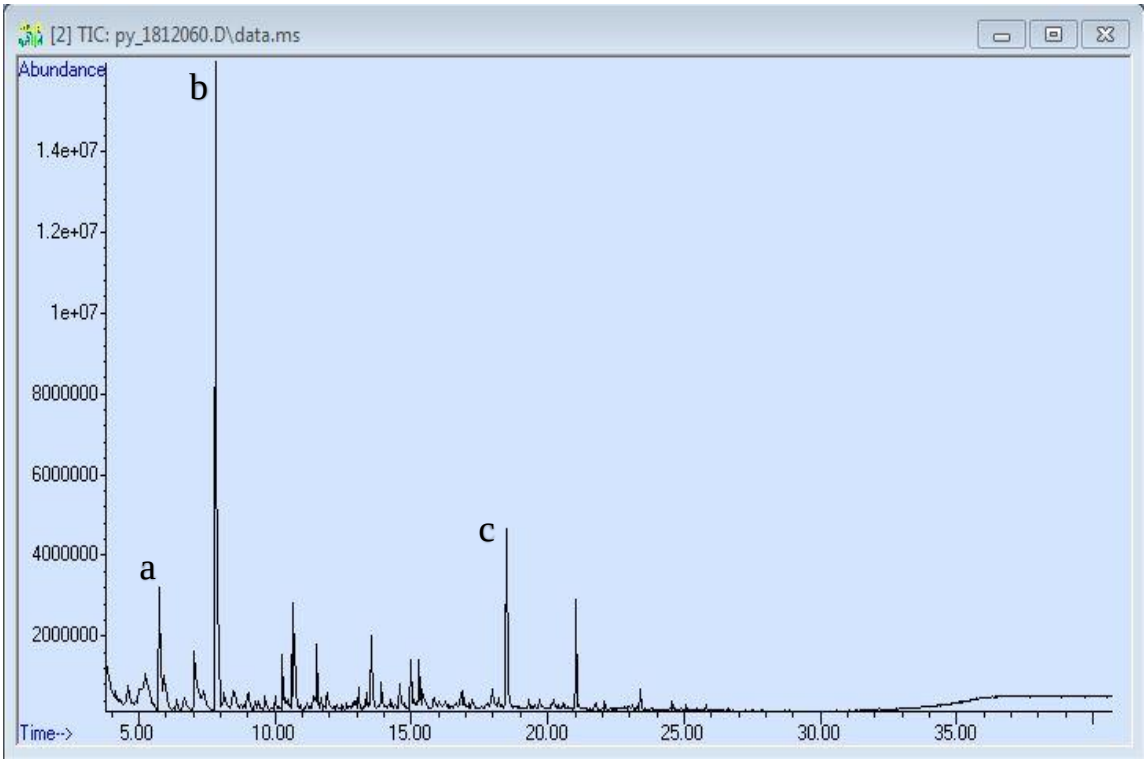

Figure S-68. TIC of L-serine

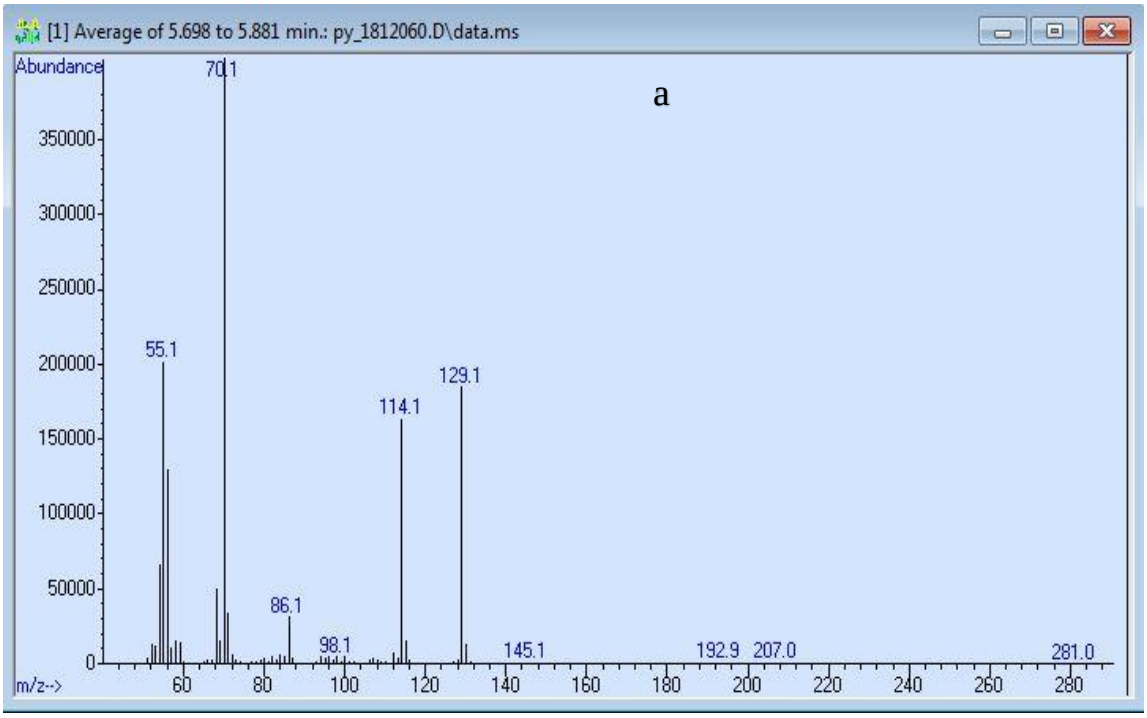

Figure S-69. MS of peak a (5.698 to 5.881 min) from Fig. S-68

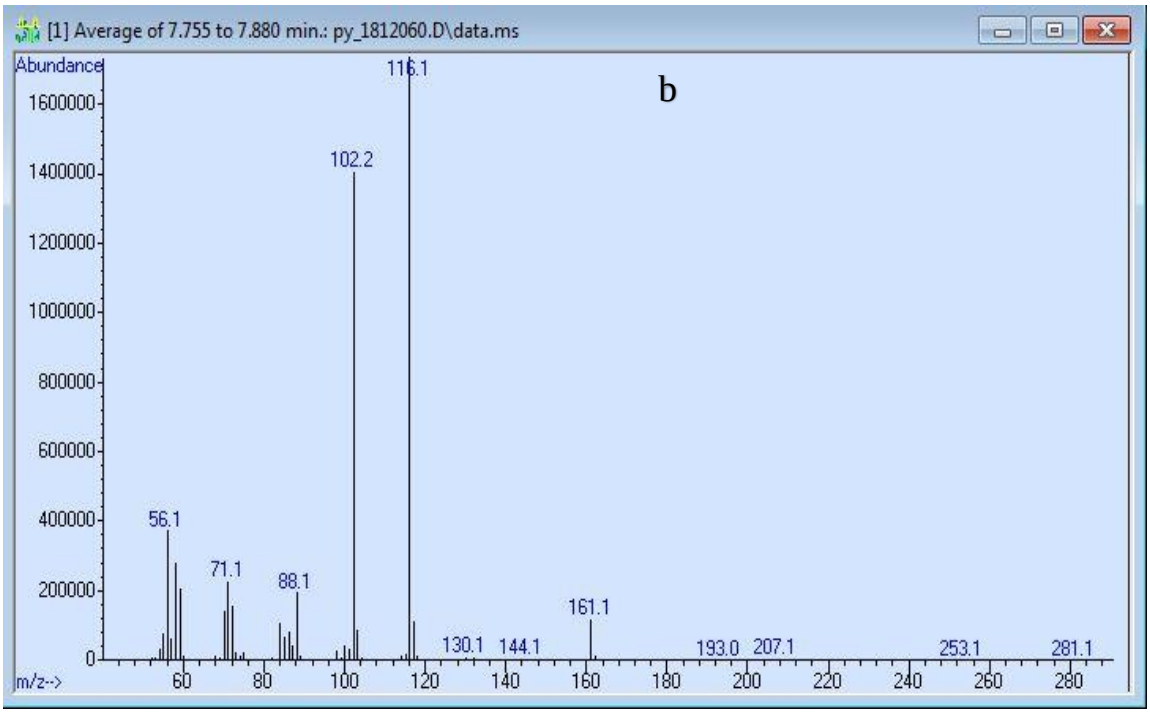

Figure S-70. MS of peak b (7.755 to 7.880 min) from Fig. S-68

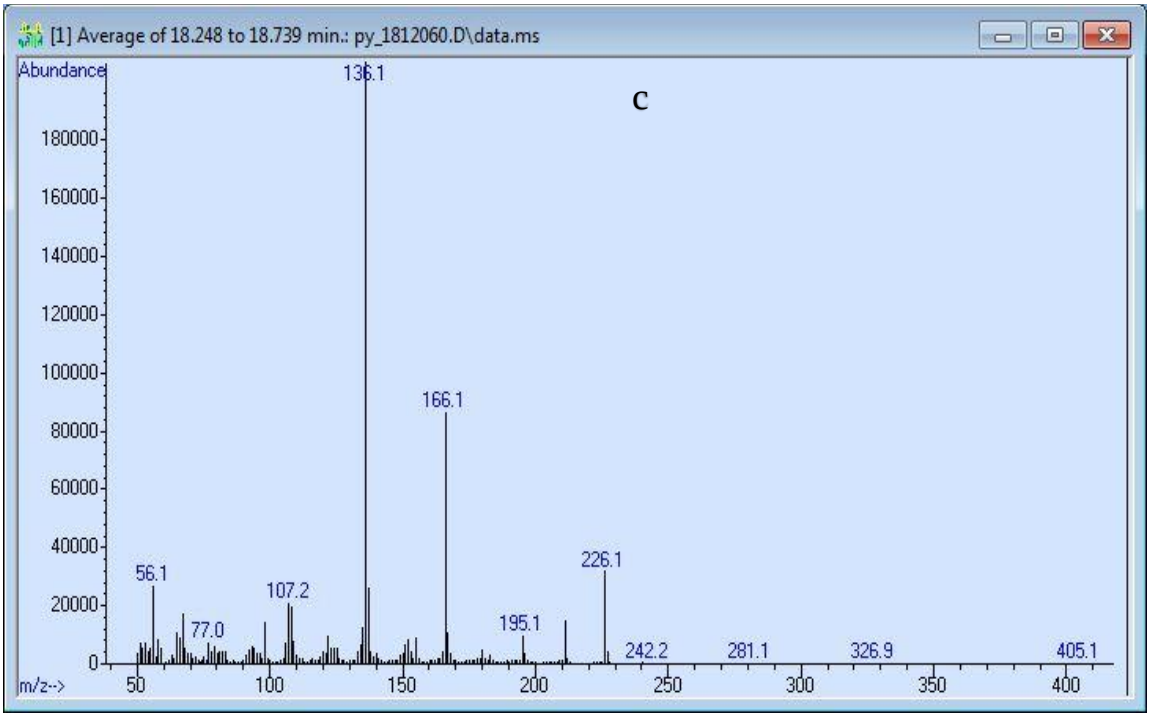

Figure S-71. MS of peak c (18.248 to 18.739 min) from Fig. S-68

L-Tyrosine: TIC

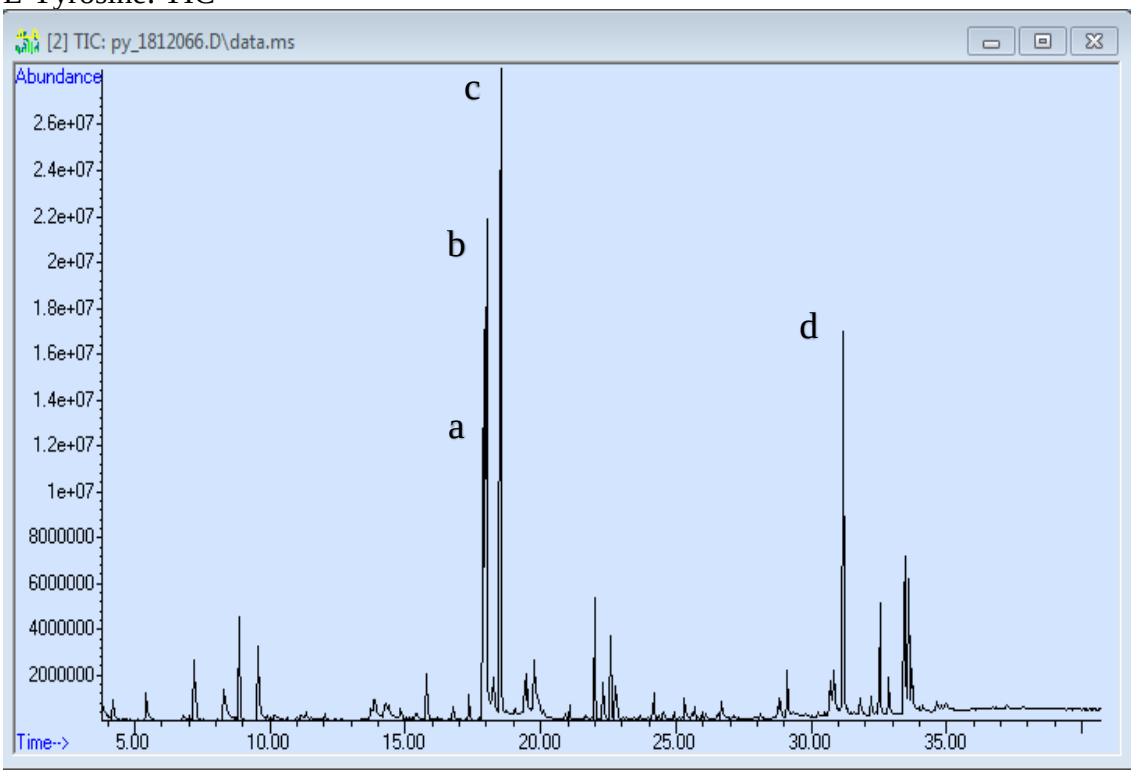

Figure S-72. TIC of L-tyrosine

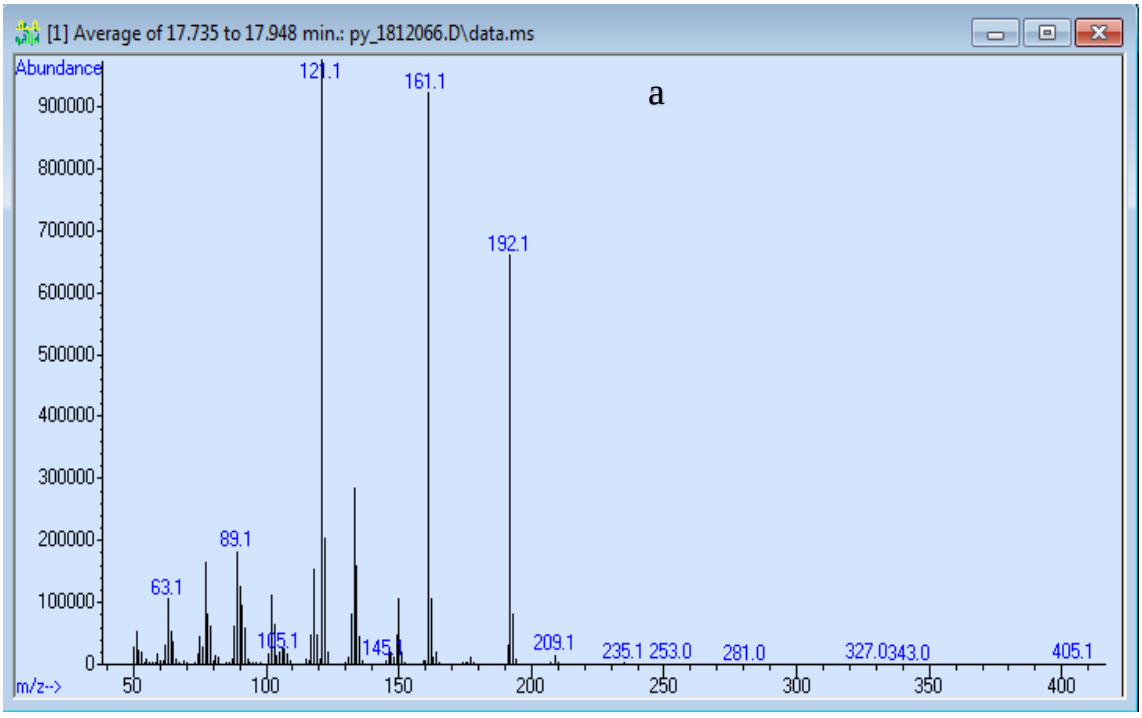

Figure S-73. MS of peak a (17.735 to 17.948 min) from Fig. S-72

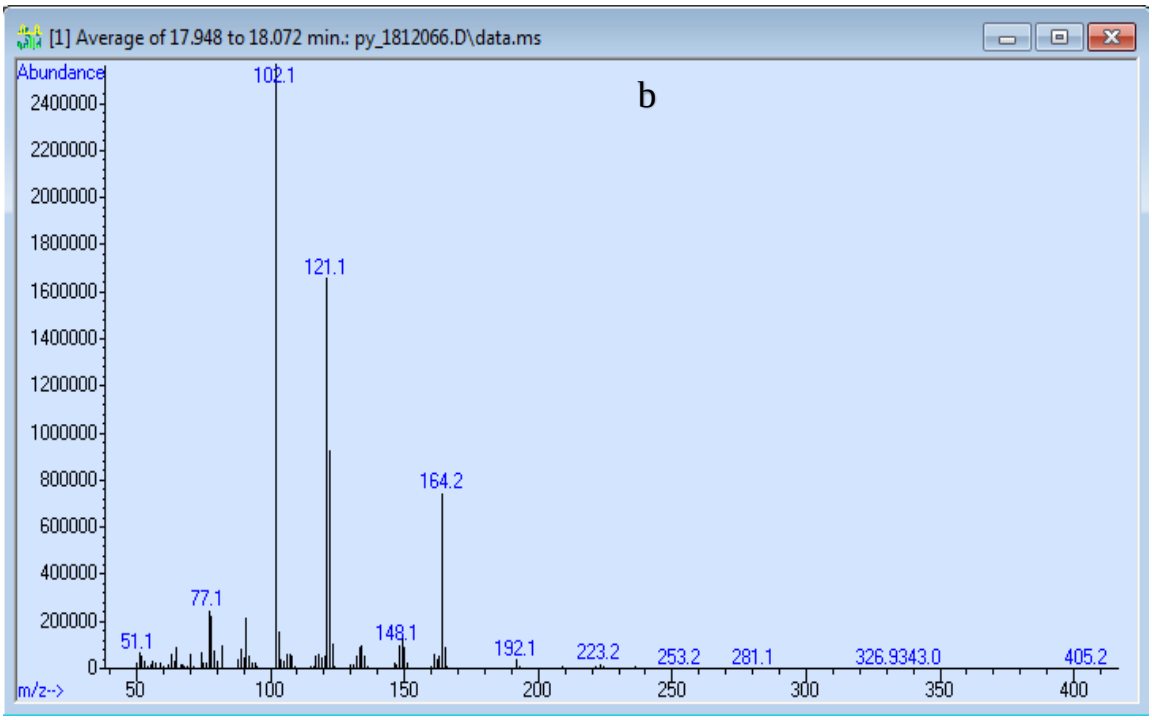

Figure S-74. MS of peak b (17.735 to 17.948 min) from Fig. S-72

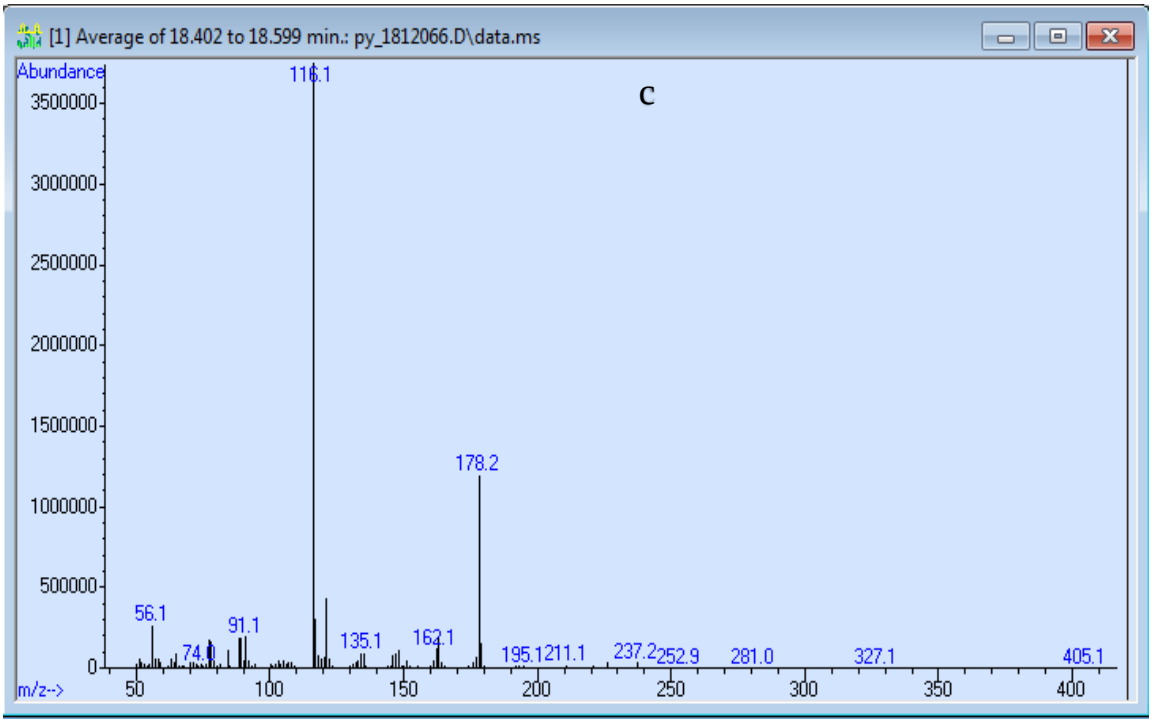

Figure S-75. MS of peak c (18.402 to 18.599 min) from Fig. S-72

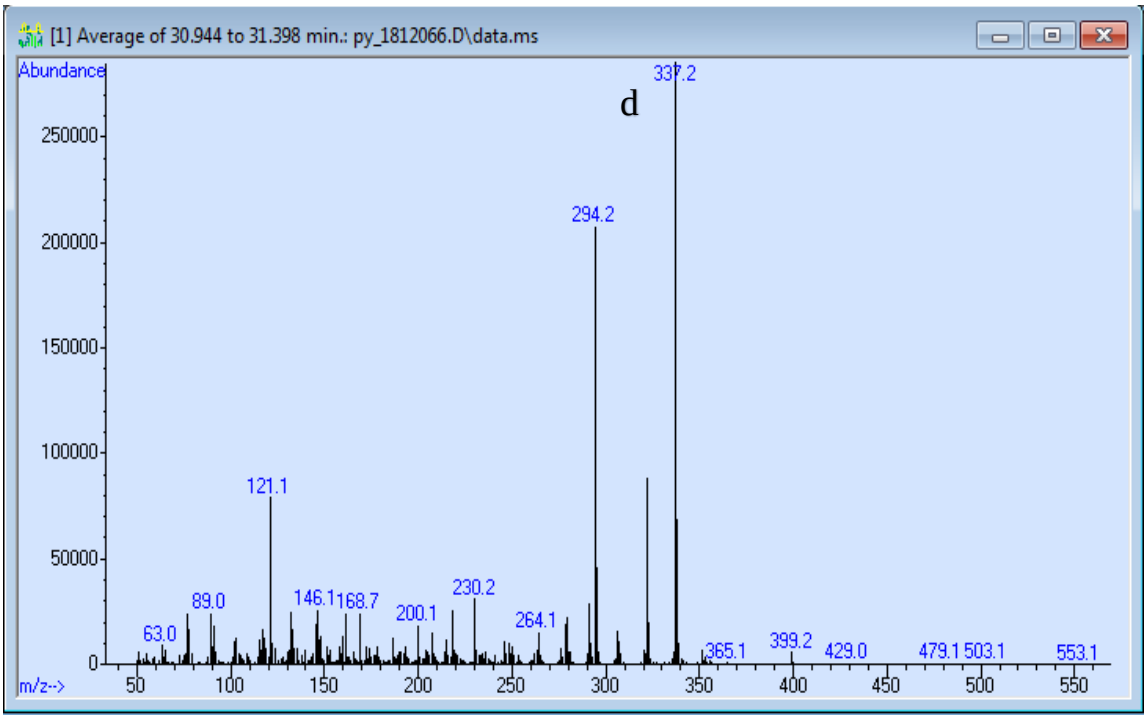

Figure S-76. MS of peak d (30.944 to 31.398 min) from Fig. S-72

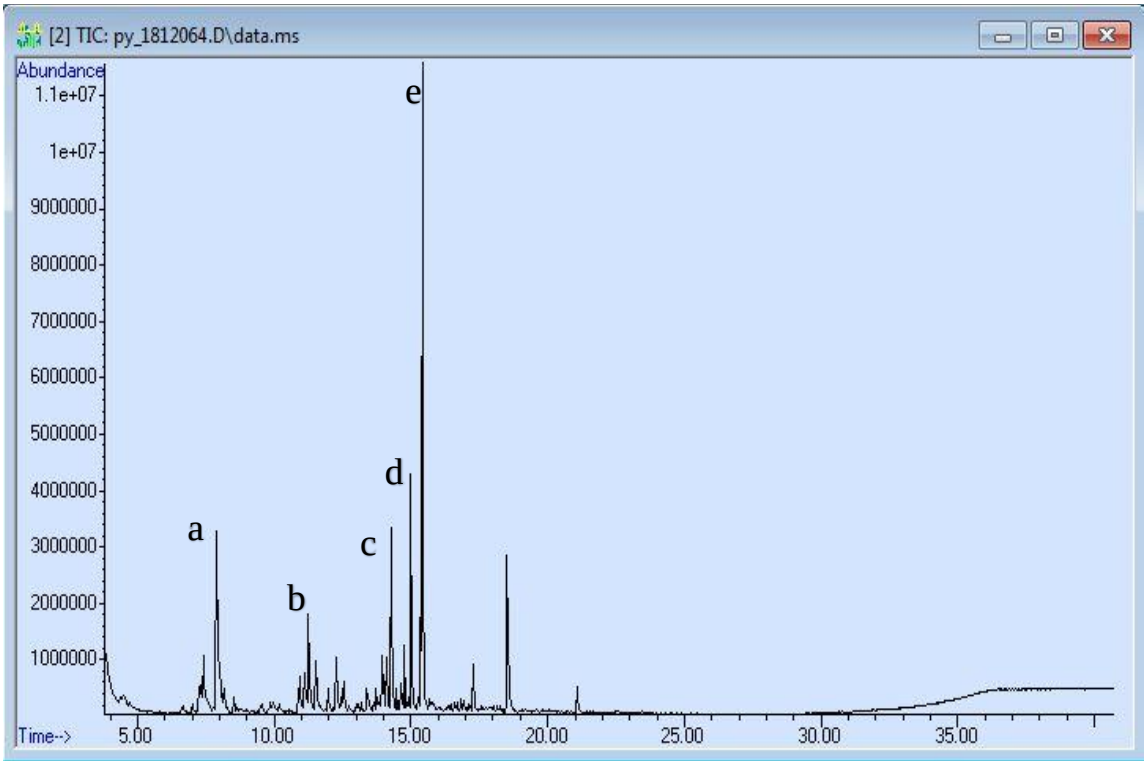

Figure S-77. TIC of Mannose

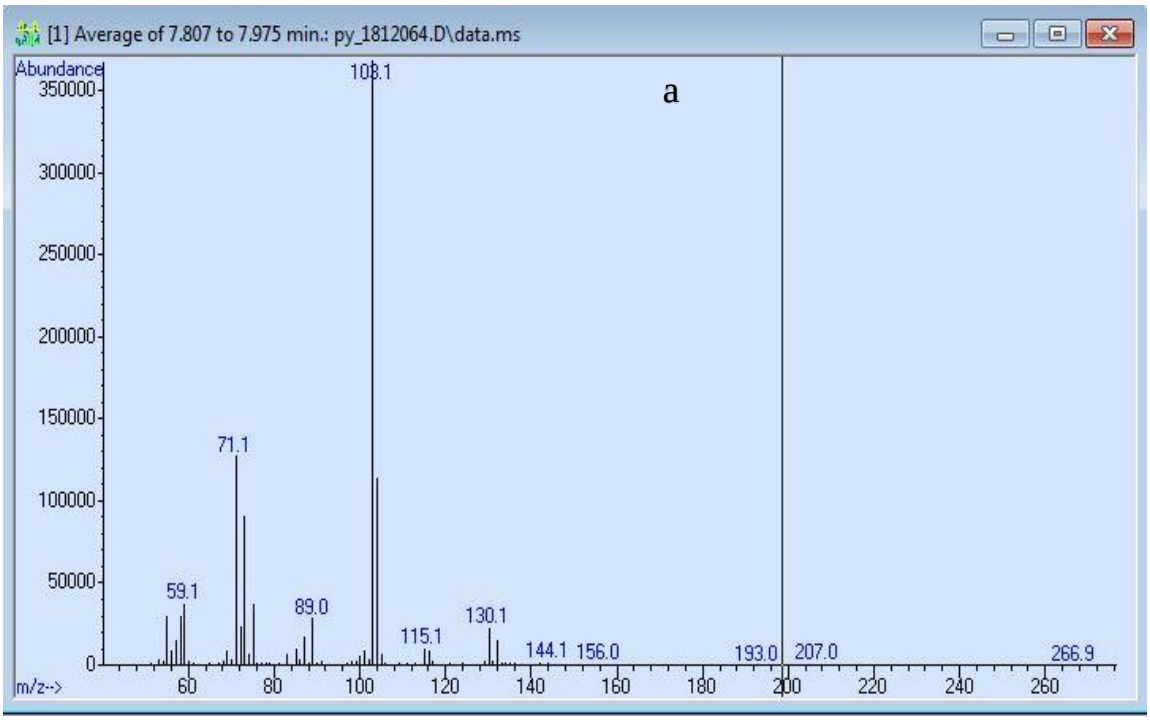

Figure S-78. MS of peak a (7.807 to 7.975 min) from Fig. S-77

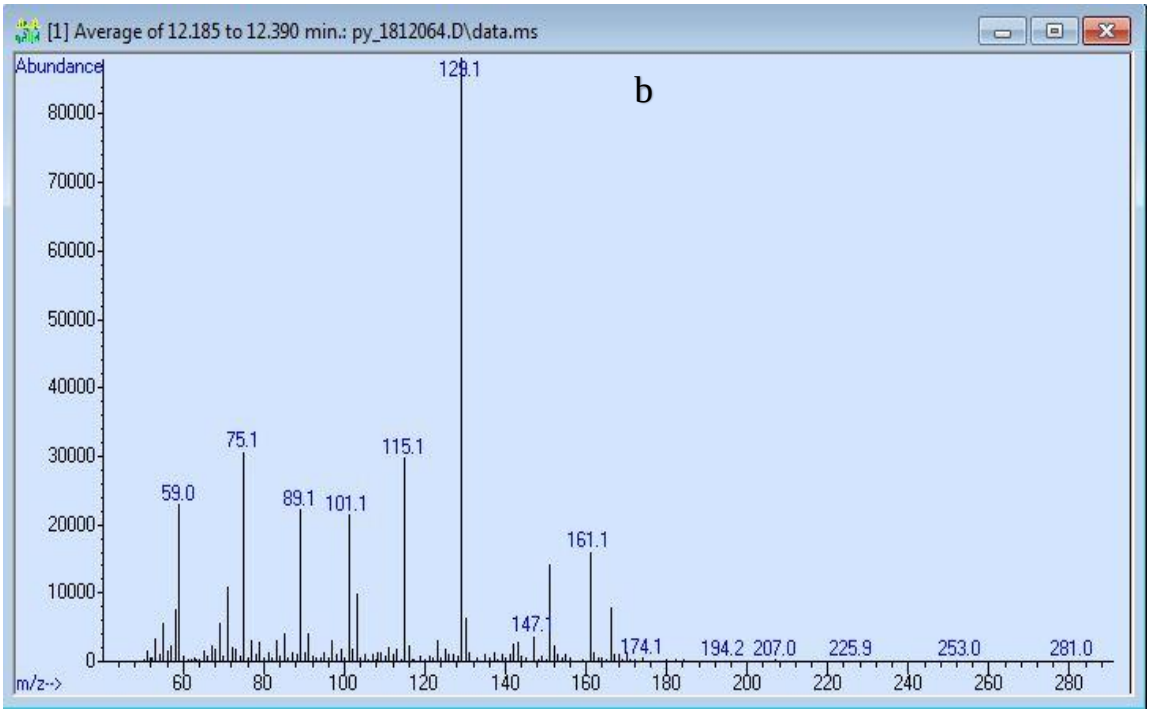

Figure S-79. MS of peak b (12.185 to 12.390 min) from Fig. S-77

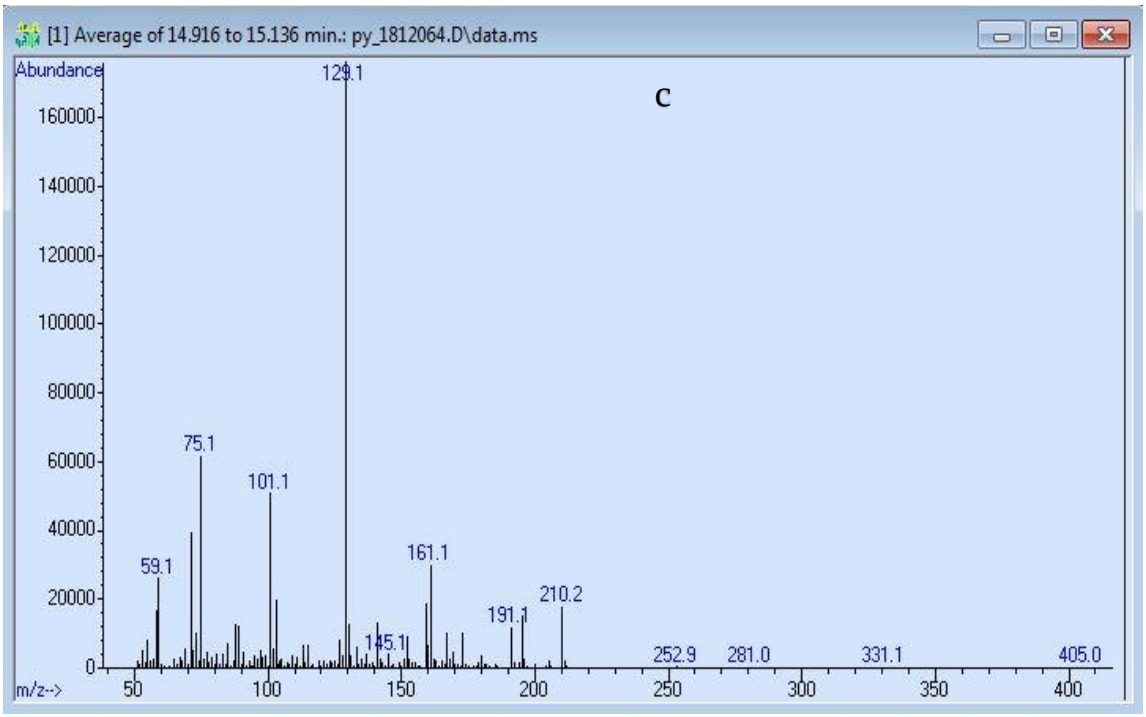

Figure S-80. MS of peak c (14.916 to 15.316 min) from Fig. S-77

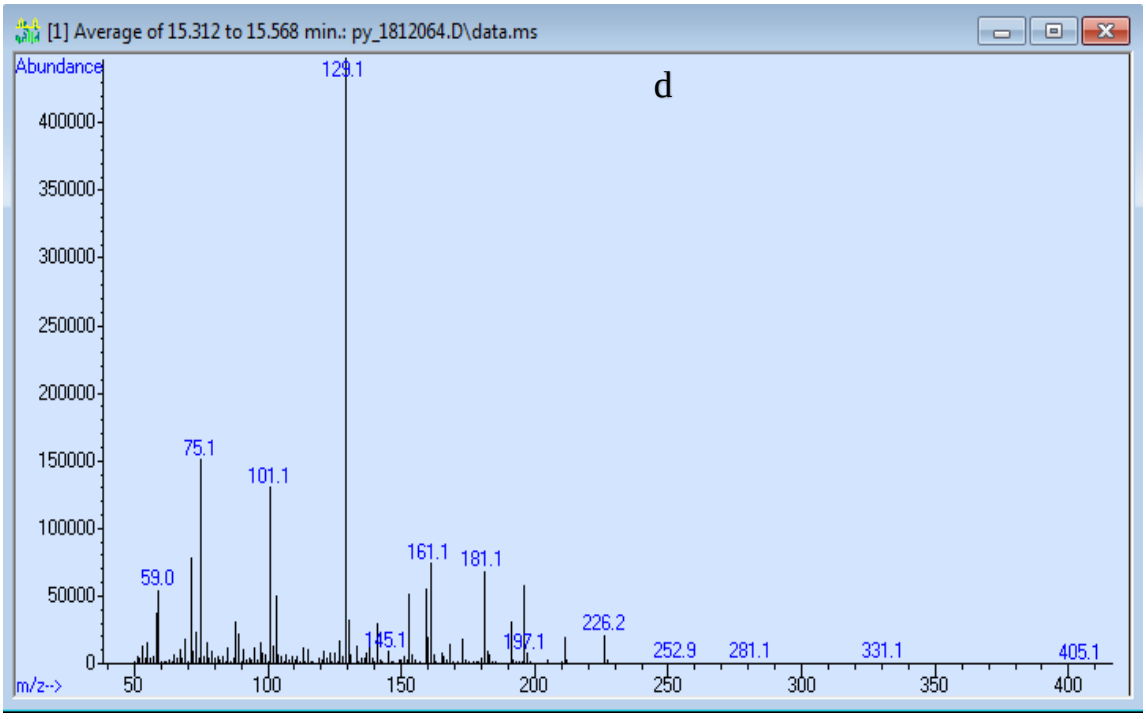

Figure S-81. MS of peak d (14.916 to 15.316 min) from Fig. S-77

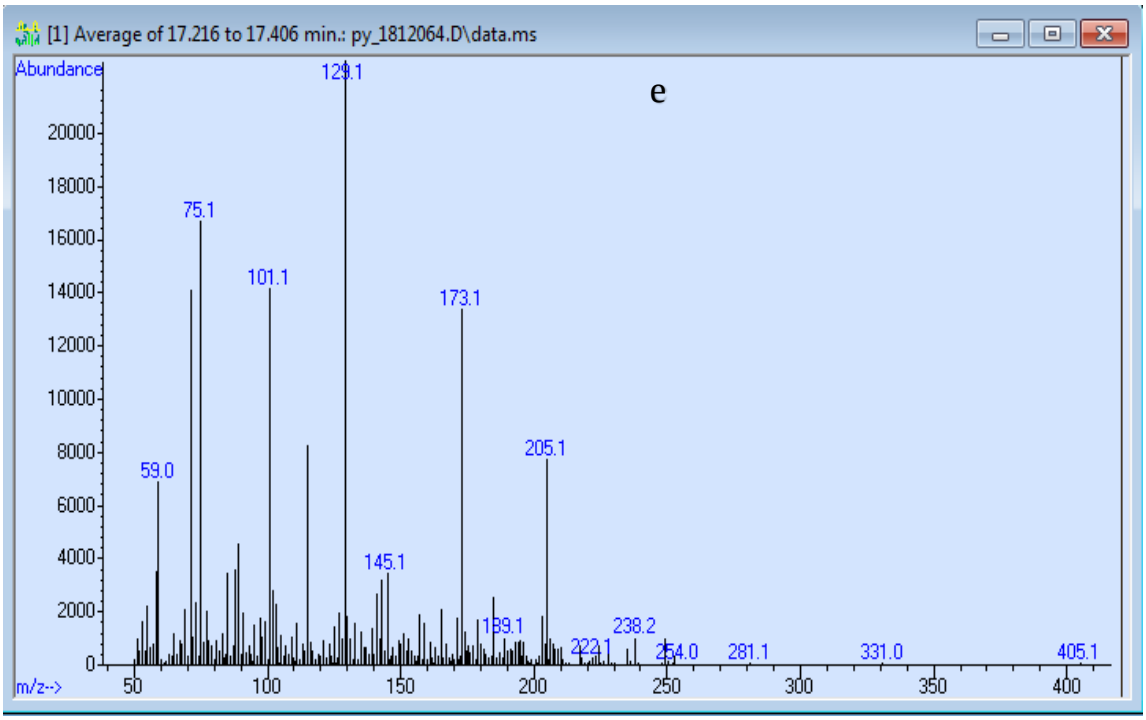

Figure S-82. MS of peak e (17.216 to 17.406 min) from Fig. S-77

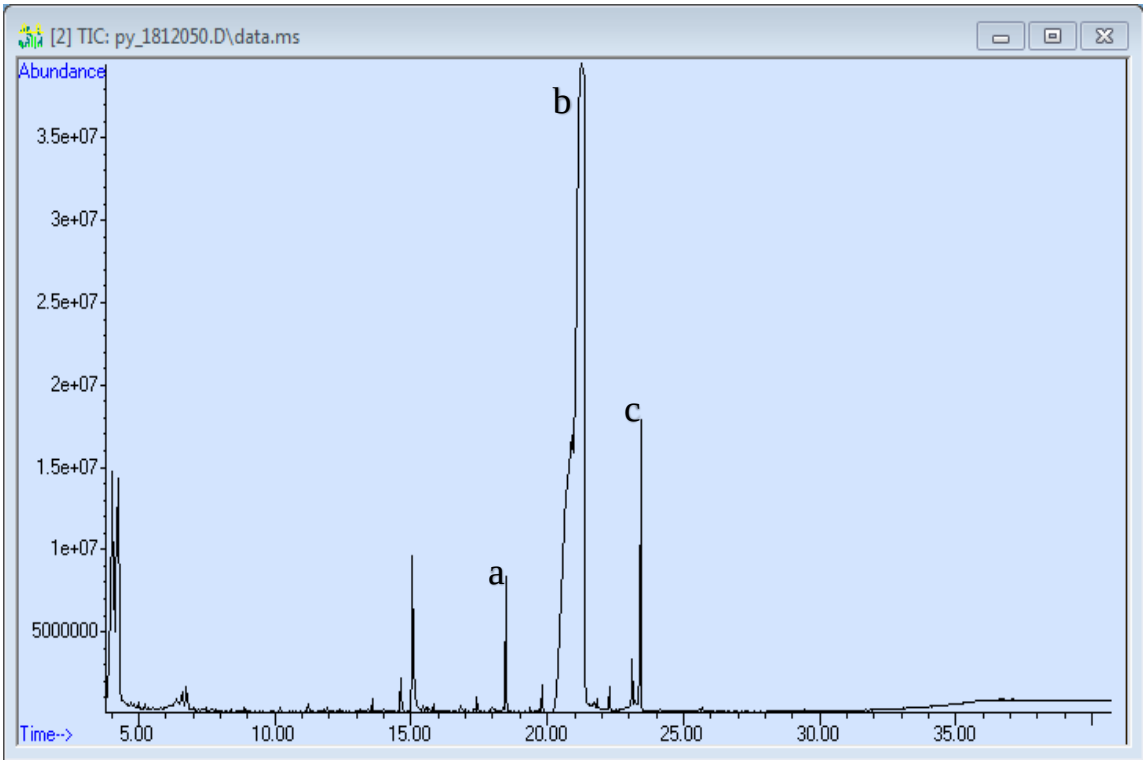

Figure S-83. TIC of palmitic acid

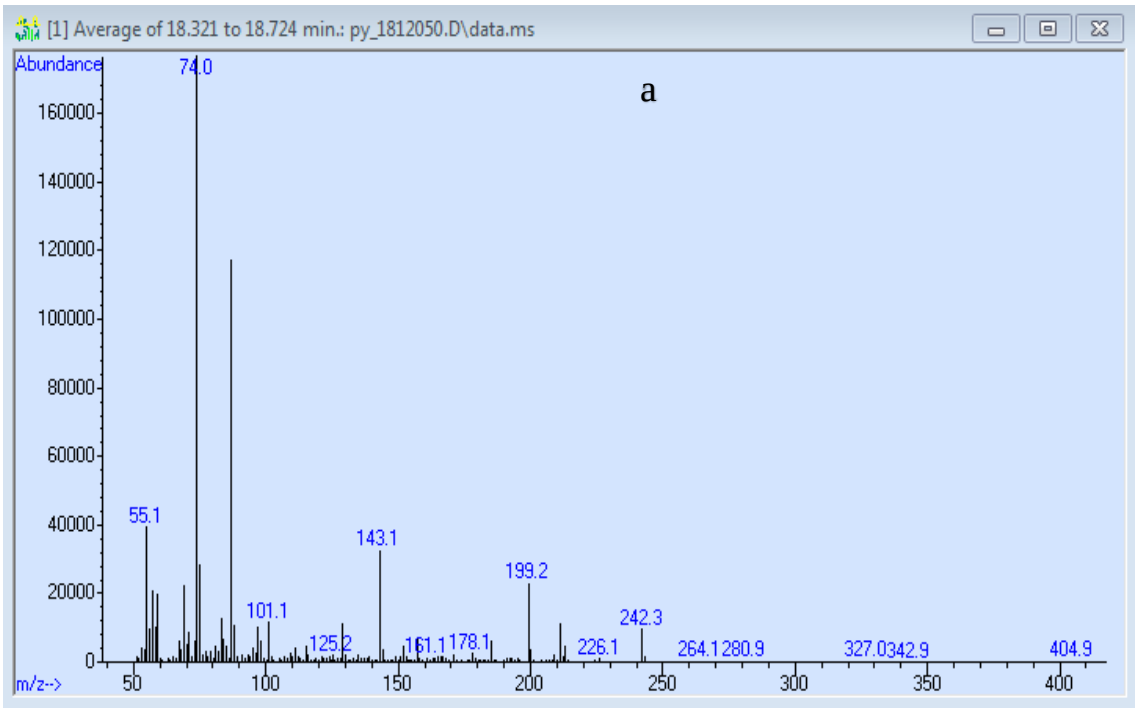

Figure S-84. MS of peak a (18.231 to 18.724 min) from Fig. S-83.

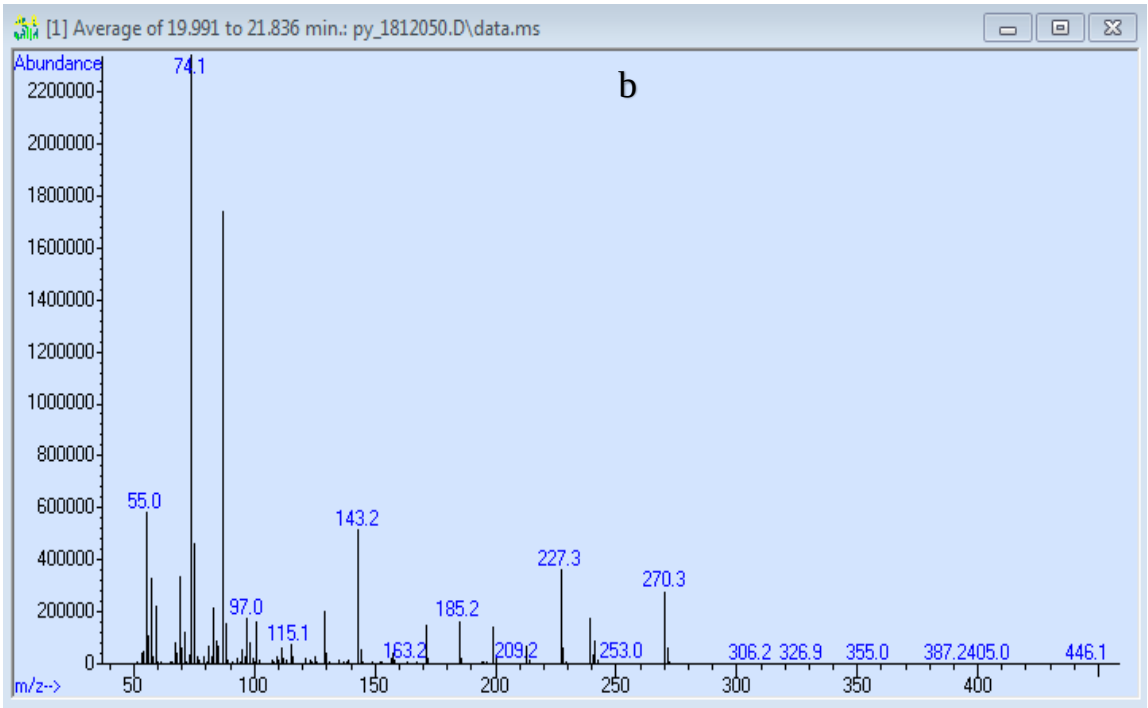

Figure S-85. MS of peak b (19.991 to 21.836 min) from Fig. S-83

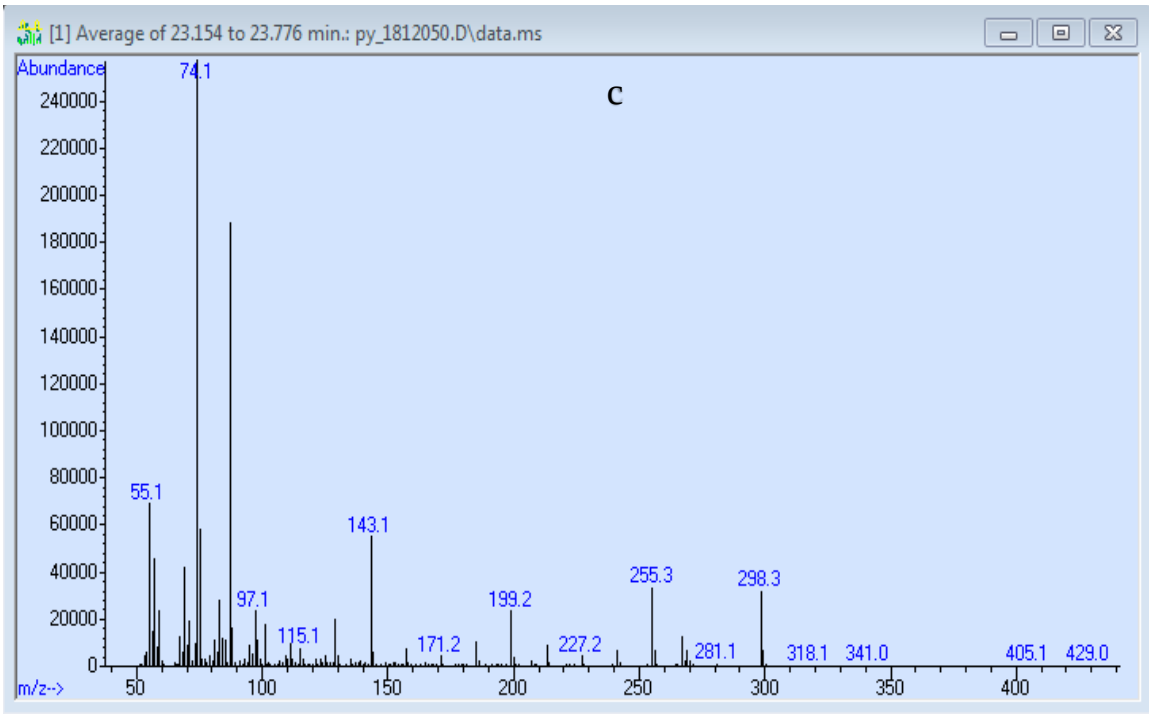

Figure S-86. MS of peak c (23.154 to 23.776 min) from Fig. S-83

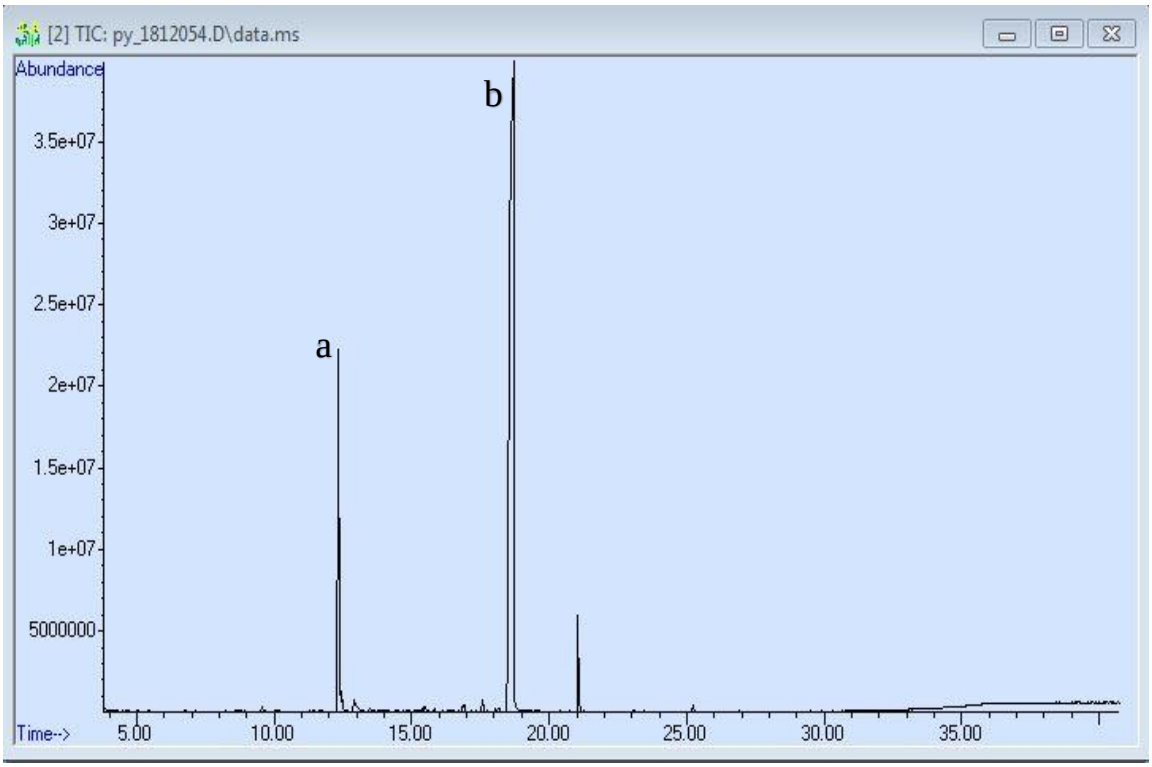

Figure S-87. TIC of tannic acid

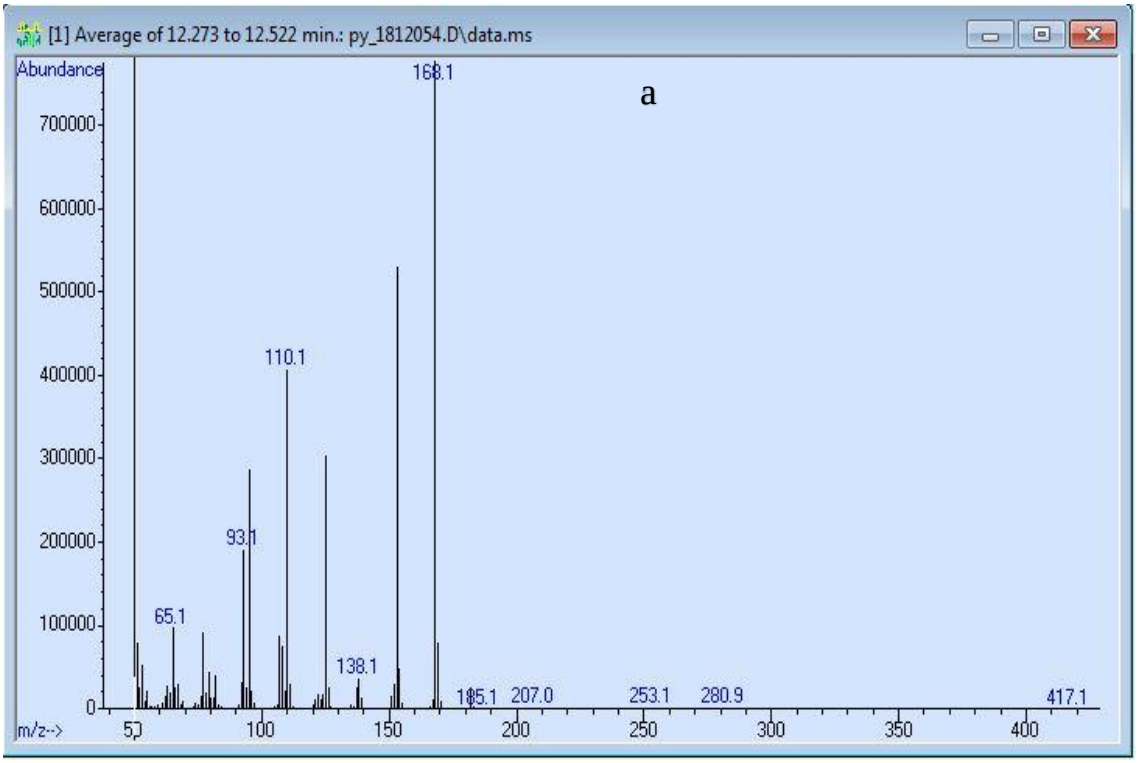

Figure S-88. MS of peak a (12.273 to 12.522 min) from Fig.S- 87

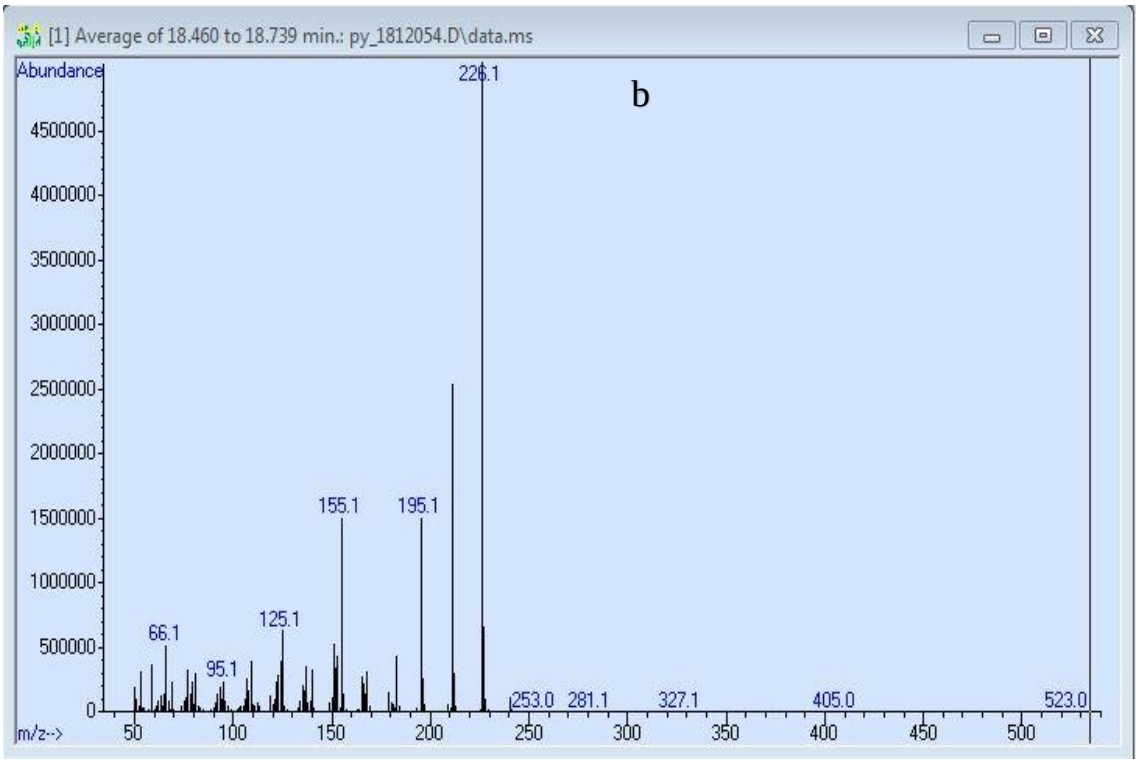

Figure S-89. MS of peak b (18.460 to 18.739 min) from Fig. S-87.

Trans Cinnamic Acid: TIC

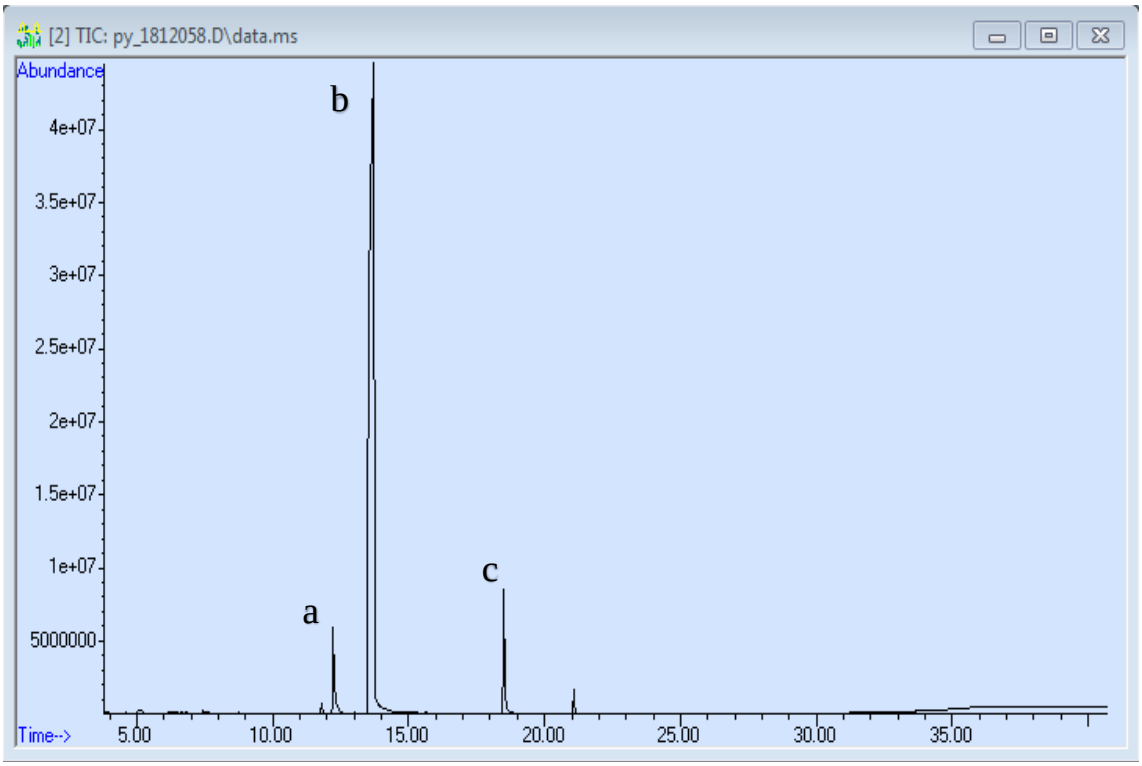

Figure S-90. TIC of trans cinnamic acid

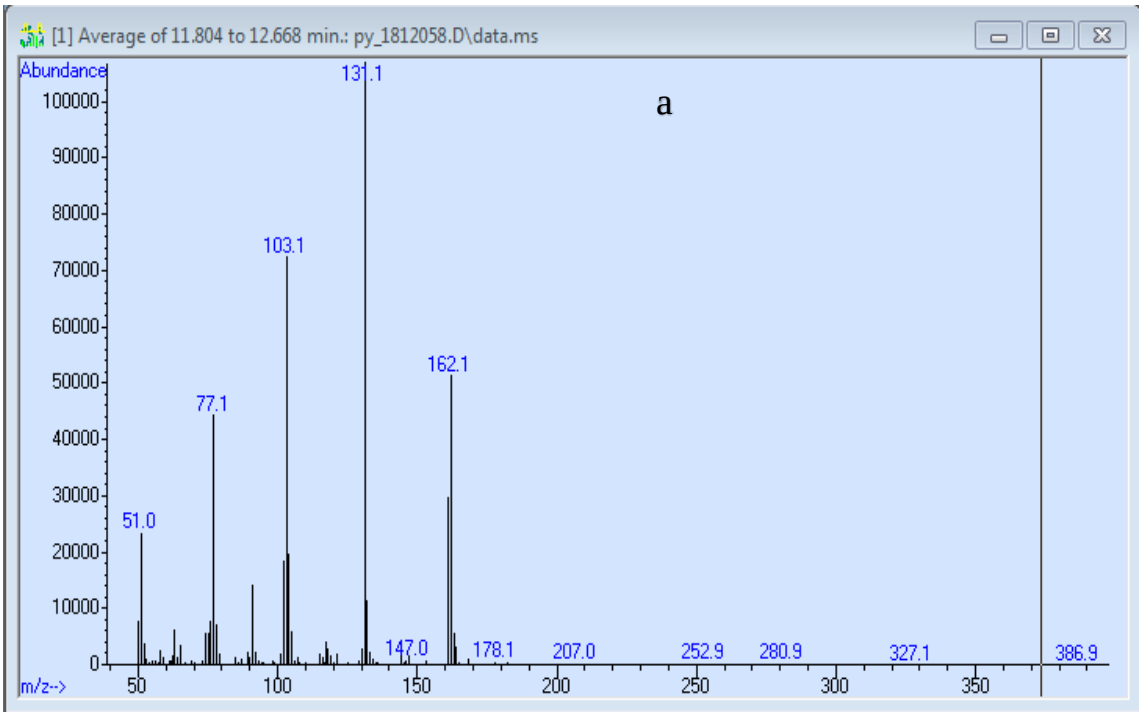

Figure S-91. MS of peak a (11.804 to 12.668 min) from Fig. S-90

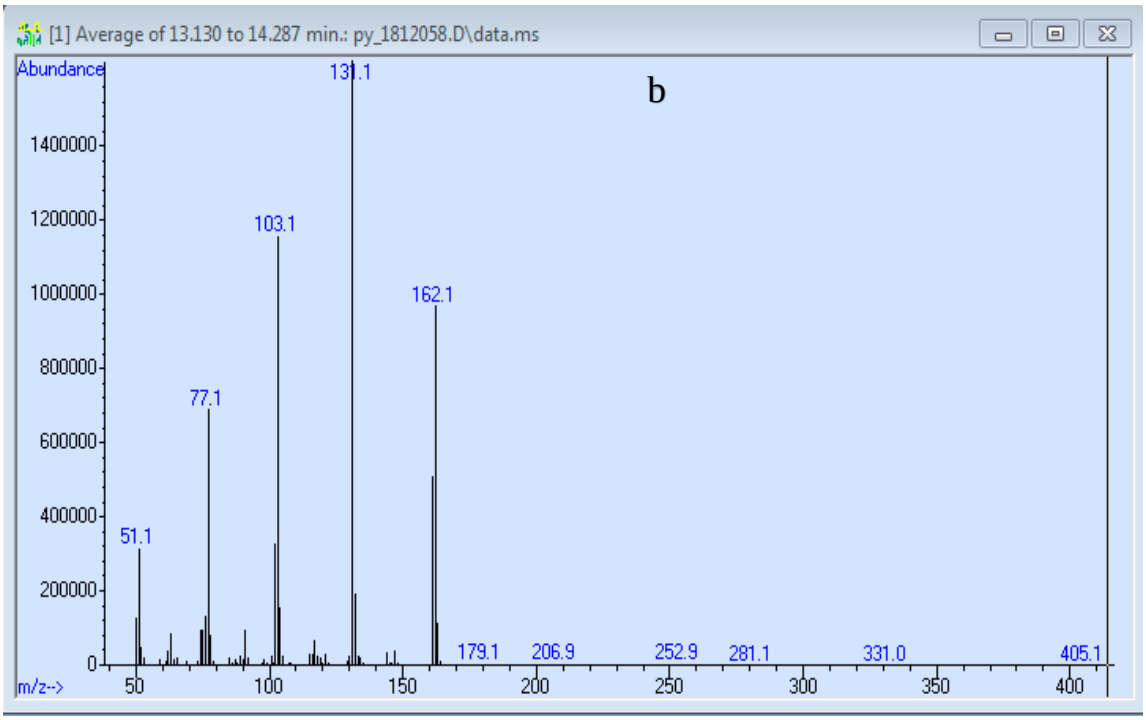

Figure S-92. MS of peak b (13.130 to 14.287 min) from Fig. S-90

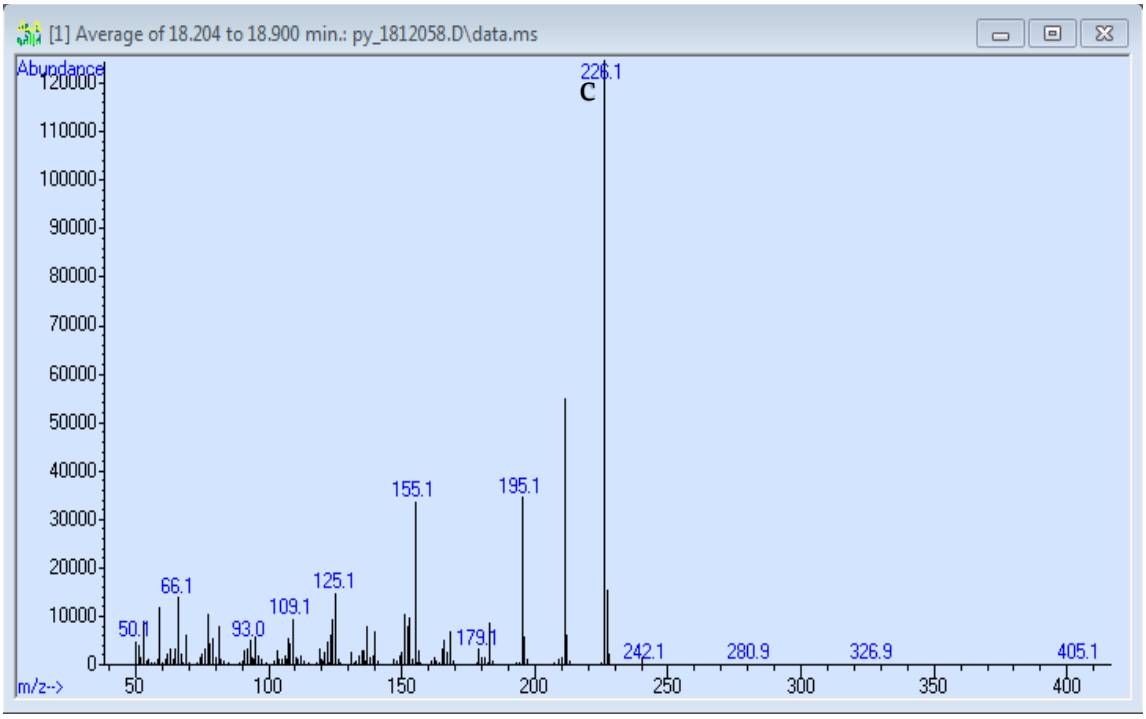

Figure S-93. MS of peak c (18.204 to 18.900 min) from Fig. S-90

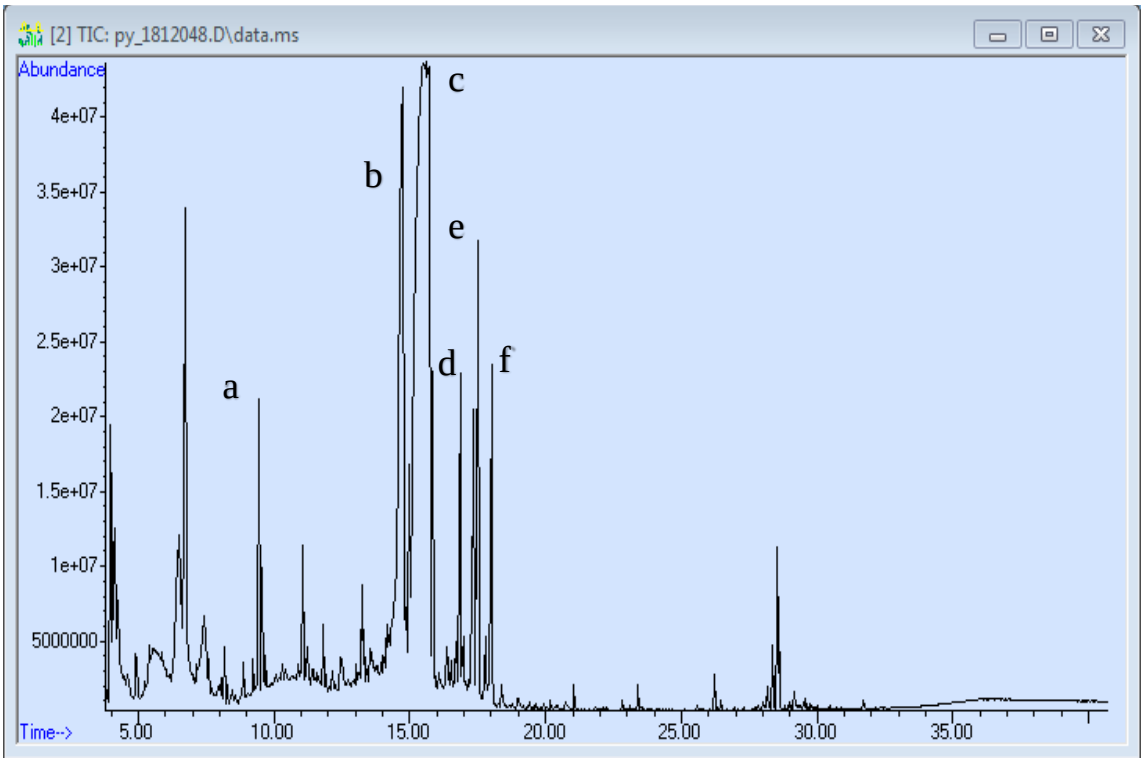

Figure S-94. TIC of vanillin

MS: 9.337 to 9.513 minutes

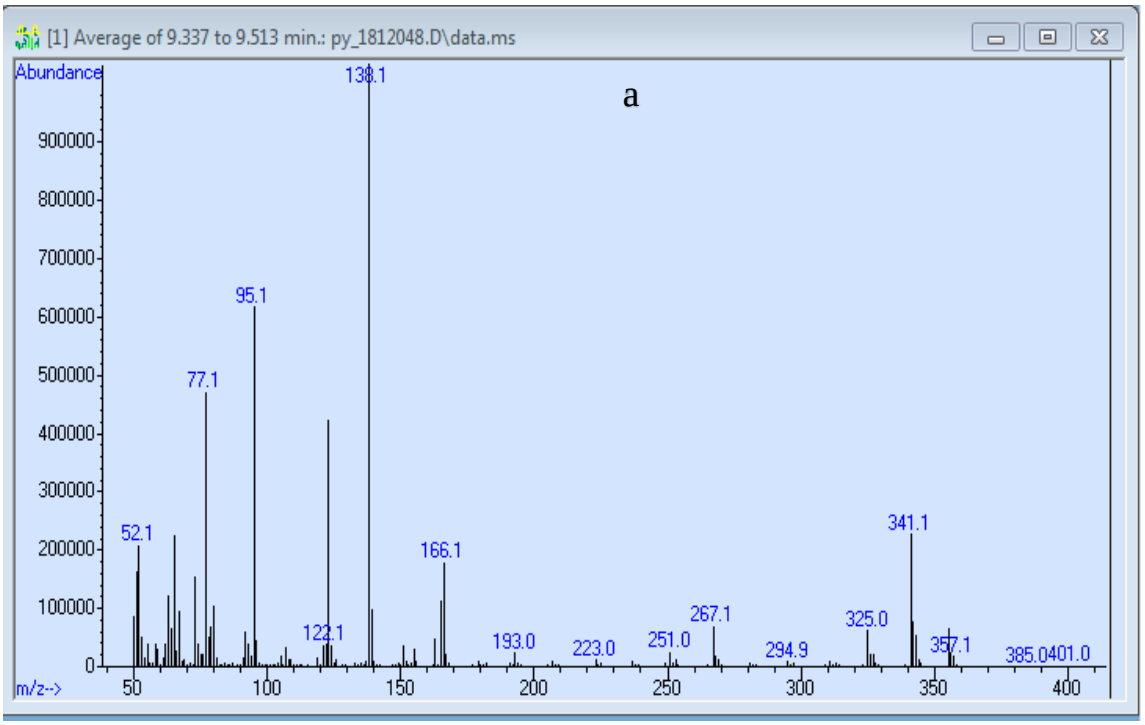

Figure S-95. MS of peak a (9.337 to 9.513 min) from Fig. S-94

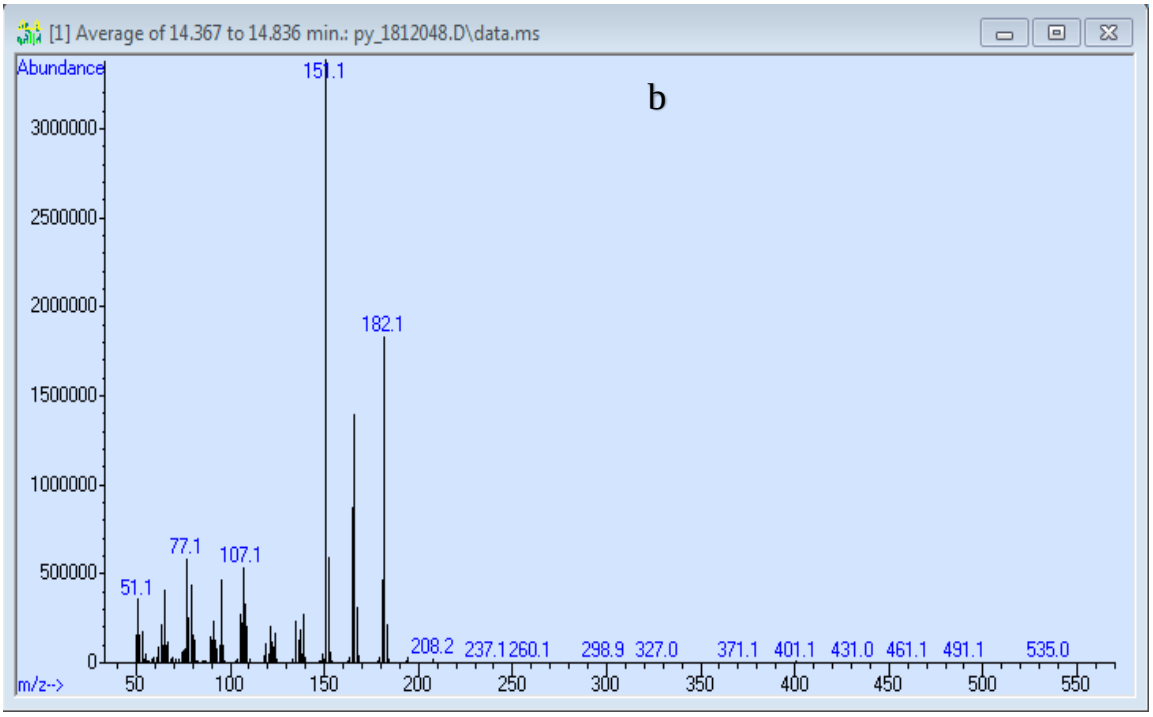

Figure S-96. MS of peak b (14.367 to 14.836 min) from Fig. S-94

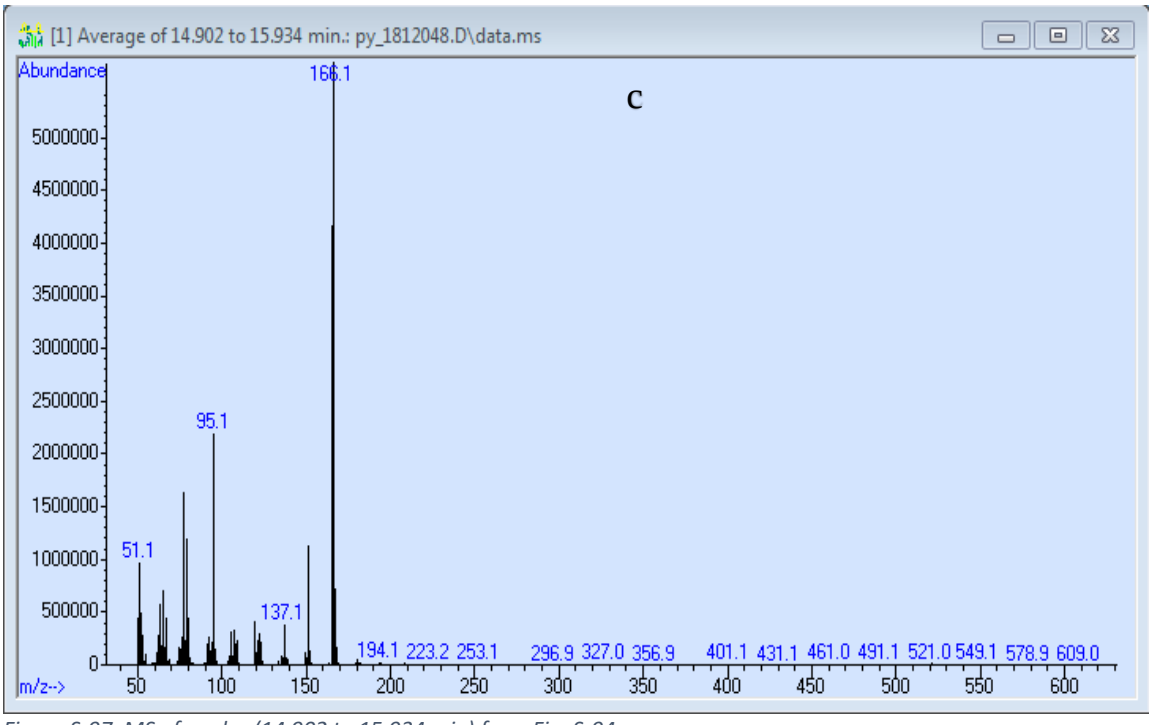

Figure S-97. MS of peak c (14.902 to 15.934 min) from Fig. S-94

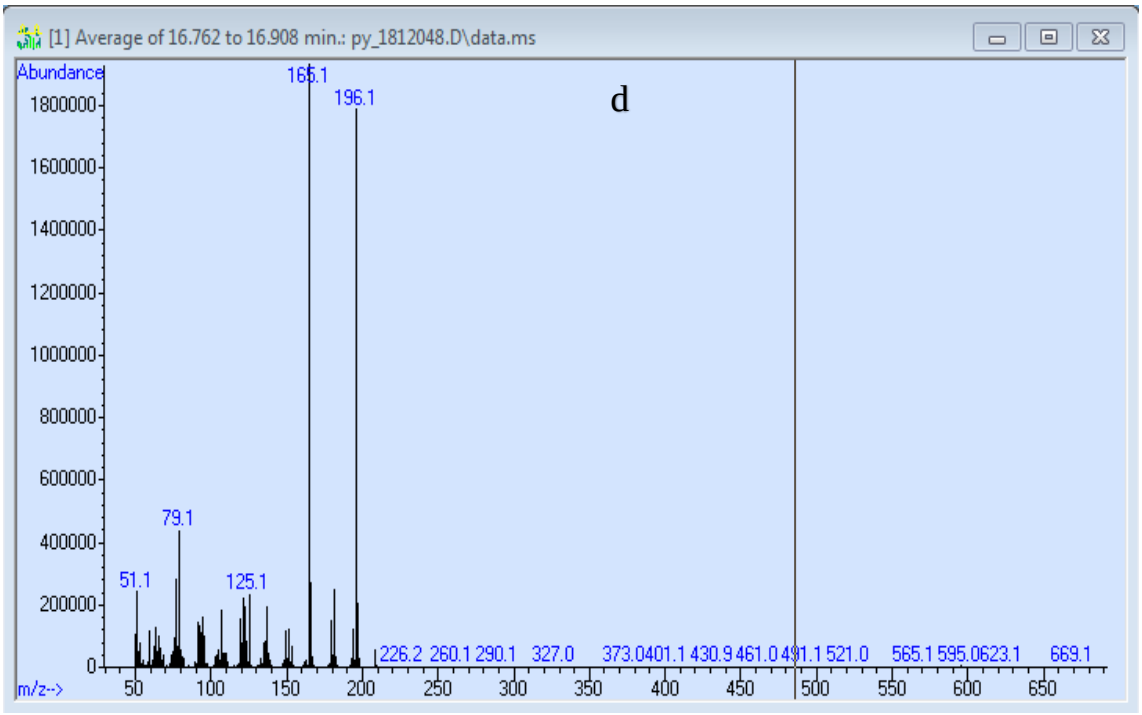

Figure S-98. MS of peak d (16.762 to 16.908 min) from Fig. S-94

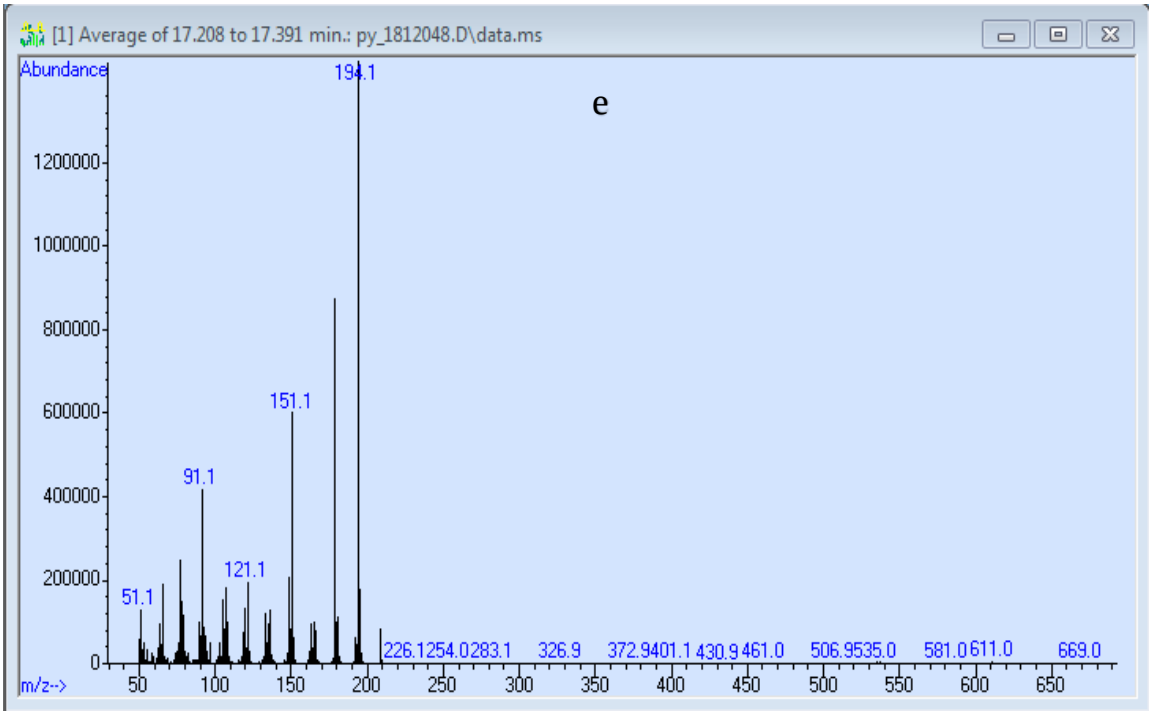

Figure S-98. MS of peak e (17.208 to 17.391 minutes) from Fig. S-94

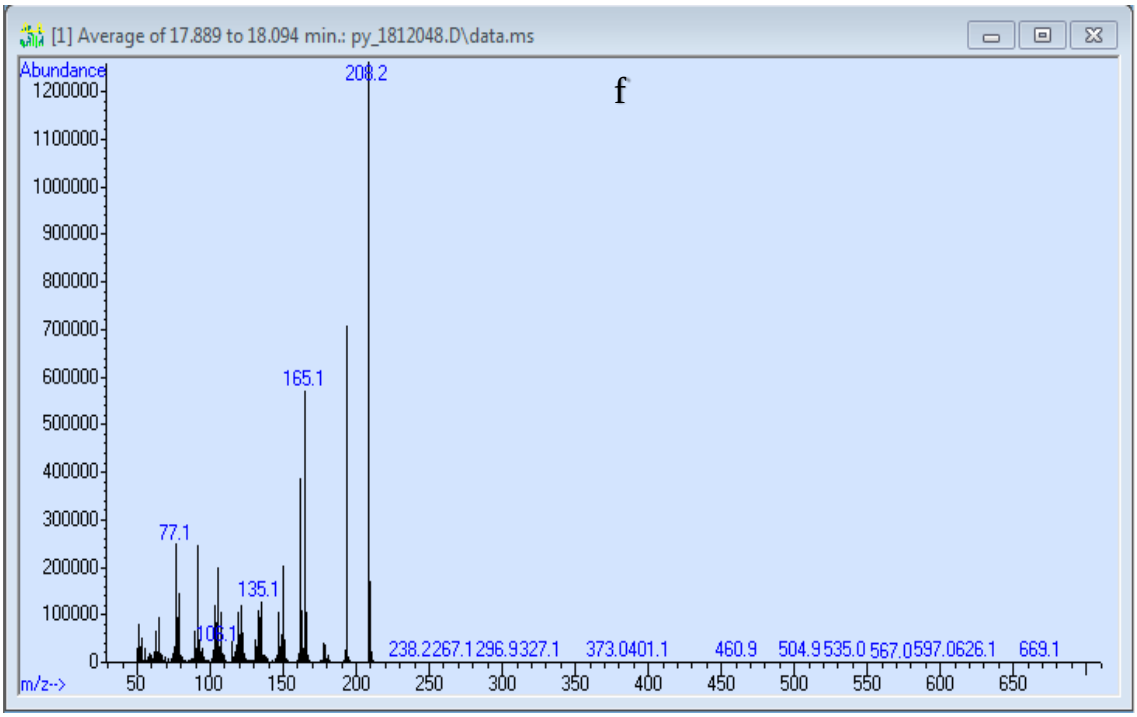

Figure S-99. MS of peak f (17.889 to 18.094 min) from Fig. S-94

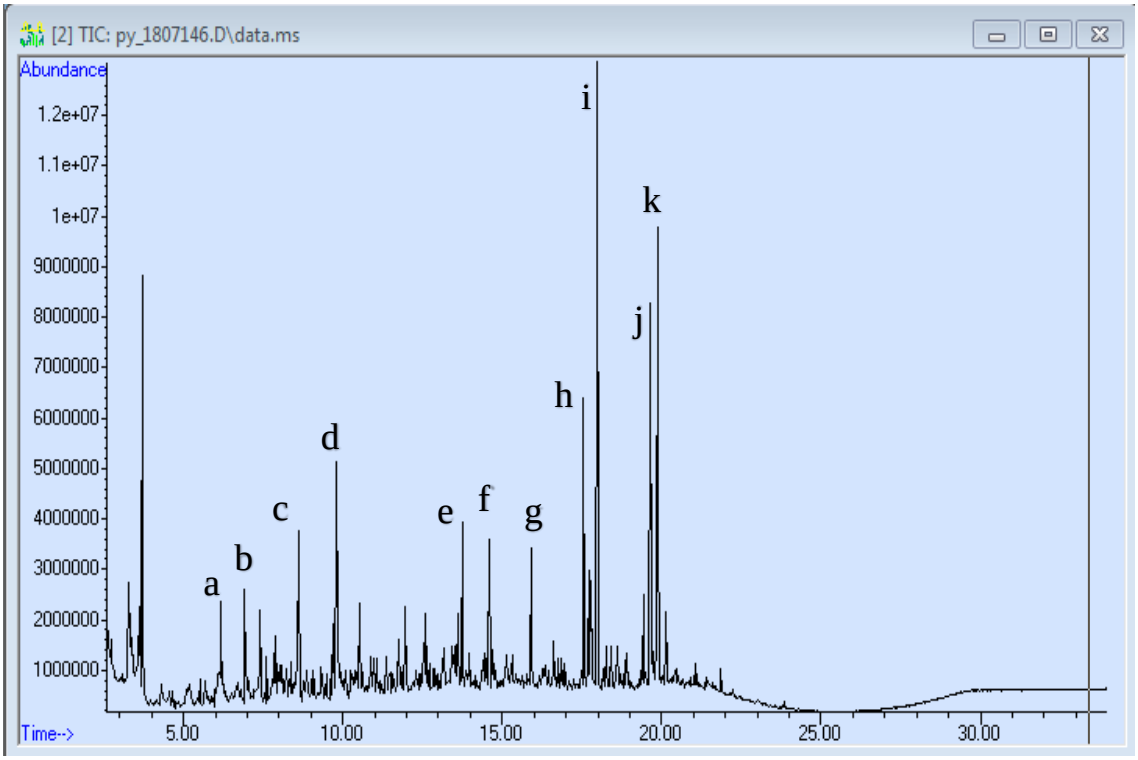

Figure S-100. TIC of Lake Superior (sample collected May 8, 2018) freeze-dried sample

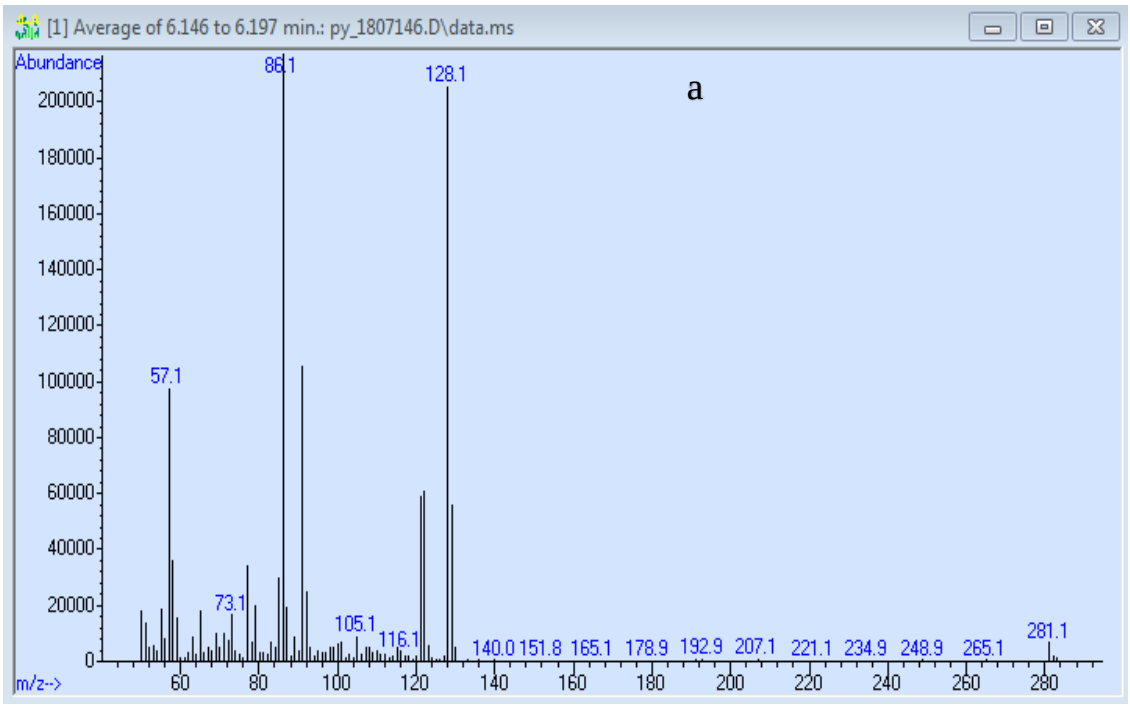

Figure S-101. MS of peak a (6.146 to 6.197 min) from Fig. S-100

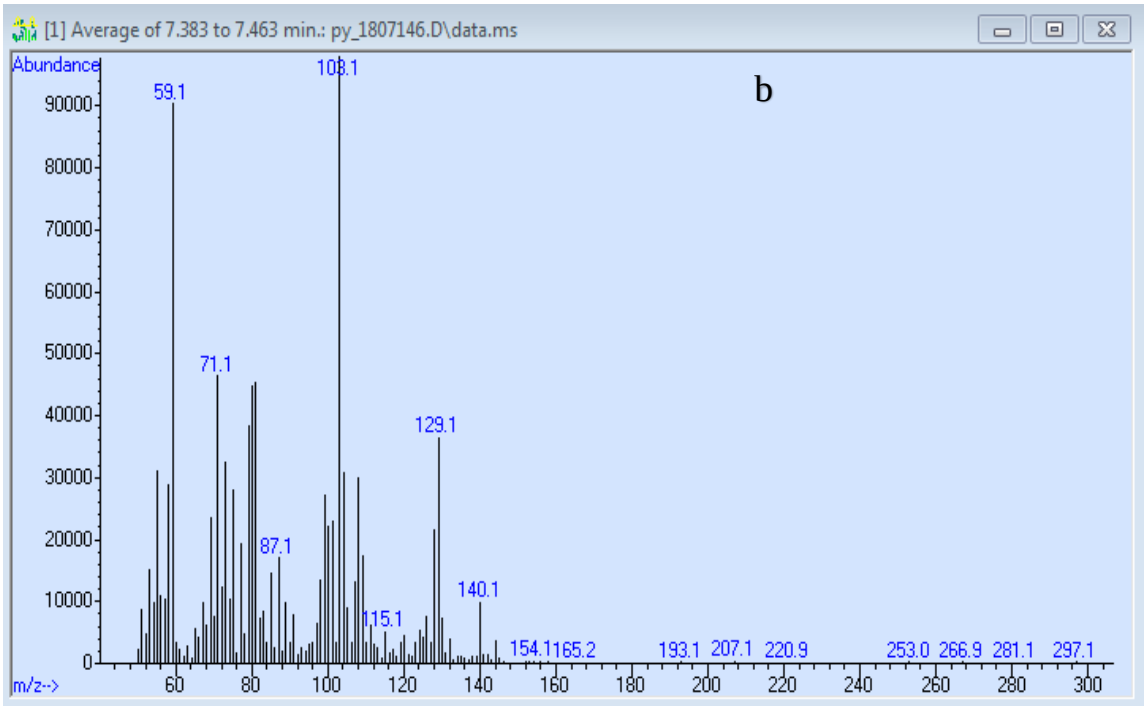

Figure S-102. MS of peak b (7.383 to 7.463 min) from Fig. S-100

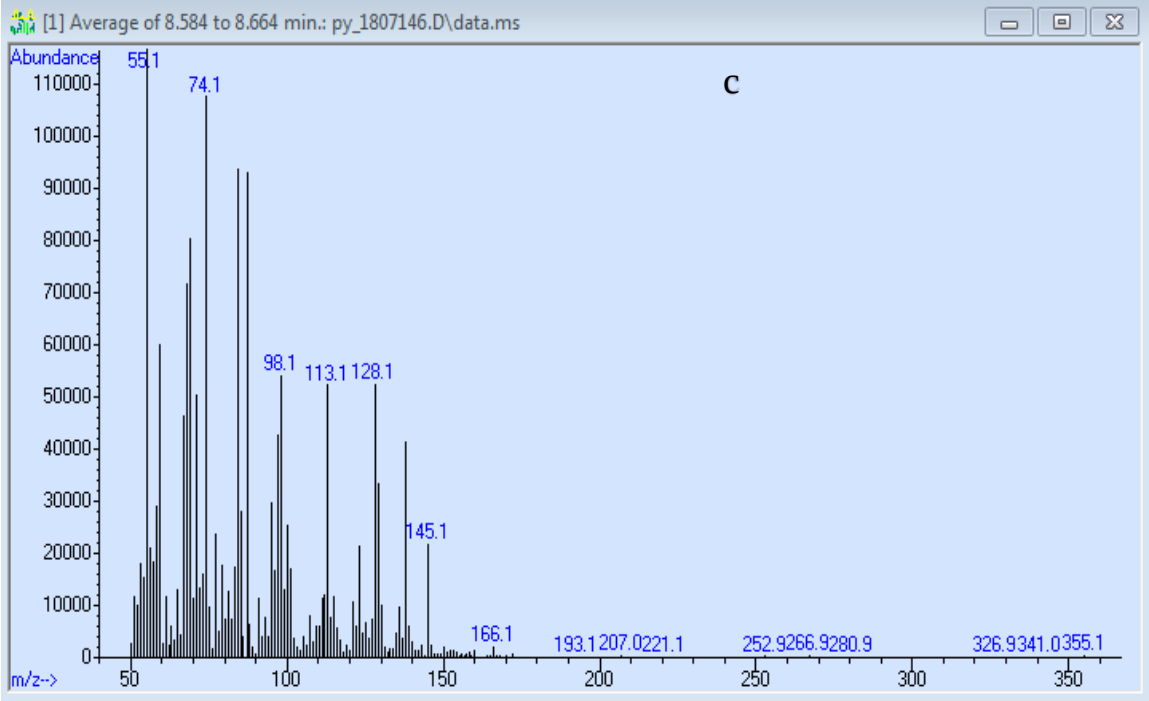

Figure S-103. MS of peak c (8.584 to 8.664 min) from Fig. S-100

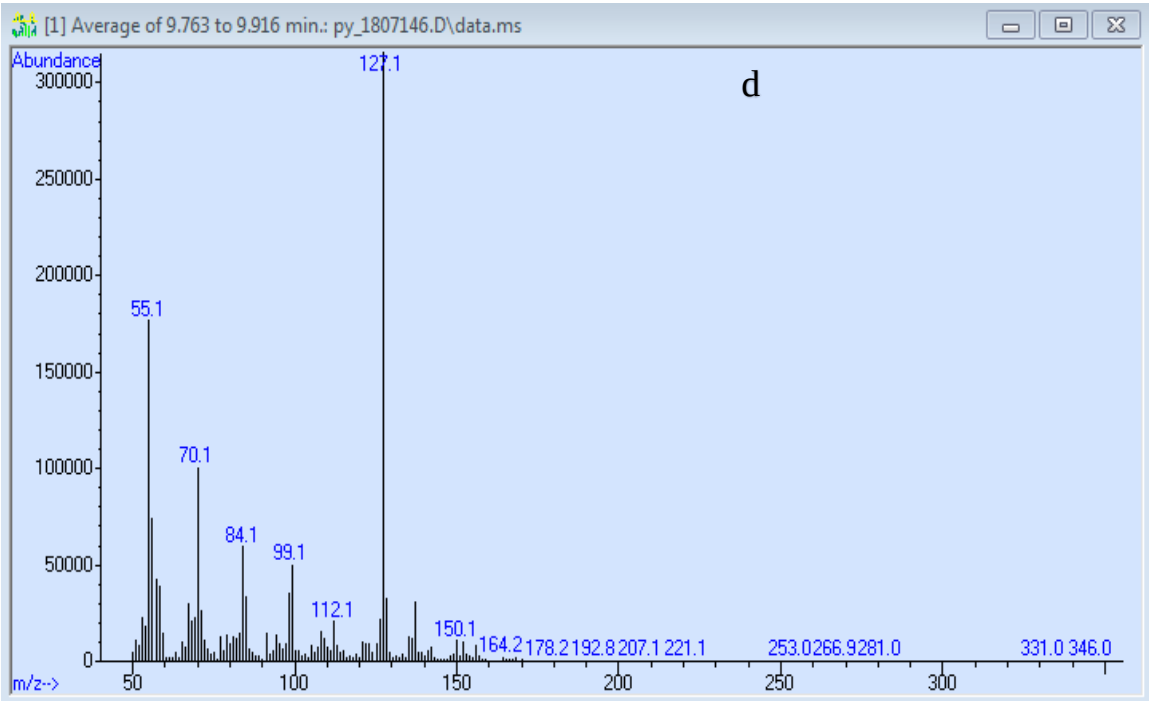

Figure S-104. MS of peak d (9.763 to 9.916 min) from Fig. S-100

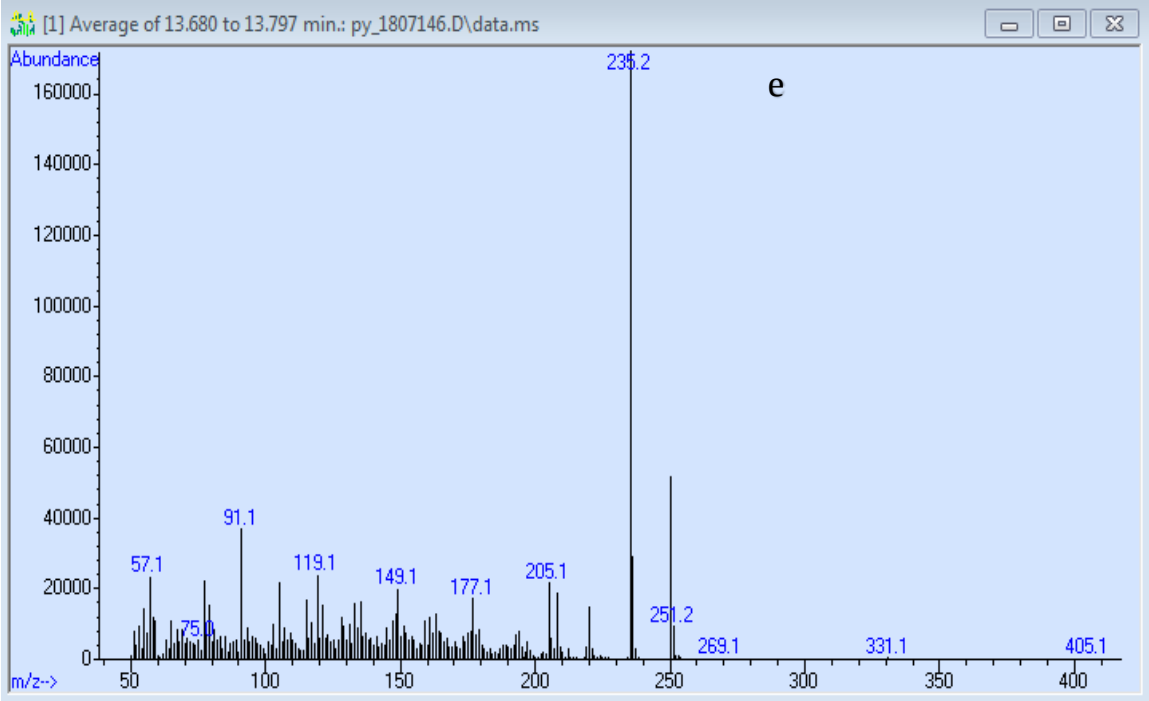

Figure S-105. MS of peak e (13.680 to 13.797 min) from Fig. S-100

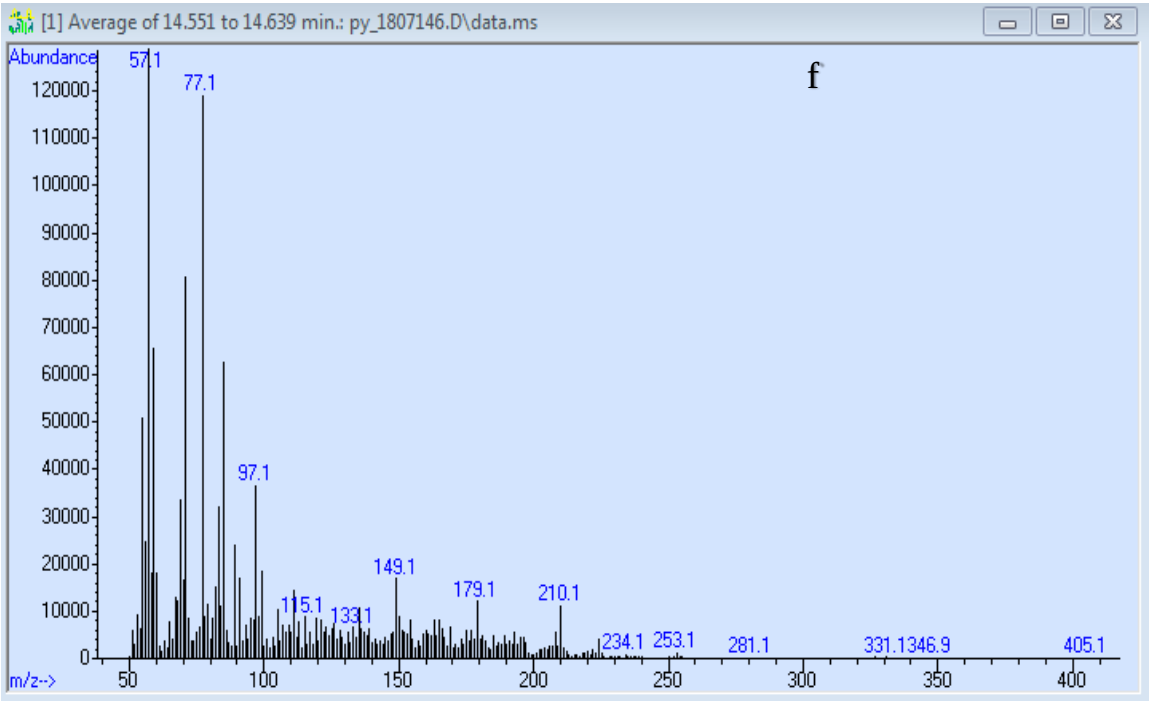

Figure S-106. MS of peak f (14.551 to 14.639) from Fig. S-100

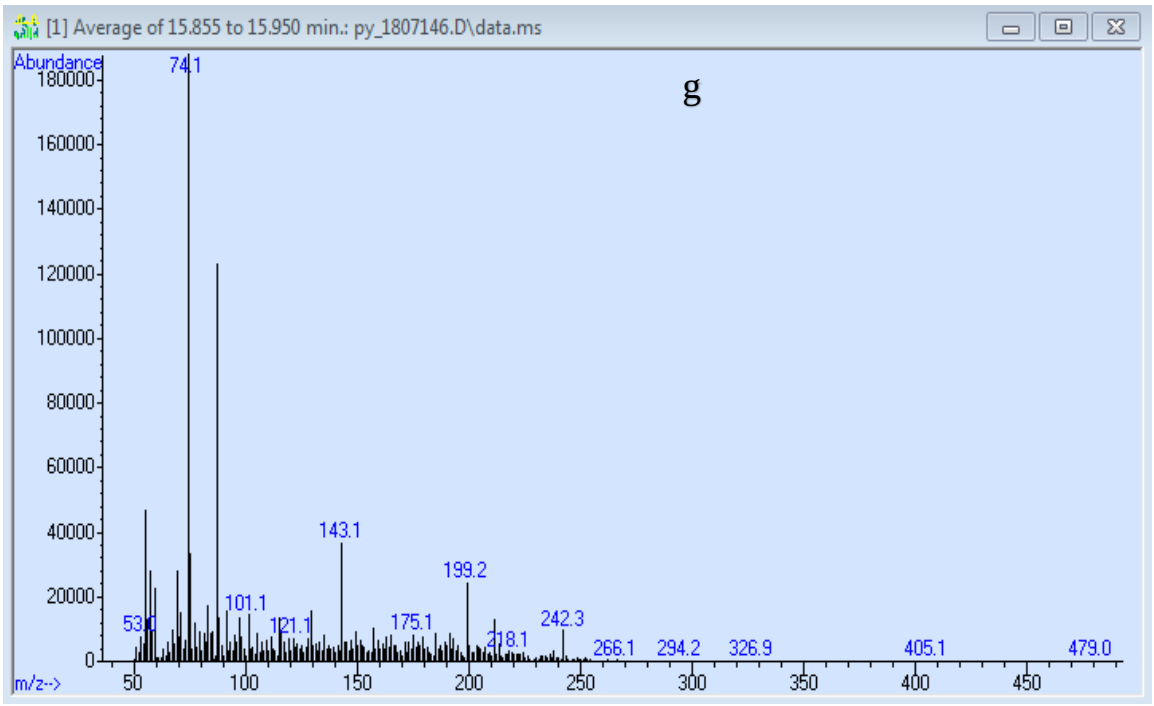

Figure S-107. MS of peak g (15.855 to 15.950 min) from Fig. S-100

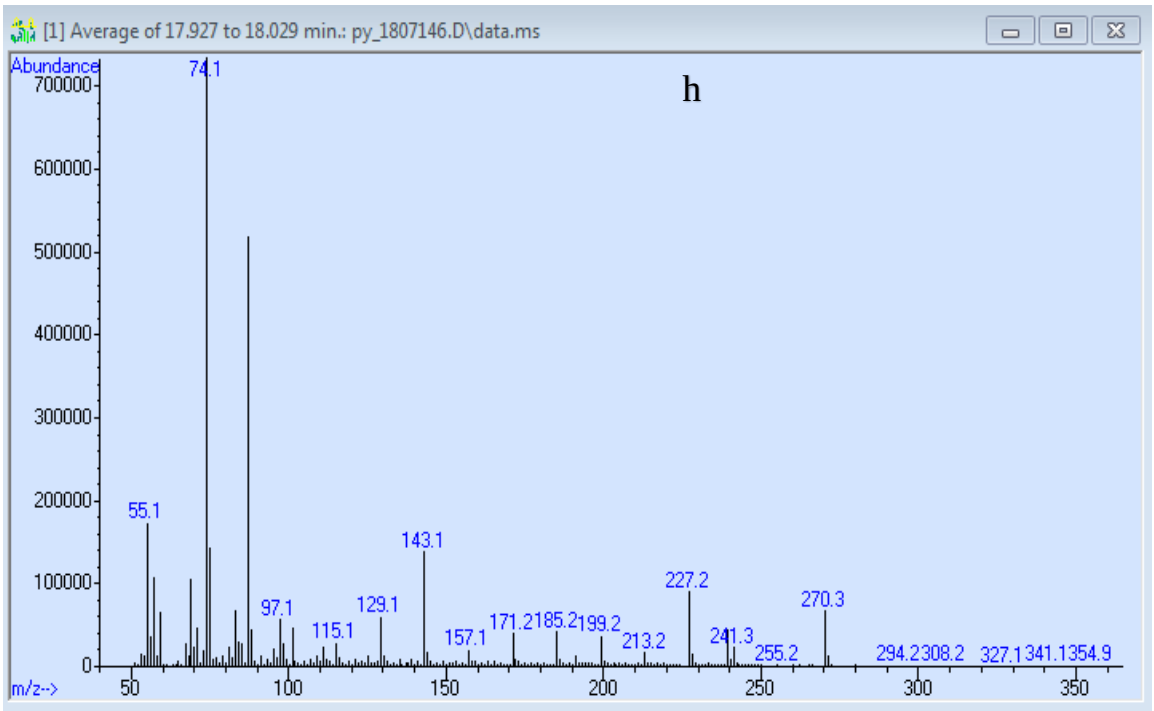

Figure S-108. MS of peak h (17.927 to 18.029 min) from Fig. S-100

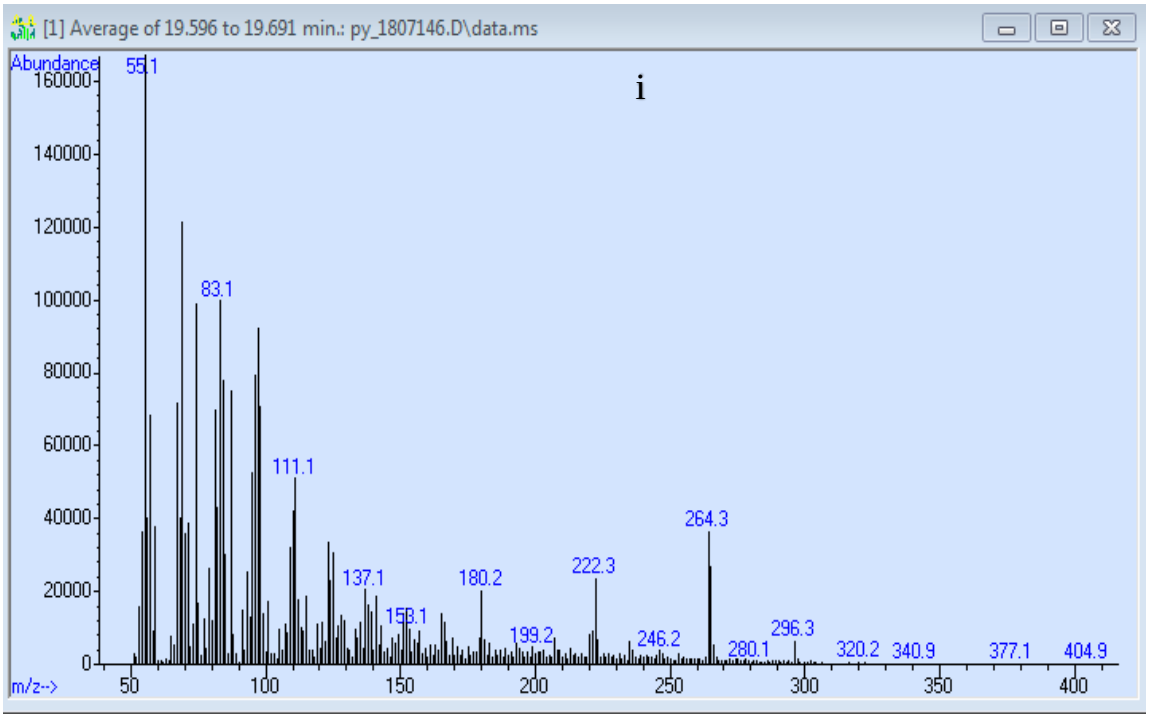

Figure S-109. MS of peak i (19.596 to 19.691 min) from Fig. S-100

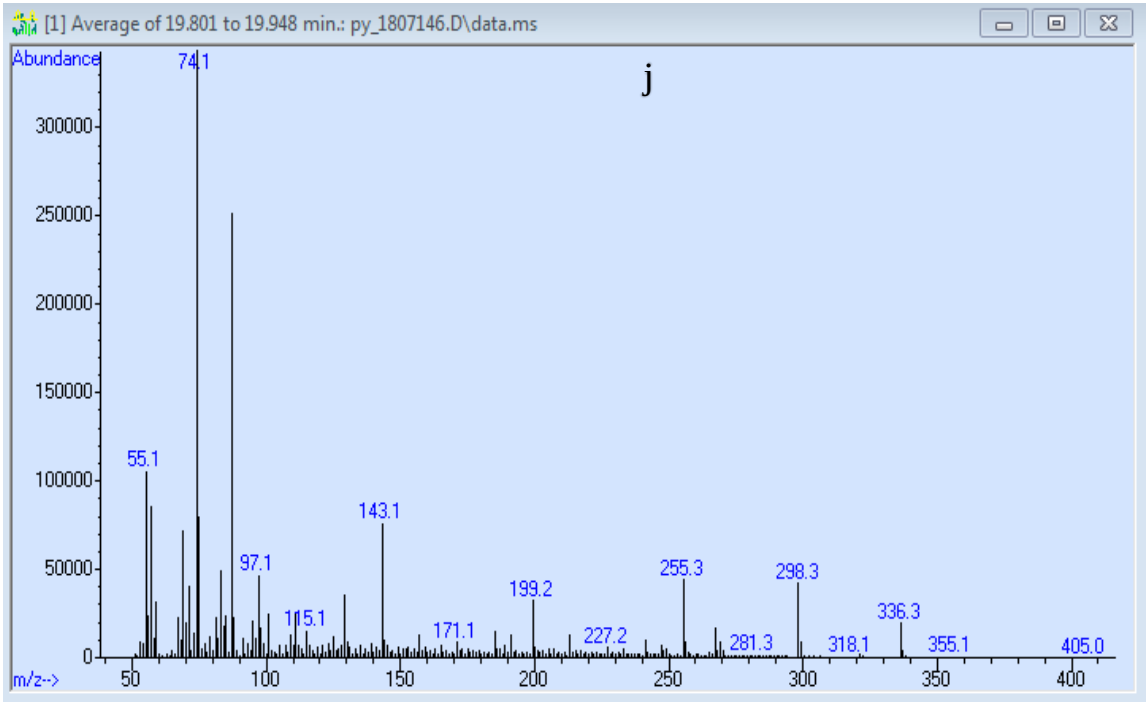

Figure S-110. MS of peak j (19.801 to 19.691 min) from Fig S-100

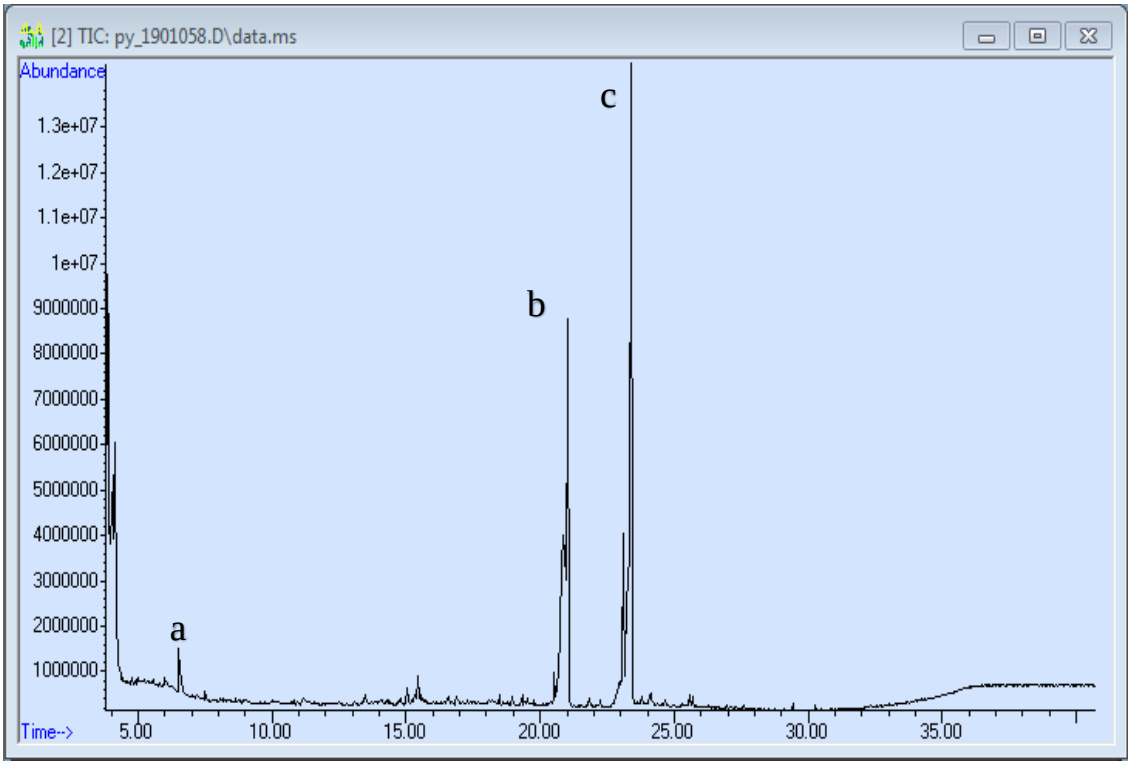

Figure S-111. TIC of Lake Superior (sample collected May 8, 2018)

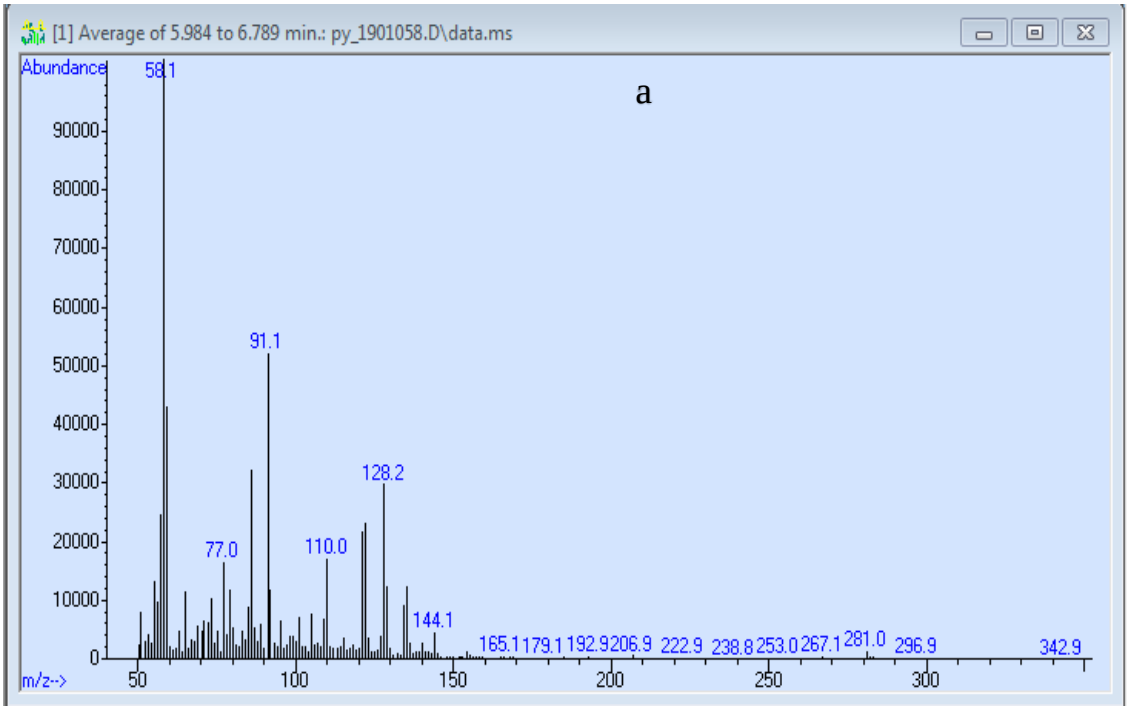

Figure S-112. MS of peak a (5.984 to 6.789 min) from Fig. S-111

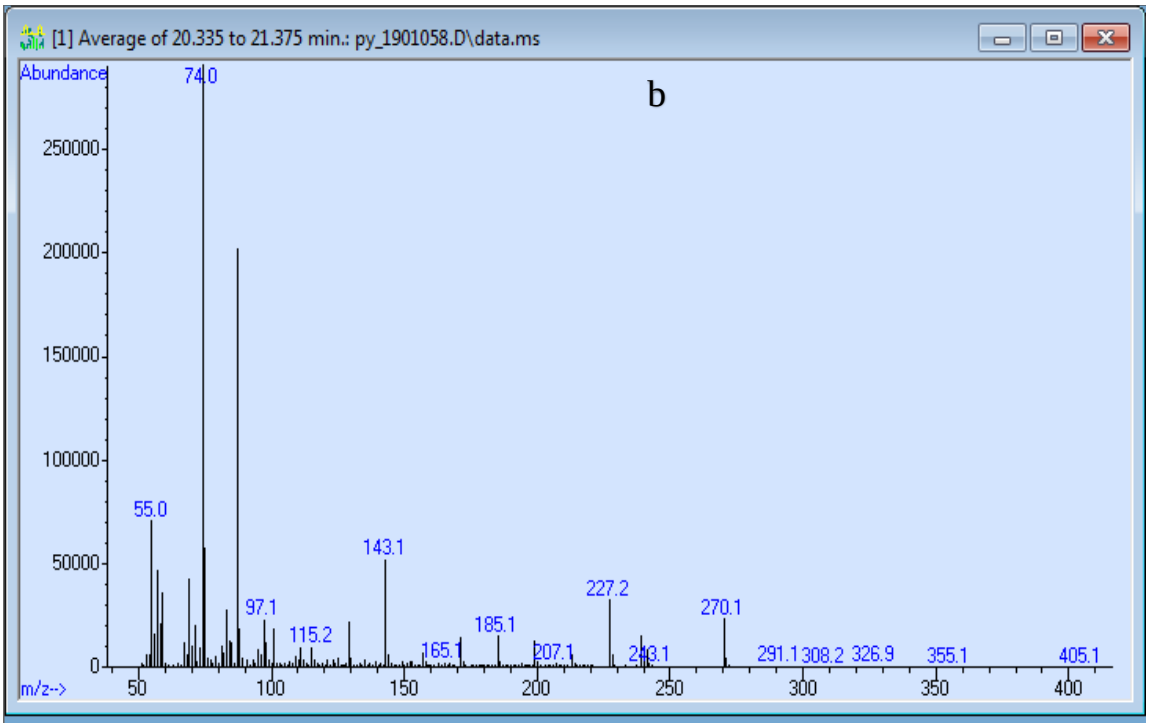

Figure S-112. MS of peak b (20.335 to 21.375 min) from Fig. S-111

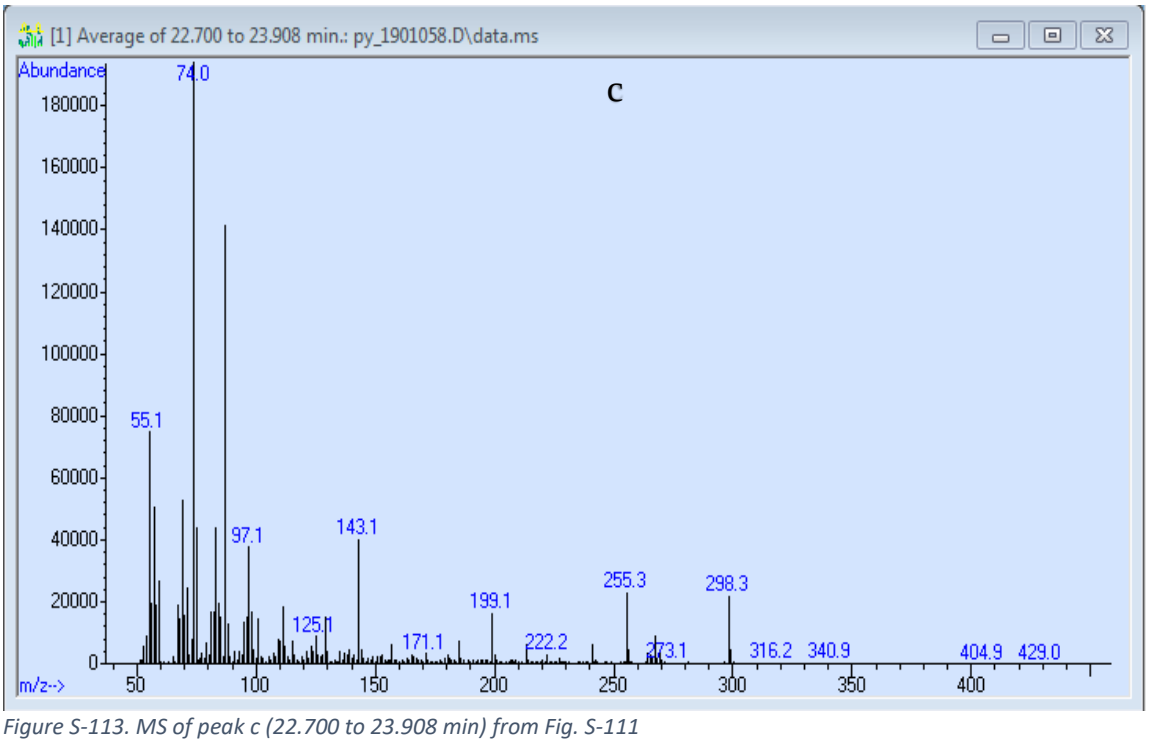

Figure S-113. MS of peak c (22.700 to 23.908 min) from Fig. S-111

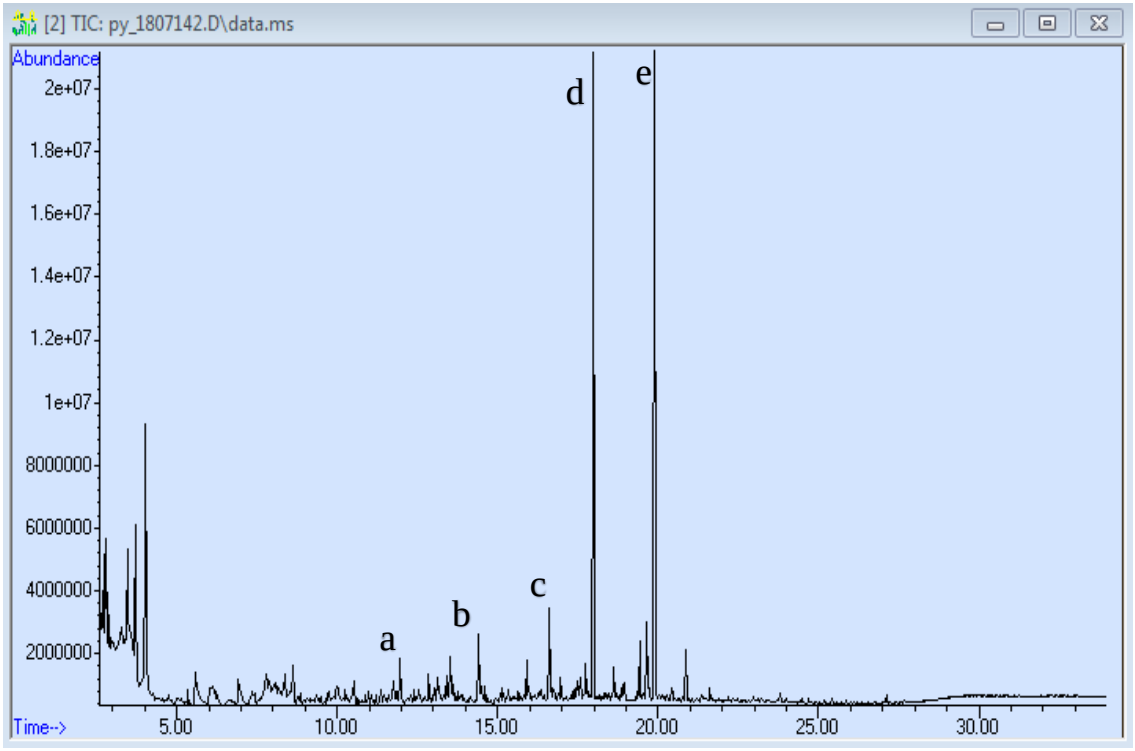

Figure S-114. TIC of freeze-dried Chester Creek (sample collected November 2017) material

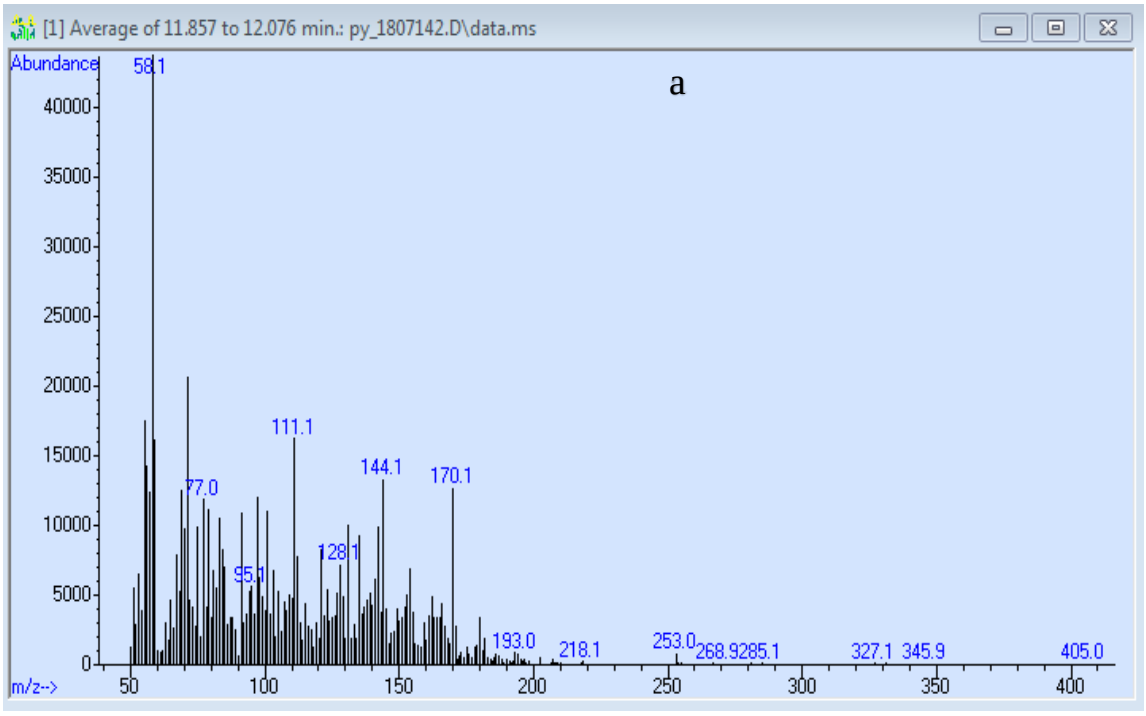

Figure S-115. MS of peak a (11.857 to 12.076 min) from Fig. S-114

MS: 14.273 to 14.515 minutes

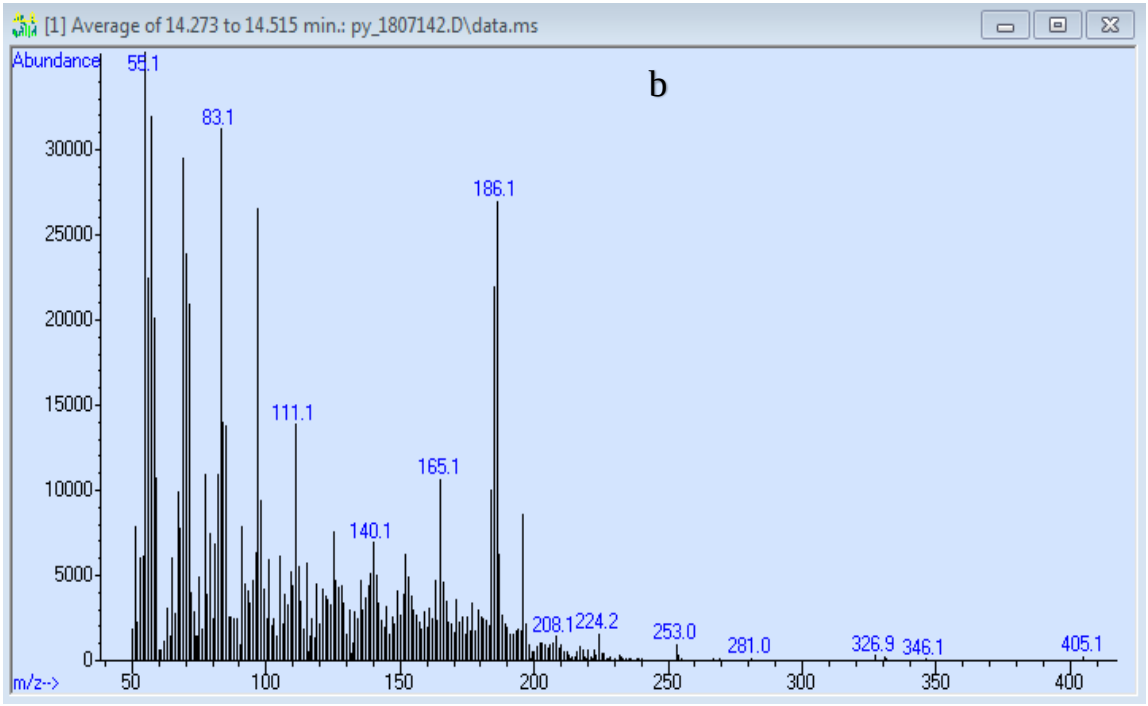

Figure S-116. MS of peak b (14.273 to 14.515 min) from Fig. S-114

MS: 16.536 to 16.733 minutes

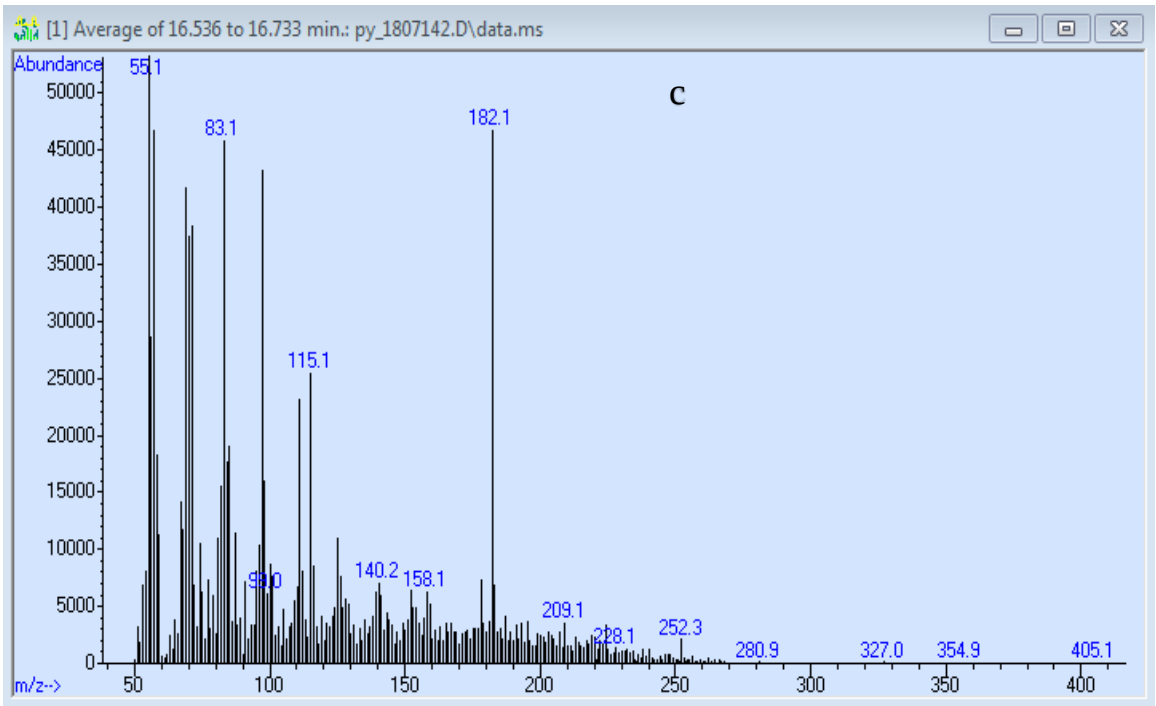

Figure S-117. MS of peak c (16.536 to 16.733 min) from Fig. S-114

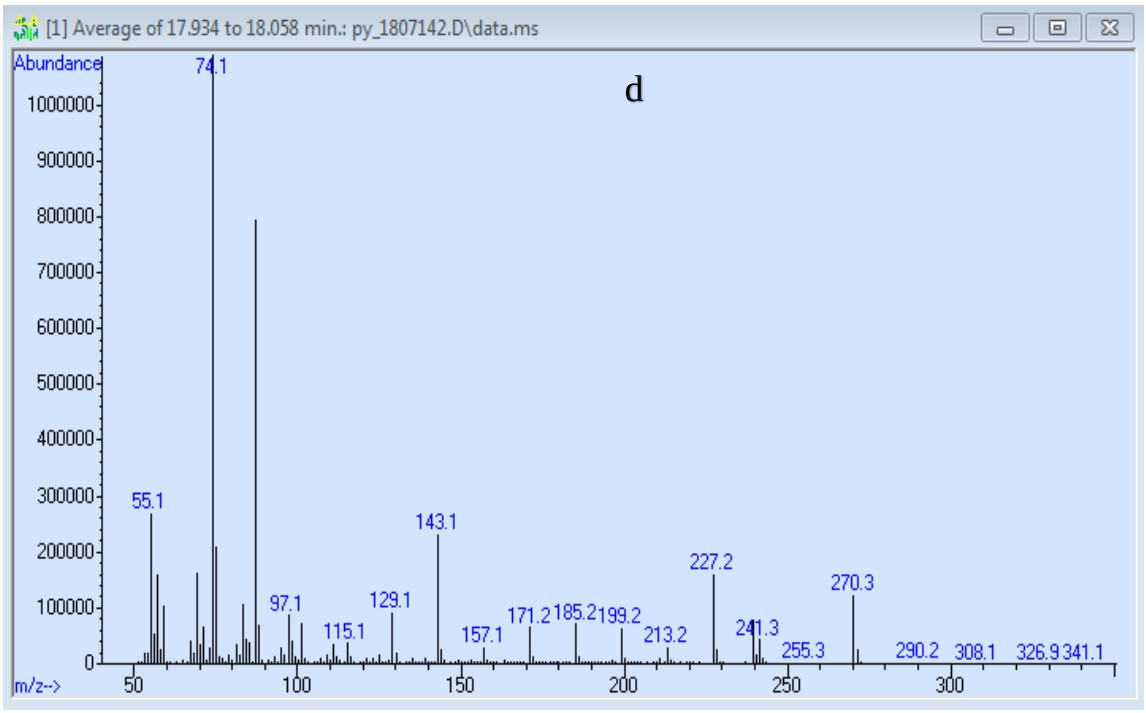

Figure S-118. MS of peak d (17.934 to 18.058 min) from Fig. S-114

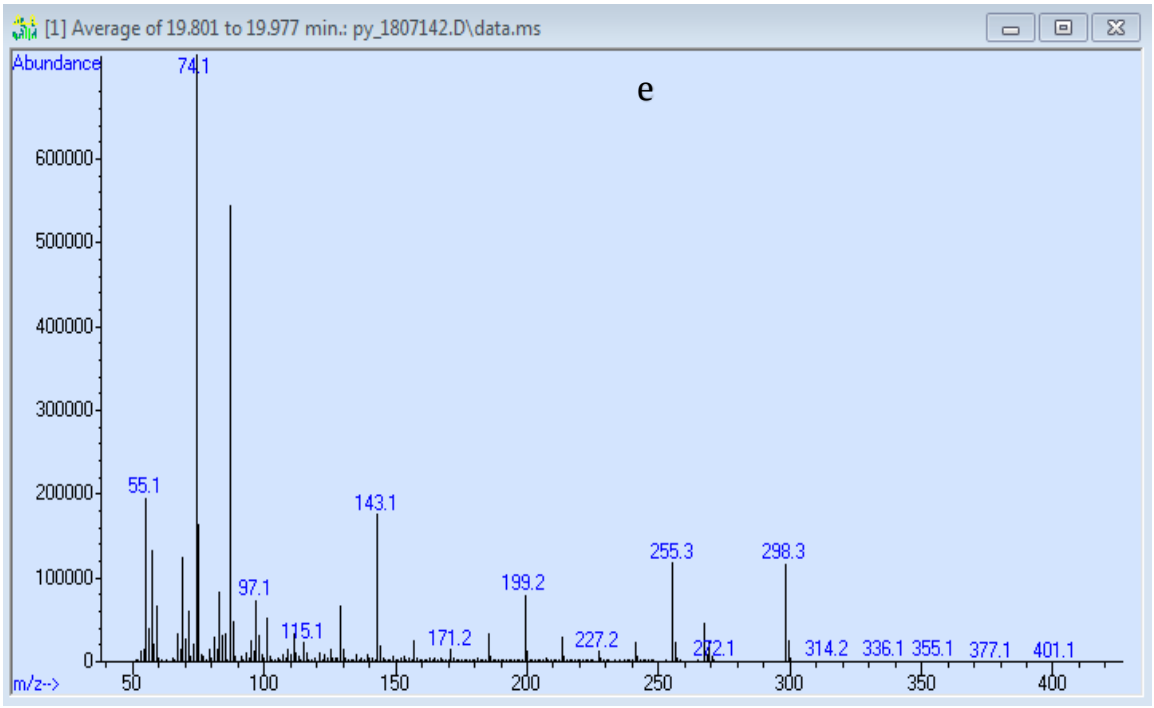

Figure S-119. MS of peak e (19.801 to 19.977 min) from Fig. S-114

Chester Creek 3 November 2018: TIC

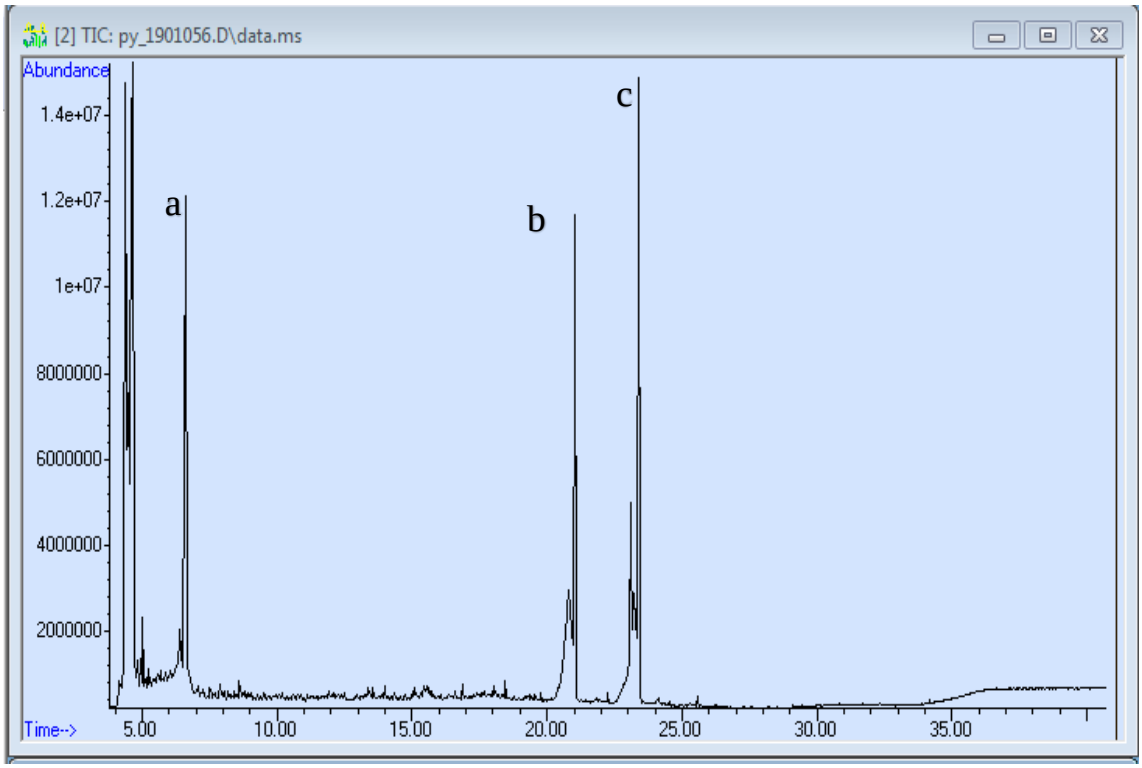

Figure S-120. TIC of freeze-dried Chester Creek (sample collected November 2018)

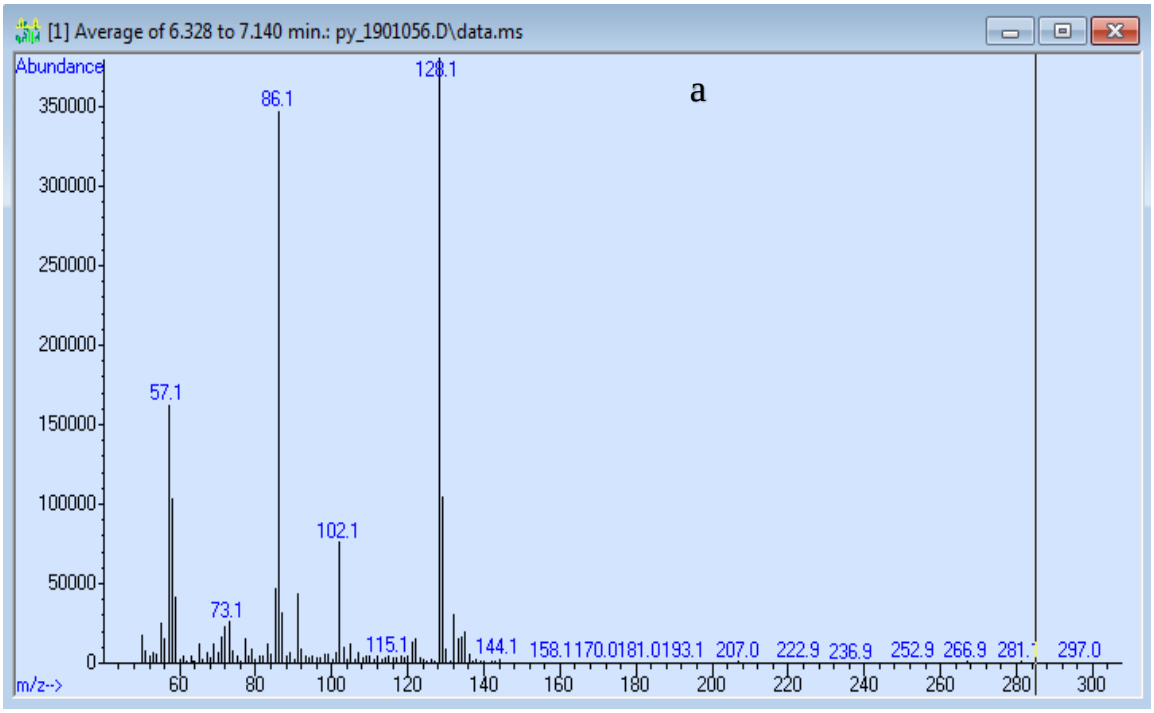

Figure S-121. MS of peak a (6.328 to 7.140 min) from Fig. S-120

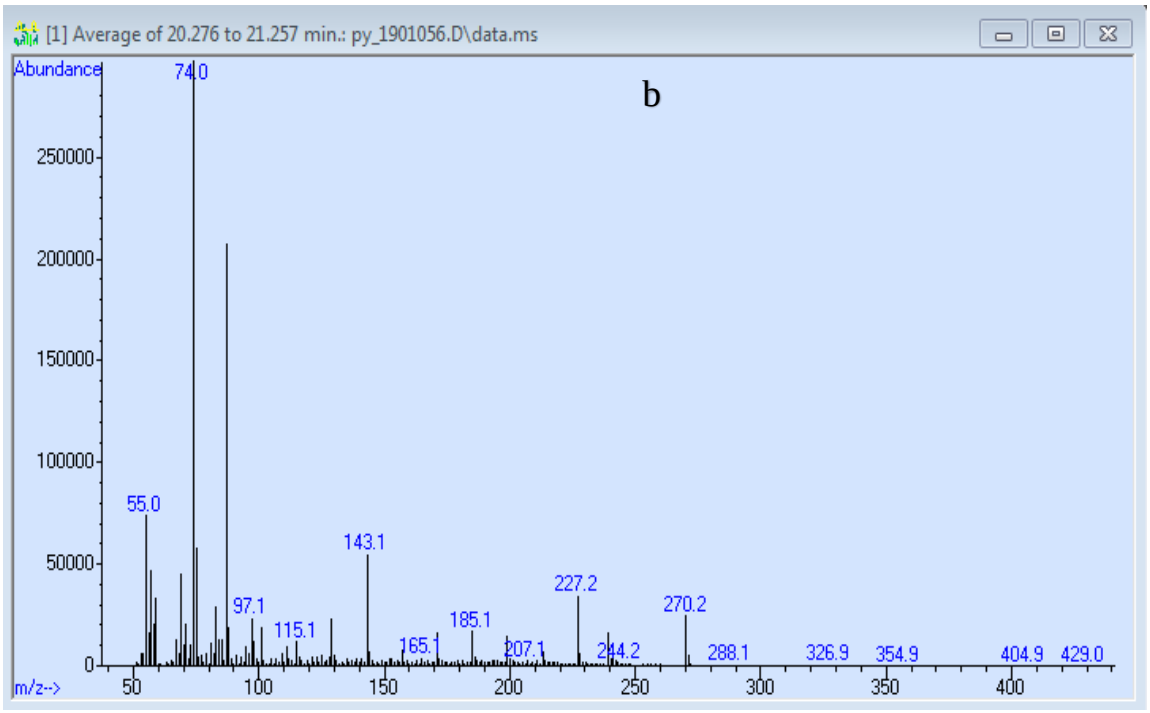

Figure S-122. MS of peak b (20.276 to 21.257 min) from Fig. S-120

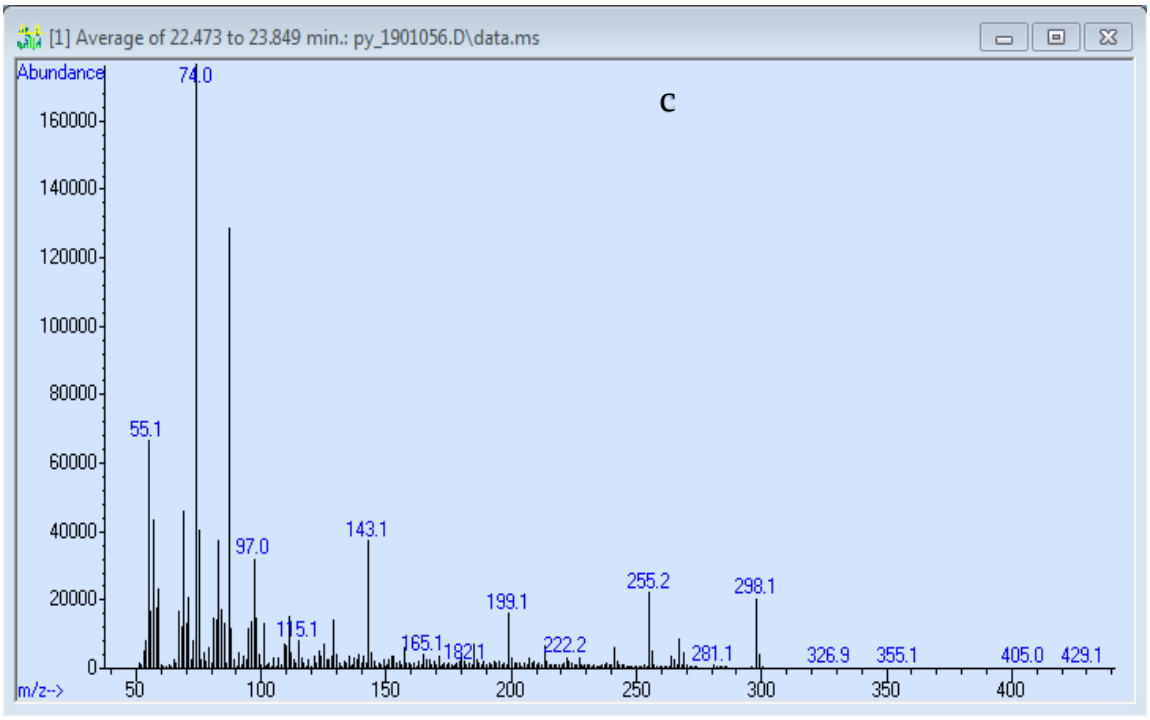

Figure S-123. MS of peak c (22.473 to 23.489 min) from Fig. S-120